Jean-Mary Martel

Series arc faults in low-voltage AC electrical installations

Ilmenauer Beiträge zur elektrischen Energiesystem-, Geräte- und Anlagentechnik (IBEGA)

Herausgegeben von
Univ.-Prof. Dr.-Ing. Dirk Westermann
(Fachgebiet Elektrische Energieversorgung) und
Univ.-Prof. Dr.-Ing. Frank Berger
(Fachgebiet Elektrische Geräte und Anlagen)
an der Technischen Universität Ilmenau.

Band 20

Jean-Mary Martel

Series arc faults in low-voltage AC electrical installations

Universitätsverlag Ilmenau
2018

Impressum

Bibliografische Information der Deutschen Nationalbibliothek
Die Deutsche Nationalbibliothek verzeichnet diese Publikation in der Deutschen Nationalbibliografie; detaillierte bibliografische Angaben sind im Internet über http://dnb.d-nb.de abrufbar.

Diese Arbeit hat der Fakultät für Elektrotechnik und Informationstechnik der Technischen Universität Ilmenau als Dissertation vorgelegen.

Tag der Einreichung:	05. Juli 2016
1. Gutachter/-in:	Univ.-Prof. Dr.-Ing. Frank Berger (Technische Universität Ilmenau)
2. Gutachter/-in:	Univ.-Prof. Dr.-Ing. Peter Schegner (Technische Universität Dresden)
3. Gutachter/-in:	Dr.-Ing. Michael Anheuser (Siemens AG, Amberg)
Tag der Verteidigung:	15. Dezember 2017

Technische Universität Ilmenau/Universitätsbibliothek
Universitätsverlag Ilmenau
Postfach 10 05 65
98684 Ilmenau
http://www.tu-ilmenau.de/universitaetsverlag

readbox unipress
in der readbox publishing GmbH
Am Hawerkamp 31
48155 Münster
http://unipress.readbox.net

ISSN 2194-2838 (Druckausgabe)
ISBN 978-3-86360-173-7 (Druckausgabe)
URN urn:nbn:de:gbv:ilm1- 2017000635

Abstract

This thesis provides a complete analysis of all the topics related to series arc faults in low-voltage electrical installations. The part played by series arc faults in the outbreak of hazardous electrical fires is explained by using fire statistics, performing an electrical and thermal characterization of the phenomenon, and comparing with other electrical faults their ability to ignite an insulation material. The analysis demonstrates that the series arc fault generates a heat stress that largely exceeds the ignition threshold of insulation polymers. Other electrical faults such as bolted short-circuit, overload, earth leakage, and glowing fault result in much lower risks of fire ignition. The principles of arc fault detection are explained and the contribution of the active protection AFDD (arc fault detection device) is taken into account in this analysis. The option of achieving a passive protection using appropriate insulation materials is also explored. The performance requirements described in the product standard of AFDD are reviewed and recommendations for improving the standards are proposed.

Abstrakt

Diese Dissertation ist eine vollständige Analyse der Problematik des seriellen Störlichtbogens in der Niederspannungselektroinstallation. Der Beitrag von seriellen Störlichtbögen in der Entstehung von Elektrobränden wird mit Hilfe der Brandstatistik, der Durchführung der elektrischen und thermischen Charakterisierung des Phänomens und des Vergleichs der Fähigkeit von den anderen elektrischen Fehlern ein Isolierungspolymer zu entzünden, erklärt. Die Analyse beweist, dass der serielle Störlichtbogen eine thermische Beanspruchung erzeugt, die die Zündgrenzen der Isolierungspolymere weitaus überschreitet. Andere elektrische Fehler wie Kurzschlüsse, Überlast, Erdschlüsse und glühende Kontaktstellen ergeben ein wesentlich niedrigeres Brandrisiko. Die Funktionsweise vom Störlichtbogenschutzschalter (auch Brandschutzschalter oder AFDD genannt) wird erklärt und der Beitrag von diesem aktiven Schutz wird in der Analyse berücksichtigt. Der passive Schutz mit geeigneten Isolationsmaterialien wird auch untersucht. Die Anforderungen, die in der Produktnorm für Störlichtbogenschutzschalter beschrieben sind, werden überprüft und Verbesserungen für diese Normen werden vorgeschlagen.

Acknowledgments

Firstly, I would like to express my special appreciation and thanks to my mentors Professor Dr. Frank Berger and Dr. Michael Anheuser, for their support, motivation, and patience during more than five years of PhD studies. They made my dream come true and ensured that this PhD thesis becomes a scientific work and not just an engineering document. I would also like to thank Professor Dr. Schegner for being my committee member and reviewer.

I would especially like to thank Bogdan Barbu for giving me advice and data on plasma physics as well as my colleagues from the R&D and product management departments of Siemens EM LP in Regensburg for reviewing my work. I would like to thank the company U.I. Lapp GmbH for providing probes of polymers as well as supporting for the UL tests. I would also like to express my gratitude to my former manager, Gerald Noerl, who strongly encouraged me and made sure that I had sufficient time and financial means for my thesis. A special thanks to my wife, Monika, my family, and my friends; they enquired regularly about the progress of my work and their encouragement has sustained me thus far.

Contents

Introduction

As electricity has become essential to our everyday lives, a genuine need for safety has followed suit. The utilization of electrical energy implies a risk of electrical faults and their potential to damage infrastructure and impact people's safety. Protection devices such as fuses, circuit breakers (MCB), and residual current detectors (RCD) have been available for decades to improve the safety of low-voltage electrical installations. Fuses and MCBs provide protection against overload and short-circuits, thus mitigating some of the risk of damage and fire. RCDs can detect current leakage to earth caused by insulation weaknesses or unintentional contact with live parts, thereby additionally increasing the safety of individuals and protection from fire.

Despite the widespread use of these electrical protection systems and continuous improvement in safety standards, electrical energy can still be a heat source that can directly cause a fire. The expression "electrical fire" in this thesis refers to this kind of fire. These fires are responsible for numerous deaths, injuries, and economic losses. One main reason is probably the series arc fault which cannot be detected and interrupted by regular protection devices. A comprehensive description of the different types of arc faults and the available detection technology (AFDD: Arc Fault Detection Device) is provided in the first chapter.

The first goal of this study is to understand the manner in which series arc faults can lead to electrical fires. The first approach is to perform a review of the fire statistics in different countries (chapter 2). The second approach is to study the published research work on electrical faults and perform one's own experimental investigations. The different types of arcing and their relationship with other electrical faults and environmental conditions are explained in chapter 3. The ability of electrical faults to generate heat and to ignite a flammable material is described with theoretical models based on electrical science, arc physics (in chapter 4), and combustion physics (in chapter 5). The thermal stresses can be expressed using different criteria such as temperature, power dissipation, and released energy. The comparison of these criteria for the different types of electrical faults is completed in chapter 6. It shows that series arcing represents a considerable risk of fire: the high

temperature of the arc column combined with a high stability over time fulfills all conditions required to ignite a flammable material.

There are two ways of addressing the problem: passive and active protection. The strategy of passive protection is to avoid emergence of the fault situation. Based on the findings on the characteristics of arc faults and the behavior under thermal stress of different polymers used for electrical insulation, concrete strategies are proposed to reduce the probability of initiation of stable arc faults in low-voltage electrical installations. Exploring the possibilities to reduce the occurrence of series arc faults based on passive protection is the second goal of this work, and the results are described in chapter 7.

The AFDD is an active protection device that was introduced for the first time in 2012 in the markets covered by IEC regulations. It is designed to detect series arc faults and limit the risk of electrical fire. Similar devices, the arc fault circuit interrupters (AFCI), have been available in North America since the nineties for protection against parallel arc faults and since 2008 for protection against series arc faults. The requirements for these devices are defined in the standards IEC 62606 and UL 1699 respectively. The main requirement is the tripping characteristic for series arcing. It prescribes a maximum break time of the device as a function of the arc current. The principle is to limit the arc energy to prevent a fire starting. The third goal of this thesis is to explain the origin of this tripping characteristic, evaluate the level of protection that it provides, check if it is appropriate for different system voltages, and suggest concrete measures for improvement (in chapter 8). Particular attention is paid to the definition of the test methods. Arc faults can take different forms such as contact arcing or arcing across a degraded insulation material. The arc conditions may strongly differ depending on the electrical parameters of the system and the material present at the fault location. In addition, the power density of arc faults is so high that they can alter their own environment and existing conditions. These facts result in inter-dependencies that give the arc fault a large variance. On the one hand, the test methods must be designed to generate arcs that are close to the arc faults observed in reality. On the other hand, the tests defined in the product standard have to be reproducible. These two requirements are not compatible regarding the arc fault phenomenon and a compromise must be found.

This thesis provides a complete analysis of all the topics related to series arc faults in low-voltage electrical installations. The part played by series arc faults in the outbreak of hazardous electrical fires is explained by using fire statistics, realizing an electrical and thermal characterization of the phenomenon, and by comparing with other electrical faults its ability to ignite an insulation material. The contribution of the active AFDD protection is taken into account in this analysis and the option of achieving a passive protection using appropriate insulation materials is explored. The performance requirements described in the product standard of AFDD are reviewed and recommendations for improving the standard are proposed.

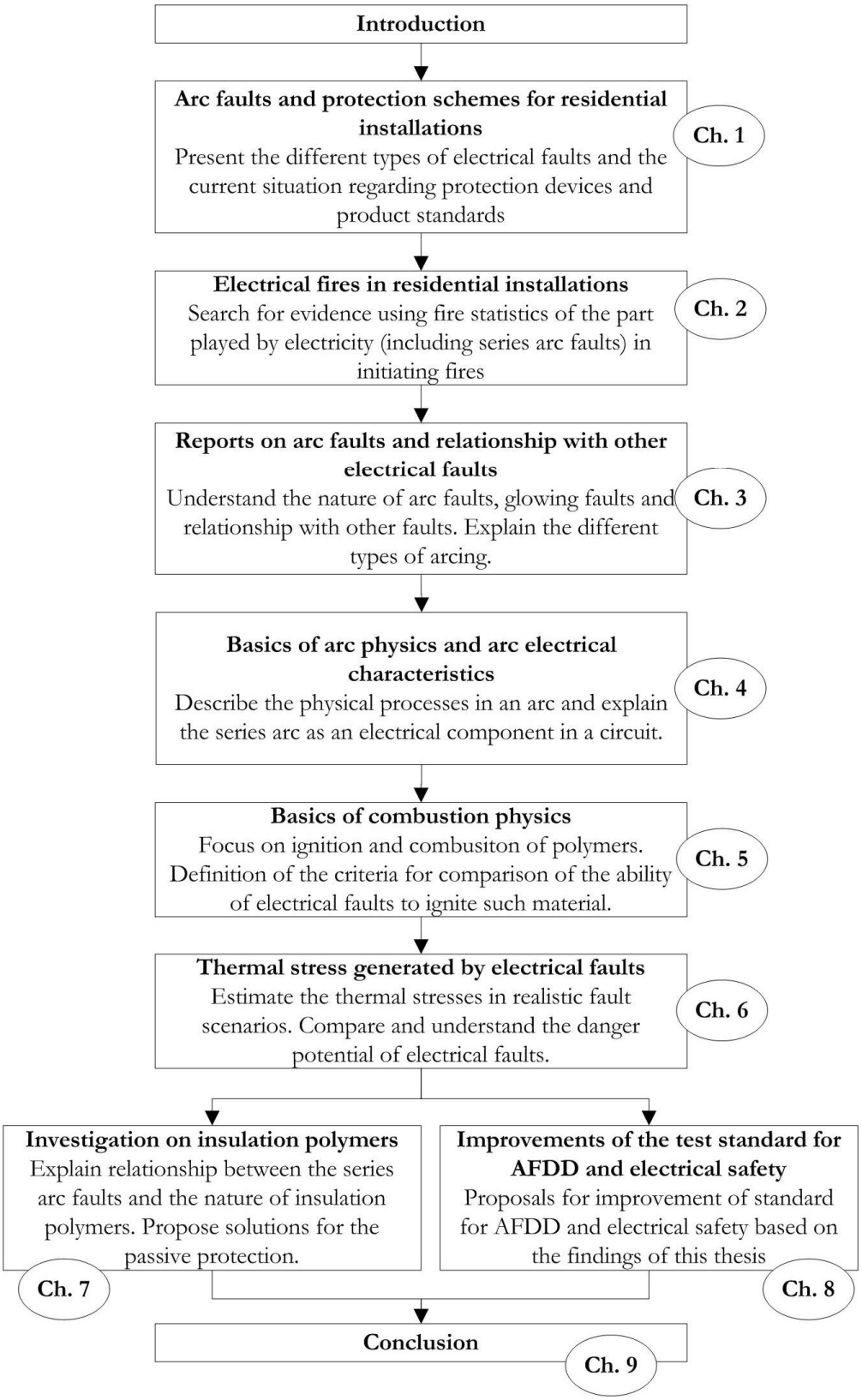

Figure 1: Structure of the thesis

1 Arc faults and protection schemes for residential installations

Arc faults are known to be possible causes of damage in different electrical applications [Ber09]. Arc faults in DC systems such as photovoltaic generators can be extremely hazardous since there is no current zero-crossing to automatically extinguish the arc. The arc continues to exist as long as it is connected to the power source. In AC systems, sustained arc faults are more seldom. Despite their low likelihood of occurrence, they cannot be neglected. If the arc fault occurs in an aircraft, the resulting fire may have dramatic consequences. In residential and industrial electrical systems, the huge number of contacts, conductors, and appliances that may be faulty at any moment and cause a hazardous arc, represent a global risk and a burden for society and insurance companies. Electrical fires are reported regularly, and many of them may be due to arc faults. In this chapter, the different types of arc faults that may occur in a low-voltage circuit are explained. The available detection and protection devices to deal with these faults as well as the related standards are described.

1.1 Series and parallel arc faults in an electrical circuit

A publication of V. Babrauskas [Bab01] contains a comprehensive analysis of the different kinds of electrical faults in electrical distribution systems. Three main kinds of electrical heat sources are reported: the arc fault, ohmic heating, and external heating. For arc faults, two sub-types are presented: the series arc and the parallel arc (Figure 2 and Figure 3).

1.1.1 The series arc fault

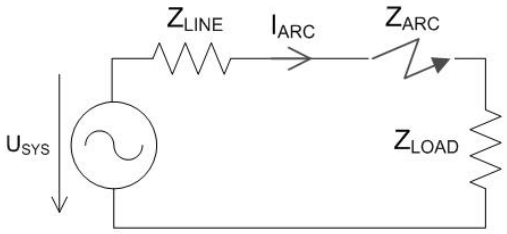

Figure 2: Series arc in a circuit

The series arc that can take place anywhere inside the electrical circuit has a limited current I_{ARC} which depends on the arc impedance Z_{ARC} and the impedance of the load in series Z_{LOAD}. This type of arc has a limited power dissipation in the range of many hundreds watts and it may last long enough to ignite a flammable material. Series arc faults were reproduced by pulling out plugs, applying vibrations on plugs, and performing make or break actions on cords [HeZu01]. The authors observed that the series arcs may last for minutes and are not detectable with conventional overload or residual current protection devices. The series arc interacts as an electrical component in series with the load and influences the load current. With resistive loads, the arc and the load together form a voltage divider and the load current decreases. The electrical power is spread between the series arc and the load in a proportion which is a function of the arc voltage and the system voltage. With active loads that have to output a constant power (e.g. power supplies), the loss of voltage due to the series arc is compensated by an increase in current consumption. This increases the complete power dissipation in the circuit and at the arc location.

1.1.2 **The parallel arc fault**

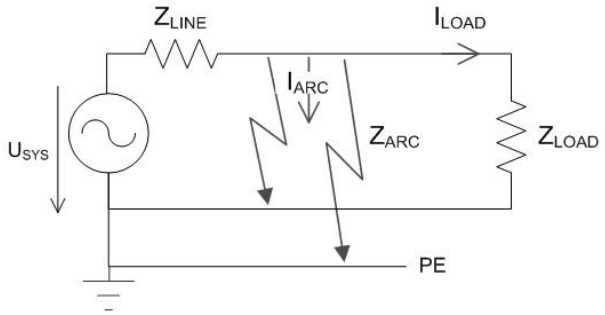

Figure 3: Parallel arcs in a circuit

The parallel arc only has its own impedance Z_{ARC} and the impedance of the distribution line Z_{LINE} as limiting impedance. The current I_{ARC} may reach many hundreds of amperes and the resulting high power dissipation may provoke a fire ignition as well. Nevertheless, the arc may not last very long: the conductors at the fault location will quickly melt, weld together, or be ejected. In [HeZu01], parallel arcs were generated by damaging or weakening the insulation of cables: the authors noticed that parallel arcs have in most cases a short duration (less than one second). In addition, if the circuit is protected with an overcurrent protection device such as a fuse or an MCB, the fault will be quickly interrupted.

1.2 Thermal stress due to arc faults

The risk of series and parallel arcs which may occur in many situations has been pointed out [PSZ09]: cords and cables exposed to mechanical stress (bent, crushed, pulled, cut, chewed by rodents, pierced by nails...), connectors, terminals, sockets, switches with weak contact force or oxidized contacts, twisted conductors as connection, insulation ageing, overheat at overload or high thermal isolation, crushed plugs etc. These faults can occur in front of the socket, behind the socket, and also inside the appliances. Figure 5 displays three examples of hazardous situations:

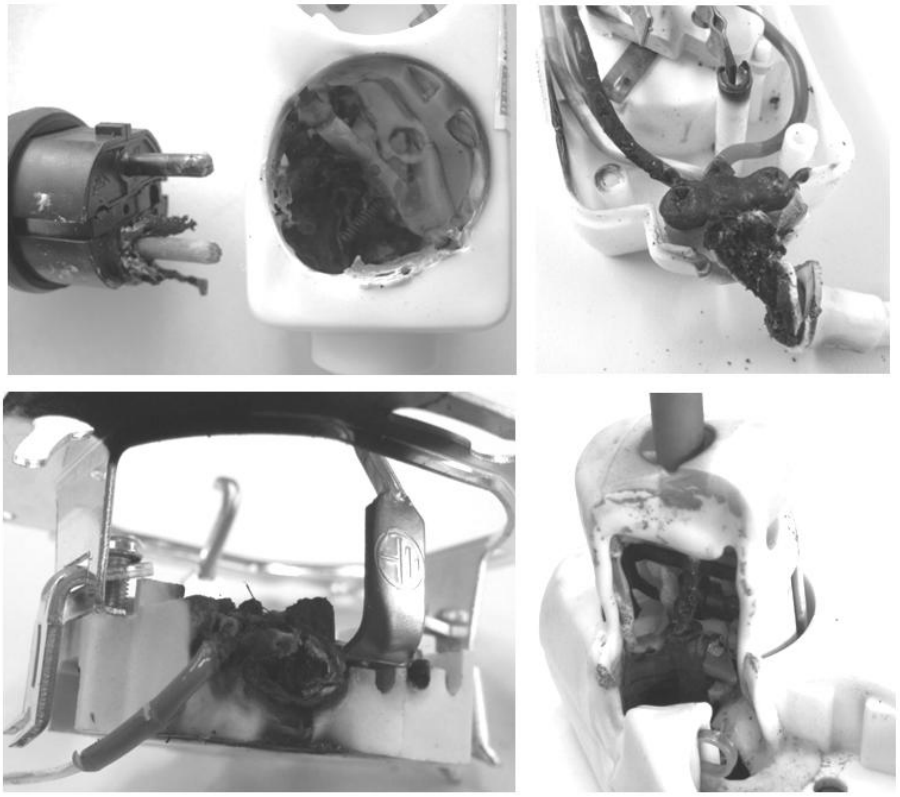

Figure 4: Effect of series arcing on various pieces of electrical equipment
A (top left): arcing at plug pin / B (top right): arcing at junction case to cord
C (bottom left): arcing at terminal / D (bottom right): arcing at plug pin

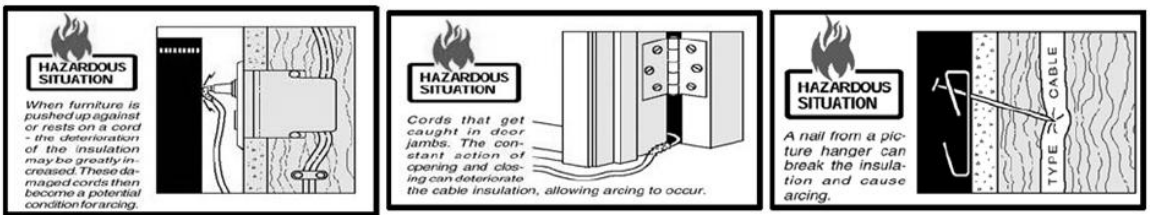

Figure 5: Examples of residential situations that lead to hazardous arcs [PSZ09]

Many electrical parts commonly used in commercial and residential applications were evaluated under series arc conditions [Rac11]. Contact arcs were produced between the pins of a plug and the contact of a socket. This could be performed by controlling the position of the plug with an electro-mechanical system as described in chapter 3.2 (
Figure 23). The effects on the insulation materials can be seen in pictures A and D in Figure 4. The same system was used to initiate arcing at a broken conductor at the feed-through of a multiple socket (picture B), and at the connection terminals of a wall receptacle (Picture C).

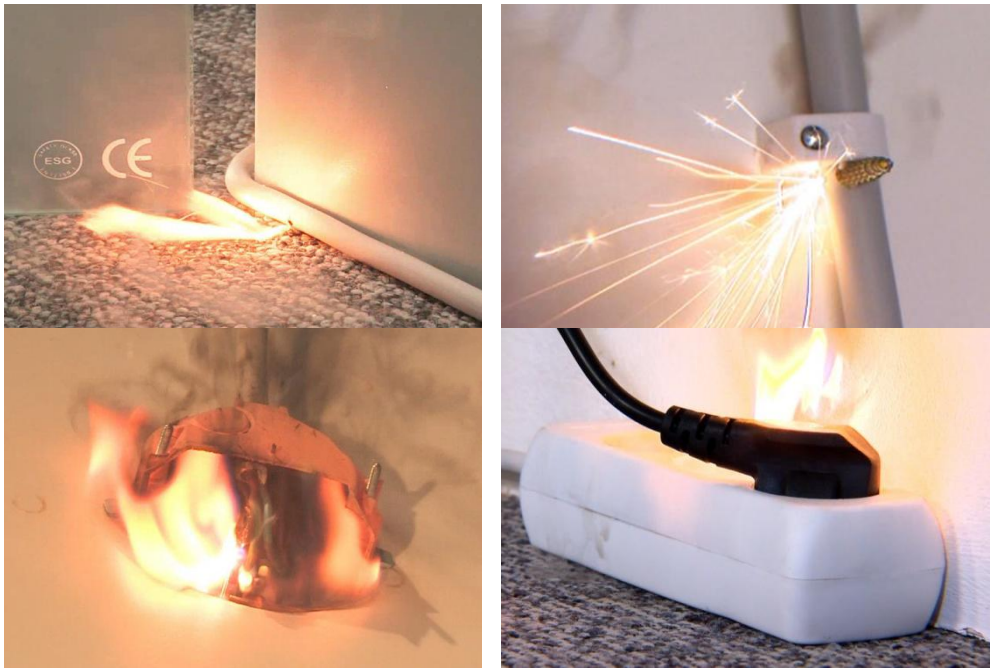
Figure 6: Video screenshots of electrical fires due to series arcing

In the scope of this thesis, videos of electrical fire situations due to series arcing were recorded in collaboration with the marketing group of Siemens. The same method was used to produce the series arcs and the conditioned electrical equipment was placed in realistic situations. The impressive results are displayed in the screenshots of Figure 6. The material

ignitions only occurred because the series arc could become stable due to a steady restrike of the arc after current zero-crossing. In many cases, the arc could not become stable or was interrupted because of a deformation or ejection of a piece of molten conductor. In other situations, melting polymer flew between the conductors and isolated them from each other.

It was observed during these tests and also reported in many publications [She07b, Bab01, Bab05] that a stable series arc has a high probability of initiation if the surrounding insulation materials at the fault location produce a carbonized residue, also called a char. This char forms a semi-conductive path between the conductors and supports the restrike of the arc after each current zero-crossing. It was supposed that the leakage current flowing through this path heats the fault location and reduces significantly the arc striking voltage, enabling striking even with gap distances of many millimeters. The causes of insulation carbonization may be a thermal stress from a previous fault situation (overload, glowing contacts, external heat source) or moisture and pollutants on the surface of the insulation that lead to a leakage current and thermal stress (also called wet tracking). The PVC is often mentioned as charring and "arc friendly" material. The relationship between the carbonization of the insulation material and the generation of stable arcs is the basis of many test methods for arc fault protection devices [IEC13, UL13]. PVC cords are used as specimens for testing.

1.3 Series arc fault detection technology

The A class AFCI was introduced in North America in 2008 (Figure 7) and the AFDD has been available since 2012 in the countries where IEC standards have been adopted. Both devices are able to detect series and parallel arc faults in low-voltage electrical installations according to the requirements defined in the applicable product standards UL 1699 [UL13] and IEC 62606 [IEC13]. The AFDD from Siemens can protect single-phase circuits with a maximum rated current of 16 A [Bra17].

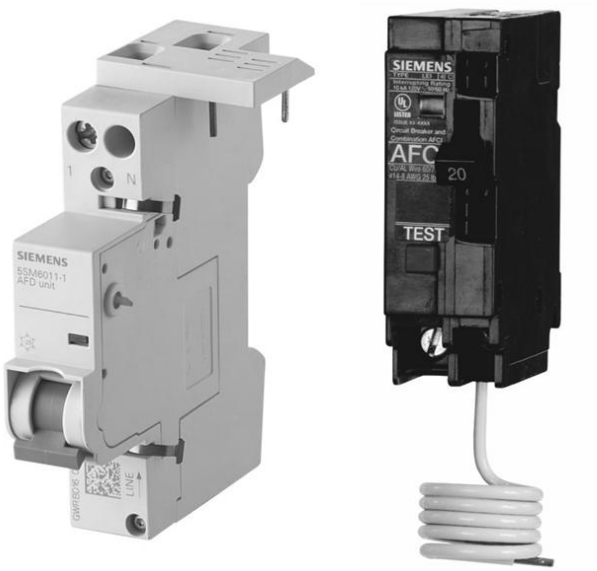

Figure 7: AFDD (left) and AFCI (right)

The detection principle used in the products of Siemens was discovered in the nineties [Bla98]. Figure 8 displays an equivalent circuit of the AFDD and a branch circuit where a series arc fault takes place. Two signals are used to detect the arc: the current at low frequency (< 1 kHz) that is changed and distorted by the impedance of the arc and the high-frequency current that is generated by the movement of the arc roots at the cathode [ShCa11]. These signals are sensed and conditioned by the analog circuit of the AFDD. The low-frequency current signal is amplified and rectified. The high-frequency current signal is transformed into an RSSI signal (Received Signal Strength Indication) that represents the noise power in the range of 23 MHz. The two signals are digitalized and analyzed by the microcontroller. Figure 9 displays the signal analysis that enables the detection of a series arc and the identification of disturbing loads. If a series arc exists, we expect an intense high-frequency noise to be generated without interruption from the striking to the extinction of the arc. During this time, the arc current will flow without interruption. During current zero-crossing, the arc will be extinguished and the RSSI will be much lower (at the ground noise level). This means that an arc must result in a periodic generation of high-frequency noise that is synchronized with the load current signal at low frequency. In addition, the strike and extinction of the arc will be very quick (less than a few microseconds) and the variations in the noise power will be very steep in these circumstances. The slope of the RSSI signal indicates these quick variations. When all these conditions are satisfied, an arc is detected and

a fault integrator is incremented. If the current-based threshold is exceeded, the AFDD trips the breaker and interrupts the current.

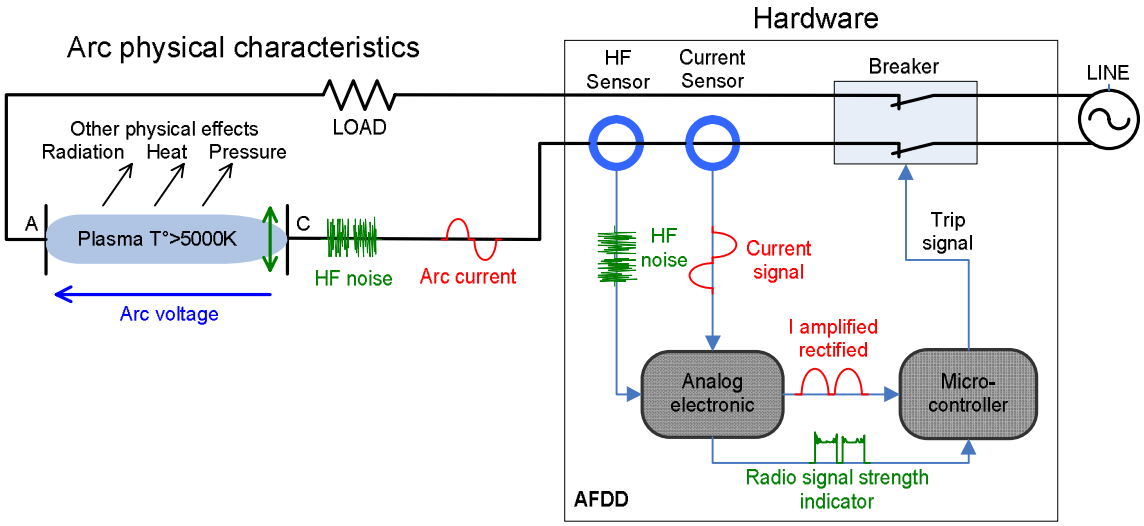

Figure 8: Equivalent circuit of the AFDD and the faulty branch circuit

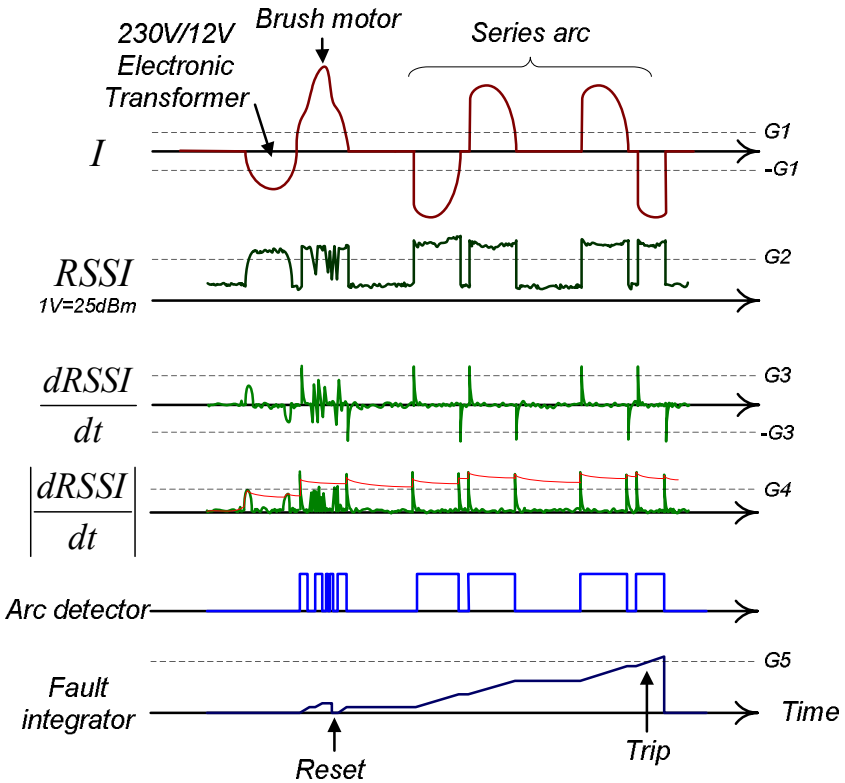

Figure 9: Signal analysis for series arc fault detection (Siemens AFDD) [MAHBE11]

An intense high-frequency noise can also be generated by disturbing loads such as brush motors or appliances with power electronics. These disturbing loads are reliably identified since the high-frequency noise they produce does not correspond to the conditions explained above. Other criteria that are kept confidential are used to ensure the detection of arc faults while disturbing loads are in use or the high-frequency signal is strongly attenuated or masked. The Siemens AFDD introduced in 2012 is the first generation of AFDD based on IEC requirements. Reports show a satisfactory performance regarding detection and immunity against unwanted tripping. This technology is constantly being further developed: the second generation of Siemens AFDD with enhanced reliability and performance will be launched on the market late 2016.

1.4 Installation standards

In Germany, the DIN VDE 0100-420 standard [IEC13] defines the electrical protection schemes for low-voltage electrical installations. Electrical circuits with up to 16 A rated current in specific buildings must be protected with an AFDD: areas of buildings where infants, retired or disabled persons live and locations which are particularly vulnerable or irreplaceable (warehouse for highly flammable materials, museum, historic building etc.). In other European countries, the AFDD is not mandatory, but this technology is being evaluated and considered by many national committees. In North America, the National Electrical Code (NEC) prescribes protection using AFCI in the living areas of residential buildings. It is applied in the majority of states in the USA and Canada.

1.5 Test standard IEC 62606

The product standard IEC 62606 [IEC13] defines the requirements for the AFDD. The German standard DIN EN 62606 [DIN14] has been available since August 2014 and is identical to the IEC standard. The investigations described in chapter 3 show that there are different types of arc faults regarding their position in an electrical circuit and their physical characteristics. IEC 62606 was written based on UL 1699 (standard for the AFCI [UL13]) and the standards for MCB and RCD breakers [DIN10b, IEC15]. Our considerations focus

on the arcing-related tests that are all described in part §9.9 of the standard. These tests include series arc and parallel arc detection, masking tests (checking the ability of the AFDD to detect arcs with disturbing loads), and immunity against nuisance trips.

1.5.1 **Series arc tests**

The series arc is initiated in a cable specimen that has been previously prepared with the procedure described in 8.2.4.1. The cable specimen is placed in the test circuit in series with a resistive load (see Figure 10). The value of the load current is adjusted to a higher value than the target test current in order to compensate the current-limiting effect of the series arc; the value is estimated for an arc voltage of 50 V. By means of switches S1 to S4, different combinations of tests are performed:

- Test §9.9.2.2: Verification of correct operation in the case of sudden occurrence of a series arc in the circuit

  Switches S1 and S3 are closed. S2 is open. The conditioned specimen is shorted with switch S4 and the load current flows normally. Then S4 is opened and the arc is initiated. This scenario is likely to occur and corresponds to the transition from a glowing fault to a stable series arc due to creepage on char as described in 3.3.2.
- Test §9.9.2.3: Verification of correct operation when inserting a load with a series arc fault

  Switch S1 is closed. S2 and S4 are open. Switch S3 is closed and the arc is initiated directly. This case corresponds to the unlikely scenario of placing a faulty load in the circuit and powering it. One scenario that is more probable is the presence of a preceding fault in series with many other loads: a glowing fault could be initiated in an extension cord that powers small loads and provides the right conditions for series arcing; Then, a powerful load like an iron or hair drier is powered with the same cord, the glowing bridge becomes astable, and the series arc starts.
- Test §9.9.2.4: Verification of correct operation in the case of closing on a series arc fault

  Switch S3 is closed. S2 and S4 are open. Switch S1 is closed and the arc is directly initiated. This scenario may happen if the AFDD has already tripped at series arcing and the user tries to reset the device.

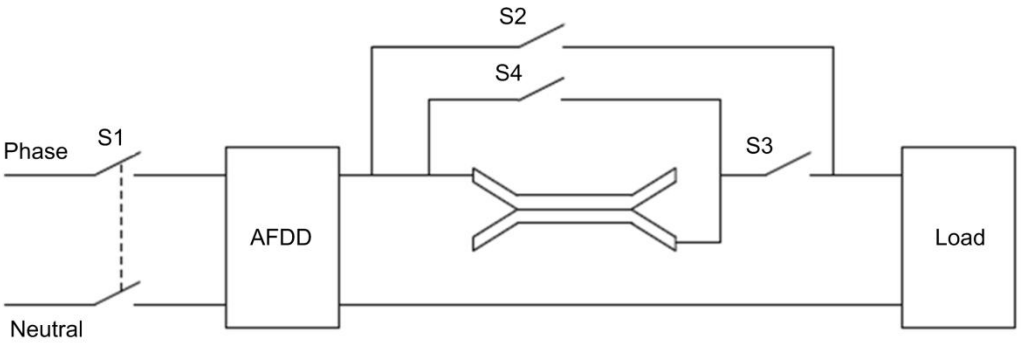

Figure 10: Test circuit for series arc fault tests [IEC13]

For every test, the break time of the AFDD and the arc current are measured and used for comparison with the thresholds displayed in Table 1 and Figure 11. The minimum arc current value for detection is 2.5 A and the values of the maximum break times at the system voltage 230 V AC are related to the limitation of the arc energy to 100 J (see 3.2 and 8.3.2). Above 20 A arc current, the maximum break time is constant at 0.12 s in order to ensure immunity against switching arcs. For the voltage 120 V AC, the minimum arc current is 5 A and the maximum break times are in general twice as high as at 230 V AC. The characteristic for 120 V AC is principally based on the requirements for the AFCI (norm UL 1699). The adequacy of the difference in the requirements at both voltages is discussed in 8.3.3.2.

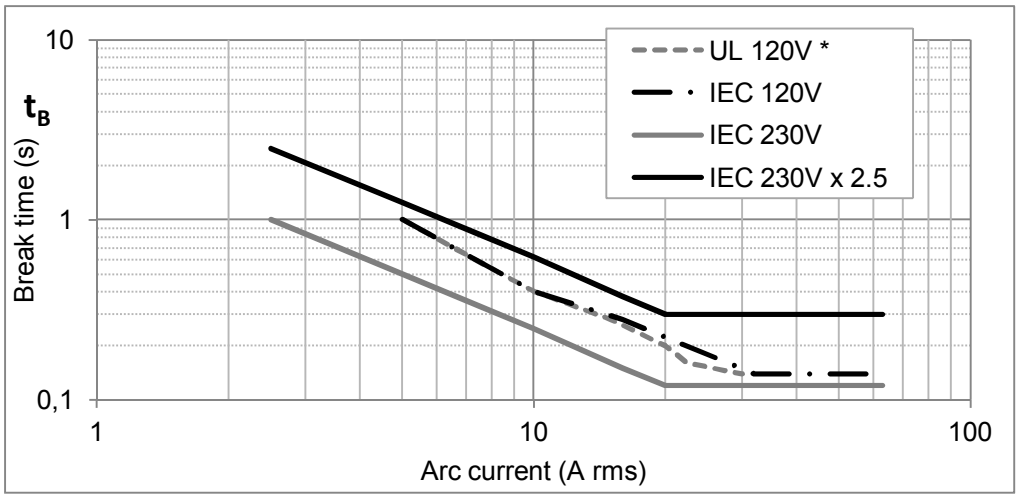

Figure 11: Tripping characteristics for AFDD and AFCI
(* for the AFCI the current axis corresponds to the load current prior to arc and not to the arc current)

Test arc current (rms value)	2.5 A	5 A	10 A	16 A	32 A	63 A
Maximum break time t_B	1 s	0.5 s	0.25 s	0.15 s	0.12 s	0.12 s

Table 1: Limit values of break times for 230 V AC according to table 1 of IEC 62606 [IEC13]

1.5.2 **Parallel arc tests**

For the parallel arc detection tests, three test conditions are defined:

- Test §9.9.3.1: Verification of correct operation in the case of a parallel arc with limited current

  A cord specimen is prepared with the same conditioning as for the series arc tests, but the connections are changed in order to initiate the arc between the phase and the neutral conductors. The short-circuit current is limited to 75 A and 100 A with an adequate length of wire upstream to the fault location.
- Test §9.9.3.2: Verification of correct operation in the case of a parallel arc cable cutting test

  The arc is initiated by slowly crushing a cable with a blade. As the blade bridges both conductors with a first contact point, a parallel arc is initiated (contact arcing explained in 3.1.2). The tests are performed with prospective arc currents from 75 A to 500 A.
- Test §9.9.3.3: Verification of correct operation in the case of an earth arc fault

  The same test conditions as in §9.9.3.1 are used, but with a parallel arc between phase and protection earth and at currents of 5 A and 75 A. The mandatory RCD will trip more quickly (less than 40 ms) than the AFDD. However, the arcs at high current levels (75 A) may be very sporadic and result in single arc half-cycles that are separated with longer time lags (see Figure 72); in this case, the correct operation of the RCD is not ensured since this device is only tested with an uninterrupted test current.

At each test, the number of arcing half-cycles is counted and compared with the maximum number defined in Table 2. Only in the case of the parallel arc to earth at 5 A, the break time is measured and compared with the corresponding value for series arcing in Table 1.

Test current (rms value)	75 A	100 A	150 A	200 A	300 A	500 A
Number of arcing half-cycles	12	10	8	8	8	8

Table 2: Maximum allowed number of arcing half-cycles within 0.5 s [IEC13]

1.5.3 **Masking and unwanted tripping tests**

The tests described in §9.9.4.2 and §9.9.4.3 of the standard aim to verify the reaction of the AFDD as various types of loads are powered with or without series arc faults. The selected appliances are assumed to be disturbing for the AFDD, for example by emitting important electrical noise or generating contact arcing:

- Contact arcing: appliances with brush motors or switches
- Non-sinusoidal current: Light dimmer and power supplies
- High inrush currents: capacitor start motor, light bulbs
- Noise generation: electronic transformers, power supplies

1.6 Conclusion

Series and parallel arc faults are electrical faults that may generate an elevated temperature at the fault location and initiate an electrical fire. The series arc fault is assumed to be more hazardous than the parallel arc fault because the regular overcurrent protection devices cannot detect it. The AFDD has been available since 2012 for the protection of low-voltage single-phase circuits according to IEC requirements with rated currents up to 16 A. This device fulfils the requirements of the IEC/EN 62606 which include verification tests for the detection of series and parallel arc faults as well as nuisance trip and masking tests.

2 Electrical fires in residential installations

Electricity is known as one possible cause of fire in residential buildings. Insurance companies, government organizations, and fire safety institutes collect and analyze statistical data on fires in order to monitor the level of financial losses sustained and implement appropriate safety measures. These data are valuable sources of information that can provide a deeper understanding of the causes and mechanisms involved in the development of fires. In this chapter, the occurrence, severity, and location of electrical fires are investigated. The contribution of arc faults in the initiation of electrical fires is also examined.

2.1 Occurrence of electrical fires

Despite improvements in technology and electrical safety standards in previous decades, electricity is still one of the major causes of fires. Table 3 displays the proportion of fire causes in different countries.

Reference	[ICF04]	[Mil13]	[Str98]	[IFS14]	[XiHu14]	[DSB17]	[FIC13]
Country	Europe	USA	Germany	Germany	China	Norway	India
Period	2004	2009-2011	1987-1996	2002-2013	2005-2010	2009-2013	2009-2012
Institute Company	ICF	CPSC	GDV	IFS	Beijing univ.	DSB	FICCI
Analyzed fires	600,000	639,000	2,804	12,000	132,000	4240	13,185
Electricity	13-20 %	5-18 %	25 %	33 %	27 %	21 %	73 %
Lightning			1 %	0 %	1 %	1 %	27 %
Explosion			9 %	2 %	n.m.	0 %	
Incendiary			26 %	9 %	6 %	6 %	
Work with fire			7 %	3 %	32 %	23 %	
Human error			2 %	16 %			
Open fire			7 %	4 %		23 %	
Self-ignition			6 %	2 %	2 %	3 %	
Overheat			9 %	9 %	n.m.	4 %	
Misc & unknown			9 %	21 %	32 %	19 %	

Table 3: Causes of fires in different countries

The proportion of electrical fires varies from 5 % to 73 %. The value of 13 % to 20 % published by the ICF (International Cable makers Federation) [ICF04] is a rough estimate based on the 600,000 fires reported annually in the European Union (25 countries in 2004). The CPSC (Consumer Product Safety Commission) in the USA estimates fires in electrical distribution systems to be 5 % and fires initiated by electrical loads to make up 13 % of the 213,000 non-confined fires annually [Mil13]. The statistical data in these two studies have been compiled by collecting data of all fires in the above countries. The sources of information are numerous and the forensic competence of the analysts is not known. We assume that the data provided by the insurance companies are more reliable since these companies usually involve forensic experts. The proportion of electrical fire data provided by the GDV (Gesamtverband der Deutschen Versicherungswirtschaft) in Germany [Str98] is 25 %. One probably very reliable estimate of electrical fires is from the IFS (Institute für Schadenverhütung und Schadenforschung der öffentlicher Versicherer e.V.) that carries out fire investigations with trained and experienced analysts on smaller number of fires. The IFS has analyzed in detail 1,200 fires per year using the same methods since 2002 [IFS14]. The institute estimates that electricity is the cause of the 33 % of fires in Germany. In China [XiHu14] and Norway [DSB17], the proportion of fires caused by electricity in recent years were 21 % and 27 % respectively. The FICCI reported in their Indian risk assessment in 2013 that 73 % of the fire incidents in Mumbai were related to electricity [FIC13].

2.2 Severity of electrical fires

The ICF reported that 13-20 % of all fires in Europe were caused by electricity. These fires seem to be particularly lethal because they accounted for 20 % to 30 % of the deaths (3,250 per year) and injuries from all domestic fires. The statistics from the CPSC are even more striking. The relatively small number (5 %) of all domestic fires caused by electrical distribution faults (see Figure 12) result in 28 % of the deaths (see Figure 13). On average, one life is lost in every 69 fires started in the electrical distribution; if the fires are due to other reasons, one life is lost in every 566 fires. Fires caused by electrical distribution faults are eight times more lethal than other fires. One of the reasons mentioned to explain this result is the difficulty in detecting this type of fire and the greater chance of being surprised

by a fire at night. Economic considerations produce a similar result: an electrical fire with costs on average $ 35,500 compared with any other fire with average costs amounting to $ 5,300. The US Fire Administration [USD08] reported that electrical fires are two times more lethal and cost 2.5 times more money than non-electrical fires.

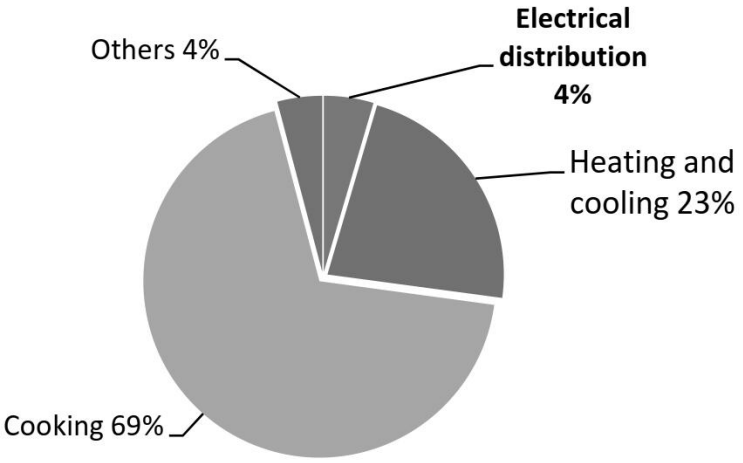

Figure 12: Causes of fire in USA, CPSC [Mil13]

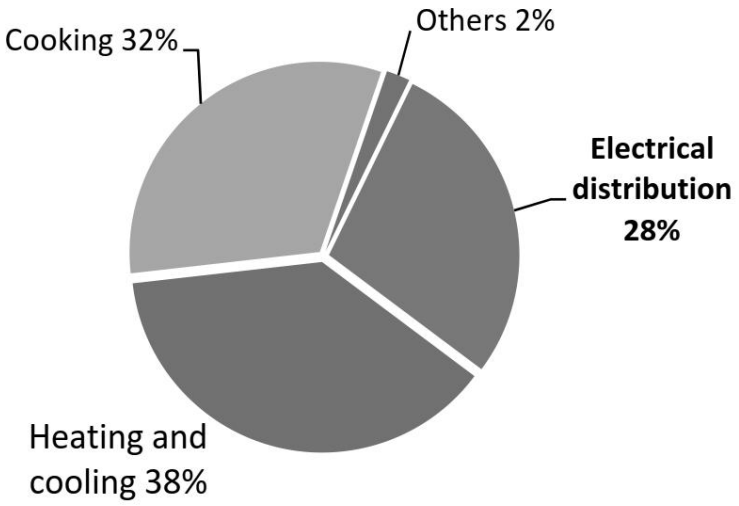

Figure 13: Causes of fires that resulted in deaths, CPSC [Mil13]

2.3 Location of electrical fires

The location where an electrical fire starts does not give a direct indication of whether the electrical fault was a series arc fault or not. A series arc fault may start anywhere in series with the load and also in the load itself. However, it is interesting to know what proportion of electrical fires start in the wiring installed between panel and socket, in the cords placed behind the sockets, and in the appliances themselves. It could be helpful to focus passive and/or active protection against series arcs on specific portions of the electrical circuit. The statistical data show that the complete electrical circuit should be protected and not only a specific part of it where fault occurrence would be much higher. In the USA, circuits may be protected with sockets incorporating GFCI and/or AFCI protection, thus protecting only the portion of wiring downstream from the socket: this protection scheme is not sensible. According to Table 4, one third of electrical fires in Germany start in the installed wiring and extension cords behind the socket. This proportion is higher in the USA at 50 % to 60 %.

Reference	[IFS14]	[Str98]	[Dah99]	[Mil13]	[USD08]	[SmCo87]
Country	Germany	Germany	Germany	USA	USA	USA
Period	2002-2013	1993-1997	1993-1998	2009-2011	2003-2005	1980-1985
Institute/Company	IFS	Allianz	Hannover	CPSC	USFA	CPSC
Analyzed fires	12,000		188	639,000	28,300	144
Electrical installation	28 %	32 %	35 %	40 %	47 %	38 %
Cords and plugs				11 %	11 %	19 %
Appliances	49 %	29 %	65 %	49 %	33 %	43 %
Misc & unknown	23 %	39 %			9 %	

Table 4: Locations of the electrical fires

A detailed and reliable investigation by the CPSC [SmCo87] on a small number of fires in the electrical distribution networks (149 fires in 16 U.S. cities) shows the high occurrence of electrical fires in older homes. As displayed in Figure 14, a majority of fires occurred in houses older than 40 years. This means that prescribing protection devices such as RCD,

MCB, or AFCI in new installations is a sensible initiative, but retrofitting older installations would also be highly recommended.

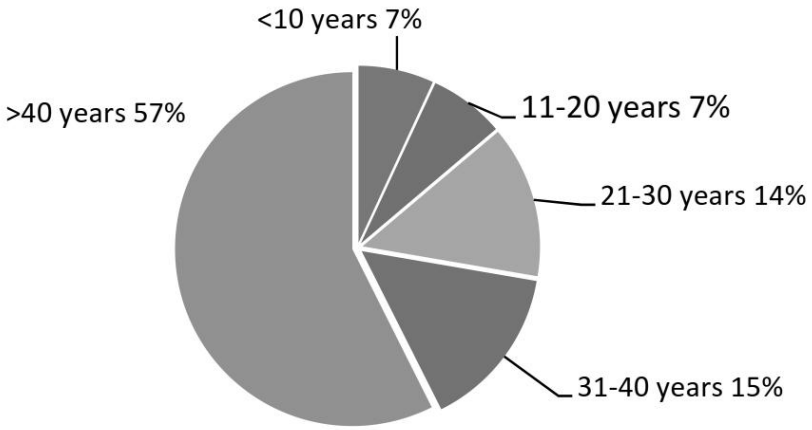

Figure 14: Distribution of electrical fires in electrical distribution networks by age of house, CPSC [HBG83]

2.4 Contribution of arc faults to electrical fires

Approximately 25 % of fires in Germany are caused by electricity. The majority of German buildings and homes are equipped with overcurrent and residual current protection devices according to the standard DIN VDE 0100. These devices are not able to mitigate or eliminate the fire causes. Neither are these devices capable of detecting series arc faults. This indicates that series arcs may make a significant contribution to the initiation of electrical fires. Hochbaum [Hoc03] stated 2003 that most electrical faults involving overloads, short-circuits, and isolation faults are detected and interrupted early enough by regular protection devices. Hence, the following electrical faults are the most probable causes of electrical fires: series electrical faults, glowing connections, and parallel faults that result in an overcurrent situation which cannot be detected (for example in the case of inadequate protection device and/or wiring).

A PhD thesis [Dah99] relating to fires in low-voltage electrical installations provides another statistical survey of 188 electrical fires in the German region of Lower Saxony (see Figure 15). The author acknowledged that the reliability of fire cause analysis is in most cases very low. Only fires which resulted in significant damage were properly investigated by the police

or experts. In most cases, the destruction was very significant and the exact nature of the electrical fault could not be clearly identified: 6 % of the faults were assumed to be contact faults and 26 % short-circuits or arc faults. For the remaining 68 % of the faults, it was not possible to distinguish between arc faults, short-circuit, or contact faults.

.

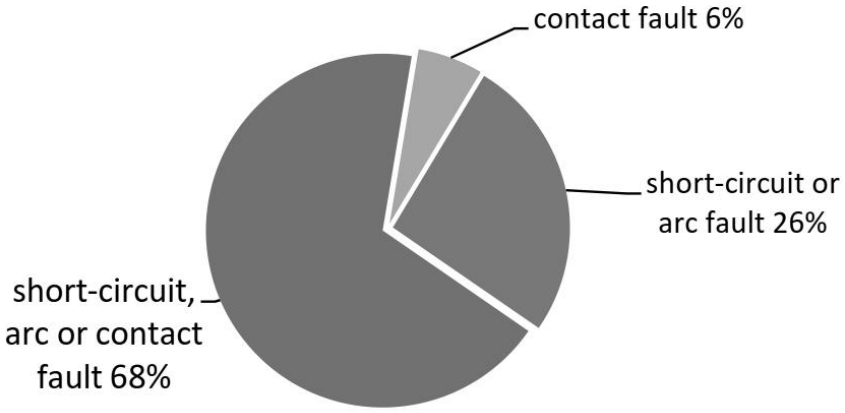

Figure 15: Causes of electrical fires, PhD Y. Dahmouni [Dah99 (p27)]

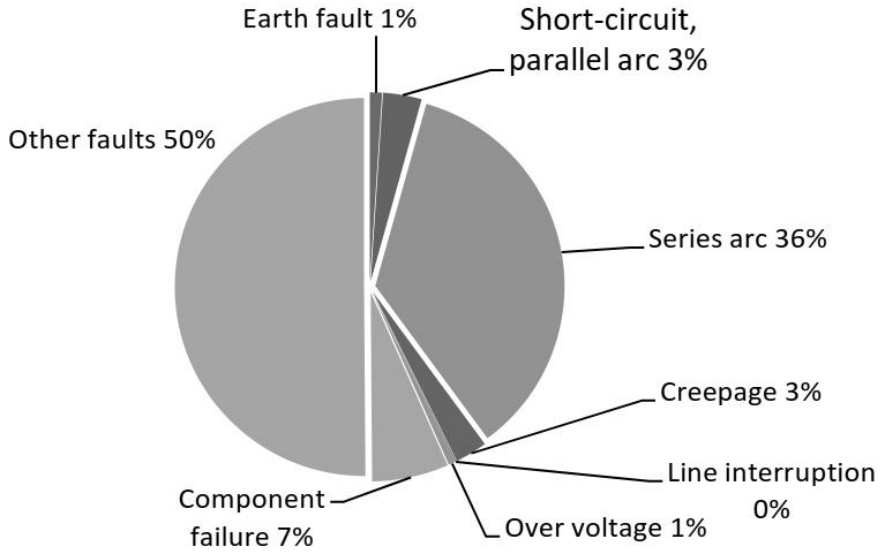

Figure 16: Causes of electrical fires estimated by DSB from 2009 to 2013 (872 cases) [DSB17]

The Norwegian directorate for civil protection, DSB, provided very precise data for the causes of electrical fires. The series arc faults are distinguished from other faults and are believed to be directly responsible for 36 % of all electrical fires [DSB17] (see Figure 16). The meaning of the category "other faults" is not clear. If the nature of these faults is unknown,

the series arc faults represent 72 % of the clearly identified electrical faults that are responsible for a fire. The FICCI in India stated that 73 % of fire incidents in Mumbai from 2009 to 2012 were due to electricity and the major cause was short-circuits due to loose wiring [FIC13 (p24)]. This term is ambiguous and can be interpreted in two ways: short-circuits and/or loose connections (that may imply series arcing or glowing).

The CPSC [SmCo87] reported that 40 % of electrical fires were due to failures like loose or poor connections. The electrical faults involved could be glowing, series arcing, or overheated connections. In another detailed study [HBG83] from the US department of commerce that relates to 105 electrical fires reported in 1980 and 1981 in 10 cities, the events that had taken place before the occurrence of the electrical fires were analyzed. In 44 % of the cases, problems had been reported before the fire. Figure 17 displays the distribution of the reported problems by type.

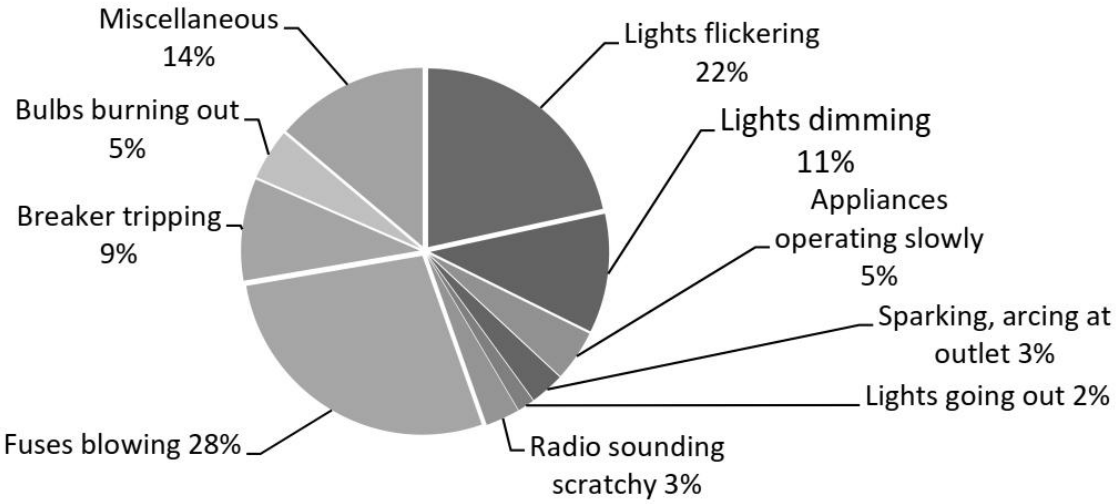

Figure 17: Reported problems prior to electrical fire, U.S. department of commerce [HBG83]

45 % of the observations suggest a series arc fault or another electrical fault in series with the load. There are direct observations like sparking and arcing at outlets, but most of the observations are indirect: lights flickering, lights dimming, appliances working slowly, lights going out, and radio sounding scratchy (arcs generate a powerful broad-band noise that may disturb or overlap the radio signals).

The Energy Safety Service of New Zealand analyzed 59,000 electrical fires that were reported from 1986 to 2003 [Pat05]. The investigators identified two causes of electrical faults which could lead to an electrical fire: the electrical arc and overheating. They reported that 38 % of electrical arc-induced fires occurred in residential dwellings and 79 % in non-residential dwellings. They explained this difference with the wider use of heating equipment in residential dwellings. In fact, heating equipment seems to increase the probability of fire due to overheating and statistically reduce the proportion of fires caused by arc faults.

2.5 Conclusion on electrical fire statistics

Based on the different reports on residential fires, we can make the following assumptions:

- 20 % to 40 % of residential fires have an electrical fault as their origin
- Electrical fires are much more lethal and costly than non-electrical fires
- The percentage of fires starting in the distribution system (board, cables, cords, and plugs) is approximately 30% to 50%
- A significant part of the electrical fires may be due to series arc faults

In a proposal [Kin02] for the U.S. National Electrical Code, the NFPA (National Fire Protection Association) technical committee argued that arc fault protection devices like AFCI might prevent 50 % of the electrical fires in the USA. A significant part of electrical fires may actually be caused by series or parallel arc faults.

The comparison of the different electrical faults in their likelihood to cause fires is important, but the mechanisms of formation and the interdependencies that can exist between these faults must be understood. The following fault scenario example combines mechanisms and situations that were observed [She06a, She07a, She07b, Zim87, PMGB01, Bab05, Bab01] and demonstrates the complexity of the problem: the contact surfaces of a faulty and sparking connector become oxidized. It leads to a glowing connection and overheats. As the oxidation of the contact progresses and the power dissipation increases, the temperature of the glowing bridge at the contacts interface may reach a critical value and vaporize. At this instant, the glowing bridge breaks and an arc is initiated. If an organic material such as an

insulation polymer is present at the fault location and has been previously carbonized by the heat of the glowing bridge, the series arc may become very stable and keep restriking after each current zero-crossing. The high power dissipation of the series arc can melt and ignite the insulation. The damage to the insulation can lead to a short-circuit and a parallel arc. This example is not unlikely. It involves many types of faults or states that people could blame for an electrical fire: contact oxidation, sparking contacts, overheating, glowing, series arcing, parallel arcing, or bolted short-circuit

Therefore, the mechanisms involved in series arc faults and also the relationships with other electrical faults must be deeply understood. The statistical data give only limited indications. Hence, the analysis of scientific publications dedicated to electrical faults, observations in a laboratory situation, and the theoretical consideration of these phenomena must be performed to reach this goal. The results are described in the next chapters.

3 Arc faults and relationships with other electrical faults

Arc faults in low-voltage AC installations may have various characteristics. On the one hand, the circuits downstream of the transformation from high-voltage to low-voltage have high prospective short-circuit currents and nominal currents: the arc faults occurring present very high power and the surrounding environment becomes seriously damaged by the radiation and pressure of the fault. On the other hand, the large majority of low-voltage circuits are further downstream where the electrical energy is used and the nominal currents are much lower (especially in residential circuits). The possible arc faults are not so powerful, but the proximity to the end user results in a greater hazard for people. The following investigations address arc faults that may occur in these end circuits.

3.1 The different types of arcs in terms of physical characteristics

The difference between a series and a parallel arc in an electrical circuit is only based on the path that the current takes. Electrical arcs can also be distinguished in terms of their appearance and physical characteristics. The definition of an electrical arc that can be deduced from the information found in the bibliography [Rie67, Mae51, Com27, Ayr03] is: an electrical arc is an electrical breakdown of a gas between two electrodes which present a sufficient electrical potential difference to enable a sustained gas ionization and high current density. It produces an ongoing plasma discharge, resulting from a current flowing through normally non-conductive media such as air.

Depending on the nature of the medium between the electrodes and the reason for the initiation, three types of arcs can be distinguished:

- Non-contact arcing due to voltage breakdown
- Non-contact arcing due to creepage on char
- Contact arcing

3.1.1 Non-contact arcing

Non-contact arcing is arcing that does not require any previous physical contact between the electrodes. The electrodes or conductors are isolated from each other by air or another insulation material.

3.1.1.1 Non-contact arcing due to voltage breakdown

If the electrodes are isolated with an air gap, a first discharge can be started by imposing a sufficient voltage. The free electrons which are always present in the air (from cosmic and natural radiation) can be accelerated by the electric field and acquire a sufficient kinetic energy to dissociate the gas molecules and release electrons from the atoms. The electrons and ions that are generated from these collisions can be accelerated and involved in a chain reaction, the electron avalanche, which results in a dramatic drop in dielectric strength.

Figure 18: Non-contact arcing due to voltage breakdown

The ionization of the gas atoms is only possible if the electron hits the molecule with a sufficient energy, 13.6 eV for oxygen and 14.5 eV for nitrogen respectively [SmWi01]. The kinetic energy accumulated by the electron is directly proportional to the electric field and the travel distance or mean free path preceding the collision. The gas composition and the pressure are the key parameters defining the mean free path and the effectiveness of an electric field to ionize a gas. The relation between the breakdown voltage, the pressure, and the gap distance is given by the Paschen's law [SiCa11], and is only true at the instant of the breakdown and initiation of the arc:

$$U_{BR} = a \frac{p \cdot d}{b + \ln(p \cdot d)} \qquad (1)\ [\text{SiCa11, FrKe11(p210)}]$$

where p *is* for pressure in atm, d for gap distance in meters and a and b constants (for air a = 43.6 10^6 V/atm m and b = 12.8).

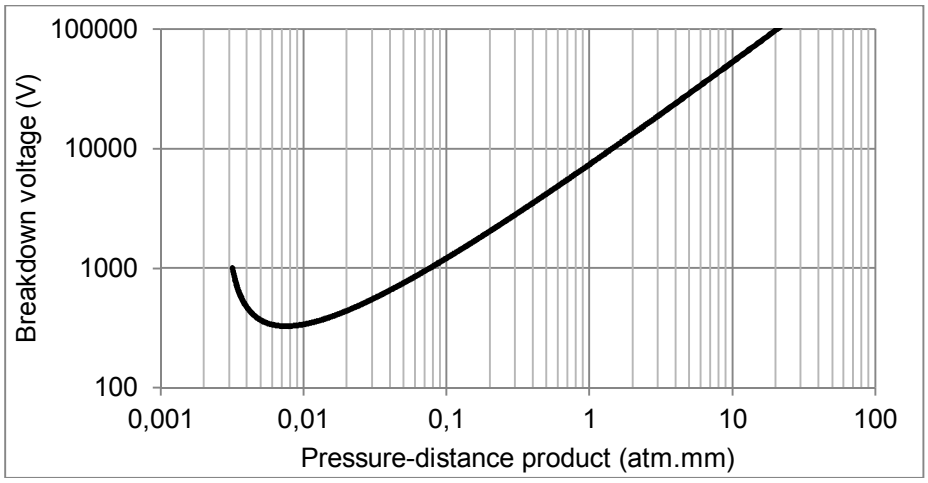

Figure 19: Breakdown voltage according to Paschen's law in air with spherical electrodes [SiCa11]

The breakdown voltage displayed in Figure 19 does not decrease indefinitely even for very low values of gap distance and pressure. For air, this minimum is approximately 330 V and corresponds to a gap distance of 7.5 µm at atmospheric pressure. This distance is slightly bigger than the mean free path of the electrons in air (4 µm at 100 kPa). Bringing the electrodes closer will not decrease the breakdown voltage because the electrons may not "statistically" travel far enough to be accelerated, provoke collisions, and ionize the air. In theory, no breakdown will occur in a low-voltage system at 120/230 V and a distance of only a few tenths of a millimeter could be assumed to be sufficient to isolate the conductors at different potentials. Nevertheless, the minimal air distances defined in electrical standards are usually 3 or 4 mm for 230 V. In fact, the breakdown voltage may be significantly reduced for different reasons: sharp electrode geometry and surface roughness with an inhomogeneous electric field, contamination of the electrode surfaces, high temperatures that result in thermionic emission of electrons, ionized air from a previous discharge or fire. Transient overvoltages resulting from lightning or high current variations in highly inductive circuits may also lead to a voltage breakdown. After the breakdown, the discharge can turn into an electrical arc if the power source can generate enough current at a sufficient voltage. Since the separation distance is very small (in the range of a few micrometers), the metal that melts at the cathodic arc root will quickly make a physical connection with the anode, short the arc and extinguish it. This outcome has been observed by attempting to generate stable non-contact arcs with an arc generator described in 8.2.3.1.

3.1.1.2 Non-contact arcing due to creepage on char

If an insulation material is in contact with two conductors at different potentials, a discharge may be initiated if a partly conductive track has been formed on the surface of the insulation [Bab03 (p312-315)]. Since it involves a surface discharge and not a discharge in a gas, the rules to determine the breakdown voltage according to Paschen's law cannot be applied. The conductive track can be formed by surface contamination or carbonization resulting from a previous electrical fault (arcing, glowing, overheat) or an aggressive environment (chemicals, radiations). This phenomenon is also called dry tracking. A conductive path can also be produced by wet tracking while moisture is present on the surface [YNN84]. A leakage current can flow in the conductive liquid, produce heat, vaporize the liquid, and initiate a discharge while the path breaks. After a significant amount of discharges has been produced, the surface may be already slightly charred. Discharges at a higher current (in the range of 100 mA), also called scintillations, may release a considerable heat on a very limited surface. The local temperature may reach 1000 °C, which is sufficient to pyrolize most insulation polymers. If the current-carrying capacity of the resulting conductive path is too low to carry the leakage current, a sustained and powerful arc can be established between the conductors (see Figure 20).

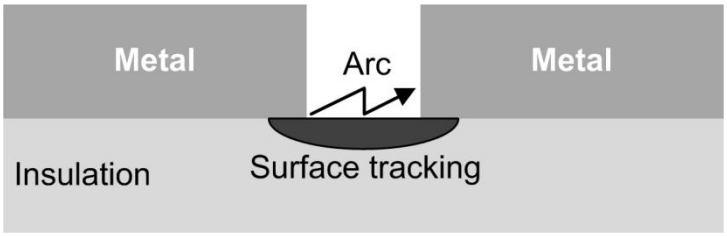

Figure 20: Non-contact arcing due to creepage on char

The molecular structure and the presence of additives giving specific mechanical and thermal properties have an influence on the quantity and composition of the material remaining after pyrolization, its concentration of carbon, and its conductive characteristics. It was observed that aliphatic polymers like PE and other halogen-free polymers may not easily char. In contrast, PVC is known to undergo arc tracking and charing. This particular topic is examined in greater detail in chapter 7.

3.1.2 Contact arcing

Any change in the state of electrical contacts like turning a switch on and off or removing a plug from an outlet creates an arc that can be more or less noticeable depending on its intensity and duration. In the case of breaking an electrical circuit under load, hot spots are created just as the contacts start to be separated. Metal bridges with a high current density are formed and elongated (see Figure 21).

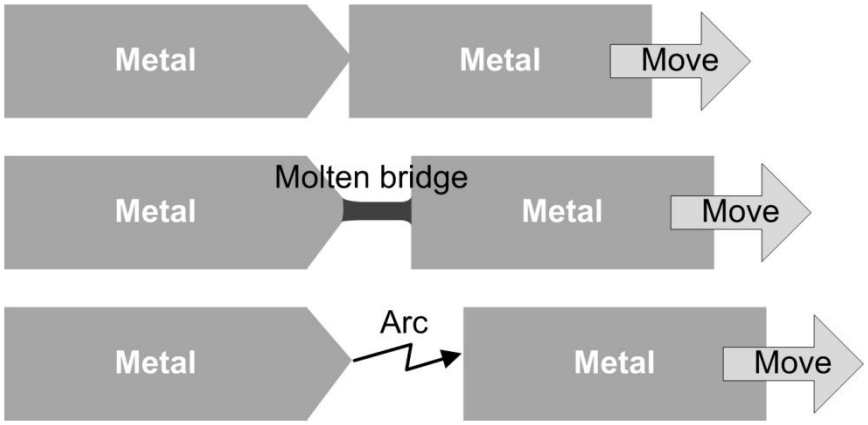

Figure 21: Contact arcing by a breaking process

Their temperature quickly rises and can exceed the melting point of the metal. Since all the metal bridges are disrupted, the voltage drop across the gap rises. If the power supply can sustain a sufficient voltage gradient across the gap, thermo-field emission and ionization can take place, and the arc starts.

The formation of molten bridges and contact arcing also occurs during the contact-making process. Depending on the speed of the contacts, the contact force, and other mechanical conditions that may result in a contact bouncing, the arc duration may strongly vary. The duration of the arc is in general shorter than at the breaking process. In low-voltage applications, parallel contact arc faults are the unintentional direct and indirect contact of live parts: cutting of a cord with a blade, crushing of a cable, shorting with a conductive object like a copper bead, a nail, a clip, or a strand.

3.2 Series arc faults in PVC installation cables

Since arcing due to creepage on char was considered as particularly likely to become very stable, this phenomenon was often studied and analyzed to define the test methods and test criteria of AFCIs [UL96, KCS07, She08]. A frequently used method to create a carbonized track is to generate discharges at the surface of the PVC probe using high voltage. Firstly, this operation is easy and convenient to implement and results in the quick formation of a conductive track for arcing tests. Secondly, it reproduces only the initial conditions to start a stable series arc and not the complete process of forming the fault prior to initiation of the arc fault. In order to prove that a PVC insulation can become sufficiently carbonized in a realistic fault scenario and lead to a very stable arc, we developed an alternative experiment. The principle was to produce contact arcing by applying make and break actions on a separated conductor and observe the evolution of the fault. We did our tests at 240 V AC 50 Hz with NYM-J cables that are widely used in Germany [MAF10]. One of the three conductors of the cable was cut (see Figure 22) and an electromechanical system controlled the bending angle of the cable and the gap distance at the fault area (
Figure 23).

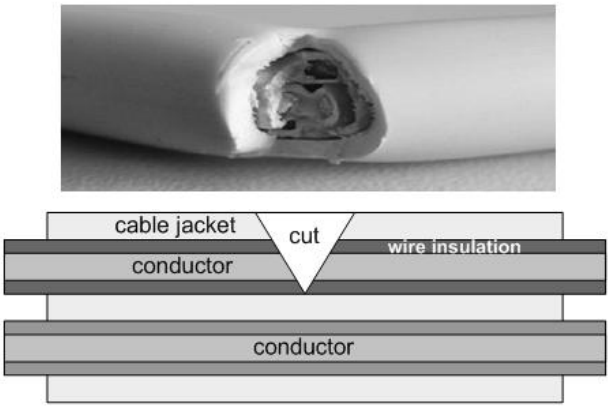

Figure 22: Conditioned test probe with cut insulation and separated conductor

An acquisition apparatus coupled with a signal processor was used to compute the different electrical and optical parameters in real time. By using a logic that could distinguish arcing from non-arcing states, the position of the actuator was controlled in order to promote arcing. The arc stability was defined as the proportion of arcing half-cycles in an observation

period of ten half-cycles of the system voltage. Figure 24 illustrates the progress of the current and voltage at the fault for a series arc signal that presents a stability of 50 %.

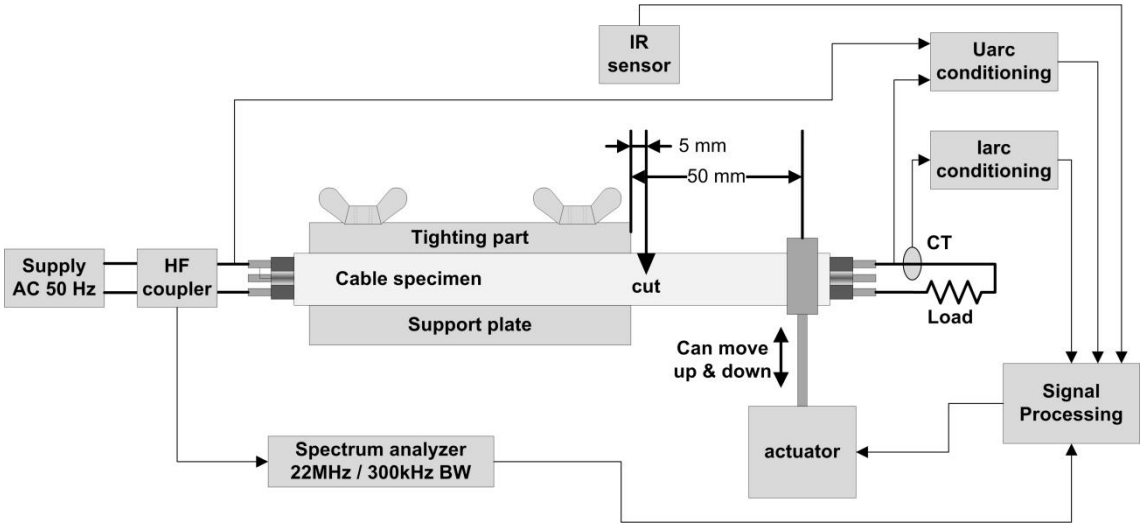

Figure 23: Test setup for series arc fault simulation by bending a damaged NYM-J cable [MAF10]

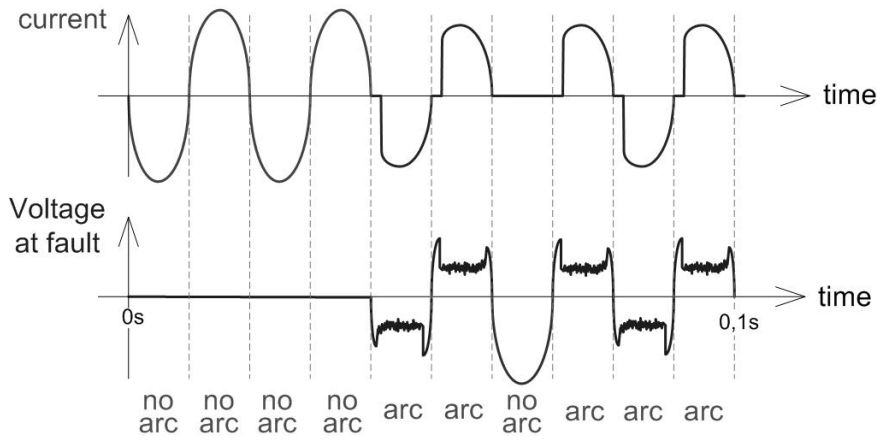

Figure 24: Determining arc stability. In this example, it is 50%.

In most cases, sustained arcs were obtained after a carbonized track had been formed between the cut conductors, thus leading to quick ignition of the PVC insulation. The energy and time required to reach a hazardous state while a sustained arc started, presented an important variance, but three main behavioral characteristics of the electrical fault could be identified depending on the current load:

- At currents below 3 A, the production of arcs was unlikely and the glowing phenomenon was predominant (even if the control system attempted to separate the glowing conductors). However, the glowing could carbonize the fault location and lead to sustained arcs and ignitions of the PVC (see Figure 25). The arcs starting after a long glowing phase suddenly presented a very high stability and could simultaneously ignite the insulation.

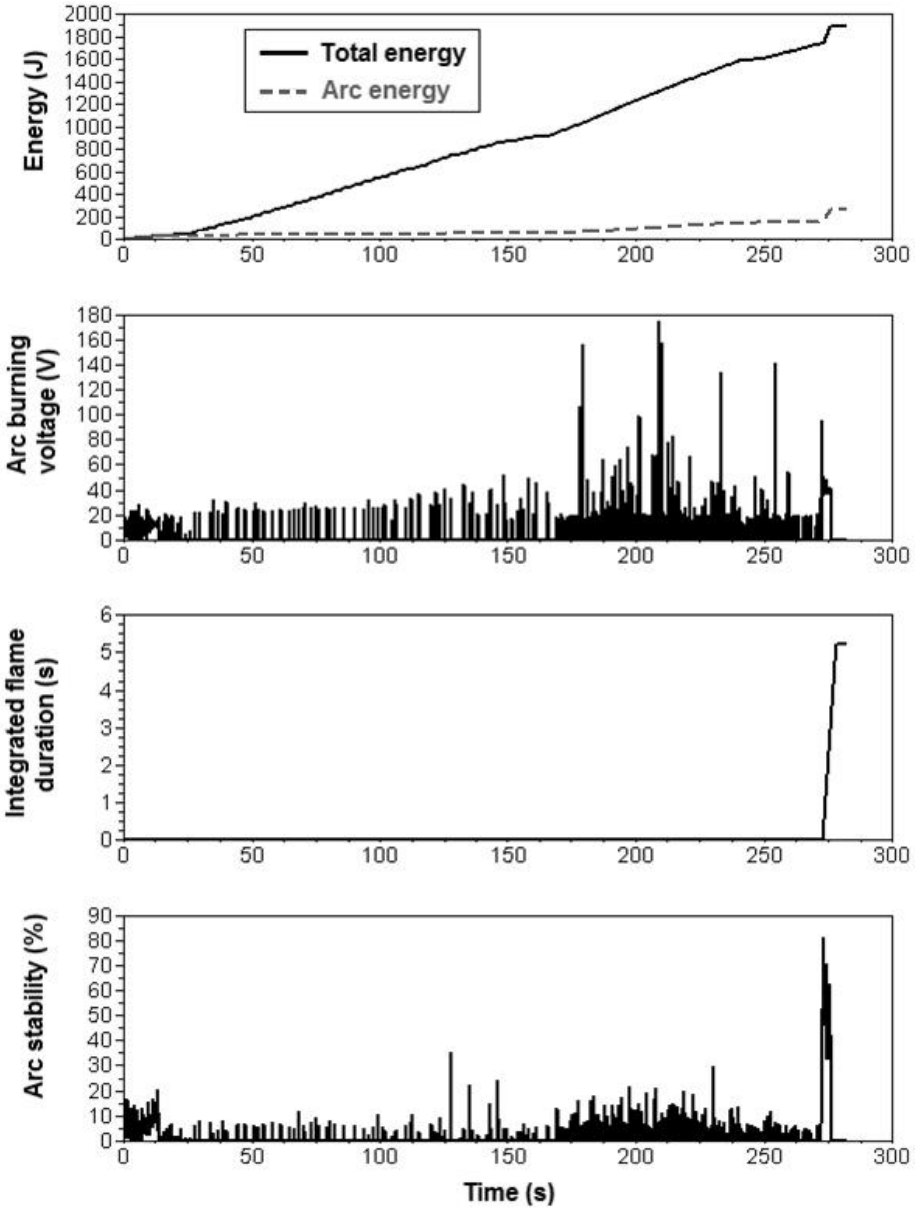

Figure 25: Series arcing in a NYM-J cable tested at 240 V AC / 2 A load

- In the range of 3 A to 10 A, the contact arcing led to a sustained arc and ignition of the PVC insulation in more than 90 % of the tests (see Figure 26). The contact arcs produced by successive make and break actions presented an intermediate phase while their stability increased progressively.

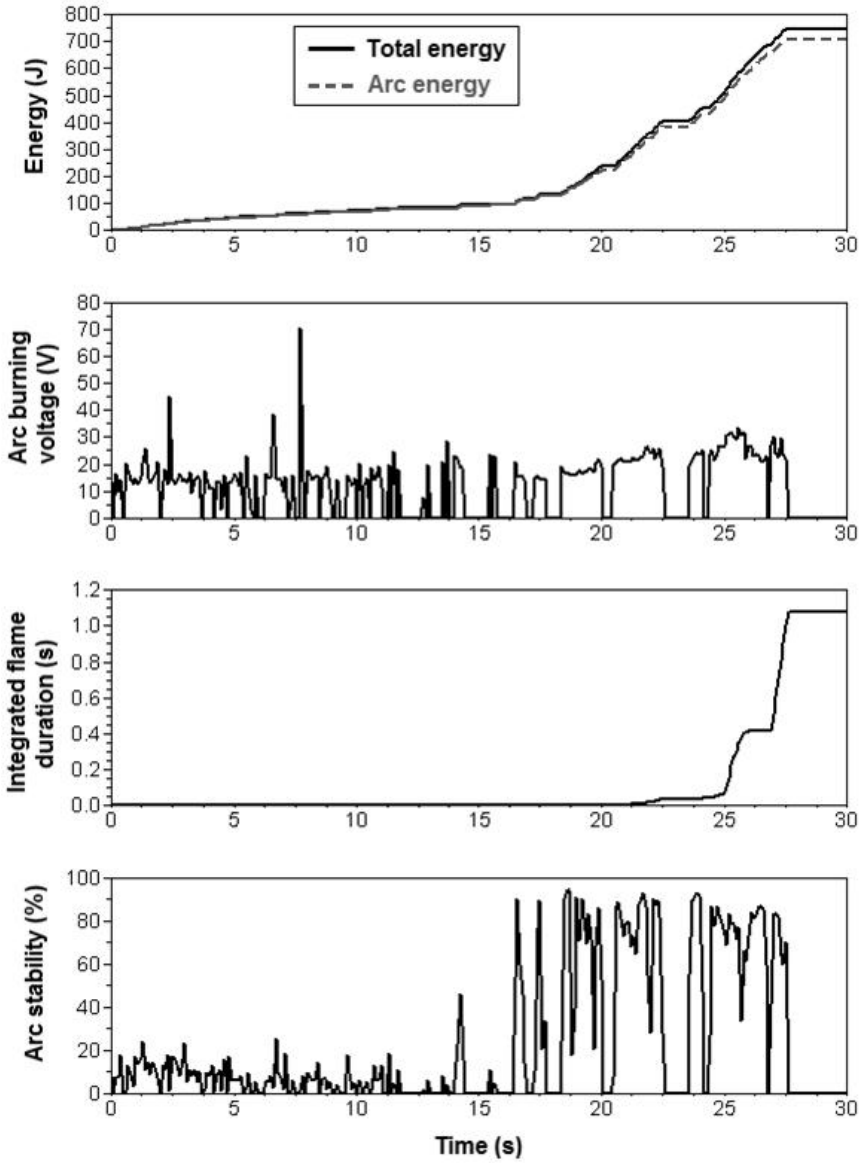

Figure 26: Series arcing in a NYM-J cable tested at 240 V AC / 5 A load

- Above 10 A the higher power of the arcs very often provoked the welding of the conductors (self-healing) or their destruction. The series arcs were very astable.

The electrical data of each test were also analyzed in order to estimate the ignition energy in the case of ignition due to a stable arc. This ignition energy was defined as the arc energy that was dissipated from time t_{STAB} when the arc became stable (at least 70 % stability) to the time t_{IGN} when a flame that lasted at least 50 ms was detected (using infrared sensors):

$$Q_{IGN} = \int_{t_{STAB}}^{t_{IGN}} U_{arc}(t)\ I_{arc}(t)\ dt \qquad (2)$$

The mean value of this ignition energy varied in the range of 200 to 500 J (see Figure 27). Based on this result, the energy value of 100 J was chosen as a reference for the extrapolation of a time-current characteristic used as a criterion for the AFDD test in the standard IEC 62606 [IEC13].

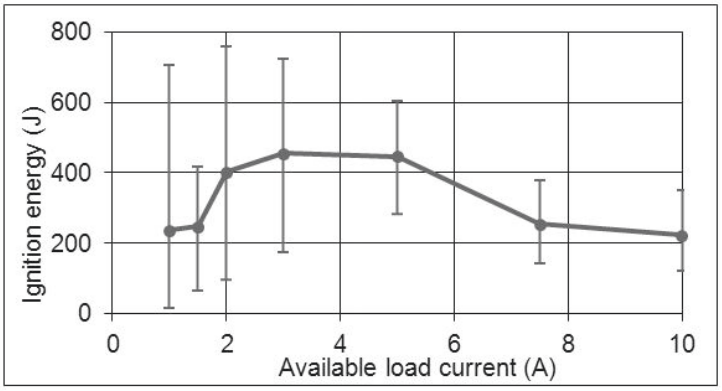

Figure 27: Ignition energy measured in [MAF10]

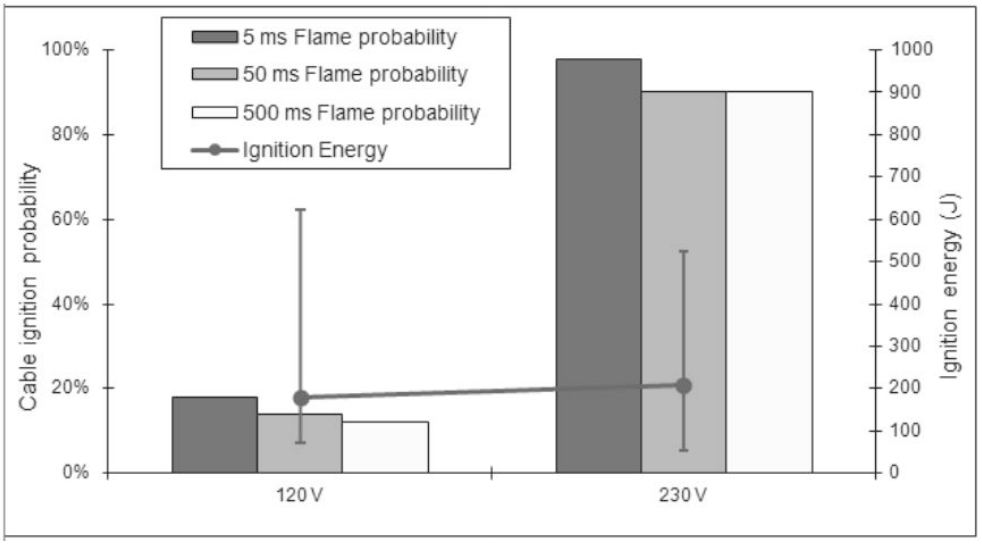

Figure 28: Ignition probability and ignition energy at series arcing at 5 A with NYM-J cable (50 samples used for each test condition)

Further tests were performed with the NYM-J cable at the system voltages 120 V AC and 230 V AC. The results are displayed in Figure 28. The ignition probability was significantly higher at 230 V than at 120 V. In most of the cables that did not ignite, a stable arc could not be initiated. A possible explanation could be the lower value of the system voltage that results in a lower probability that it will exceed the required striking voltage of the arc after the current zero-crossing. The ignition energy was in the range of 150 to 500 J and a clear correlation with the system voltage could not be observed.

The main findings from these series arc tests on PVC cables were:

- The standard deviation of the value of the ignition energy in such test conditions is large. The results may only be reproducible if a large number of samples are tested.
- The probability of igniting a cable is higher at a higher system voltage because the probability of initiating a stable arc is higher, not because the ignition energy is lower.
- The initiation of a stable series arc due to creepage on char is more probable in the current range 3 A to 10 A.
- There are clear transitions between contact arcing, glowing, and arcing due to creepage on char.

3.3 Relationship between glowing and series arcing

3.3.1 The glowing connection

Much well researched work about glowing connections in residential installations has been published by J. Shea and X. Zhou [She06b, She07a, ShZh07, ZhSh07]. They used a similar test apparatus as described in
Figure 23 with the difference that only copper conductors without insulation were used as electrodes and the gap distance was adjusted with a precision translator. In addition to the acquisition of the electrical parameters, the temperature of the glow was measured with a thermocouple. In an upgraded version, the emitted radiation could be analyzed with a spectroscope. J. Shea observed initially that a glowing connection begins to form after the surface of the conductors has been conditioned by contact arcing. The heat of the short arcs

oxidized the surface of the copper conductors and by drawing out the conductors from each other a glowing bridge could be formed. Figure 29 displays such a bridge with a dark solid material assumed to be copper oxide and a light-emitting track. Microscopic and X-ray mapping analysis of the bridge confirmed that the dark material was made up of copper and oxygen. The black color indicated the copper(II) oxide CuO or a copper oxide with a lower stoichiometry $Cu_{1-x}O$. A similar diagnosis was done for the track that was glowing and emitting visible light. Its red color suggested a copper(I) oxide Cu_2O. The formation of copper(I) oxide is promoted at higher temperatures and the semi-conducting properties of this material would explain the high current density in the glowing track. During the glowing, the measured temperature of the dark oxide was in the range of 250 °C to 500 °C. The measured temperature of the glowing track was from 700 °C at 1 A up to 1400 °C at 7.5 A. Most of the captured temperatures were in the range of the melting point of copper(I) oxide Cu_2O (1235 °C). The relationship between oxidation and the glowing was proven by attempting to produce a glowing connection in an oxygen-deprived environment: no glowing could be initiated. A glowing connection which was already established in air could not be sustained in such an environment.

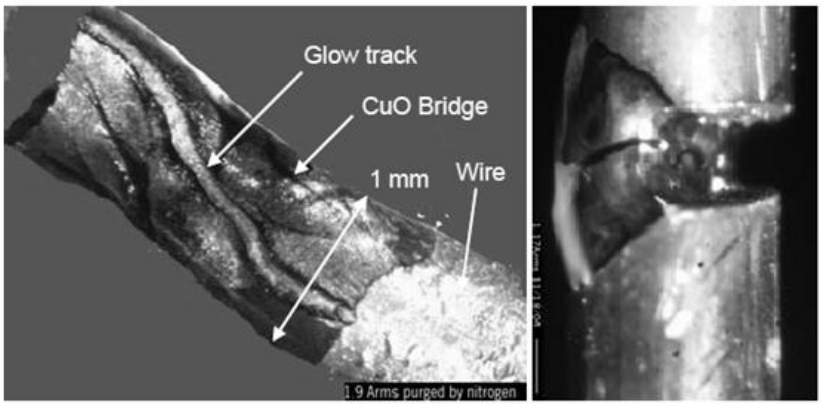

Figure 29: Glowing bridges between two copper conductors [She06a]

J. Shea extended the study to different materials which are commonly used for electrical connections. He observed two different types of behavior. Glowing with copper-based metals (copper, brass, and bronze) was very dependent on the formation of an oxide filament and initiation required sufficient contact arcing as a precondition. The second group formed by iron-based metals quickly produced a glowing zone with few contact arcs and it could be

sustained without having to manually expand an oxide bridge. The electrical characteristics of glowing with these materials were also different: the glowing involving copper-based metals had a higher resistivity and dissipated more power. Conductivity measurements of the oxide bridge involving copper were performed: they showed variations corresponding to a semi-conducting behavior of the oxide (exponential variation according to $e^{-Eg/kT}$) resulting in a resistivity of around 0.1 Ω m at temperatures in the range of 1000 °C and around 10 Ω m below 500 °C. The strong temperature dependency of the oxide resistivity had direct consequences on the electrical impedance of the glowing bridge. We performed our own investigations: glowing connections were reproduced using the same method with 1.5 mm² massive copper conductors. The electrical parameters displayed in Figure 30 confirm the strong interdependency between current, temperature, and resistance of the glowing bridge. The phenomenon is easy to observe at currents below 5 A. At higher currents, the variations of the impedance are less distinct since the average temperature is higher and the oxide bridge doesn't cool quickly enough at the current zero-crossing to provoke a significant impedance change (see Figure 31). If the load current is higher, in general above 10 A, it is very difficult to obtain a sustained glowing connection. The assumption of J. Shea that the bridge temperature approaches the vaporization point of the copper(I) oxide (1800 °C) and leads to an astable liquid/vapor interface is logical.

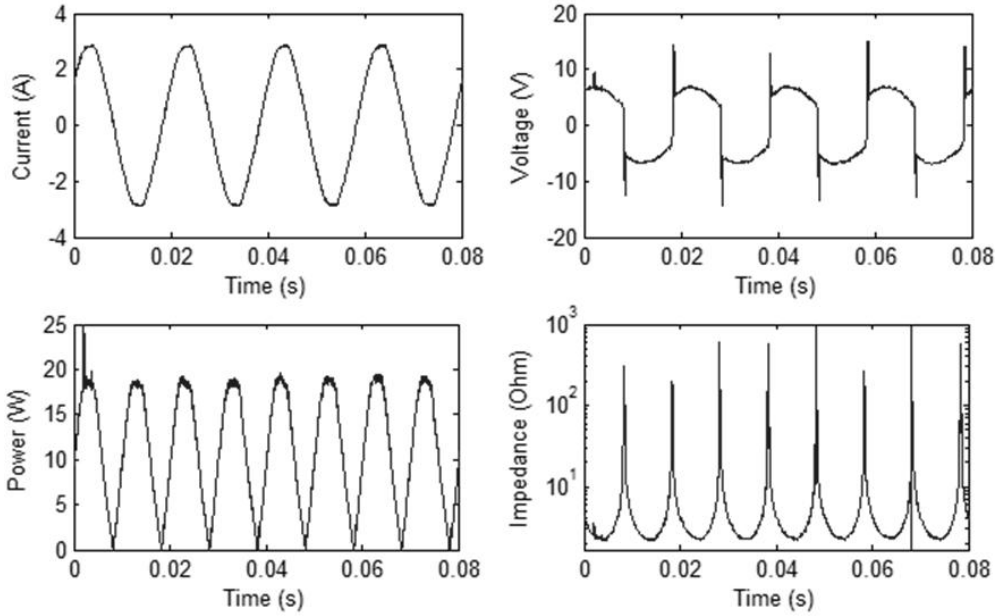

Figure 30: Electrical characteristics of glowing between two copper conductors at 2 A load current

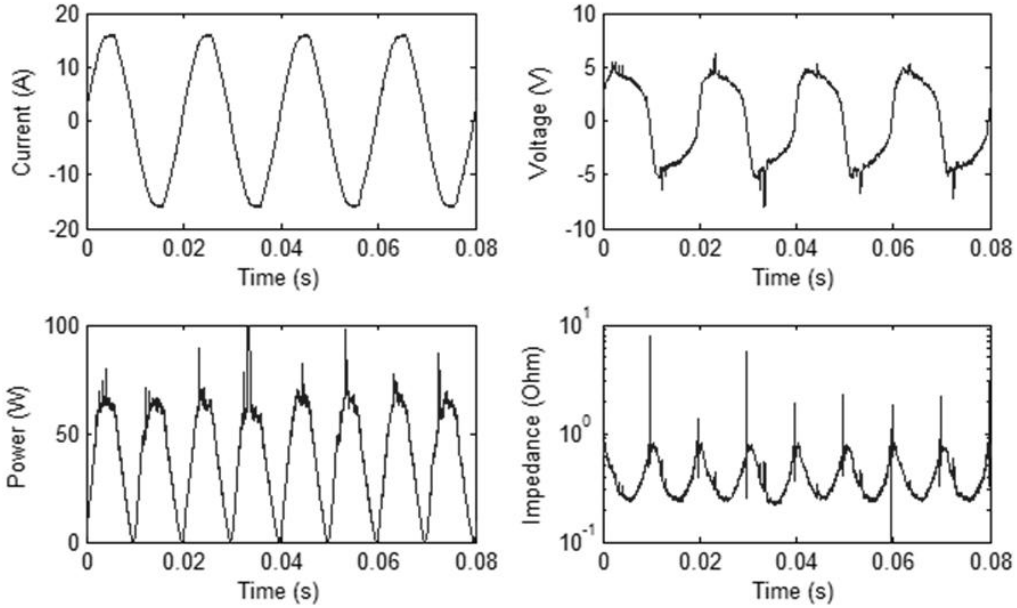

Figure 31: Electrical characteristics of glowing between two copper conductors at 11 A load current

3.3.2 **Transition from glowing to arcing and fire ignition**

The temperature of the glowing bridge is sufficient to carbonize the PVC of the cable jacket or wire insulation: the decomposition temperature of the PVC is in the range of 250 °C [Tro90], so approximately 1000 K lower than the temperatures observed at glowing. In these conditions, a conducting carbonized track can be formed. While the glowing connection finally breaks (the vaporization temperature of the oxide is reached or there is a mechanical stress), a very stable series arc may start and ignite the polymer surrounding the fault. This phenomenon could be observed as ignition attempts were performed by applying different flammable materials on the glowing fault. The mechanical stress and/or the strong cooling (due to the application of the probe) were the reasons that disturbed the glowing. The electrical parameters at this instant are displayed in Figure 32. The transition from glowing to series arcing is clearly visible at the trigger time of 0 s. After arc initiation, the dramatic increase of the power dissipation by a factor of 6 was the reason for the ignition of the test material.

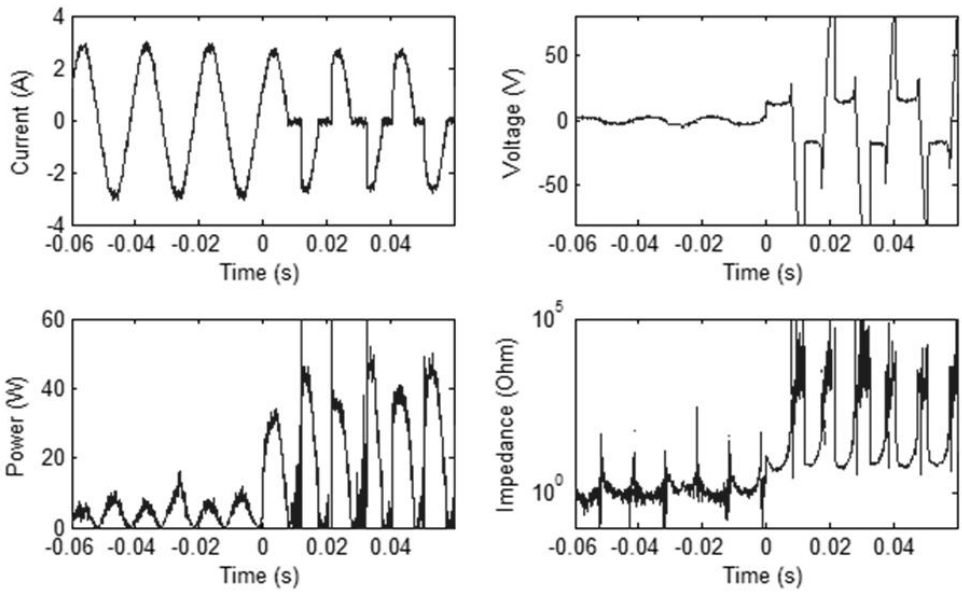

Figure 32: Electrical characteristics at a transition glowing to series arcing between two copper conductors at 2 A load current and 230 V AC system voltage

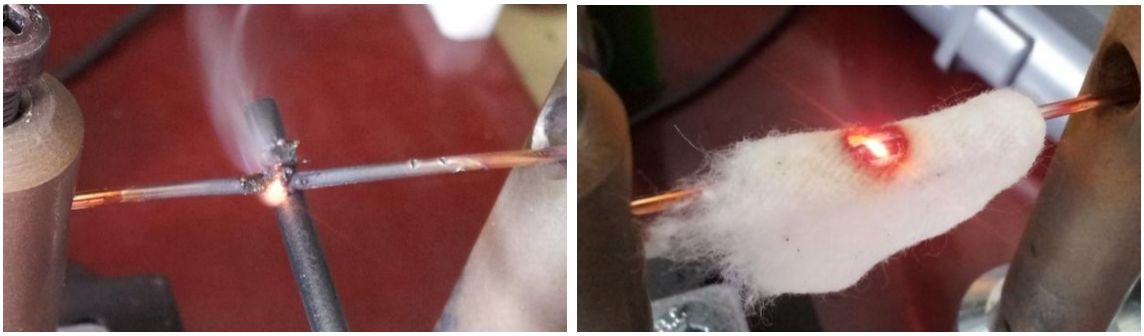
Figure 33: Ignition attempt with glowing at 2 A with PVC (left) and cotton (right)


Figure 34: Effect on polymers of thermal stress from glowing
Left: PUR / middle: PVC / right: halogen free polymer

The same ignition attempts were performed with 18 different insulation materials provided by a cable manufacturer. The base components of the polymers were polyurethane, PVC,

PE, and polypropylene. The probes were applied with different forces on and under the glow. None of these materials could be directly ignited by the glowing. Most polymers melted and released smoke as displayed in Figure 33 (left) and in Figure 34 (left and middle). They could only be ignited after initiation of a stable series arc. Many of the PE-based and halogen-free polymers were hardly damaged at all by the thermal stress (see Figure 34, right) and could not be ignited since no arc started. The cotton that is usually used as a flame indicator in standard tests was also used. The glowing could not ignite this material: it only smoldered and retracted away from the fault area (Figure 33, right).

Other authors reported similar observations and tried to initiate glowing in practical cases involving screw connections, bad contacts in receptacles, or separated conductors [MeBe77]. The glowing connections were produced with loose connections or by applying vibrations on terminals. J. Urbas tried to reproduce an electrical fire that was probably caused by a glowing connection [Urb08]. It was supposed that glowing occurred at a connection of a receptacle switch stressed with vibrations. The actual device current flow was 0.6 A at 120 V. Urbas observed in the same conditions that glowing occurred on all test specimens after 25 to 82 minutes. The studies showed that glowing connections could already be initiated at very small currents in the range of 0.15 A to 0.8 A and the stability of the glowing decreased above 6 A. Many ignitions of flammable materials by glowing were observed, but it was not reported if arcing was involved or not. In contrast to our observations above, Sletback [SKSNR91] stated that the glowing phenomenon must be the best explanation for the many electrical fires caused by series faults. It must be mentioned that J. Sletback reported exclusively on the formation and the observation of glowing contacts. He did not consider the arc phenomenon and did not perform ignition tests based on glowing.

3.3.3 **Conclusions on the glowing phenomenon**

The different studies published on glowing are mostly very consistent and match our own observations. The main facts about this phenomenon are:

- The formation of an oxide layer is necessary to start the glowing. The initial formation of the oxide can be due to contact arcing.

- The specific electrical properties of the oxide lead to an important fault impedance and power dissipation in the range of 5 W to 50 W. The temperature of the glowing bridge may exceed 1250 °C (for a copper-copper connection) and this promotes the growth of the oxide bridge.
- Most metals, copper and iron-based, as well as aluminum, can glow.
- Small currents above 0.15 A may be sufficient to start and sustain glowing.
- Glowing can last for hours or days without interruptions and can be restarted after a current interruption.
- Glowing connections are unlikely to be sustained at higher load currents above 6 A. The high temperature of the filament makes it less stable and tends to break. A mechanical or electrical disturbance may stop the glow by destroying the bridge and initiate a series arc fault.
- Glowing connections may carbonize insulation materials at the fault location, lead to stable series arcing, and consequently to a higher probability of fire ignition.

Our main finding was the fact that a glowing connection could not ignite directly the organic materials being tested. A series arc was always involved in the ignitions. We cannot guarantee that a glowing fault alone is not able to initiate an electrical fire because it may be possible in other scenarios that we did not consider. Nevertheless, the observations and analysis of the fault characteristics tend to show that series arcing is much more likely to ignite a flammable material; the main hazard from glowing would be the fact that it is a fault preceding series arcing. It must be mentioned that the glowing fault can also be related to other electrical faults. The thermal stress may alter and deform the insulation materials and lead to short-circuits or earth leakages. R. Wagner [Wag01] conducted a study to evaluate the performance of AFCIs B type (no detection of series arc faults) from five different manufacturers to mitigate glowing faults. The AFCIs with ground fault protection were tripped in many cases. Since these devices are not designed to detect a glowing connection, we can assume that the glowing faults turned to bolted short-circuits, parallel arc faults, or ground faults. It seems that if an electrical fire is the result of a chain of many fault situations, the glowing fault is very often at the beginning of this chain, seldom at the end.

3.4 Relationship between the types of arcing and other electrical faults

Figure 35 presents an overview of the different types of arcs, the abnormal situations, or defects leading to arc faults, and their interactions with other electrical faults. This result is based on bibliographic researches, our own observations, and interviews with electricians. The argumentation for the considered interactions between these phenomena and the electrical faults are listed below:

- Interaction A: Contact arcing leads to arcing due to creepage on char

The heat of intermittent contact arcs caused by make and break operations between two unintentionally broken conductors can carbonize and degrade the insulation or other materials at the fault location [part 0, She07a, Bab05, Bab01, MAF10].

- Interactions B and C: Arcing leads to glowing

The heat generated by any kind of series arcing facilitates and accelerates the formation of oxide on the surface of conductors and can lead to a glowing connection. This phenomenon was observed by most scientists who studied glowing and arcing phenomena [part 3.3.1, She07a, MAF10, She06b, Urb08, SKSNR91]. The transition from arcing to glowing is more probable at currents below 7 A. Above this current, the high power of the arc damages the surface of the conductors and inhibits the formation of a stable oxide bridge.

- Interaction D: Glowing leads to arcing due to creepage on char

The temperature of a glowing connection can easily exceed 1000 °C and carbonize materials in the vicinity of the fault [part 3.3.2, She07a, MAF10, She06b, Urb08, SKSNR91]. If the glowing bridge is disturbed and interrupted, a series arc due to creepage on char can be initiated and sustained.

- Interaction E: Arcing due to breakdown leads to arcing due to creepage on char

Arcing through normal insulation is seldom, but possible under specific conditions. Overvoltages due to lightning can provoke discharges between live parts and possibly carbonize the insulation [Bab05]. Leakage currents may flow in the formed carbonized path, intensify the carbonization of the insulation, and initiate a parallel arc or an arc to ground. Electrical fires have been reported that occurred a long time after lightning struck.

- Interaction F: Sustained series arcing leads to parallel arcing

The heat from a sustained arc can destroy or deform the insulation separating the conductors at different polarities, leading to a bolted short-circuit or parallel arc.

- Interactions G, H, I, and J: Overheating leads to arcing

Overloads and overvoltages combined in most cases with inadequate wiring, faulty equipment, and thermal isolation [She07b, Bab01] can damage the connections, carbonize the insulation, thereby yielding favorable conditions for arcing.

- Interactions K and L: Bolted short-circuit leads to parallel arcing

A bolted short-circuit with physical contact between live parts may easily turn to a parallel arc. The high current involved in the fault is only limited by the impedance of the system and short-circuit currents in the range of 1000 A are expected. Since the metal-to-metal contact area is in most cases small and with a limited current carrying capacity, the local temperature may quickly reach the melting point of the metal, destroying the conductive bridge, and initiating a parallel contact arc [PNGB01, Bab01].

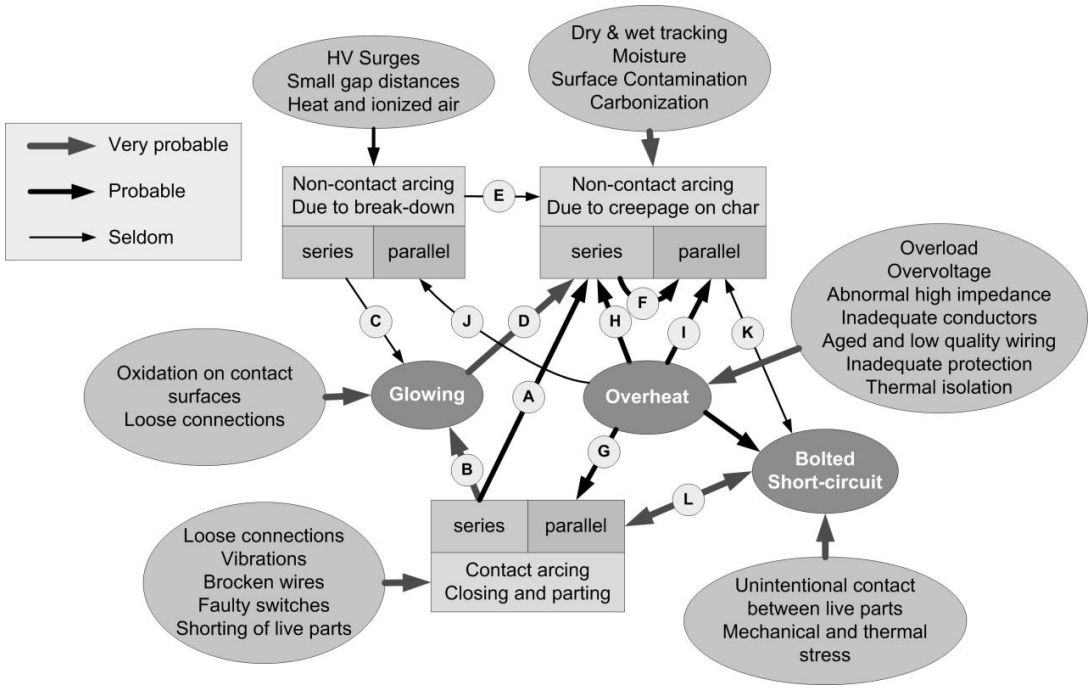

Figure 35: Causes, evolution of arcing, and interactions between the electrical faults

All these different types of faults and possible interactions show the real complexity of electrical faults. Determining with precision the occurrence of each individual fault type and the probability of the different transitions seems to be barely possible. However, concerning

the series arc faults, we can notice a tendency of the different types of arcing to lead to the stable arcing form that is due to creepage on char.

3.5 Electrical faults and current dependency

One of the most influential parameters on the occurrence and outcome of the different forms of arcing and electrical faults is the current. The overview in Figure 36 is based on an article by UL experts [UL95], our own findings, and the most recent developments in circuit protection. Below the rated current of the branch circuit, the abnormal heat leading to a fire can be dissipated by series arcing, glowing, and abnormal high impedance. Above the rated current, the major sources of heat are overloads, short-circuits, parallel arcs, and arcs to ground. It seems that the available circuit protection offers suitable protection against most electrical faults. However, there is no protection against glowing and the protection against series arc faults starts at 5 A with the AFCI [UL13] and at 2.5 A with the AFDD [IEC13]. A comprehensive comparison of the thermal stresses of electrical faults with the consideration of the protection devices is described in the chapter 6.

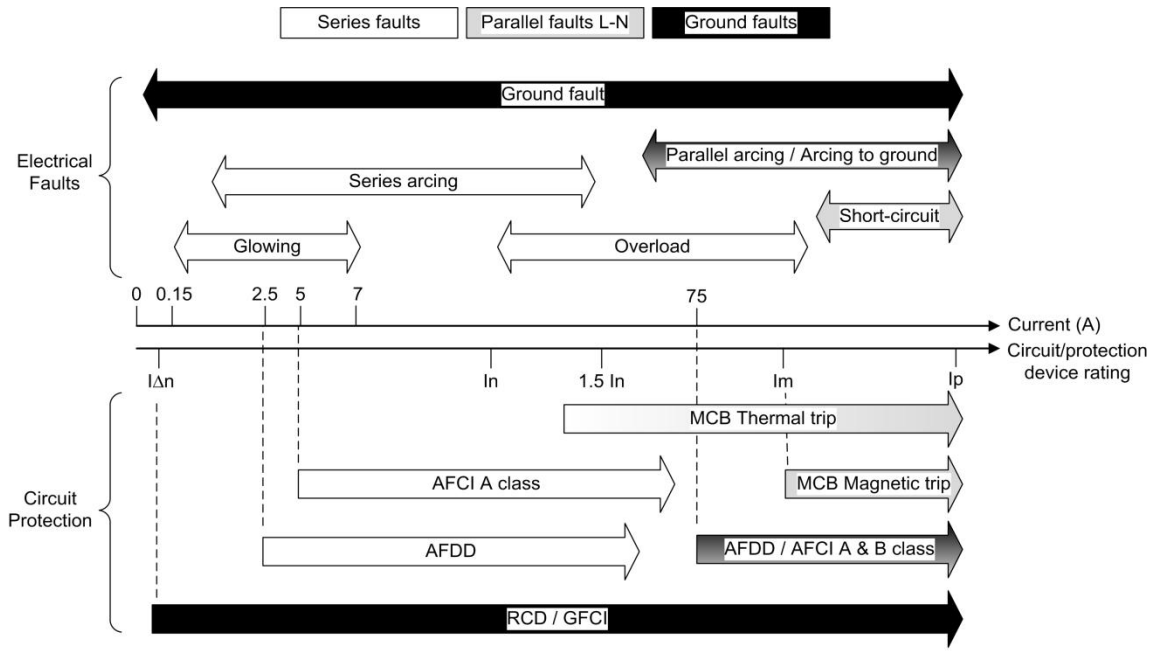

Figure 36: Electrical faults and available UL/IEC protection technologies
IΔn: rated operating residual current of the RCD / In: rated current of the branch circuit
Im: Instantaneous trip threshold of MCB / Ip: Prospective short-circuit current

3.6 Conclusions regarding arc faults and other electrical faults

The occurrence of the different types of series arcing, the contact and non-contact arcing, strongly depends on the electrical parameters, the initial conditions, and prior electrical faults. Many realistic scenarios were described and the non-contact series arcing that is due to creepage on char could be identified as the most hazardous form of series arcing: it can be the result of many other phenomena like glowing and contact arcing, become self-sustained, and dissipate a significant amount of heat. The other types of arcing do not have the same capability to sustain themselves and dissipate a lot of heat. Their probability of directly causing an electrical fire may be much lower. However, they cannot be neglected since they are often observed and create the conditions for the initiation of glowing and sustained series arcing on char.

4 Basics of arc physics and electrical arc characteristics

4.1 Basics of arc physics

The electrical arc is an electric discharge which produces an ongoing plasma between two electrodes at different polarities. If the conditions for stability are satisfied, especially a sufficient supply of electrical energy to sustain the heating of the plasma column, it may exist indefinitely or at least much longer than a non-sustained discharge like a spark. As displayed in Figure 37, the arc differs from the other types of discharge with its characteristic voltage and current values. The conduction of electrical current is enabled with the travel of negative charge carriers (electrons) from the cathode to the anode. There is also a flow of positive charge carriers, the ions, in the opposite direction. They have a lower mobility and contribute to a lesser extent to conduction. For arcing in low-voltage electrical installations, the processes of generating electrical charge carriers are the thermofield emission [MuGo56, FrKe11 (p513)] of electrons at the cathode and the thermal and impact ionizations in the plasma.

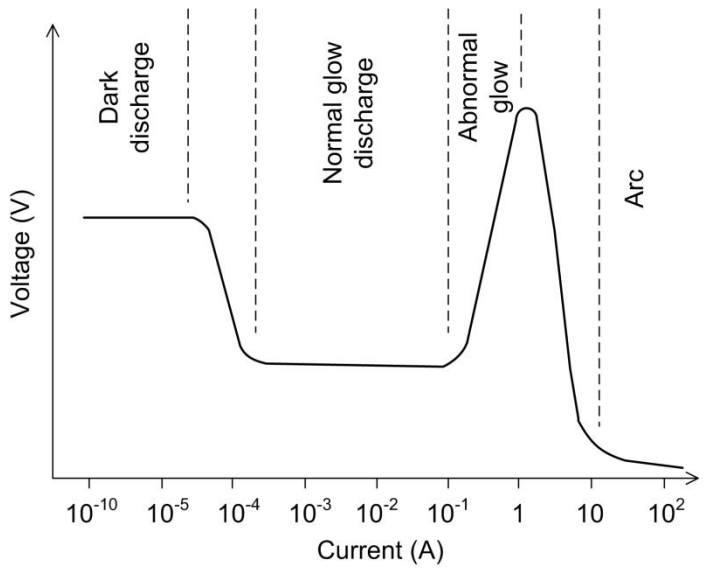

Figure 37: Voltage and current characteristics of electrical discharges [Rie67 (p61)]

In a plasma with a high concentration of charge carriers and energy density, the thermal ionization process that produces new charge carriers in the column to replace the lost ones is predominant. The self-sustained generation of charged particles and the high electrical

conductivity of the plasma do not necessitate a high electric field. The arc exists as long as the power input is sustained and no disturbing event like damage to the electrodes or important cooling occurs. A part of the arc energy is dissipated in the form of radiation. The frequency distribution depends on the plasma temperature, thereby radiations are always emitted in the visible light domain, giving the arc its bright aspect. The power dissipation of the electric arc is many orders of magnitude higher than for the spark or other discharges. It is known as a heat source capable of igniting a flammable material. The purpose of this chapter is to explain the main physical processes involved in the electrical arc in order to give the reader a comprehensive understanding of the mechanisms involved in this phenomenon. It leans on the publications of Rieder [Rie67] and Maecker [Mae51] which are easily understandable for anyone with a scientific background. Physicists should consult more recent and detailed contributions of Fridman and Kennedy [FrKe11].

4.1.1 **Energy balance**

The physical phenomena involved in the electrical arc are well understood and explained. Like every phenomenon, the plasma of the arc column obeys the first law of thermodynamics, and its energy balance can be expressed as:

$$E\ (j_i + j_e) = div(\kappa\ \ grad(T)) + \rho\ \ c_p\ \ v_c\ \ grad(T) + rad(T) + W_i\left(\frac{n_e}{t} - \frac{1}{e} div(j_e)\right) - \rho\ \ c_p\ \ \frac{dT}{dt} \quad (3)$$

[Rie67(p76)]

where E is the electric field, j_i and j_e the current densities with the ions and the electrons, κ the thermal conductivity, ρ the plasma density, c_p the specific heat capacity, v_c the plasma velocity, W_i the ionization energy, n_e the electron density, e the charge of the electron, and T the temperature.

Each term of this equation is a power density (W/m³). This equation can also be expressed in simple words: Joule heating = conducting loss + convection loss + radiation loss + work to produce charged particles + heating or cooling of the plasma

Each term can be described mathematically, but the complete solution is nearly impossible because many parameters are interdependent. In most cases, simplifications of the models must be used and many interactions and dependencies must be determined empirically.

A common approach consists in the following simplifications [Rie67 (p77)]:

- Stationary arc: no time dependency
- Plasma considered as electrically neutral: no space charge $n_e = n_i$
- Vertical and cylindrical shape of the arc: symmetry of the column
- Negligible convection velocity compared with the particle velocity $v_c << v_{ions} << v_{electons}$

In this case, the energy balance equation can be simplified as follows:

$$E\ (j_i + j_e) = E^2\ \sigma = -\frac{1}{r}\ \frac{d}{dr}\ r\ \left(\kappa\ \frac{dT}{dr}\right) + W_i\ D_{am}\ \frac{dn_e}{dr} + rad(T) \qquad (4)$$

[Rie67 (p78)]

where σ is the electric conductivity, r the radial coordinate of the cylindrical column, and D_{am} the diffusion speed of the electrons. Further simplifications may be used by neglecting the two last terms of power loss: the ionization to replace the diffused electrons and the radiation loss. The thermal conductivity may also be considered as constant in the plasma core. The most simplified energy balance equation of the stationary arc with the canal model is:

$$E^2\ \sigma = -\frac{\kappa}{r}\ \frac{d}{dr}\left(r\ \frac{dT}{dr}\right) \qquad (5)$$

[Rie67(p80), Mae51 (p305), FrKe11(p526)]

The purpose of the following parts is to present the determination and the meaning of the key parameters such as the plasma temperature, the radiated power, and the electrical and thermal conductivities.

4.1.2 **Thermal equilibrium**

The temperature of the plasma is of the greatest importance since most plasma characteristics depend on it. The determination of a temperature is only sensible if the system is in thermal equilibrium, otherwise the temperatures and the velocities of the different particles must be taken into account.

Two assumptions can be made for a thermal equilibrium:

- The energy increase of the charged particles due to acceleration by the electric field is negligible compared with the thermal energy:

$$E\ e\ \lambda << \frac{3\ k_B\ T}{2} = \frac{m_e\ v^2}{2} \tag{6}$$

[Rie67 (p34-35), Mae51(p298)]

where k_B is the Boltzmann constant, m_e, λ, and v the mass, the mean free path, and the velocity of the electron.

- The temperature change over a distance in the range of the mean free path of the charged particles is small if compared to the absolute temperature itself:

$\lambda\ \ grad\,(T) << T$ [Rie67 (p34-35), Mae51 (p298)]

The mean free path of an electron in air at 100 kPa is in the range of 3.7 µm [Rie67 (p24)] and the plasma of the low current arcs, from 1 to 50 A, in air has a temperature of at least 5000 K [Mae (p304)]. With a radius of the arc column in the range of the millimeter, the product of the mean free path of the electron with the temperature gradient is approximately 20 K; it is 250 times smaller than the temperature of the arc column and the plasma should be in thermal equilibrium.

4.1.3 **Electrical conductivity**

The electrical conductivity of the plasma is proportional to the concentration of charged particles and their mobility. Considering the respective masses of the ions and the electrons, the ions have a much lower mobility and contribution to the conduction of current (~ 1 %). The contribution of the ions can be neglected for simplicity's sake:

$$\sigma = e\ n_e\ b_e + e\ n_i .\ b_i \approx e\ n_e\ b_e \tag{7}$$

[Rie67 (p47), Mae51 (p310)]

where n_e and n_i are the concentrations of electrons and ions, b_e and b_i the corresponding mobilities. The electron mobility can be expressed as:

$$b_e = \frac{e\ \lambda_e}{m_e\ \bar{v}_e} \tag{8}$$

[Rie67 (p33), Mae51(p310)]

where λ_e is the free mean path of the electron, m_e the electron mass, and $\bar{v}_e$ the mean electron velocity.

The mean electron velocity in a plasma at thermal equilibrium is:

$$\bar{v}_e = \sqrt{\frac{3 \; k_B \; T}{m_e}} \tag{9}$$

[Rie67 (p28), Mae51 (p310)]

The mean free path in a pure gas is:

$$\lambda_e = \frac{1}{\sqrt{2} \; \left(n_0 \; Q_0^C + n_i \; Q_i^C \right)} \tag{10}$$

[Rie67 (p23-24), ChCo90(p91)]

where n_0 and n_i are the volumetric concentrations of the neutral particles and ions, Q_0^C and Q_i^C the corresponding effective cross-sectional areas.

Fridman obtains the electrical conductivity in weakly ionized plasma with the frequency of electron-neutral collisions f_{en} :

$$\sigma = \frac{n_e \; e^2}{m_e \; f_{en}} \tag{11}$$

[FrKe11(p190)]

Values of the parameters are provided for air at 100 kPa [FrKe11 (p191)]:

$\lambda_e = 40 \; \mu m \qquad f_{en} = 3 \; 10^{12} \; s^{-1} \qquad b_e = 600 \, cm^2 / V \, s$

If the gas is composed of different particles, the different concentrations and effective cross-sectional areas must be taken into account. The concentrations can be determined using Saha's equation [BHSL06]:

$$\frac{n_i \; n_e}{n_0} = 2 \; \frac{\left(2\pi \; m_e \right)^{3/2}}{h_P^3} \; \frac{g_i}{p \; g_0} \; \left(k_B \; T \right)^{5/2} \; e^{-W_i / k_B T} \tag{12}$$

[Rie67 (p41), Mae51 (p371)]
[BHSL06 (p576]

where g_i is the statistical weight at i th ionized state, g_0 the statistical weight of the atoms, W_i the ionization energy, p the pressure, and h_P the Planck's constant.

The positive influence of the temperature on the electrical conductivity can be deduced from the equations described above:

$$\sigma = const \ \frac{T^{3/4}}{\sqrt{p}} \ e^{-W_i / 2 k_B T} \qquad (13)\ [\text{Rie67(p47)}]$$

At higher temperatures, the electrons have a higher kinetic energy and their probability to ionize a gas molecule in a collision is greater. The concentrations of electrons and ions increase as well as the mobility of these particles.

Figure 38 displays the value of the electrical conductivity of the plasma in air and at different concentrations of copper at a pressure of 100 kPa (physical characteristics of plasma in air were provided by Reichert and Barbu [ReBa15], valuable data is also available in [AnLü09, Kos11]). Below 4000 K, the conductivity is very low and the plasma will not be sustained at low voltage. The column of the arc has in general a temperature of at least 5000 K. We observe a steep increase in the conductivity up to 10,000 K. It saturates above 20,000 K because the gas becomes completely ionized and the degree of ionization of the atoms cannot increase indefinitely [Rie67 (p43)]. A possible contamination of the plasma with copper from the electrodes has a minor influence on the electrical conductivity.

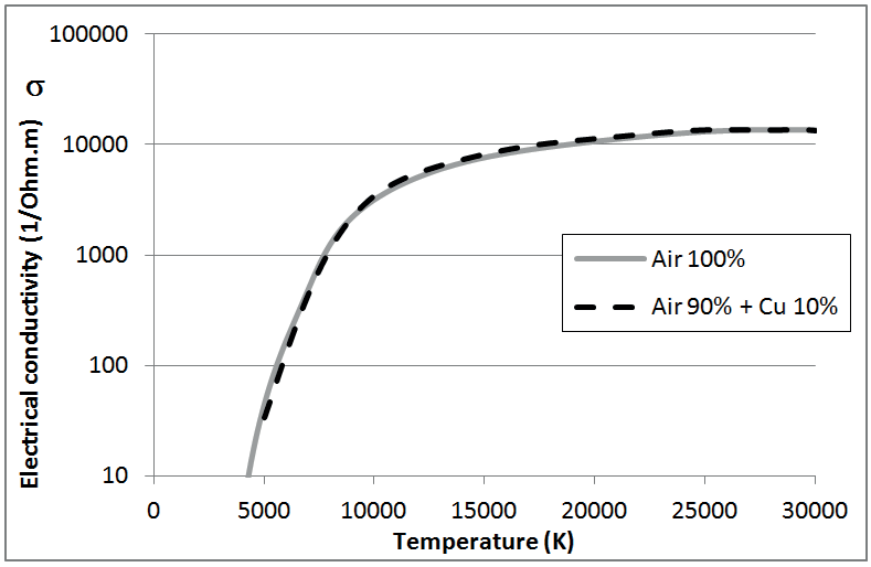

Figure 38: Electrical conductivity of air at 100 kPa [ReBa15]

4.1.4 **Specific heat capacity and thermal conductivity**

Thermal conductivity is the ability of a medium to conduct a quantity of energy in a given direction presenting a temperature gradient. For a gas and also for a plasma, thermal conductivity depends on the mobility of the particles and the quantity of energy they can transport. Each particle in movement is an energy carrier which can transmit a quantity of energy by colliding with the next particle. In a given direction (for instance in the axis z), the quantity of particles crossing a perpendicular surface per second is:

$$F_p = \frac{n\ v}{6} \qquad (14)\ [\text{Mae51 (p312)}]$$

where n is the concentration of particles and v their velocity. The factor 1/6 represents the portion of the particles pushed in the direction of interest (6 possible directions in a three-dimensional space). This first term represents the flow of "energy carriers".

The transported energy of a single particle on a distance z is:

$$W_{sp} = -c_{sp}\ \frac{dT}{dz}\ z \qquad (15)\ [\text{Mae51 (p312)}]$$

where c_{sp} is the heat capacity per particle. The minus sign is due to the negative temperature gradient. The particles have a free mean path λ, and are supposed to move in the domain $z \pm \lambda$: the travel range of the "energy carrier" is $2\ \lambda$.

The product of the flow of energy carriers and the transported energy per carrier over the travel range is the total quantity of energy transported through the defined area per second:

$$\dot{W}_t = W_{sp}\ F_p = -\frac{n\ v\ c_{sp}\ \lambda}{3}\ \frac{dT}{dz} = -\kappa\ \frac{dT}{dz} \qquad (16)\ [\text{Mae51 (p312)}]$$

The thermal conductivity can be deduced as follows:

$$\kappa = \frac{-W_t}{dT/dz} = \frac{n\ v\ c_{sp}\ \lambda}{3} \qquad (17)\ [\text{Rie67 (p32), FrKe11 (p203)}]$$

The average particle velocity in an ideal gas can be obtained from this energy equation:

$$\overline{W}_{cinetic} = \frac{m\ \bar{v}^2}{2} = \frac{3\ k_B\ T}{2} \qquad (18)\ [\text{Rie67 (p29)}]$$

$$\bar{v} = \sqrt{\frac{3\ k_B\ T}{m}} \qquad (19)\ [\text{Rie67 (p29)}]$$

The plasma is a mixture of different particles: molecules, single atoms, ions at different degrees of ionization, and free electrons are present. The relative concentrations depend on the temperature. Below 4000 K, the air composition remains almost unchanged. Between 4000 K and 12,000 K, the plasma has enough energy to dissociate the molecules into single atoms. Above 12,000 K, the majority of the atoms are ionized and the electron density is at a maximum. Each particle has a corresponding effective cross-sectional area regarding the other particles. This results in a mean free path for each particle that depends on the concentrations and effective cross-sectional areas of the other particles. The mean free path [ChCo90] of a specific particle i in a mixed gas is:

$$\lambda_i = \frac{1}{4\ \sqrt{2}\ \left(n_1\ Q_1^i + n_2\ Q_2^i + \ldots + n_j\ Q_j^i\right)} = \frac{1}{4\ \sqrt{2}\ \sum_{j=1}^{j=m} n_j\ Q_j^i} \qquad (20)\ [\text{Mae51 (p313)}]$$

where n_j is the concentration of the particle j and Q_j^i the effective cross-sectional area of the particle j for the particle i. The thermal conductivity of the plasma that is composed of different particles is:

$$\kappa = \frac{1}{12\sqrt{2}} \sum_{i=1}^{i=m} \frac{n_i\ \bar{v}_i\ c_{spi}}{\sum_{j=1}^{j=m} n_j\ Q_j^i} \qquad (21)\ [\text{Mae51 (p313)}]$$

The heat capacity c_{sp} of each particle has still to be determined. It represents the ability of a particle to store energy. For a monoparticle like an electron or a single atom, the energy can be transformed into kinetic energy in the three possible dimensions of space. This particle has three degrees of liberty and its energy can be calculated with the equation (18). The heat capacity of the single particle can be deduced with a derivation from the temperature:

$$c_{sp} = \frac{d\overline{W}_{cinetic}}{dT} = \frac{3\ k_B}{2} \qquad (22)\ [\text{Rie67 (p30), Mae51 (p314)}]$$

Since such a monoparticle has a concentrated mass, a rotation cannot store a lot of energy. In contrast, high rotation torques can be obtained for molecules. This gives additional degrees of liberty for the molecules and a higher heat capacity per particle. A number of degrees of liberty f can be used for the heat capacity of the different particles:

$$c_{spi} = \frac{f_i \ k_B}{2} \qquad (23) \text{ [Rie67 (p31)]}$$

The dissociation of the molecules, the excitation of atoms, and the ionization give additional degrees of liberty (f_i can reach the number of 45). Figure 39 and Figure 40 display the specific heat capacity at constant pressure and the thermal conductivity of air at 100 kPa. The different peaks are due to the important variations of the degrees of liberty. Similar values are published by Fridman and Kennedy [FrKe11 (p206)].

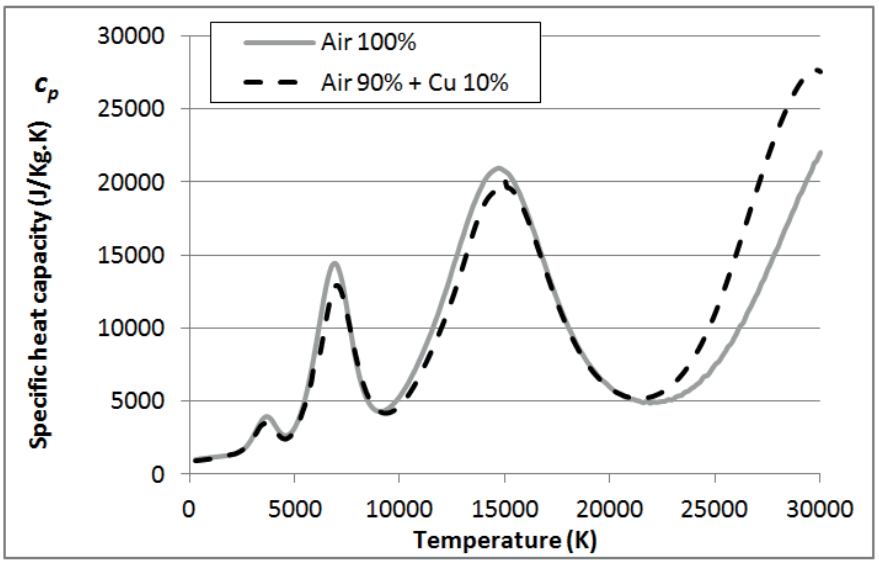

Figure 39: Specific heat capacity of air at different concentrations of copper at 100 kPa [ReBa15]

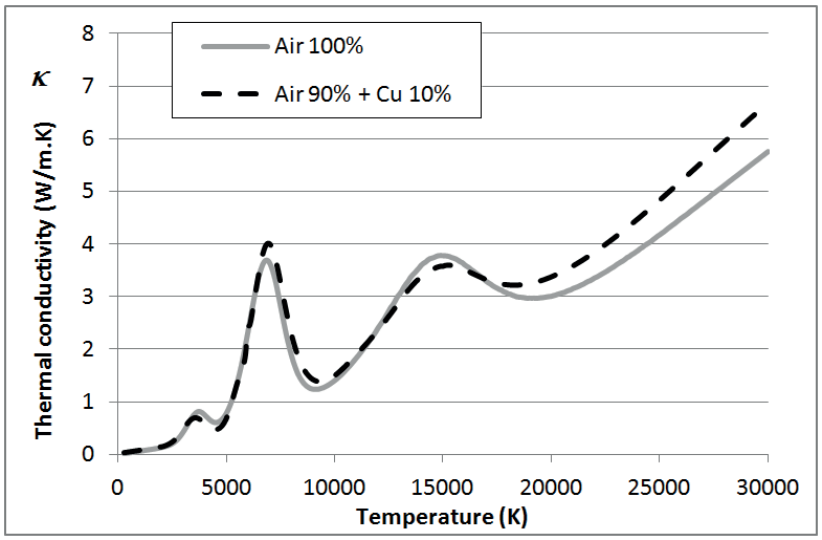

Figure 40: Thermal conductivity of air at different concentrations of copper at 100 kPa [ReBa15]

4.1.5 **Radiation**

In the plasma, most ionizations result from inelastic collisions where a free electron e^- transfers to an atom X an amount of energy which is at least higher than the ionization energy of this atom. The result is an ion and an additional free electron:

$$X + e^- \rightarrow X^+ + 2\ e^-$$

If the energy is not sufficient, no ionization occurs, the atom is excited with a quantity of energy ΔW, and an electron jumps to a higher-bound level:

$$X + e^- \rightarrow X^* + e^- - \Delta W$$

By jumping back to a lower-bound level, a photon at the frequency f_P is emitted.

$$X^* \rightarrow X + h_P\ f_P$$

This is called a bound-to-bound transition and the resulting photon energy or wave-length depends on the difference of energy involved in the electron jump. The relation energy – wave length is given by Planck's law and the energy levels are described by Bohr's atomic theory. For simple atoms like hydrogen and helium, the number of spectral lines is limited, but for heavier atoms, the number of possible transitions increases with the atomic number.

These discrete transitions between bound states result in spectral lines and their intensity per unit of volume can be expressed by:

$$I_f = N_m \; A_n^m \; h_P \; f_P \qquad (24)\ \text{[Rie67 (p39)]}$$

where N_m is the density of atoms excited at the level m and A_n^m is the transition probability from m to n. The total radiation power of the spectral lines can be estimated with the mean transition probability $\overline{A}_L$, the mean excitation energy $\overline{W}$ [ChPo72], and the pressure p:

$$\dot{q}_L''' = \overline{A}_L \; \frac{p}{T} \; e^{-\overline{W}/k_B T} \qquad (25)\ \text{[Rie67 (p39)]}$$

The arc plasma is a thermal plasma and the other radiation phenomena, the Bremsstrahlung and the electron-ion recombination, result in a continuous spectrum. For plasma with a low ionization level, which is the case at low arc currents below 20 A and column temperatures below 10,000 K [Rie67 (p43), Mae51 (p304)], the radiated power from the recombination can be estimated by:

$$\dot{q}_R''' = \overline{A}_R \quad p \quad e^{-\overline{W_i}/k_B T} \qquad (26)\ \text{[Rie67 (p40)]}$$

where $\overline{A}_R$ is the recombination probability and $\overline{W_i}$ the mean ionization energy.

At high plasma temperatures where the gas ionization is complete, the recombination probability is very low and the Bremsstrahlung becomes predominant. Its power density can be approximated with:

$$\dot{q}_B''' = 1.4 \; 10^{-40} W m^3 / K^{0.5} \; Z^2 \; n_e \; n_i \; \sqrt{T} \qquad (27)\ \text{[Rie67 (p40)]}$$

where Z is the degree of ionization.

Determining all transition probabilities and summing all contributions from the different transitions is virtually impossible; in most cases, the radiated power is directly measured. The emitted radiation of an electrical arc is mostly in the ultraviolet domain and a part is reabsorbed by the colder regions surrounding the arc. This is the case with arcs at low currents and atmospheric pressure which are optically thick to these radiations. Hence, the contribution of radiation to energy dissipation is often neglected. For high current arcs, this simplification is not possible. Latham [Lat80] showed that the proportion of radiated power in low-current arcs (below 30 A) is lower than 1 %. Above 100 A, the radiated power becomes predominant: at 1500 A, the measured radiated power represents 99.8 % of the power losses.

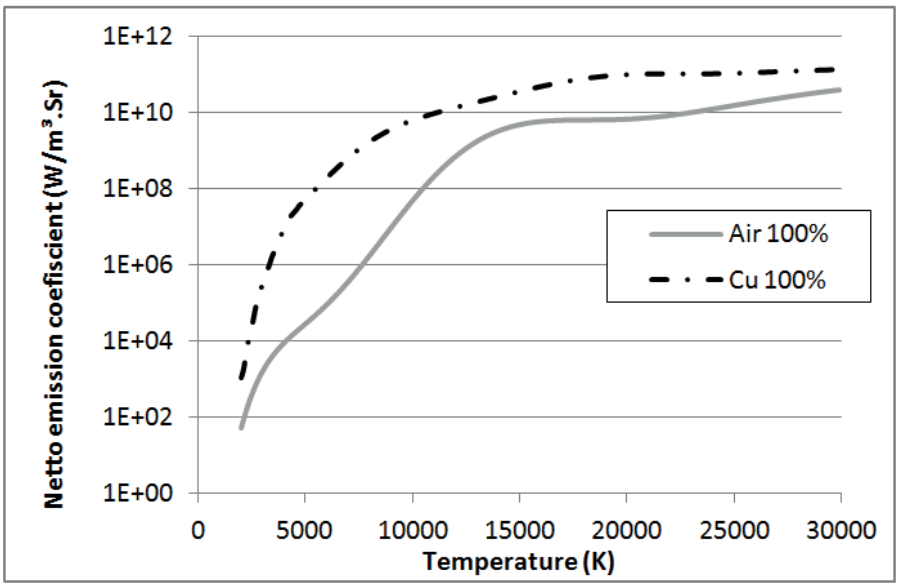

Figure 41: Net emission coefficient of air and copper vapor at 100 kPa [ReBa15]

The radiated power per cubic meter and steradian is called the net emission coefficient (NEC) [Low74, BCTG12]. Figure 41 displays the value of the NEC for air and copper vapor at 100 kPa. In contrast to the electrical and thermal parameters of the plasma, the copper concentration has a huge influence on the value of the radiated power: between air and pure copper vapor, the ratio of emitted power can reach 1000.

4.1.6 **Energy density**

The energy content of the plasma at a temperature T is obtained by integrating the specific heat capacity at constant pressure with the temperature and multiplying it by the density:

$$Q'''(T) = \rho(T) \int_{T_0}^{T} c_p(T)\, dT \tag{28}$$

A discrete integration up to 30,000 K with a temperature step of 1 K results in the values displayed in Figure 42 (blue curve). The effect of the variations in specific heat capacity is noticeable with the small peaks at the same temperatures (see Figure 39). The energy density does not increase any more above 7000 K and remains in the range of 1 MJ/m^3. The reason is the decrease of the plasma density with the temperature. In order to reach these energy densities, the plasma volume must be previously heated with a quantity of energy that can be estimated with the equation (29) (displayed with the red curve in Figure 42):

$$Q_H'''(T) = \int_{T_0}^{T} \rho(T)\ c_p(T)\ dT \tag{29}$$

The increasing difference between this accumulated heating energy and the actual energy density is due to the decreasing density of the plasma. Since we are considering here a constant pressure of 100 kPa, the heated plasma must expand and leave the defined volume. This energy is lost to the environment and/or contributes to expanding the diameter of the arc column.

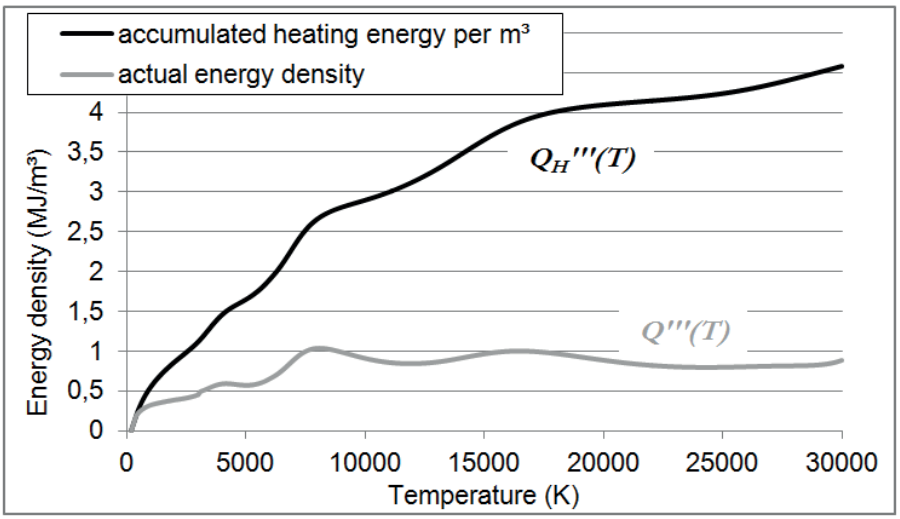

Figure 42: Actual energy density and accumulated heating energy for an air plasma at 100 kPa. Extrapolated from [ReBa15]

4.2 The stationary arc

4.2.1 The different regions of the arc

After initiation, the arc can be sustained if the conditions are favorable. The key factors are the arc voltage and the current. These two parameters are self-influencing and are also dependent on the gap distance, the nature of the isolation medium, and the electrodes. The electrons leave the cathode from a spot and are accelerated by the electric field in the direction of the anode. Very high current densities in the range of 10^2 to 10^7 A/cm² can be obtained and heat the surface at the cathodic spot. A solid and rough cathode surface allows a higher emission of electrons and is beneficial for the stability of the arc. Therefore, the cathodic spot may split into many spots and keep moving at the surface in order to reduce the erosion of the surface asperities [Noa03]. The collisions with the gas molecules support the continuous ionization, sustain the plasma, and increase the diameter of the arc in this region. The cathodic region has a thickness in the range of 10 µm and the voltage drop in this zone is usually between 8 and 20 V. The resulting electric field is in the range of 1.5 MV/m and promotes the field emission of electrons.

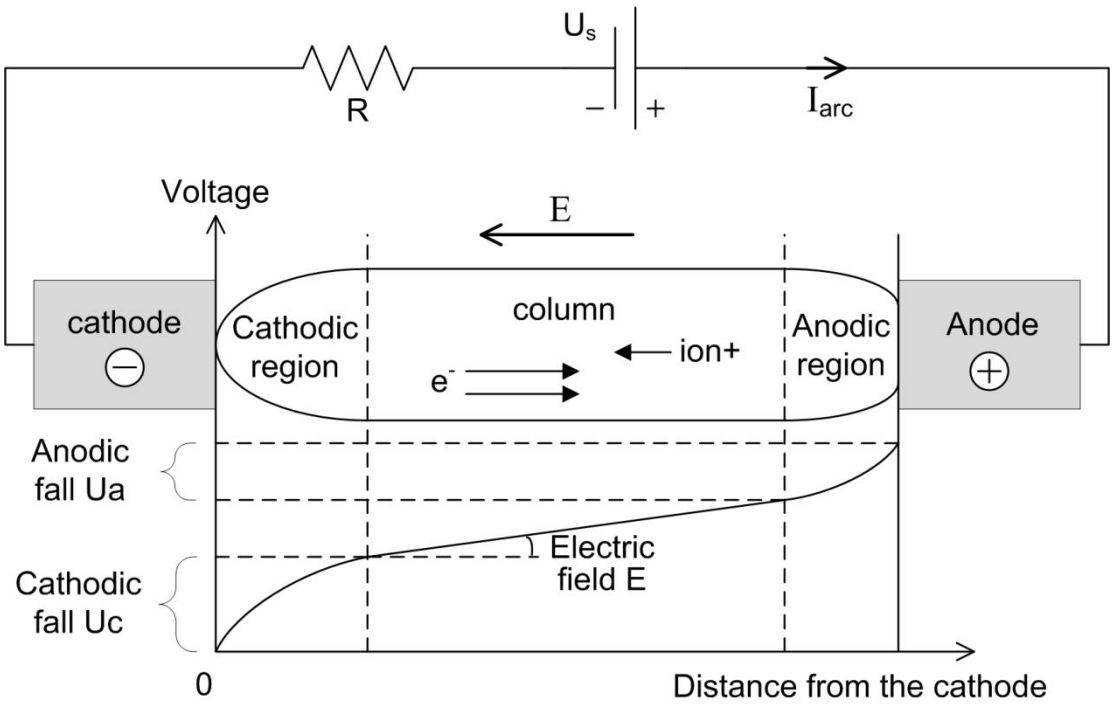

Figure 43: Regions of an arc, voltage drops, and particles in motion

The electrons meet the anode on a wider area and the current densities are usually two orders of magnitude lower than at the cathodic arc root. The thickness of this zone is smaller (~1 μm) and presents a voltage drop of 2 to 6 V. The cathode and anode regions are separated by a long column with a uniform electric field E in the range of 0.8 to 3 kV/m. The temperature of the plasma in the long column is typically an order of magnitude higher than the temperatures of the electrodes and thermal ionization is predominant; the anodic and cathodic regions are transition regions with an important temperature gradient.

4.2.2 The voltage-current characteristic of the arc

The sum of the voltage drops in the three regions is the arc voltage. If the distance between the electrodes is so small that a long column cannot be formed, the arc is called a short arc, otherwise it is a long arc. For a short arc, the arc voltage is the sum of the cathodic and anodic voltages, which represents the minimum arc voltage to sustain the arc. There is also a minimum current limit which is only valid if a sufficient arc voltage and electric field can accelerate the electrons. The minimum current and arc voltage depend on the electrode material, the gas composition, and the pressure. The minimum values at 100 kPa in air are 13 V and 0.45 A for copper and 20 V and 0.01 A for carbon [Bab03 (p546)]. Alternative metals and alloys used in electrical installations such as brass, tungsten, aluminium, and silver have similar minimum arc voltages as copper. For this reason, it is not possible to have arc fault issues in board systems with a 12 V DC supply. Conditions that are more favorable for arcing can be found in vehicles with a 48 V DC supply. For the common AC low-voltage systems with rated voltages from 120 V to 690 V and photovoltaic equipment with up to 1500 V DC, the arc faults represent a real fire hazard. It is noticeable that carbon, the only non-metal material from this list, differs greatly with the highest minimum arc voltage of 20 V and the lowest minimum arc current of 10 mA. Carbon is an efficient thermionic emitter of electrons and is likely to be found in the vicinity of the arc fault (directly at the gap or on the surface of the electrodes). This is, for example, the case of arc faults involving carbonization of an insulation material. The relation between arc current, voltage, and gap distance was studied intensively and several empirical equations were proposed to describe it [Com27, Ayr03]. The most famous is the equation proposed by Ayrton:

$$U_{arc} = a + b\ \ gap + \frac{c + d\ \ gap}{I_{arc}} \qquad (30)\ \text{[Ayr03 (p184)]}$$

where U_{arc} is the arc voltage, I_{arc} the arc current, *gap* the gap distance, *a*, *b*, *c*, and *d* constants. For carbon electrodes and air, Ayrton obtained the values *a* = 38.88 V, *b* = 2.074 V/mm, *c* = 11.66 V A, *d* = 10.54 V A/mm. Voltage *a* corresponds to the minimum arc voltage of the carbon electrode system used by Ayrton and factor *b* to the electric field of the long column. Factors *c* and *d* are used to describe the current dependency. Figure 44 displays the theoretical arc voltage obtained in air and with carbon electrodes.

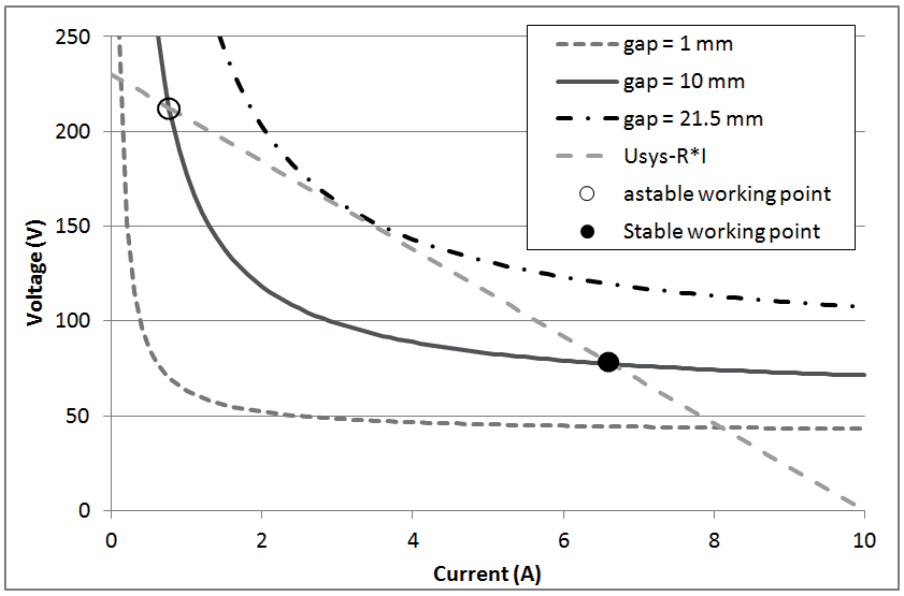

Figure 44: Voltage-current characteristics of stable arcs at different gap distances between carbon electrodes according to the equations of Ayrton [Ayr03]. Representation of the working points in a circuit at the system voltage
U_{sys} = 230 V DC, load R = 23 Ω, and gap = 10 mm

The arc voltage-current equation can be further optimized to take into account the influence of many parameters like the nature of the isolating medium, the geometry of the system, or the cooling power. These equations are static and only valid for stationary arcs at DC supply voltage and as long as the arc does not significantly modify its environment (for example if the electrodes material melts or the arc with the convection moves). They can also be used to describe the electrical parameters of arcs at AC current if the period is much bigger than the time constant of the arc [Rie67 (p119)].

4.2.3 **The arc in the electrical circuit**

The electric arc can be considered as an impedance dependent on current and gap distance that interacts with the complete electrical circuit [Noa03 p(280-283)]. The arc resistance and power can be expressed by:

$$R_{arc} = \frac{U_{arc}}{I_{arc}} = f(I_{arc}, gap) \tag{31}$$

$$\dot{q}_{arc} = U_{arc} \quad I_{arc} \tag{32}$$

The arc requires a defined resistance in series to remain stable. If the arc burns in a circuit at a system voltage U_{SYS}, with a resistance R in series, and a negligible inductance, the arc voltage can be expressed by:

$$U_{arc} = U_{SYS} - R \;\; I_{arc} \tag{33}$$

There are only two possible working points for the arc: where the parabolic current-voltage characteristic intersects with the $U_{SYS} - R \;\; I_{arc}$ curve as represented by black and white dots in Figure 44. The stable working point is the one at the highest current level (black dot). Under these conditions, any small current change Δi results in a reaction of the arc to mitigate the change and restore the electrical parameters of the working point. For example, a small current increase will result in a voltage difference between the real voltage of the arc (which follows its voltage-current characteristics) and the theoretical arc voltage that can be sustained by the circuit. This leads to a higher impedance of the arc, an automatic decrease of the current, and a return to the stable working point. The same compensation takes place if there is a small decrease in current. The second working point (white dot) is not stable: an increase in current will lead to a quick transition to the stable working point and a decrease in current will result in the extinction of the arc. While the gap distance increases, the arc voltage-current is shifted, but the circuit characteristic remains unchanged. If only one single working point is available, the breaking distance of the arc is reached (at gap = 21.5 mm in Figure 44), and any further separation or current decrease will lead to the extinction of the arc [Rie67]. If a load is placed in parallel with the arc, the current provided by the system will be shared between the arc and this additional load. This will result in a shift of the arc working point. If the bypass current is too high, the power supplied to the arc will not be sufficient any more to maintain it at this given distance and the arc will extinguish. The static

arc characteristics and the description of the stable working point are only valid for stable arcs without any quick changes or disturbances. At quick variations, the dynamic nature of the arc must be taken into account. The arc is mainly a thermal process and the electrical conductivity is strongly temperature-dependent. The heat capacity acts as a damper of the thermal and also electrical variations. If the thermal and electrical characteristics of an arc present significant variations, which can be the case in series arc faults at AC applications, a dynamic model is necessary to describe the arc (see part 8.3.3.1).

5 Basics of combustion and considerations on the flammability of electrical cables

Comparing the hazards of different types of electrical faults requires an estimate of their ability to ignite a flammable material and sustain the combustion to spread the fire. The physical rules involved in the ignition and combustion processes must first be understood. The primary rule is the fire triangle as displayed in Figure 45. Three conditions must be fulfilled to start and maintain a combustion reaction: a source of heat, a fuel, and an oxidant in sufficient quantities. The oxidant is the oxygen from the air and it is always available. The heat source can be any component within the electrical circuit. In the case of an electrical fire, the material that is ignited first must be close to the electrical parts and this is in general the electrical insulation. The majority of the flammable insulation materials used in low-voltage applications are polymers. This is the reason why this chapter focuses on the processes involved in the combustion of these materials.

Figure 45: Fire triangle [Tro90 (p12)]

The combustion reaction takes place in the flame in the gaseous phase [Bab03 (p540-548), HoPr01 (p1-9)]. A solid polymer cannot burn directly. The heat must first pyrolize the surface of the polymer and generate a flammable fuel that can mix with the air (see Figure 46). The air-fuel mixture is ignited if the temperature is sufficient to initiate the combustion reaction. This reaction that involves free radicals is exothermic and produces heat in addition to the primary external heat source. If the heat feed-back from the flame to the pyrolized surface of the polymer is sufficient, the combustion can continue even if the primary external heat source is removed. Soot is produced if the fuel is not completely consumed. The

incandescence of the soot particles emits light in the visible domain and gives the flame its coloration.

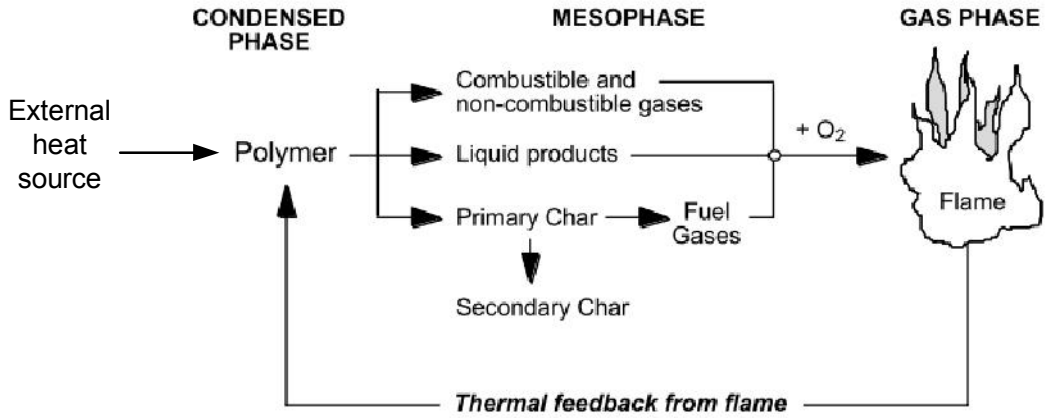

Figure 46: Phenomenology of polymer burning as described in [Tr090 (p16), FAA05 (p8)]

5.1 Polymers used in low-voltage equipment

The excellent performance and ease of production of polymers make them preferred components in the majority of objects that we find in our everyday life. The properties of insulation and mechanical flexibility are the main reasons for their use in electrical equipment. Despite the benefits provided by the use of polymers, many disadvantages exist: use of fossil resources, recycling difficulties, and toxicity. The flammability of these organic materials is also a problem that manufacturers try to reduce depending on the application. Polymers are chemical compounds or mixtures of compounds that consist of repeating structural units, namely, monomers [Cro06]. The formula of poly(vinyl chloride) (PVC) and polyethylene (PE) [Wyp12 (p336&592)] can be expressed as:

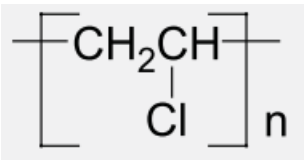

for PVC

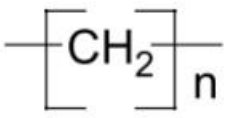

for PE

The monomer is depicted within the brackets. The number n of monomers usually exceeds many thousands: the polymer macromolecule has a huge size and molar mass. The polymers

are seldom used in pure form: colorants, fillers, softeners, and additives are incorporated to save costs and add the necessary functionalities to the materials. Additional processes such as cross-linking or vulcanization may also modify the properties of the materials.

Polymer type	Generally observed fire performance and specificities	Decomposition temperature	Char yield μ
ABS	Highly flammable / burns readily with dense smoke Use of halogens and PVC to reduce flammability	390 °C	0 %
PA Nylon	Known as self-extinguishing because of dripping Flammability may increase if reinforced with fibers	350-411 °C	4 %
PBT	Burn with smoky flame accompanied by dripping, melting, and little char formation	382 °C	7 %
PC	Reduced flammability with significant char formation	476 °C	25 %
PE	Burn readily with dripping and melting Low smoke and char Better performance with cross-linking and fire retardants	399-411 °C	0 %
PP	Burn readily with dripping and melting Low smoke and char	354 °C	0 %
PPO	Low flammability / Char forming polymer	441 °C	25 %
PVC	Low flammability Release of irritant and corrosive gas	249-273 °C	8 %

Table 5: Fire performance observed in general for pure polymers [LAN83 (p33-57)], decomposition temperatures, and char yield [FAA05]

The polymers that are commonly used in electrical equipment for low-voltage installations in Europe were identified by an internet research. It shows that the main polymers used for the insulation of conductors are the soft PVC and the PE. Polyamide (PA 4.6 or 6.6), poly(phenylene oxide) (PPO), poly(butylene terephtalate) (PBT), and polycarbonate (PC) are used for terminals, connector blocks and housings. Poly(acrylonitrile-co-butadiene-co-styrene) (ABS) and thermoplastics are also used often for housings. Table 5 displays the behavior of these polymers that are usually observed if they are exposed to heat. The decomposition temperatures, while the pyrolysis and generation of flammable gases start, can vary from 249 °C for PVC to 476 °C for PC.

5.2 Decomposition process and residues

Polymers start to dissociate and release gases if sufficient energy is provided. The required energy is called the enthalpy of gasification of the fuel L_g which is the sum of the stored energy in the material, the enthalpy of fusion for semi-crystalline polymers, the enthalpy of bond dissociation and of vaporization. Many polymers are not completely dissociated into a gas. A fraction μ of charred residue, also called char yield, may remain during and after combustion (see right column of Table 5). Depending on the type of polymers, the formation of char may strongly vary. Those polymers with a high carbon-to-hydrogen ratio (C/H), especially with aromatic cycles, produce more char. Inserted additives such as fillers (e.g. CaCO3) may remain as ash during combustion: these ashes do not contain carbon. Polymers in pure form with a low C/H ratio such as PE or PP burn completely and do not leave any char. The formation of char and ash is a phenomenon that retards or inhibits sustained combustion. The fraction of polymer which remains as ash is not released in the form of volatile fuel and results in a poorer fuel-air mixture. The ash may also act as a barrier between the external heat source and the polymer and reduce the heat flow to the intact polymer. In addition, the higher viscosity of the mesophase with solid residue may inhibit the transfer of fuel from the decomposed polymer to the air. The formation of char is a strategy used by the manufacturer to improve the fire properties. If residues are formed, the enthalpy of gasification of the solid polymer is:

$$h_g = L_g \ (1 - \mu) \qquad (34)\ [\text{FAA05}]$$

where L_g is actually the enthalpy of gasification of the vaporizable part of polymer. The enthalpy h_g is for most polymers in the range of 1.5 to 2.5 kJ/g. The resulting evaporation rate of the polymer is:

$$\dot{m}'' = \frac{\dot{q}''_{ext} - \dot{q}''_{loss}}{h_g} \ (1-\mu) \qquad (35)$$

where $\dot{q}''_{ext}$ is the heat flow from the external heat source and $\dot{q}''_{loss}$ the surface losses dissipated in the environment.

5.3 Combustion reactions

The combustion reactions of the fuel released by polymers in decomposition involve active radicals. The initiation takes place with the formation of radical hydrogen from the fuel molecule RH [Tro90 (p17), FAA05 (p3)]:

$$RH \xrightarrow{k_1} R + H$$

By reacting with the oxygen in the air, the radical hydrogen produces two new radical hydroxyl and oxygen:

$$H + O_2 \xrightarrow{k_2} OH + O$$

The recombination of these radicals with carbon monoxide and dihydrogen produces most of the heat in the flame. Water and carbon dioxide are produced and the new radical hydrogen can react again:

$$OH + CO \xrightarrow{k_3} CO_2 + H$$

$$OH + H_2 \xrightarrow{k_4} H_2O + H$$

The role of the radical hydrogen may be terminated if it is associated with the dioxygen and forms a molecule which is less reactive:

$$H + O_2 \xrightarrow{k_5} HO_2$$

The presence of halogen atoms (X) such as chlorine or bromine in the polymer decreases the intensity of the flame by capturing the radicals and reduces the reactivity of the mixture:

$$H + HX \xrightarrow{k_6} H_2 + X$$

$$OH + HX \xrightarrow{k_7} H_2O + X$$

The evolution of the combustion depends on the proportion of fuel and the reaction rates k_i. If the reactions producing active radicals dominate the reactions of termination and inhibition, the combustion is sustained and only limited by the flux of fuel from the polymer degradation.

5.4 Ignition and burning

The combustion reaction can only take place if the energy balance is favorable. This is the case if the generation of power in the flame is at least greater than the rate of power losses from convection, conduction, and radiation. This state is reached if a sufficient density of energy Q''' is obtained. This energy density is almost independent from the nature of the flammable material and is on average 1.9 MJ/m^3 [FAA05]. For an air-fuel mixture at atmospheric pressure, this state corresponds to a temperature of 1600 K. The minimum energy density can also be expressed as a function of the vapor density ρ_f, the heat of complete combustion of the fuel h_c^0, and the lower flammability limit LFL. The LFL is the lowest volumetric fraction of fuel in the fuel-air mixture that can sustain the ignition.

$$Q''' = \rho_f \; h_c^0 \; LFL \tag{36}$$

[FAA05 (p18), Tur12 (p293-295)]

The heat of complete combustion h_c^0 is the energy released if the fuel undergoes a complete combustion with carbon dioxide and water as end products. It can be calculated by the product of the heat of complete combustion of organic fuel per mass of oxygen (~13 kJ/g) and the stoichiometric quantity of oxygen to react with the carbon and hydrogen atoms of the monomer. The values are in the range of 10 to 45 kJ/g since the composition of the fuel produced during the pyrolysis strongly differs between the polymers. The combustion of the fuel gases is not necessarily complete. The combustion efficiency χ is the ratio between the effective heat of combustion HOC and the heat of complete combustion h_c^0.

$$HOC = h_c^0 \; \chi \tag{37}$$ [FAA05 (p18)]

Combustion efficiency is almost 100 % for polymers with a low C/H ratio such as polyethylene. Polymers with a high C/H and polymers containing fire retardants (halogen) have much lower combustion efficiencies (59 % for flexible PVC, 38 % for ABS with fiber glass). A low combustion efficiency results in the generation of smoke and toxic gases.

A sufficient fraction of fuel for combustion can be obtained if the pyrolysis releases enough flammable fuel. The corresponding critical mass flow or evaporation rate of fuel at the lower flammability limit LFL is:

$$\dot{m}''\Big|_{ign} = \frac{HRR}{h_c^0} \qquad (38)\ [\text{FAA05 (p18)}]$$

where HRR is the heat release rate which represents the heat release per unit of polymer surface during the combustion. The lowest HRR is obtained at LFL and varies in the range of 13 to 35 kW/m. The corresponding critical evaporation rate for ignition is in the range of 0.6 to 2 g/m^2 s.

Polymers have low thermal conductivities in the range of 0.2 W/m K and high specific heat capacities (in general above 1 kJ/kg K). They can be considered as thermally thick with common thicknesses used for the insulation of electrical conductors. The equation (39) is adequate to estimate the time to ignition of a thermally thick object:

$$t_{ign} = \frac{TRP^2}{\left(\dot{q}''_{ext} - \dot{q}''_{loss}\right)^2} \qquad (39)$$

[FAA05(p21), MoGi06 (p71)]

The term TRP is the thermal response parameter which is a function of the material properties:

$$TRP = \frac{\sqrt{\pi\ \rho\ \kappa\ c}}{2}\ \left(T_{ign} - T_{AMB}\right) \qquad (40)$$

[FAA05 (p21), MoGi06 (p71)]

where ρ is the density, κ the thermal conductivity, c the specific heat capacity, T_{ign} the ignition temperature, and T_{AMB} the initial and ambient temperature of the polymer.

5.5 Steady and unsteady burning

After initiation of the combustion reaction, a fraction of the heat generated by the flame is radiated to the polymer surface in addition to the external heat. This accelerates the pyrolysis and the evaporation of flammable gases. The heat release rate HRR increases and becomes stabilized in general at 2 to 3 times the HRR at the ignition point. At steady burning, the HRR is:

$$HRR = \chi\ h_c^0\ \dot{m}'' = \frac{\chi\ h_c^0}{L_g}\ \left(\dot{q}''_{ext} + \dot{q}''_{flame} - \dot{q}''_{loss}\right) \qquad (41)\ [\text{FAA05 (p22)}]$$

The ratio of the heat of combustion HOC to the heat of gasification is a key parameter called heat release parameter HRP:

$$HRP = \chi \ (1-\mu) \ \frac{h_c^0}{h_g} \qquad (42)\ [\text{FAA05 (p23)}]$$

The HRP of the highly flammable polyethylene is approximately 21. This means that during combustion, 21 J of heat is dissipated for each Joule that was used for the pyrolysis of the polymer. Flexible PVC is much less flammable with a HRP of 4.

The heat release rate can be split in 2 terms:

$$HRR = HRP \ \dot{q}''_{ext} + HRP \ \left(\dot{q}''_{flame} - \dot{q}''_{loss}\right) = HRP \ \dot{q}''_{ext} + HRR_0 \qquad (43)\ [\text{FAA05 (p24)}]$$

The first term of the equation is the forced heat release rate that represents the fraction of heat release due to the external source. The second term, HRR_0, is the unforced heat release rate corresponding to the fraction of heat release from the combustion reaction. If the external heat source is removed ($\dot{q}''_{ext} = 0$), the polymer will self-extinguish if:

$$HRR_0 < HOC \quad \dot{m}''_b = HRR^*_b \qquad (44)\ [\text{FAA05}]$$

where $\dot{m}''_b$ is the critical mass flux and HRR^*_b the critical HRR for the sustained burning of the polymer. Most polymer compounds used as insulation have a high HRR^*_b and can self-extinguish quickly.

5.6 Flame power

If the insulation burns, the flame heats the insulation in addition to the external source and this contribution must be taken into account in the calculation of the evaporation rate. The power radiated by a flame with well-distributed temperature T_F can be calculated with the Stefan-Boltzmann equation:

$$\dot{q}_{F,rad} = A_F \ \varepsilon \ \sigma_{SB} \ \left(T_F^4 - T_{AMB}^4\right) \qquad (45)\ [\text{Fen95}]$$

where A_F is the surface of the flame, ε the flame emissivity, σ_{SB} the Stefan-Boltzmann constant, and T_{AMB} the ambient temperature. The surface A_F, length L_F, and volume V_F of the flame depend on the flame power and diameter D_F of the base of the flame. For a vertical flame with a cylindrical shape, these dimensions are:

$$A_F = \pi \; D_F \; \varepsilon \left(\frac{D_F}{2} + L_F \right) \qquad (46)\ [\text{Fen95}]$$

$$V_F = \frac{\pi \; D_F^2 \; L_F}{4} \qquad (47)\ [\text{Fen95}]$$

$$L_F = a \; \dot{q}_F^{2/5} - b \; D_F \qquad (48)\ [\text{Fen95}]$$

where flame power $\dot{q}_F$ must be expressed in kW. The constants $a = 0.23 \, / \, kW^{2/5}$ and $b = 1.02 \, / m$ are valid for the range $7 < \dot{q}_F^{2/5} / D_F < 700 \; kW^{2/5} / m$. If we assume $D_F = 2 \; r_2 = 6 \; mm$ (the size of the exposed PVC insulation in our model presented in 6.1.1.1), this condition is fulfilled for flame powers from 0.36 W to 36 kW.

The flame emissivity is obtained with an equation based on the effective emissivity coefficient K and the mean beam length $\overline{L}_B$:

$$\varepsilon = 1 - \exp\left(- K \; \overline{L}_B\right) \qquad (49)\ [\text{Fen95, Dry11 (p77)}]$$

$$\overline{L}_B = 3.6 \; \frac{V_F}{A_F} \qquad (50)\ [\text{Fen95}]$$

Responsible for the emission of light in a flame are the soot particles: the emissivity coefficient is directly related to the concentration of soot particles. Unfortunately, there are very few values of this coefficient in the literature and no information was found for the combustion of PVC. The values for the combustion flame of three polymers are provided in Table 6. There is a clear relationship between the emissivity coefficient and combustion efficiency: a low combustion efficiency is mainly due to the generation of soot, thus increasing the emissivity. Since the flexible PVC used for cable insulation has a combustion efficiency of 0.59, it can be assumed that the effective emissivity coefficient for PVC is slightly greater than the value of 5.3 /m for PS (the value of 6 is used in part 6.1.1.3). The PVC burns with a yellow flame and the flame temperature will be in the range of 1250 K [Dry11 (p60)].

Polymer	Flame temperature T_F (K) [Fen95]	Emissivity coefficient K (/m) [Fen95]	Combustion efficiency χ (kJ/kJ) [FAA05]
PMMA	1400	1.3	0.99
PP	1350	1.8	0.97
PS	1190	5.3	0.66

Table 6: Flame temperature, emissivity coefficient, and combustion efficiency of PMMA, PP, and PS

The radiated power of the flame in the direction of the polymer surface can be estimated with this equation:

$$\dot{q}_{F,rad\to INS} = A_{INS} \ \varepsilon \ \sigma_{SB} \ \left(T_F^4 - T_{INS}^4\right) \tag{51}$$

with A_{INS} the exposed surface of insulation and T_{INS} the surface temperature of the insulation that is assumed to be equal to the decomposition temperature (see Table 5). Figure 47 displays the radiated power to the environment and to the insulation surface for a flame power up to 1 kW. The radiated power to the environment increases with the flame power, but the radiated power to the insulation surface remains almost constant: as the power of the flame increases, length L_F of the vertical flame increases too, thus increasing the mean distance between the radiating volume and the constant exposed surface A_{INS}. The radiated power to the insulation will increase if the surface of the insulation is vertical. The equation (35) can be updated with the additional radiated power from the flame to the insulation:

$$\dot{m}'' = \frac{\dot{q}''_{ext} + \dot{q}''_{F,rad\to INS} - \dot{q}''_{loss}}{h_g} \ (1-\mu) \ \text{ with } \ \dot{q}''_{F,rad\to INS} = \frac{\dot{q}_{F,rad\to INS}}{A_{INS}} \tag{52}$$

Finally, the flame power can be estimated with the equation (53) whereas the contribution of $\dot{q}''_{F,rad\to INS}$ is nearly constant and independent of the flame power $\dot{q}_F$:

$$\dot{q}_F = \frac{A_{INS} \ \chi \ h_c^0 \ (1-\mu)}{h_g} \left(\dot{q}''_{ext} - \dot{q}''_{loss} + \dot{q}''_{F,rad\to INS}\right) \tag{53}$$

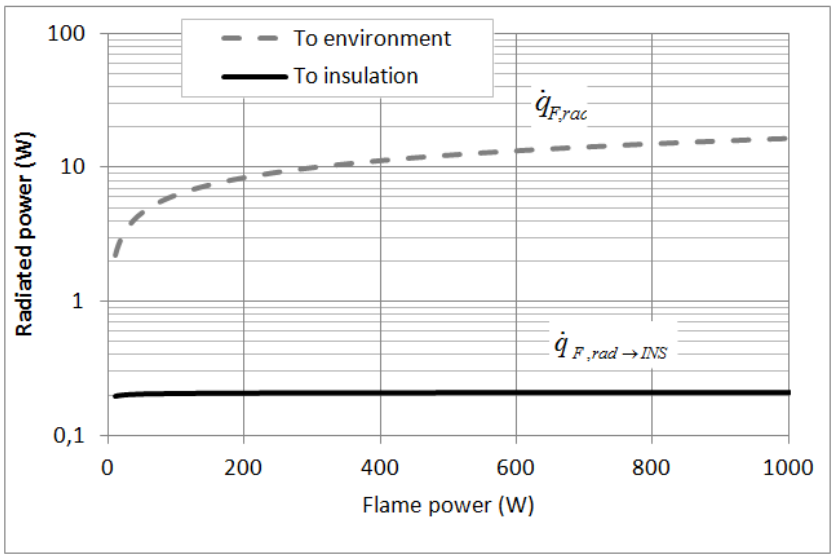

Figure 47: Radiated power from the flame as a function of the flame power (PVC combustion with vertical flame and horizontal probe surface, D_F = 6 mm, K = 6 /m, and T_{INS} = 522 K)

5.7 Requirements and standard tests for electrical wiring

5.7.1 Testing the flame resistance of electrical polymers

The standard test methods involve different types of heat sources. A glowing wire with increasing temperature is used in IEC 60695-2-12 [IEC10a], IEC 60695-2-13 [IEC10b], and ASTM D 3874-12 [AST10a]. In IEC 60695-11-10 [IEC04] and UL 94 [UL12a], a flame with a power of 50W is applied on a horizontal sample. The burning rate (velocity of the flame on the surface) is measured and must be below a maximum value depending on the thickness of the sample. If this criterion is fulfilled, the HB performance level is reached. A similar test is performed on a vertical sample: the flame is applied during a limited time and the capability to self-extinguish is determined by measuring the duration of burning. Performance levels V0 (the best), V1, and V2 (the worst) are defined. Electrical discharges are also used as heat sources: in the UL 746A [UL12b], the ignition time is measured during the application at the surface of the material of arcs at 32.5 A / 240 V AC and low current discharges at 2.36 mA / 5200 V AC.

5.7.2 Requirements for the flame resistance of cables and other insulation parts

The majority of the fire resistance requirements for electrical equipment in UL [UL01, UL10] and DIN VDE standards [DIN01] are related to the self-extinguishing property, the limitation of the burning rate, and formation of smoke [GrSe05]. The ability to avoid initial ignition is not taken into account. It seems that the requirements are focused on limiting the spread of the fire and the direct hazard to people. The fact that the material may burn at high thermal stress is considered to be unavoidable. It is also mostly assumed that PVC as an insulation material is flame resistant. This material is even recommended for buildings and installation which present a very high risk of fire [DIN03a] and it is not subject to further flammability testing if it is used in equipment [DIN11]. It is often mentioned that the main reasons for the high flame resistance of PVC-based materials are the high concentration of halogens and the tendency to char. In contrast, our investigations show that PVC can enable sustained series arcs and ignite for the same reason.

5.8 Criteria for estimating the hazards of electrical faults

This thesis considers that the hazard of an electrical fault is related to its ability to ignite the insulation material and continue to generate heat in order to make the combustion sustainable even if the material has self-extinguishing properties. The ability to start, maintain the combustion of a polymer, and possibly spread the fire can be evaluated with the following criteria:

- Heat flow to the insulation

Ignition can only occur if a critical evaporation rate of the fuel is exceeded and the energy density and the temperature of the fuel-air mixture are sufficiently high. It has been considered that the mass flow of fuel is proportional to the heat flow generated by the fault that is oriented to the insulation surface. The temperature of the fuel-air mixture prior to ignition is difficult to estimate, but we can assume that it is also strongly dependent on the heat flow. Therefore, we use this heat flow to the insulation surface as a first criterion. A minimum heat flow of 13 kW/m² [FAA05] is defined as the threshold for the ignition of PVC.

- Temperature of the fault location

The evaporation of flammable fuel can only take place if the ignition temperature of the material is exceeded: the higher the temperature of the fault location, the higher the rate of vaporization of gaseous fuels and the probability of initiating the combustion reaction. The ignition temperature of PVC (318 °C) [FAA05] is used as a threshold value.

- Accumulated energy of the electrical fault

The mixing of fuel with air and the heating of this mixture take time. If we assume that the first two criteria are already fulfilled (heat flow and temperature), these conditions must last long enough and impact a large enough surface to obtain a sufficient energy density in the mixture to reach the ignition point. The combination of power dissipation and the duration at the fault can be an interesting indicator. This criterion corresponds to the accumulated energy of the fault in Joule.

- Duration of the thermal stress

The ignition of the polymer does not necessarily mean that a hazardous electrical fire will start. Most insulation polymers have self-extinguishing properties and the situation can only turn into a dangerous electrical fire if the flame spreads to other flammable materials. Therefore, the danger potential of the electrical fault is much higher if the fault can generate a thermal stress during a time that exceeds the time to ignition.

- Time to ignition

If the temperature and heat flow are sufficient to ignite the insulation, the time to ignition can be determined by the equation (39). If it is shorter than the duration of the thermal stress, the insulation ignites.

- Flame power

In addition to the maximum duration of the fault, the probability of the fire to spread to other materials increases with the power of the flame $\dot{q}_F$. This criterion can be estimated with the equation (53).

The values of these six criteria are analyzed in chapter 6 (see Figure 78) for different types of electrical faults including the series arc faults. The protection devices (MCB, RCD, AFDD) can limit the thermal stresses and their contributions are taken into account.

6 Thermal stresses from electrical faults

All possible electrical faults that would normally generate excessive heat are displayed in Figure 48. Depending on the value and path of the electrical current, four categories of faults are defined:

- The series faults present current values below the nominal current of the circuit and a correct current path: glowing connections and series arcs faults.
- The earth leakage also results in a low current fault, but the current flows from the phase conductor to earth.
- The current of the overload fault takes the correct path, but the current rating of the circuit is exceeded.
- The short-circuit results in over-exceeding the current rating and bypassing the load. It can take two forms: a bolted short-circuit or a parallel arc.

The purpose of this chapter is to analyze these faults, to estimate the thermal stress that they are capable of generating, and to make a comparison with the series arc fault. Other faults where the current flow is not directly responsible for the overheating are not considered in this study. This includes cases of misuse such as excessive thermal insulation, blocking of the cooling slots, insufficient distances between appliances and flammable objects, and technical failures like excessive friction in appliances.

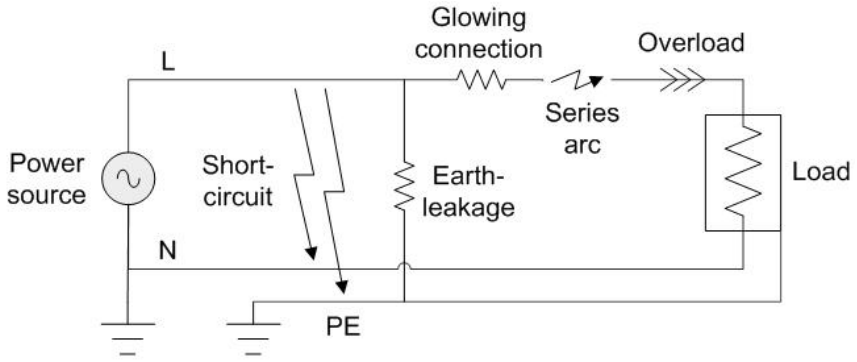

Figure 48: Possible electrical faults in a low-voltage circuit

Standard conditions must be defined for the comparison of the electrical faults. Our approach is to consider a circuit that is representative of a majority of residential branch circuits in Germany:

- Overcurrent protection: MCB rated 16 A, B tripping characteristic, rated breaking capacity of 6 kA and energy limitation of class 3.
- Residual current protection: RCD A type with rated residual operating current of 0.3 A (most of RCDs have a rated residual operating current of 0.03 A for people protection, but we prefer here to use 0.3 A since this value is defined for fire protection)
- Installed cable of type NYM-J according to DIN VDE 0250-204 [DIN00]: three copper conductors with 1.5 mm² cross-section, insulation of the wires and the jacket in PVC (operation permitted up to 70 °C)

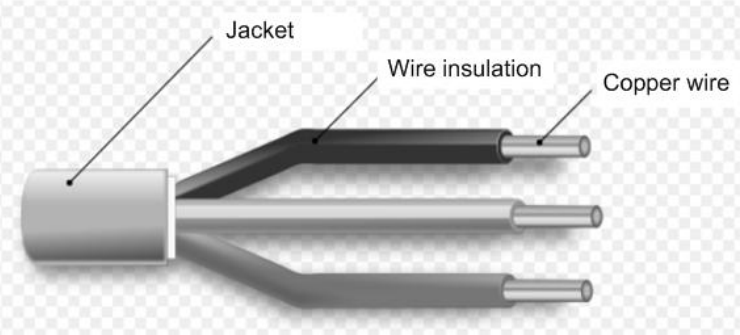

Figure 49: Cable NYM-J 3x1.5 mm²

6.1 Series faults

6.1.1 Series arc fault

Together with the glowing fault, the series arc fault is supposed to represent a very hazardous electrical fault. Recently, arc fault detection devices, AFDD, have been introduced in the markets where IEC standards are applicable. The detection performance at series arcing of the AFDD at 230 V AC is displayed in Table 1 (part 1.5.1). Since the use of the AFDD in electrical installations is not mandatory everywhere, the thermal stresses due to series arcing are estimated for the scenarios with and without AFDD protection. Hence, the contribution of the AFDD to fire protection may be estimated by using this approach.

6.1.1.1 Electrical and thermal model of a series arc fault

The heat generated by a series arc and its effects on the insulation material must be assessed. Direct measurement of the thermal effects of the arc is both time-consuming and resource-intensive, and the introduction of a probe in the system may influence the results. An alternative approach is to realize a simplified theoretical model as presented in [MABB13], verify it with electrical measurements (see 6.1.1.2), and use it to estimate the temperatures and other interesting parameters at the fault location (arc energy, power dissipation to the insulation). The simple geometry displayed in Figure 50 represents a conductor break inside a wire of the NYM-J cable (the rest of the cable with the other conductors and jacket is not represented).

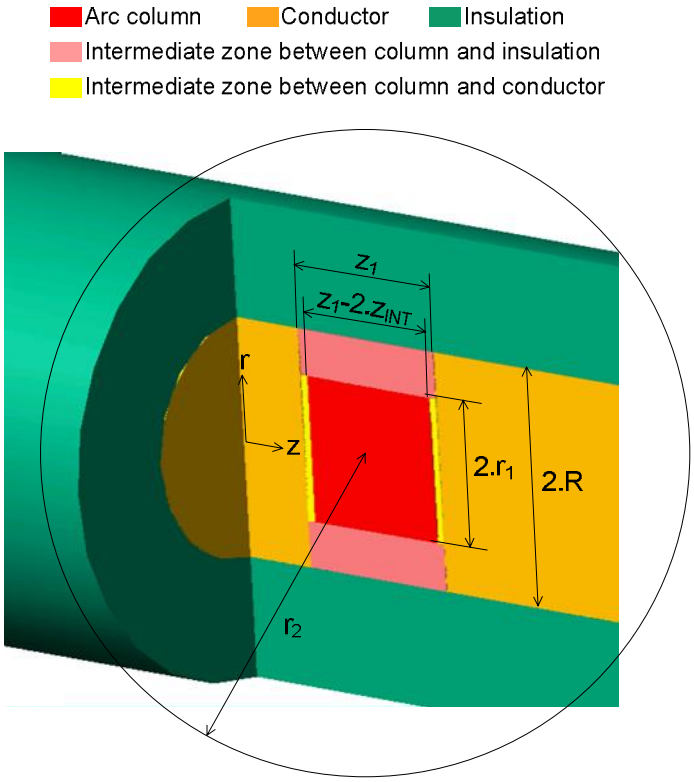

Figure 50: Model geometry of a broken wire with series arc

The conductors are separated by a distance z_J and the arc is divided into three zones, each having the radius r_1: the intermediate zones with thickness z_{INT} that represent the anodic and cathodic domains and the arc column with length z_J-2*z_{INT}. The use of the cylindrical and symmetrical geometry saves computing resources. It was also decided to ignore the differences of the work functions at the anode and the cathode and define the same power dissipation in the intermediate zones according to the equation (54):

$$\dot{q}_{INT} = I_{arc} \ \frac{U_{AC}}{2} \tag{54}$$

where U_{AC} is the sum of the anodic and the cathodic falls. The power dissipated in the column is:

$$\dot{q}_{COL} = I_{arc} \ \left(U_{arc} - U_{AC}\right) \tag{55}$$

The remaining gas volume is the intermediate zone that starts from the arc column and ends at radius R where the insulation is present. This zone presents an important temperature gradient and heat flow from the arc to the insulation. The solid parts (conductors and insulation) are divided into single elements that are very small near the internal elements and become increasingly bigger with distance. This finite-element geometry results in a higher resolution of the physical values in the elements of interest.

The estimate of the arc radius r_1 is based on the canal model described by W. Rieder [Rie67] and the simplified energy balance of the arc expressed with equation (5) in part 4.1.1. After a double integration in the radial direction, the equation becomes:

$$\sigma(T_1) \ E^2 = \frac{\int_{T_R}^{T_1} \kappa \ dT}{r_1^{\,2} \ \ln\left(\frac{R}{r_1}\right)} \tag{56} \text{ [Rie67 (p81)]}$$

where T_1 is the temperature of the arc column and T_R the temperature of the insulation. According to the principle of minimum energy, the power density and electrical field will be as small as possible. This condition is given at an optimal value of the radius r_1 that can be calculated with these equations:

$$\frac{dE}{dr_1} = 0 \tag{57} \text{ [Rie67 (p79-80)]}$$

that results in:

$$r_1 = R \ \exp\left(-\frac{1}{2}\right) \approx 0.606 \ R \tag{58}$$

For a 1.5 mm² massive conductor, we obtain r_1 = 0.425 mm with R = 0.7 mm.

The temperatures in the gaseous elements of the model, the arc zones, and the intermediate zone between arc and insulation, are estimated using the theoretical curves of energy density displayed in Figure 42 of part 4.1.6. For every time interval $\Delta t = t_B - t_A$, the powers generated and lost in these elements (see Figure 51) result in a variation of energy density:

$$\Delta Q'''_H(t_A) = \left(\frac{\left(\dot{q}_{COL}(t_A) + 2 \;\; A_z \;\; \dot{q}''_z(t_A) + A_r \;\; \dot{q}''_r(t_A)\right)}{volume} - \dot{q}'''_{RAD}(t_A) \right) (t_B - t_A) \qquad (59)$$

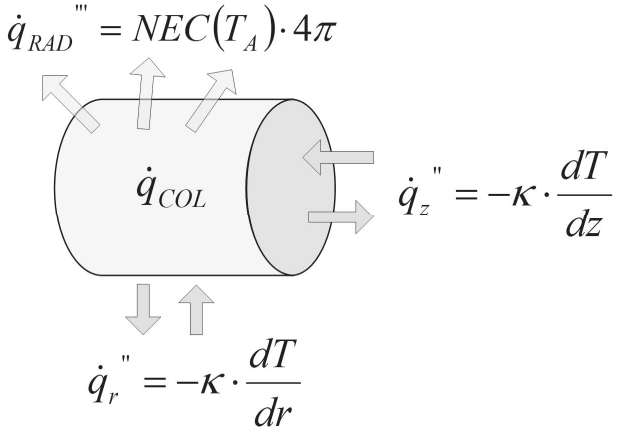

Figure 51: Internal generation of power and losses in the arc column

We consider that the elements have constant dimensions, so the expansion or contraction of the gases at the temperature changes result in mass movements that correspond to an additional heat flow. Therefore, the new temperature of the gaseous element cannot be directly calculated using a linear relation. The temperature change ΔT between times t_A and t_B is estimated using the following method:

- The heating energy calculated in the equation (29) (see 4.1.6) is already known for each temperature and its new value at time t_B after the variation of energy density is:

$$Q'''_H(t_B, T_B) = Q'''_H(t_A, T_A) + \Delta Q'''_H(t_A, T_A) \qquad (60)$$

- The corresponding new Temperature T_B and actual energy density $Q'''(T_B)$ at the time t_B are deduced by means of a graphical method displayed in Figure 52:

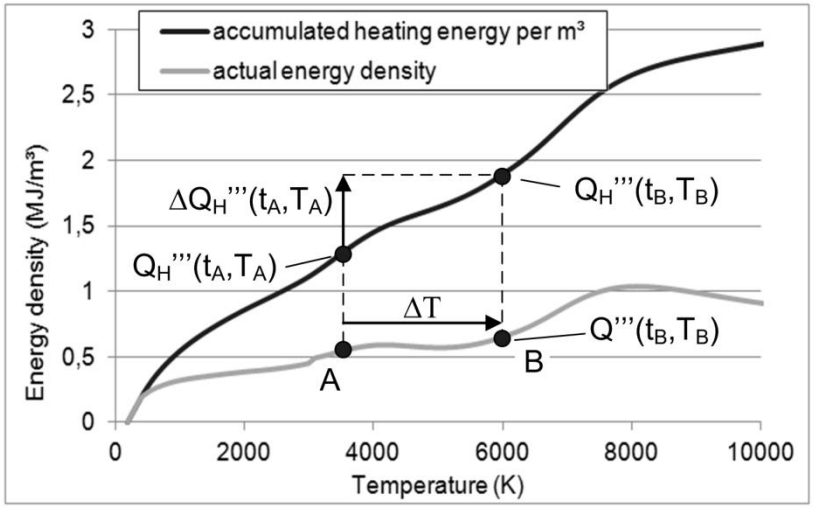

Figure 52: Graphical method for estimating the temperature change as a function of the energy density change

The difference between the initial variation of energy density $\Delta Q_H'''(t_A)$ and the real variation of energy density $Q'''(t_B,T_B) - Q'''(t_A,T_A)$ is lost for the considered element because it leaves its volume in the form of a heated and expanding gas. The first law of thermodynamics is respected by adding the corresponding energy to the next elements, regardless of whether they are gaseous or solid. The portion of energy that is transferred to a next element is proportional to the product of its heat capacity and the available exchange surface with the element that generates the heat flow. This simple method has limitations:

- The pressure in this simple model is constant (100 kPa); therefore the mass transfers between the elements are not damped. This results in numerical instabilities in the calculation and errors as the arc current and power increase. Decreasing the time interval provides a limited improvement and requires significantly greater computing resources: the modelization provided plausible results at arc currents up to 16 A.
- The dynamic changes in the arc are not correctly computed. Only the results after stabilization of the values can be interpreted. This means that after a change, the result can be interpreted after a duration that is significantly bigger than the thermal time constant. This time constant is estimated with the ratio between the energy density and the power dissipation per unit of volume. Its value is in the range of 10 µs according to equation (149). This implies that the rate of rise of the arc power will remain low enough. Many trials show that the value of 200 W/ms (increase of

2 W during a period equal to the time constant) is optimal regarding the computation results and the computation time.

The power transfer between two elements at different temperatures is established by conduction and radiation. Since the system is closed and the time required to ignite the insulation is in the range of the second, the contribution of a natural convection process can be neglected. The determination of the conducted losses is based on the Fourier's law. The values of the thermal conductivities κ of the solids are taken from handbooks [Yaw11]. The theoretical data for plasma provided by [ReBa15] are used for the gases. The heat losses by radiation are calculated with the net emission coefficients provided in 4.1.5. The insulation releases gases as it becomes pyrolized and the cooling effect of the gas must be taken into account. The equation (35) is used to calculate the evaporation rate whereas the term $\dot{q}''_{ext} - \dot{q}''_{loss}$ is replaced by the part of the arc power $\dot{q}_{INS}$ part power that heats the exposed insulation:

$$\dot{m}''_g = \frac{\dot{q}_{INS}}{h_g \ A_{INS}} \ (1-\mu) \tag{61}$$

with

$$\dot{q}_{INS} = \alpha \ (\dot{q}_{COL} + 2 \ \dot{q}_{INT}) \tag{62}$$

α is the proportion of heat flow oriented to the insulation surface. A cooling effect from this evaporation is expected. It was observed in [RSZ11, GBP11] that the gassing reduces the radius and the temperature of the arc column. The vaporized gas at decomposition temperature T_d that reaches the arc column is heated at column temperature T_l, and the necessary additional power is provided by an increase of arc power and arc voltage. This effect increases with evaporation rate $\dot{m}''_g$ and specific heat capacity c_g of the gas [GCT10]. The cooling power resulting from a polymer being degraded on a surface A_{INS} can be expressed with the equation (63):

$$\dot{q}_g = \int_{T_d}^{T_l} c_g \ \dot{m}''_g \ A_{INS} \ dT \tag{63}$$

6.1.1.2 Verification of the model

The computation algorithm is designed to enable a simplified comparison between the calculation based on the model and the measurements. The procedure to verify the model includes many steps that are displayed in Figure 53:

- define the electrical power of the arc $\dot{q}_{ARC}$ as an input variable (initial value is 30 W)
- make a rough estimate of the arc current by dividing the power by a hypothetic initial arc voltage of 50 V
- estimate the power dissipation in the column and in the anodic and cathodic regions with the equations (54) and (55)
- obtain the temperature of column T_1 with the graphical method based on the energy density (see 6.1.1.1)
- obtain the corresponding value of electrical conductivity σ of the plasma at T_1 from the curve provided in 4.1.3
- calculate the electric field of the arc column with equation (64):

$$E(T_1) = \frac{1}{r_1} \sqrt{\frac{\dot{q}_{COL}}{(z_1 - 2\ z_{INT})\ \pi\ \sigma(T_1)}} \tag{64}$$

- calculate the arc voltage and the arc current with equations (65) and (66):

$$U_{ARC} = U_{AC} + E(T_1)\ (z_1 - 2\ z_{INT}) \tag{65}$$

$$I_{ARC} = E(T_1)\ \sigma(T_1)\ \pi\ r_1^2 \tag{66}$$

- increase the electrical arc power at a rate of 200 W/ms
- calculate the new arc current by using the previously calculated arc voltage
- continue the simulation as long as the arc current remains below 16 A

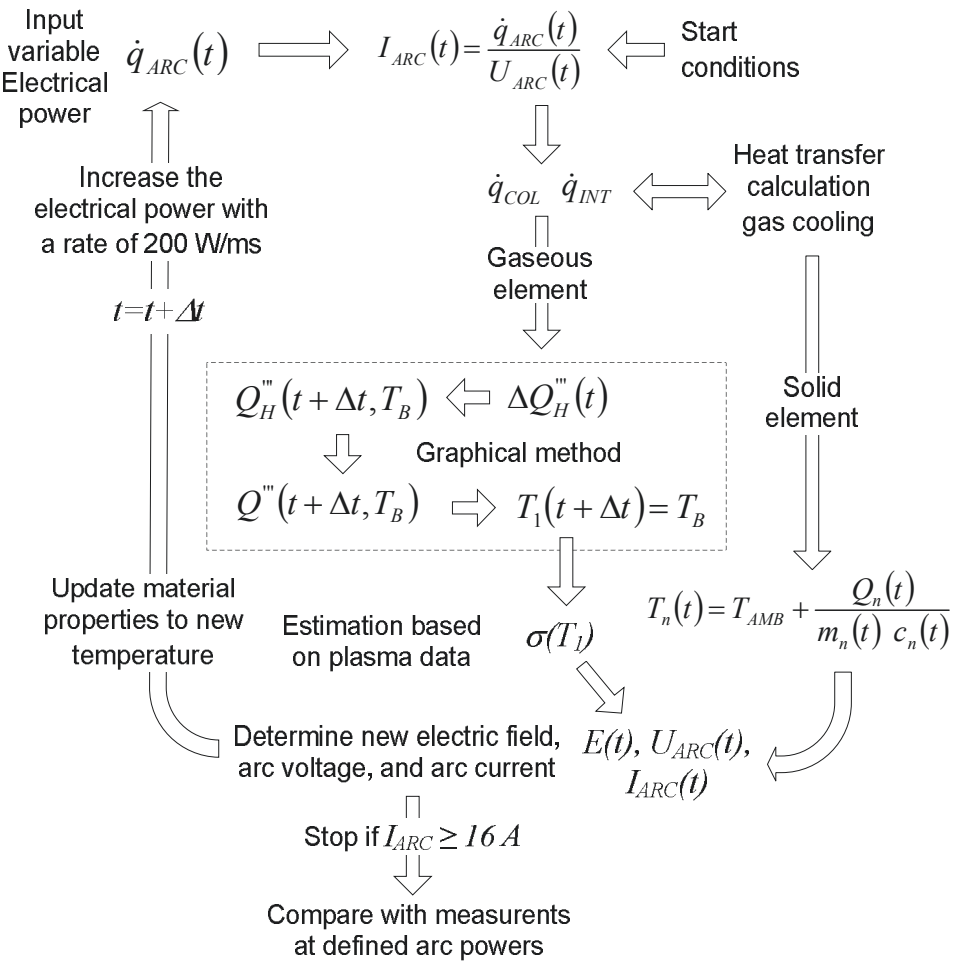

Figure 53: Process to compute the arc electrical data and the comparison with the experimental results

The constant parameters are: U_{AC} = 13 V, r_1 = 0.425 mm, R = 0.7 mm, z_{INT} = 40 µm, Δt = 100 ns, T_{AMB} = 23 °C. The simulations were performed for separation distances z_1 from 0.3 mm to 2 mm and the specific heat capacity of the polymer gases, c_g, was the same as for air. The simulation starts with a first period of heating that lasts 30 µs with a constant electrical arc power of 30 W. In addition, the first elements of the conductors in contact with the arc (thickness of 100 µm) have an initial temperature of 1084 °C (melting point of copper). With these initial conditions, long simulation times to reach a first stable working point can be saved (a single millisecond of simulated time represents nearly 3 hours of computing time). After this initial period, the electrical arc power is steadily increased at a rate of 200 W/ms and the simulations interrupted as soon as the extrapolated arc current

exceeds the value of 16 A. The values of the plasma properties (c_v , κ , σ , and NEC) are updated at each calculation loop for the actual element temperature [ReBa15].

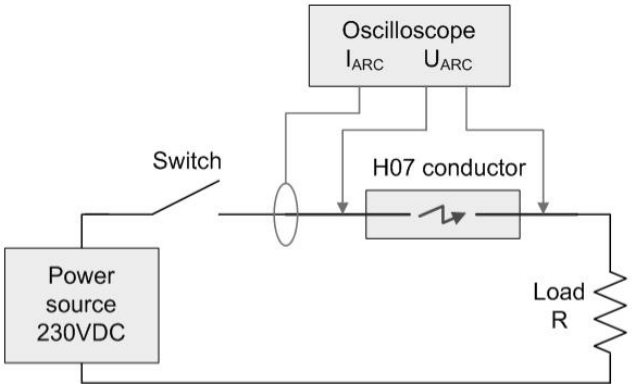

Figure 54: Electrical equivalent circuit of the test setup and picture of a tested sample

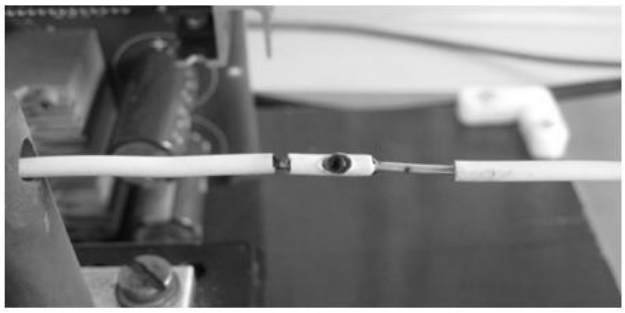

Figure 55: Picture of a tested sample

The experimental setup consists of a H07 type wire (similar to the wires of a NYM-J cable) with 1.5 mm² copper cross-section and PVC insulation placed in series with a resistive load, a switch, and a power source (see Figure 54). The wire is cut, the insulation is removed from the ends, and each conductor piece is tightened on a fixture that can control the gap distance and quickly separate the conductors (within 20 ms) at a defined gap. A piece of insulation is placed at the gap location to cover the conductors. Figure 55 displays such a sample after a test. The arc current and arc voltage are recorded with an oscilloscope at the sampling frequency of 100 kHz. The tests are performed at a supply voltage of 230 V DC in a circuit that has a negligible inductivity. The use of a DC power source allows the initiation of very stable arcs with an excellent reproducibility and is as appropriate as AC power to study the thermal effects of arcing. Measurements were also performed without insulation (only with

air all around the conductors) in order to evaluate the contribution of the gassing in the cooling of the arc column.

Figure 56 displays the measured arc electrical parameters in the form of a voltage-current graph for a separation distance of 1 mm. Because of the gassing and other interactions between the arc and the insulation, the variations are very important and the display of the data results in a fuzzy cloud of points. In order to improve visibility, the data are filtered and only the outer contour of the cloud is displayed. The "230V-R×I" curves (dashed black lines) symbolize the electrical characteristic of the circuit where the stable arc can exist. They all intersect the voltage axis at the supply voltage 230 V DC and intersect the current axis at the available load currents of the circuit (see Figure 44). The black curve symbolizes the calculated arc's electrical characteristics and matches the average working points of the real arcs (red clouds). The green curve corresponds to a simulation without the gas cooling effects (polymer evaporation discarded in the simulation script); the difference between both curves represents the contribution of gas cooling. The contribution of heat conduction to the insulation and evaporation enthalpy is the difference between the green curve and the measurements without PVC insulation (blue clouds). The influence of the separation distance is visible in Figure 57. A longer distance means a longer arc column and a higher arc power. The calculated temperature of the arc column as a function of the arc power is displayed in Figure 58. The values are compatible with the estimates or measurements from other authors [Rie67, Mae51, Lat80]. The gassing results in a temperature decrease of at least 1000 K.

The calculated contribution of radiation to power dissipation is 0.01 % with the net emission coefficients for air and 1.5 % for pure copper vapor. This result is in agreement with the estimates of D. Latham [Lat80]. The results of the simulation model are plausible and match the measurements. Therefore, we consider this model to be appropriate for the simulation of series arc faults at low-voltage and low current (below 16 A).

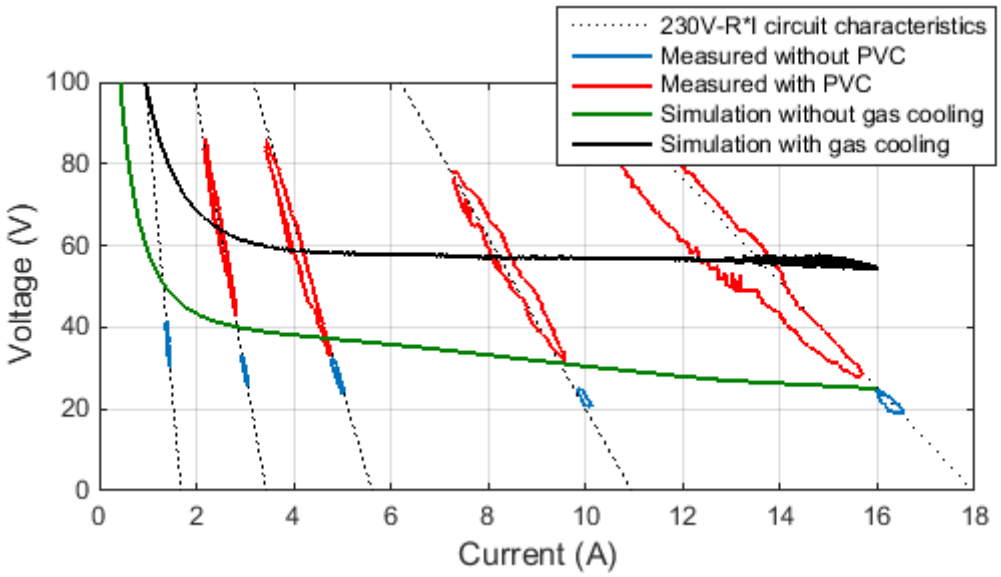

Figure 56: Comparison between measured and calculated arc electrical characteristics. 1 mm distance / Influence of load impedance.

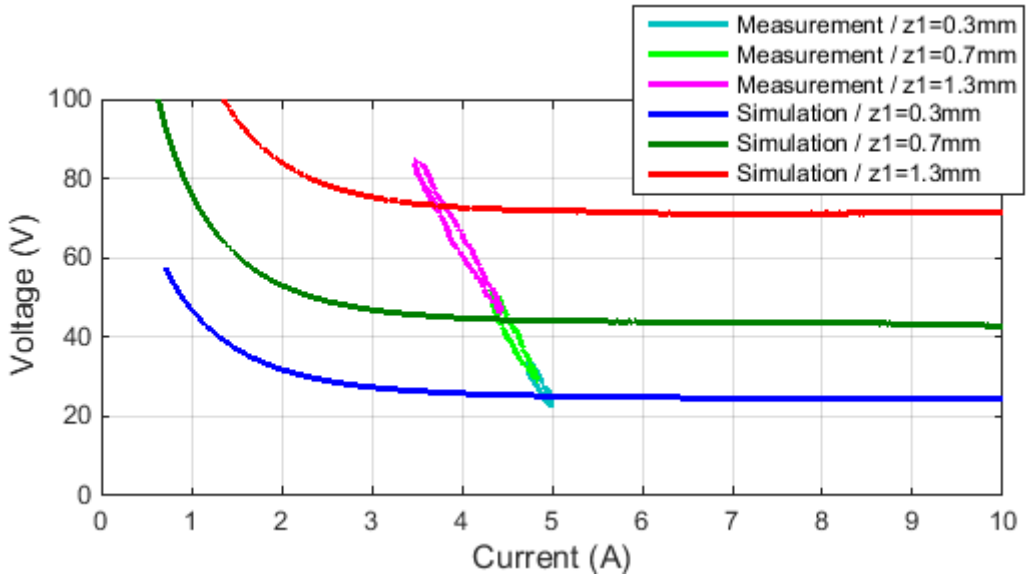

Figure 57: Comparison between measured and calculated arc electrical characteristics. Influence of separation distance.

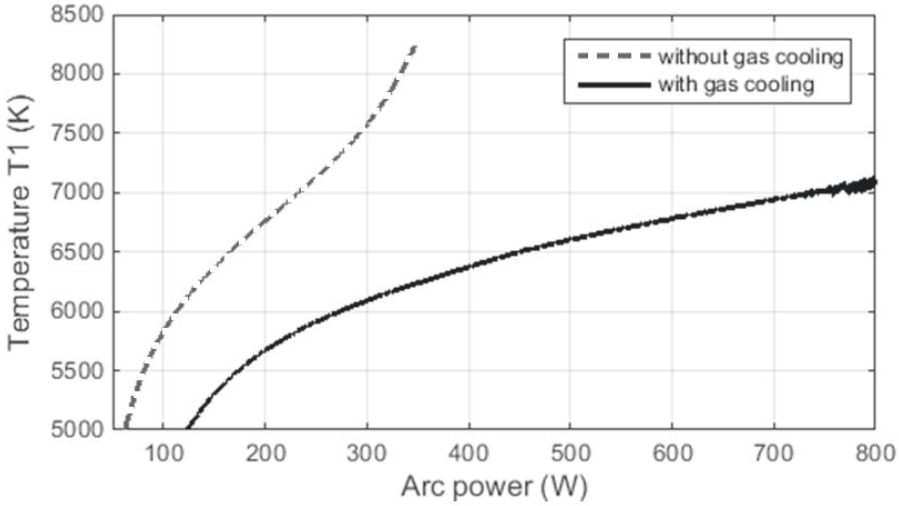

Figure 58: Temperature T_1 with and without gas cooling

6.1.1.3 Analysis

The proportion of arc power dissipated in the copper conductors is harmless because it directly heats a non-flammable material and is rapidly conducted away from the fault location. In contrast, the power directly dissipated in the insulation results in the evaporation of flammable gases. Therefore, the heat flow to the insulation is a very important parameter to determine in this analysis. Estimating its value requires firstly understanding the different contributions involved in cooling the arc:

- Conduction and radiation to the conductors
- Conduction and radiation to the insulation
- Cooling due to gassing

Cooling due to gassing can be regarded as forced convection because it involves the flow and heating of a cooler gas into the arc column. This heating energy is lost for the arc column and dissipated to the environment. Therefore, the absolute value of the heat flow to the insulation must be estimated with the following equation (67) by considering the contribution of this gas cooling:

$$\dot{q}''_{INS} = \frac{\alpha \ \left(\dot{q}_{ARC} - \dot{q}_{GAS}\right)}{2 \ \pi \ R \ z_1} \tag{67}$$

where α is the proportion of power radiated and conducted in the direction of the insulation and $\left(\dot{q}_{ARC} - \dot{q}_{GAS}\right)$ represents the contribution of arc power that can heat the system; the

contribution of gassing to arc power is subtracted because it does not directly contribute to heating the electrodes and the insulation.

The theoretical model shows that the proportion α of radiated and conducted power in the direction of the insulation is nearly independent of the absolute value of the overall conduction and radiation losses; it increases in a linear fashion at 15 % for each millimeter of gap distance as long as the gap distance is not too big and the electrical circuit can supply the arc with a sufficient power. The values of the heat flow dissipated to the insulation are displayed in Figure 59. We observe a logical increase in the gap distance and the arc current. The values are in the range of 5 to 30 MW/m² and are at least two orders of magnitude higher than the minimum heat release rate at the lowest flammability limit of PVC (see 5.4).

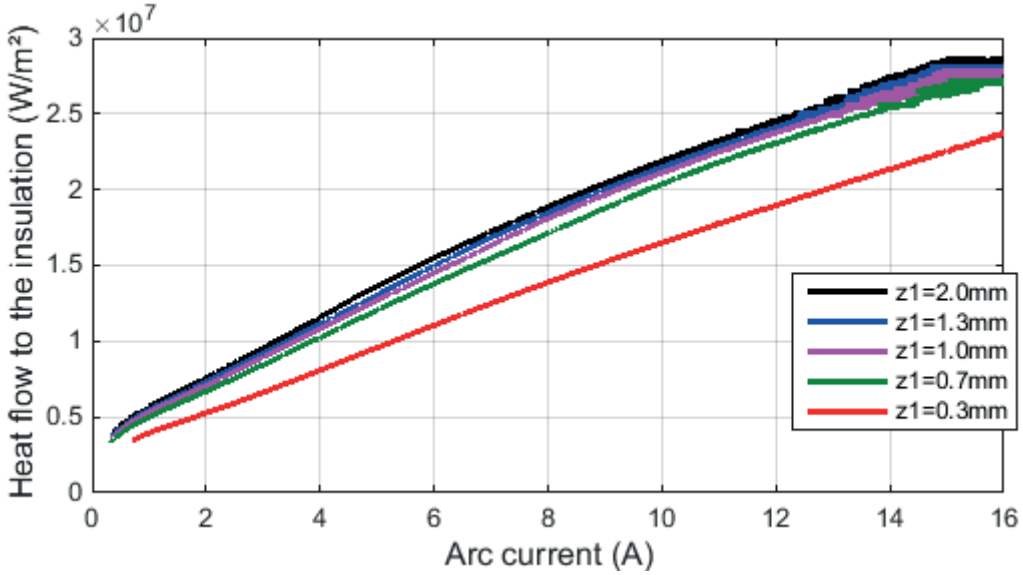

Figure 59: Heat flow in the direction of the PVC insulation

The accumulated arc energy that is dissipated to the environment can be calculated with this equation:

$$Q_{ACC} = \dot{q}_{ARC} \; t_B \tag{68}$$

where t_B is the maximum break time of the AFDD (see Table 1).

In contrast to the electrical protection schemes against overcurrent and earth faults, the AFDD is not mandatory in all electrical circuits. For this reason, the estimate of the energy

release in the event of a series arc fault must also be done for the scenario without AFDD protection. The maximum duration while a series arc at AC supply can be sustained can only be roughly estimated based on the following assumptions:

- The sustained series arc requires a carbonized track (see 3.1.1.2 and 7.3.3).
- The thermal degradation of the insulation involves carbonization that sustains a carbonized track, but also an oxidation that disintegrates this track.
- If the insulation in the vicinity of the fault is completely oxidized and only inert ashes remain, the arc cannot be sustained any more.

If we consider the case of a series arc in a PVC NYM 3x1.5 mm² cable and define an influence radius r_2 (see Figure 50) around the series arc fault where the degraded insulation could provide carbonized residue for arcing, the maximum arc fault duration t_{AF} is:

$$t_{AF} = \frac{h_g \ m_P}{\dot{q}_{INS}} \tag{69}$$

with

$$m_P = \rho \ \left(V_{INS} - V_{Cu\_Gap}\right) = \rho \ \left(\frac{4}{3} \ \pi \ r_2^3 - 2 \ r_2 \ \pi \ R^2\right) \tag{70}$$

m_P is the mass of the polymer in the influence range, V_{INS} the volume of the polymer, V_{Cu_Gap} the volume occupied by the separation and the conductors, r_2 is the influence range of the arc fault to pyrolize the polymer, ρ the density, and L_g the enthalpy of vaporization of the insulation which are 1255 kg/m³ and 1.9 kJ/g for the PVC respectively (see 7.3.2). Figure 60 displays the arc fault duration for different gap distances and arc currents. The series arc may last from 1 s (at higher arc power) to 1 minute (at the lowest power levels). If no AFDD protection is available, the break time t_B in the equation (68) can be replaced with the maximum arc fault duration t_{AF}: the accumulated arc energy becomes proportional to the mass of the polymer in the influence range of the arc and the enthalpy of evaporation:

$$Q_{ACC} = \frac{h_g \ m_P}{\alpha \ z_1} \tag{71}$$

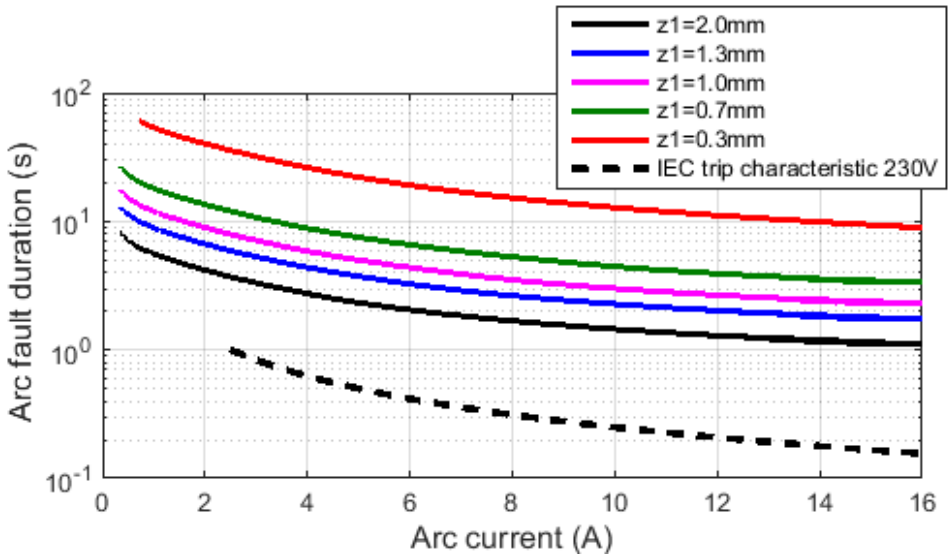

Figure 60: Arc fault duration in a PVC NYM cable with influence range r_2 = 3 mm

The estimated accumulated energies are displayed in Figure 61. The AFDD protection has no effect on the heat flow to the insulation because it is only intended to reduce the duration and energy of the arc. Thanks to the AFDD protection, the accumulated energy is reduced by a factor of 5 to 50. The zone where the dashed and continuous curves meet corresponds to the arc current of 2.5 A. Below this threshold, the AFDD protection may not be available (see Table 1) and the thermal stress is the same as without AFDD protection.

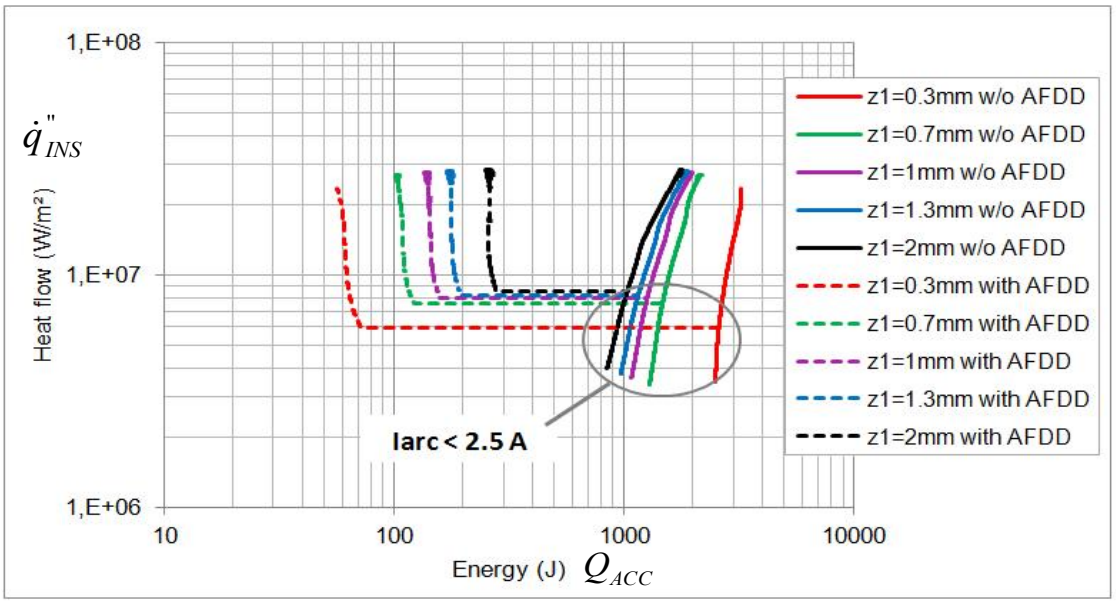

Figure 61: Heat flow to the insulation as a function of the accumulated energy for series arcing from 1 to 16 A in PVC NYM cable (with or without AFDD protection)

The ignition time can be estimated with the equation (39). The expected surface losses $\dot{q}''_{loss}$ are in the range of many tens of kW/m² and are negligible when compared to the heat flow dissipated by the arc fault. Therefore, the equation can be changed to:

$$t_{ign} = \frac{TRP^2}{\dot{q}''^{\,2}_{INS}} \tag{72}$$

We obtain theoretical ignition times in the millisecond range for arc currents from 1 A to 16 A. The real ignition times are longer; we observed ignition times in the range of one second during our tests. The equation (39) for the ignition time was verified at heat flows in the range of 10 to 100 kW/m². The thermal stress from arcing is at least one order of magnitude higher and this equation may not be valid in this case. In addition, ignition takes place when the gas mixture above the fault location reaches a sufficient temperature and a proper concentration of fuel and oxygen. This process apparently takes much more time than the time required to decompose the surface of the polymer and release gases.

After the ignition point, the resulting flame power can be obtained by using the equation (53) whereas $\dot{q}''_{ext} - \dot{q}''_{loss}$ has the value of $\dot{q}''_{INS}$:

$$\dot{q}_F = \frac{A_{INS}\ \chi\ h_c^0\ (1-\mu)}{h_g}\ \dot{q}''_{INS} \tag{73}$$

The radiated heat flow from the flame to the insulation $\dot{q}''_{F,rad\rightarrow INS}$ is negligible because it is a factor of 1000 lower than the heat flow from the arc column $\dot{q}''_{INS}$. The resulting flame power varies from 10 W to 1500 W for the current range 2.5 A to 16 A and for gap distances from 0.3 mm to 2 mm. The length of the flame can be estimated with the equation (48): it varies from 30 mm to 260 mm and corresponds to the observations made at the arcing tests described in part 0. The product of flame power and fault duration is the accumulated flame energy that is an adequate indicator of the risk of the fire spreading:

$$Q_F\big|_{NO\ AFDD} = \left(t_{AF} - t_{ign}\right)\ \dot{q}_F \tag{74}$$

Ignition time t_{ign} is negligible if compared to the fault duration. The equation can be simplified and the flame energy has a constant value: it is equal to the heat that can be dissipated by burning the mass of the polymer in the influence range of the arc (see equation (75)), whereas the production of ash and the combustion efficiency are taken into account. The obtained value is 1414 J for an influence radius of 3 mm.

$$Q_F\big|_{NO\,AFDD} = h_c^0 \;\; m_P \;\; \chi \;\; (1-\mu) \tag{75}$$

If an AFDD protects the circuit and a flame is initiated anyway, the flame energy is:

$$Q_F\big|_{AFDD} = \left(t_B - t_{ign}\right) \;\; \dot{q}_F \tag{76}$$

We obtain energy values between 3 and 12 J (see part 6.6 for details). If the arc current is lower than the detection current (the standard value is 2.5 A), the AFDD does not trip and the flame energy is the same as without AFDD protection (1414 J).

6.1.2 **Glowing fault**

Figure 62 displays the measured power of the glow involving copper conductors at different currents. The observations and measurements of other authors [ShZh07, MeBe77, SKSNR91] could be reproduced. Glowing bridges could be initiated at 1 A and then sustained at 0.5 A. Above 7 A, the electrical characteristics could be measured, but the glow was not stable and was quickly interrupted. This behavior is related to the semi-conductive properties of the copper oxide that forms the glow. The maximum power dissipation is limited by the boiling temperature of this material at 1800 °C (see 3.3.1). Experiments with different metals [ShZh07] have shown that the copper-copper glow presents the highest power dissipations and the scenario of a glow involving copper can be considered as a worst case in terms of thermal effects.

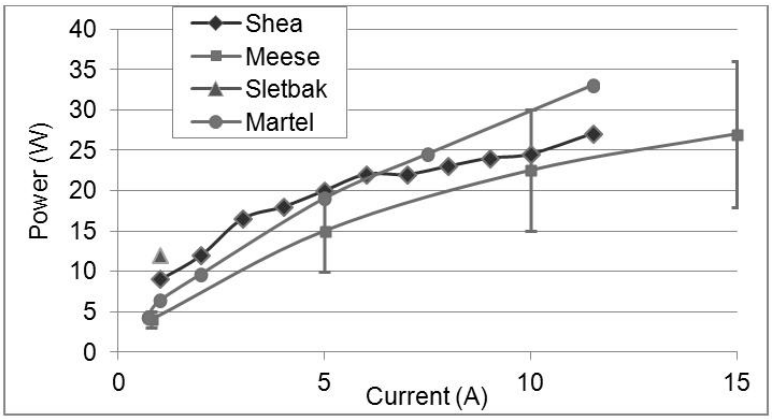

Figure 62: Power dissipation of copper-copper glows in references [ShZh07, MeBe77, SKSNR91] and own measurements

The glowing bridge consists of a small and hot glowing track where the current flows and a larger and colder element. Both are made of copper oxide, but they present different oxygen stochiometries and electrical conductivities [She06b, ShZh07, SKSNR91]. The temperature of the glowing track is in the range of the melting point of Cu_2O at 1235 °C and the colder element has in general a 50% lower temperature [She06b]. If a flammable material comes into direct contact with the glowing bridge, the conducted power dissipation results in additional cooling at the contact zone (see Figure 63). Regarding the semi-conductive properties of the copper oxide, this cooling provokes a local increase in the electrical resistance and will interrupt the glowing track if the material is in contact at this particular

spot. If the current continues to flow and the glow still exists, it means that the glowing track has moved away from the zone where the test material has been applied. This means that in the event of direct contact, the external material is not directly exposed to the temperature of the glowing track, but to the temperature of the colder zone.

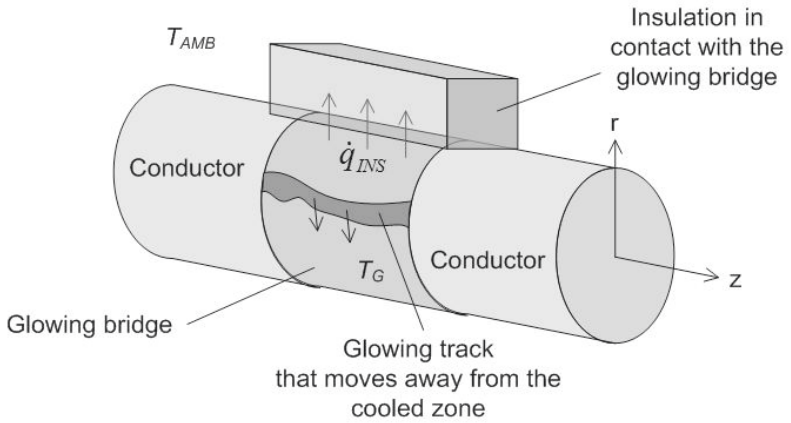

Figure 63: Sketch of the glowing bridge with cooling and movement of the track

The glow is not a fault that can be initiated instantaneously like a short-circuit. It must first be established with initial contact arcing and copper oxidation. The power dissipation at the fault location starts at only a few watts and increases steadily to the values displayed in Figure 62. If any insulation material is in direct contact with the glow or around the conductors near the glow, it must progressively undergo degradation at the temperature of the colder zone of the glow (in the range of 600 °C). This progressive degradation will result in a low evaporation rate of the flammable gases and continuous depletion of the vaporizable materials. These assumptions could be explanations for the inaptitude of the glowing to ignite polymers (see parts 3.3.2 and 7.5).

The heat flow through the insulation at sustained glowing can be estimated using equation (77). The values of thermal resistances provided in Table 8 (see part 6.2) for NYM-J PVC cables installed in different fashions can be used.

$$\dot{q}''_{INS} = \frac{T_G - T_{AMB}}{R_{th}\ 1m\ 2\ \sqrt{\pi\ S}} \tag{77}$$

where R_{th} is the thermal resistance of one meter of cable, S the cross-section of the copper conductor, T_G the temperature of the glowing bridge, and T_{AMB} the ambient temperature. If

we consider an ambient temperature of 23 °C and a temperature of 600 °C for the glowing bridge in the current range 0.5 to 7.5 A, the heat flow varies between 12 kW/m² and 21 kW/m². These values are in the range of the critical heat rate release for the ignition of polymers (13 to 35 kW/m², see 5.4). The thermal stress conditions at glowing are exactly at the flammability limit of the insulation. The expected time to ignition can be estimated using equation (39) but the term $\dot{q}''_{loss}$ is not negligible and must first be estimated. In [Bea05 (C.6)], the time to ignition of PVC was measured at different heat fluxes:

Applied heat flow	Time to ignition +/- 2 s	Extrapolated surface losses
$\dot{q}''_{ext}$	t_{ign}	$\dot{q}''_{loss}$
kW/m²	s	kW/m²
40	50	19.9
80	14	42.0
120	6.5	64.3
180	3	98.0

Table 7: Test of time to ignition of grey PVC in cone calorimeter [BEA05 (C.6)]

The surface losses can be extrapolated using the following equation and a linear relationship to the external heat flow is verified:

$$\dot{q}''_{loss} = \dot{q}''_{ext} - \frac{TRP}{\sqrt{t_{ign}}} \approx 0.58 \ \dot{q}''_{ext} \tag{78}$$

The estimated surface losses for an external heat flow of 21 kW/m² are 12.2 kW/m² and we obtain a time to ignition of 260 s. The glowing fault can be sustained as long as no disturbance occurs and no detection system is available, thus the accumulated energy tends to infinite and the ignition is unavoidable in theory. However, the real duration where the fault is hazardous is limited: the quantity of insulation around the fault that is exposed to the thermal stress is limited and it steadily loses mass. The variation of the volume of the polymer near the glowing fault is:

$$\frac{dV}{dt} = \frac{-\dot{m}_P}{\rho} = \frac{-\dot{q}_{INS}}{\rho \ h_g} \approx -2 \ \pi \ z \ r \ \frac{dr}{dt} \tag{79}$$

where $\dot{m}_P$ is the evaporation rate of the polymer, z the length of the glowing bridge, and r the radius of the exposed surface of the polymer. The steady evaporation of the polymer results in an increase in the radius and of the exposed surface of the polymer:

$$\frac{dr}{dt} = \frac{1}{r} \frac{\dot{q}_{INS}}{2 \pi z \rho h_g} \tag{80}$$

The solution of the differential equation (80) is:

$$r(t) = \sqrt{r(0)^2 + \frac{\dot{q}_{INS}}{\pi z \rho h_g} t} \tag{81}$$

The increase in the exposed polymer surface results in a decrease in the heat flow to the insulation that can be deduced with the following equation:

$$\dot{q}_{INS} = \dot{q}''_{INS}(0) \; 2 \pi \; r(0) \; z \tag{82}$$

$$\dot{q}''_{INS}(t) = \frac{\dot{q}_{INS}}{2 \pi \; r(t) \; z} = \dot{q}''_{INS}(0) \; \frac{r(0)}{r(t)} \tag{83}$$

Figure 64 displays the evolution of the heat flow to the insulation during the fault. We observe that its value drops below the minimum HRR to ignition after only 50 s, so 210 s before the estimated time to ignition. Ignition seems to be impossible in these conditions. This conclusion matches our observations as we attempted to ignite different insulation materials (see 7.5). The material usually retracts away from the heat source and does not ignite. The glowing fault does not seem to represent an immediate and direct risk of ignition of the insulation polymer in the scenario that we considered.

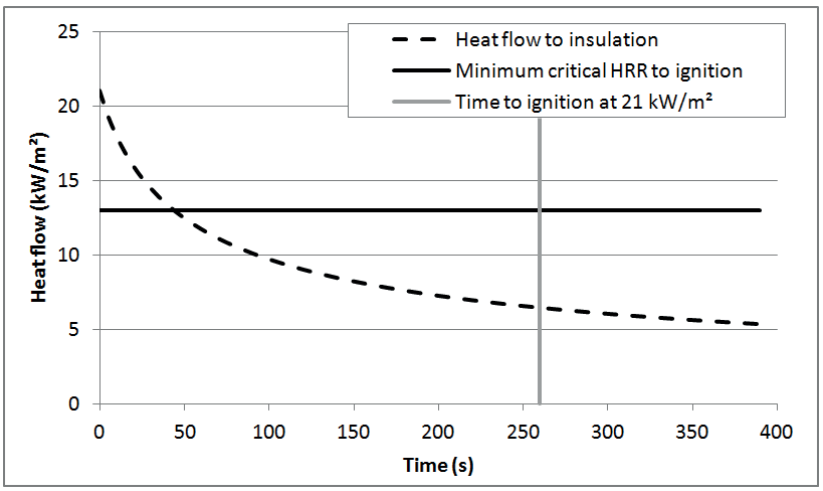

Figure 64: Evolution of the heat flow to insulation during the glowing fault

6.2 Overload2

Overload is a situation where the current in the circuit is larger than the rated current and results in the generation of excessive heat in the conductors. Fuses and circuit breakers (MCB) can distinguish between a normal load and an overload situation and interrupt the current if the thermal tripping characteristic (see Figure 65) is exceeded.

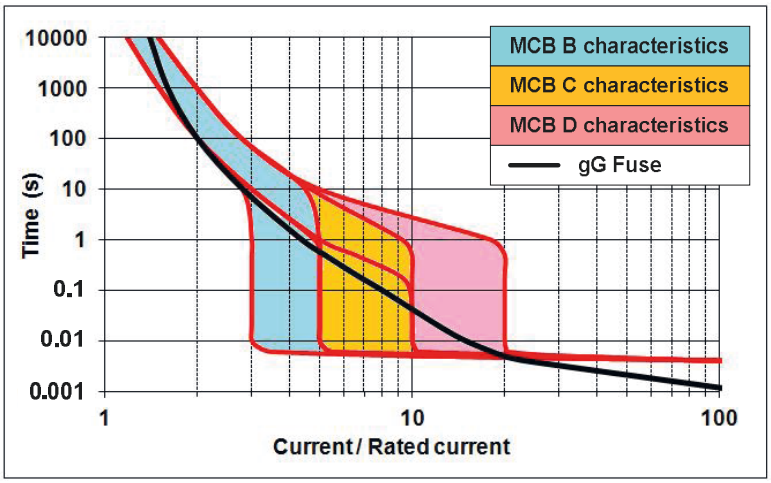

Figure 65: Typical MCB characteristics according to IEC 60898 [IEC15] and gG Fuse according to DIN VDE 0636 [DIN99]

We chose for our theoretical consideration an MCB B16: the intended load current in the circuit must be equal to or lower than 16 A and the required minimum conductor loading capacity can be determined using this equation:

$$I_{\min} = \frac{I_N}{f(A)\ f(T)} \qquad (84)\ [\text{Kal12}]$$

where I_N is the rated current, *f(A)* the factor of accumulation, and *f(T)* the temperature factor.

The factor of accumulation is used if many conductors are installed together in a bundle over a length of more than one meter. For a single conductor, this factor is equal to 1. The temperature factor has, for reference purposes, an ambient temperature of 30 °C and it decreases as the ambient temperature increases. The values of these factors are defined in DIN VDE 0298-4 [DIN03b]. For a single cable with two loaded conductors (phase and neutral) at 30 °C ambient temperature and protected with an MCB B16, the current carrying

capacity will be at least 16 A. According to Table 3 of DIN VDE 0298-4, the cross-section of the conductor will be at least 2.5 mm² if installed in tubes through the thermal insulation and 1.5 mm² if installed in tubes or directly on the wall without a tube (see Table 8).

Installation type	Conductor Cross-section S	Maximum load current	For one meter of cable			
			Electrical resistance R_{elec}	Power at maximum load current $\dot{q}_{elec}$	Thermal resistance R_{th}	Thermal time constant θ
	(mm²)	(A)	(Ohm)	(W)	(K/W)	(s)
Tube in thermal insulation	1.5	15.5	0.0230	5.52	7.24	859
	2.5	18.5	0.0138	4.72	8.47	1005
Tube	1.5	16.5	0.0230	6.26	6.39	758
	2.5	23	0.0138	7.30	5.48	650
Clamped on the wall	1.5	19.5	0.0230	8.74	4.58	543
	2.5	27	0.0138	10.06	3.98	472

Table 8: Determining conductor ratings for PVC cable with copper conductors rated at 70 °C at an ambient temperature of 30 °C and physical characteristics for one meter of cable

Table 8 also provides an estimate of electrical power dissipation $\dot{q}_{elec}$ at the maximum load current, thermal resistance R_{th} between the conductors and the environment, and the thermal time constant θ for one meter of cable using the following equations:

$$\dot{q}_{elec} = R_{elec} \; I_{Load}^2 \tag{85}$$

$$R_{elec} = \frac{1m}{\sigma \; S} \tag{86}$$

where σ is the electrical conductivity of copper and S the cross-section of the conductor.

$$R_{th} = \frac{\Delta T}{\dot{q}_{elec}} = \frac{40K}{\dot{q}_{elec}} \tag{87}$$

$$\theta = R_{th} \; C_{cable} \tag{88}$$

$$C_{cable} = m_{Cu} \; c_{Cu} + m_{PVC} \; c_{PVC} \tag{89}$$

The equivalent circuit of a simple thermal model of the cable is displayed in Figure 66. There is no thermal resistance between the power source and the cable because the power source is

internal. The heat capacity of environment C_E is considered as infinite. The heat capacity of cable part C_{cable} is determined using the dimensions of the NYM cable prescribed in the standard VDE 0250-0204 [DIN00]. The density and the specific heat capacity values are available in the Yaw's handbook [Yaw11] for copper and in the handbook of polymers [Wyp12] for PVC.

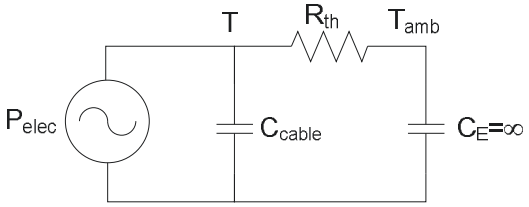

Figure 66: Thermal equivalent circuit of the heated cable

Equations (90) and (91) lead to the differential equation (92):

$$T(t) = T_{amb} + \frac{Q(t)}{C_{cable}} \tag{90}$$

$$Q(t) = \int_0^t \left(\dot{q}_{elec} - \frac{T(t) - T_{amb}}{R_{th}} \right) dt \tag{91}$$

$$\frac{dT(t)}{dt} = -\frac{T(t)}{\theta} + \frac{\dot{q}_{elec}}{C_{cable}} + \frac{T_{amb}}{\theta} \tag{92}$$

The solution of this differential equation is:

$$T(t) = T_{Amb} + R_{th} \quad \dot{q}_{elec} \quad \left(1 - \exp\left(-\frac{t}{\theta} \right) \right) \tag{93}$$

The maximum temperature of the cable is obtained at the maximum break time t_B of the MCB. The following equation fits with the upper thermal trip characteristic of the MCB:

$$t_B = 55000 \quad \left(\frac{I_{Load}}{I_N} \right)^{-7.3} \tag{94}$$

Figure 67 displays the maximum temperature that can be reached as a function of the load current. For correct installation and for currents below the rated current, the temperature remains below the specified temperature of 70 °C. This value can be exceeded in the case of overload (at a break time of 30 minutes) and reach 117 °C; we expect the insulation to be able to withstand these conditions for a limited time. For an installed circuit where the

accumulation factor for a bundle of three cables (value of 0.7) is ignored, the trend is the same, but the maximum temperature may reach 208 °C. At the rated current, the maximum temperature can exceed 100 °C. These conditions are below the lowest decomposition temperature of pure PVC (249 °C) and self-ignition is not possible. Nevertheless, if overheating occurs too often, the additives of the polymer may become degraded. A loss of electrical and mechanical properties is expected and it may lead to a further electrical fault such as a short-circuit or an earth fault.

The maximum heat flow to the insulation is a function of the temperature difference between the conductors and the environment:

$$\dot{q}''_{INS} = \frac{T_{\max} - T_{Amb}}{R_{th} \ 1m \ 4 \ \sqrt{\pi \ S}} \tag{95}$$

Equation (95) is similar to Equation (77) used for glowing, but it is divided by an additional factor of 2 because there are two conductors that generate heat in the cable, thus doubling the exchange surface. The heat source is the ohmic heating in the conductor and the accumulated energy in the complete wiring before the current interruption of the MCB is given by:

$$Q_{ACC} = 230V \ I \ t_B \tag{96}$$

The worst-case conditions are 1.75 kW/m^2 with 7 MJ for the correct installation and 3.5 kW/m^2 with the same energy dissipation for the wrong installation (with ignored accumulation factor). These conditions of thermal stress are less intense than at series arcing and glowing. Since the decomposition temperature of the PVC cannot be exceeded, we can assume that an imminent fire risk in the case of overload is very low. The installation rules and available protection devices ensure an acceptable safety level against overloads if such rules and devices are applied. Other mistakes could increase the severity of the thermal stress:

- choosing an inappropriate conductor cross-section or breaker rating.
- installing the wiring in an incorrect fashion and increasing the effect of heat accumulation.
- neglecting the effect of external heat like sun radiation or cooling slots of appliances.

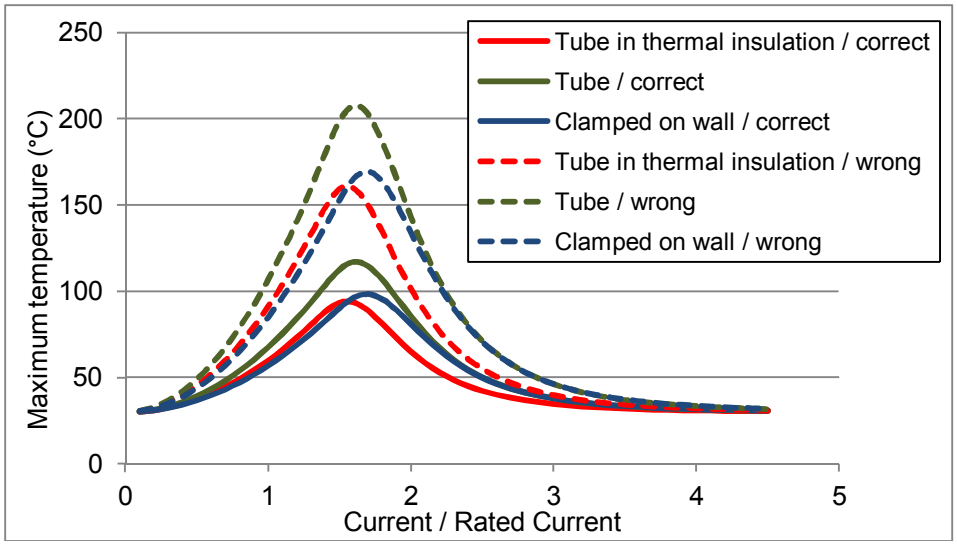

Figure 67: Maximum temperature of the cable for the 3 highlighted installation scenarios from Table 8

Correct: correct installation according to the rules

Wrong: incorrect installation by neglecting the accumulation factor f(A) for a bundle of 3 cables

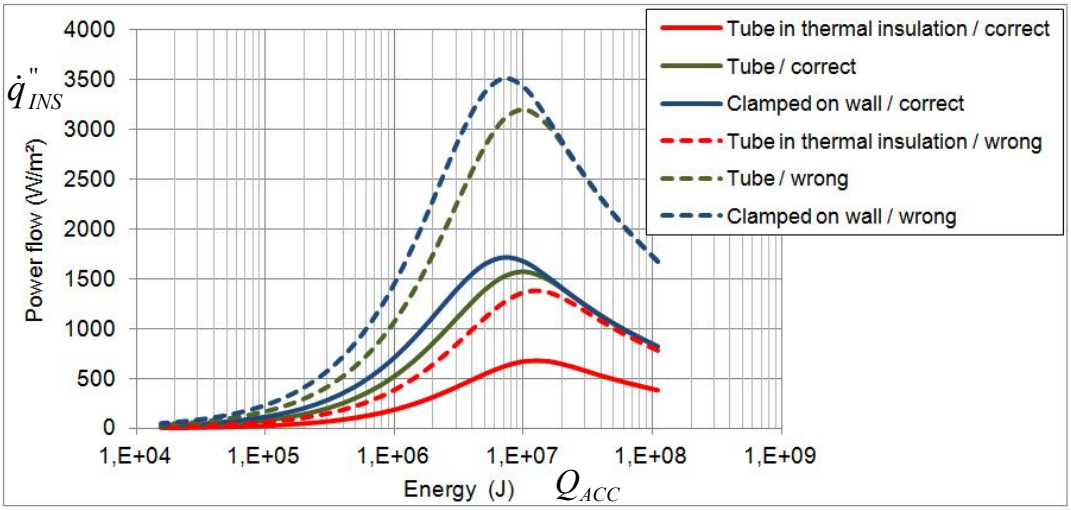

Figure 68: Heat flow to the insulation as a function of the accumulated energy for the 3 highlighted installation scenarios from Table 8

6.3 Short-circuit

In the case of a short-circuit, a closed loop is formed between the energy source (Transformer T), the phase conductor, and the neutral or protection earth conductors. The resulting short-circuit current exceeds the rated current of the circuit and the current does not take the normal conducting path that it is intended to use (see Figure 69).

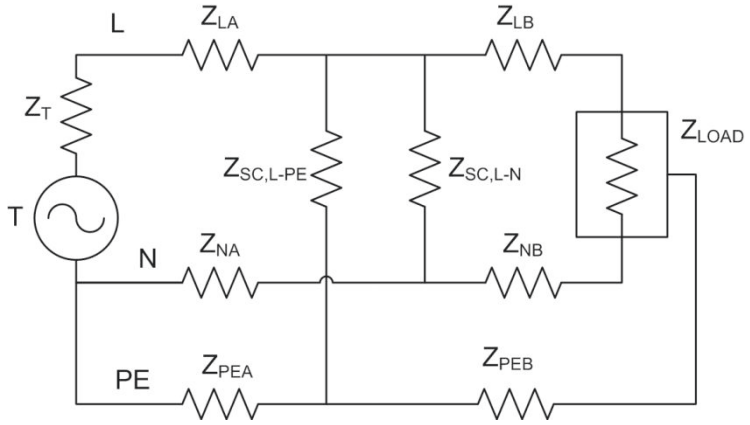

Figure 69: Equivalent circuit of a short-circuit between phase and neutral or phase and protection earth

6.3.1 **Bolted short-circuit**

This situation can occur if the conductors at different polarities come directly into contact. If the conductor-to-conductor contact is stable and its impedance ($Z_{SC,L-N}$ or $Z_{SC,L-PE}$) is low, the heat dissipation caused by the important current flow will be spread evenly in the wiring. In this case, the fault is a bolted short-circuit.

The requirement for short-circuit protection in Germany is defined in DIN VDE 0100-430 [DIN10a]. The current must be interrupted within a maximum break time t_B that is calculated using this equation:

$$t_B = \left(\frac{S \ k_M}{I_{SC}} \right)^2 \qquad (97) \text{ [Kal12]}$$

where I_{SC} is the short-circuit current and k_M the material coefficient that is 115 10^6 A $s^{1/2}/m^2$ for PVC insulated wires. The maximum temperature is reached at the maximum break time t_B and the equation (93) becomes:

$$T_{\max} = T_{Amb} + R_{th} \;\; R_{elec} \;\; I_{sc}^2 \;\; \left(1 - \exp\left(-\frac{S^2 \;\; k_M^2}{\theta \;\; I_{SC}^2}\right)\right) \tag{98}$$

The term $I_{sc}^2 \;\; \left(1 - \exp\left(-\frac{S^2 \;\; k_M^2}{\theta \;\; I_{SC}^2}\right)\right)$ tends to $\frac{S^2 \;\; k_M^2}{\theta}$ if $I_{sc}^2 >> \frac{S^2 \;\; k_M^2}{\theta}$

This is the case because the term $\frac{S^2 \;\; k_M^2}{\theta}$ is in the range of 30 A² and the value I_{sc}^2 will be greater than 10,000 A². The maximum temperature rise is independent of the short-circuit current:

$$T_{\max} = T_{Amb} + R_{elec} \;\; \frac{S^2 \;\; k_M^2}{C_{cable}} \tag{99}$$

Based on this equation, we can understand the origin of the material coefficient k_M which is a function of the material properties of the conductor:

$$k_M = \sqrt{\Delta T \;\; \sigma \;\; \rho \;\; c} \tag{100}$$

where σ is the electrical conductivity, ρ the density, c the specific heat capacity of the conductor, and ΔT the maximum allowed temperature rise above the ambient temperature for a specific insulation material. The resulting temperature rises for the three highlighted scenarios from Table 8 are between 5 K and 10 K. These values are small in comparison to the temperature rise curves extrapolated for the overload faults because it is possible that the cables are previously heated by the load current to the maximum operating temperature (e.g. 70 °C for PVC). The definition of the break time in the standard [DIN10a] was probably decided by considering this combination of previous heating from the load and short-circuit fault. In this case, the absolute temperature of the cable may reach 80 °C (see Figure 70).

The mistake of ignoring the factor of accumulations for bundles will not have a significant impact in the case of the short-circuit. The contribution of the other cables during the short duration of the fault will be negligible. Another mistake with greater effects at short-circuit could be the choice of an inappropriate conductor cross-section. According to Table 8, the installation of the cable in a tube in thermal insulation requires a cross-section of 2.5 mm². With a cross-section of 1.5 mm², the temperature rise would be 16 K instead of 10 K.

The maximum current for instantaneous tripping of the B16 MCB is 5 times the rated current (80 A) [IEC15]. The electrician must always verify that this current will flow in the case of short-circuit at any point of the protected circuit. This is ensured by measuring the impedance of the system at each socket and extrapolating the short-circuit current (a margin of 30 % is usually observed). At this current or above, the MCB must trip within 100 ms according to the standard. However, the common design of such high current protection (plunger moved by the magnetic force of the current flowing through a bobbin) ensures a reaction time that is lower than the duration of a half-cycle of the current (10 ms for 50 Hz). In addition, the breaker design ensures a limitation of the short-circuit current by opening the contacts quickly and initiating an arc with increasing voltage and impedance. This results in an energy limitation that is expressed as I^2t value. The limit for an MCB B16 with a rated breaking capacity Icn = 6 kA and an energy limit of class 3 is 35,000 A^2 s. The maximum break time of the MCB can be expressed as follows:

if $\frac{35{,}000\ A^2\ s}{I_{sc}^2} < 0.01\,s$ then $t_B = \frac{35{,}000\ A^2\ s}{I_{sc}^2}$ else $t_B = 0.01\,s$

The corresponding maximum temperature at the maximum break time is also estimated with the equation (98) and the result is displayed in Figure 70 for currents up to the rated breaking capacity.

As expected, the MCB protects the circuit better against short-circuits than a hypothetical protection device that would fulfill the minimum requirements of the standard DIN VDE 0100-430. The mistake of using the next lower cross-section results in an additional temperature rise of only a few Kelvin. Figure 71 displays the thermal stress from the short-circuit current if the current flows in a cable that is previously heated to 70 °C at the load current. The values of heat flows to the insulation and energy densities are much lower than with the other faults studied previously. A bolted short-circuit does not seem to be particularly hazardous if it is detected by a conventional protection device. For the protection with MCB, the heat flow to the insulation and the accumulated energy increase steadily until point a is reached. In this portion of the curve, the break time of the MCB is defined as constant with a value of 10 ms. The heat flow continues to increase after this point a, but the accumulated energy decreases. This portion of the curve corresponds to higher short-circuit

currents (above 2000 A) that result in an important decrease of the break time; the break time decreases faster than the power of the fault and limits the energy.

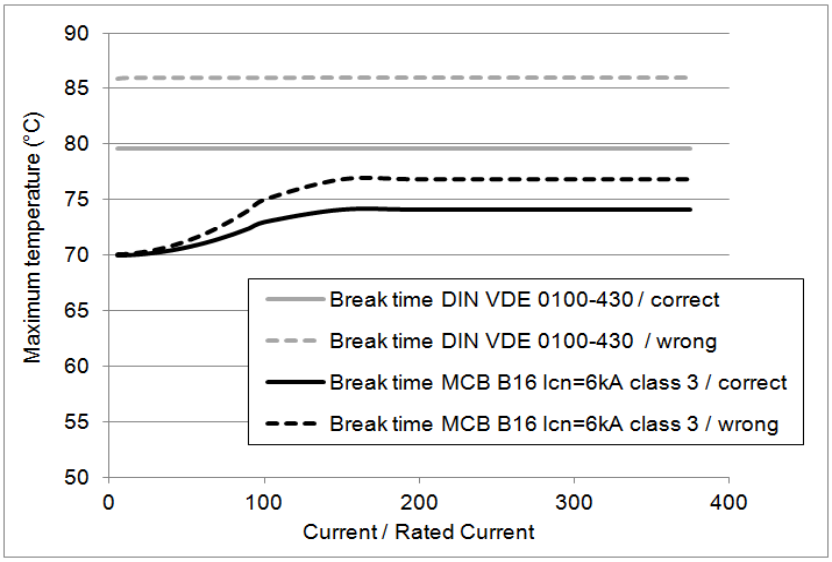

Figure 70: Maximum temperature of the cable for installation in a tube in thermal isolation
Correct: correct installation according to rules
Wrong: incorrect installation by using a cross-section of 1.5 mm² instead of 2.5 mm²

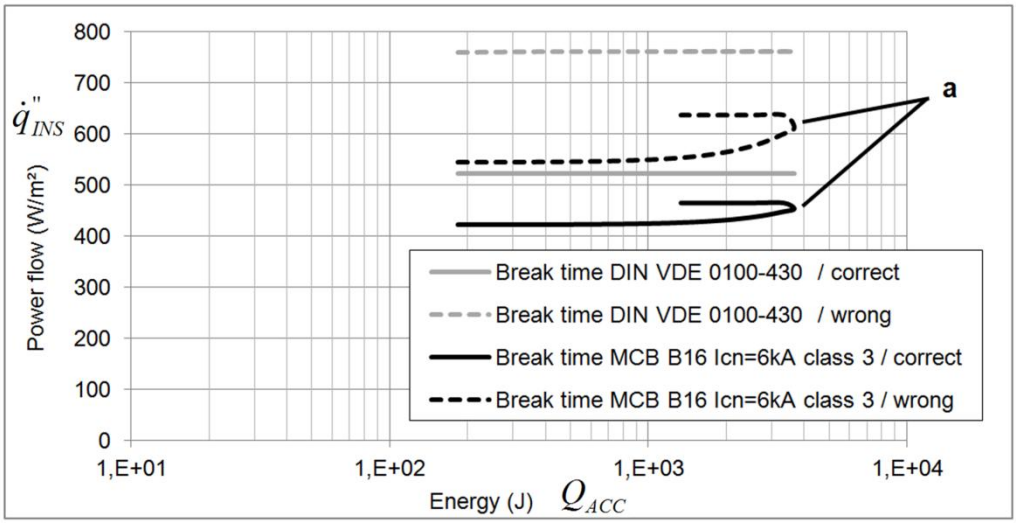

Figure 71: Heat flow to the insulation as a function of the accumulated energy for installation in a tube in thermal isolation (Table 8)

6.3.2 **Parallel arc fault**

If the impedance of the short-circuit ($Z_{SC,L-N}$ or $Z_{SC,L-PE}$ from Figure 69) is not negligible, the heat dissipation is not spread evenly through the system. A significant part of the heat is dissipated at the fault location and results in a higher thermal stress. This is the case of the parallel arc that can be the result of these two events:

- Contact arcing: Transition from bolted short-circuit to parallel arc

If the current-carrying capacity of the conductor-to-conductor contact is exceeded, the metal quickly heats up and melts. The temperature of the molten bridge increases, resulting in a steady increase of the electrical resistivity and power dissipation. Finally, the molten bridge reaches boiling point, is vaporized, and a parallel arc is initiated. This complete sequence is usually observed within a half-cycle. Since the conductor-to-conductor distance is extremely small at the instant of the separation, the arc is a short arc and will present the lowest arc voltage (13 V to 20 V in general).

- Non-contact arcing due to creepage on char: spontaneous initiation of a parallel arc

The parallel arc may be directly initiated with the same carbonization process as explained in 3.1.1.2 and 7.3.3. Considerations based on a simple model of a carbonized path show that the arc will start within the first half-cycle of the system voltage if the conductivity of the track is sufficiently high. The required minimum conductivity decreases with the power of the load in series (see part 7.3.3). In the case of a parallel arc, the corresponding load in series is only the impedance of the wiring and the power source. This means that a reduced carbonization of the fault area will be sufficient to initiate the parallel arc. The initiation of longer arcs is possible and higher arc voltages are expected (20 V to 70 V).

Regardless of the fault scenario, an AFDD will be able to detect and interrupt the parallel arc current according to the requirement in Table 2 (see 1.5.2). A maximum number of half-cycles is defined because the high power of the arc most often results in a very astable fault. As displayed in Figure 72, time interruptions between the arcing half-cycles are usually observed. The shortest possible break time in the case of a stable parallel arc is the number of half-cycles multiplied by the duration of the half-cycle, for example 80 ms for a parallel arc at 500 A / 50 Hz.

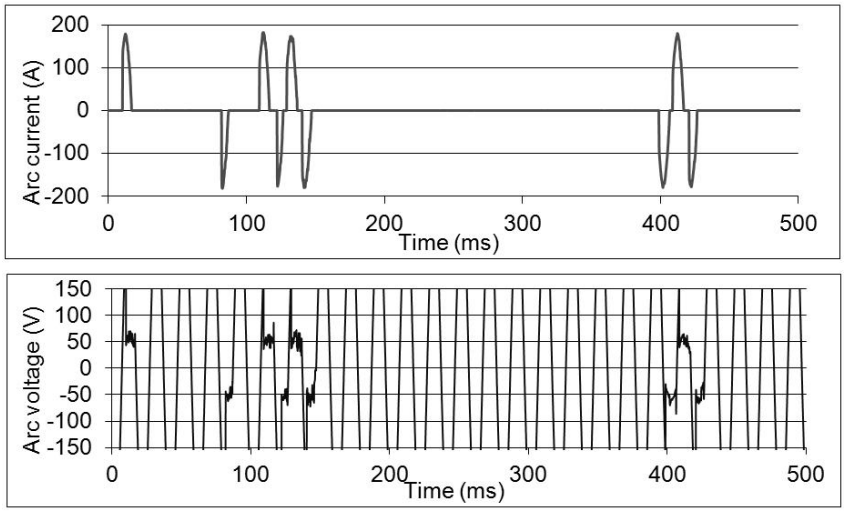

Figure 72: Parallel arc voltage and current in SPT2 cord at guillotine test according to IEC 62606 / §9.9.3.2 [IEC13] for 150 A prospective short-circuit current at 230 V AC 50Hz

The parallel arc detection of the AFDD is not the only means of protection that may interrupt such a fault: if the parallel arc current is below the minimum test current of 75 A, the series arc detector may detect it and trip (see 1.3). The thermal release system of the MCB can be sensitive to the low current parallel arcs too and the instantaneous magnetic release system will interrupt the current within a half-cycle if it exceeds 80 A. If the parallel arc shorts the phase conductor with the protection earth, the RCD will trip within 40 ms. The maximum break times of all these devices are displayed in Figure 73.

Since the current is much higher than at series arcing, the temperature of the arc column must also be higher. J. Latham [Lat80] estimated the arc temperature to be 10,000 K at 140 A and 11,800 K at 1000 A. B. Babrauskas [Bab03 (p540-548)] reported temperatures in the range of 11,000 K to 15,000 K for the same current values. The power of the arc can be roughly estimated by using the equations and extrapolated values of the heat flow obtained in the analysis of the series arcing fault (6.1.1.3). The geometry of the fault is slightly different, but at least the correct order of magnitude can be obtained. In a PVC NYM-J 3x1.5 mm² cable, the distance between two conductors is 0.7 mm. This distance can be used as separation distance z_J. The duration of fault t_B is the break time of the quickest protection device that can detect the fault (see Figure 73). The values of heat flow and accumulated energy are displayed in Figure 74.

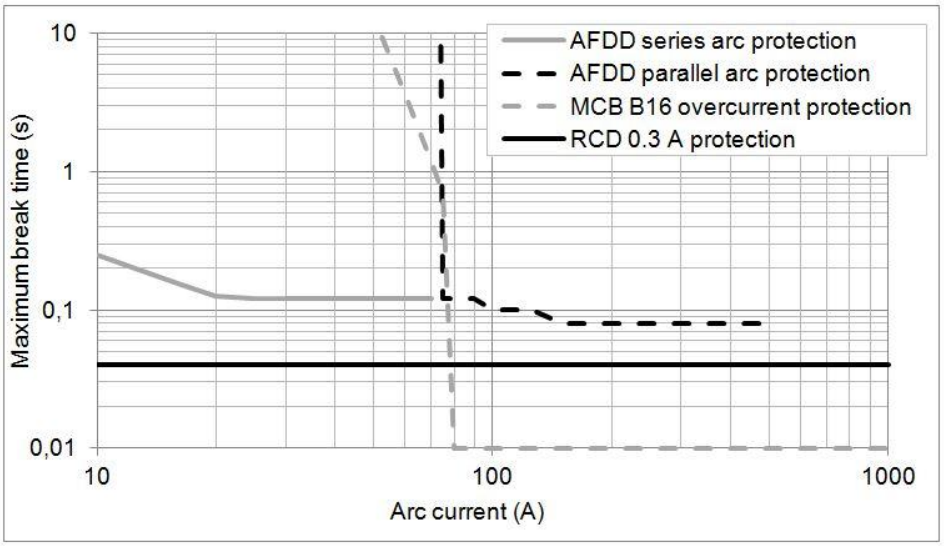

Figure 73: Maximum break times of the AFDD 230 V AC, MCB B16, and RCD 0.3 A according to applicable standards

The domain where all the curves are together (portion a) corresponds to high arc currents above the maximum instantaneous tripping current of the MCB (80 A) and a break time of 10 ms. Below 80 A, the MCB can only trip with the slower thermal trip system (portion d of the curve). If an AFDD is installed, the parallel arc is interrupted much more quickly (portion c of the curve). In the case of a parallel arc to earth, the RCD will limit the energy with a maximum break time of 40 ms (portion b of the curve). The contribution of the AFDD in the case of such a parallel arc fault is significant in theory, but in practice it is only useful if the current is below the instantaneous tripping threshold of the MCB. This scenario will occur very rarely because according to the standards [DIN10a], the protection devices and wiring must be installed and tested in such a fashion that the short-circuit current is always at least 30 % above this threshold, regardless of where the fault takes place [MAHBE11]. The heat flows are extremely high when compared with other faults. They are 10 times higher than at series arcing and 10,000 times higher than at a glowing fault. The accumulated energy is moderate because the fault duration is in general very short.

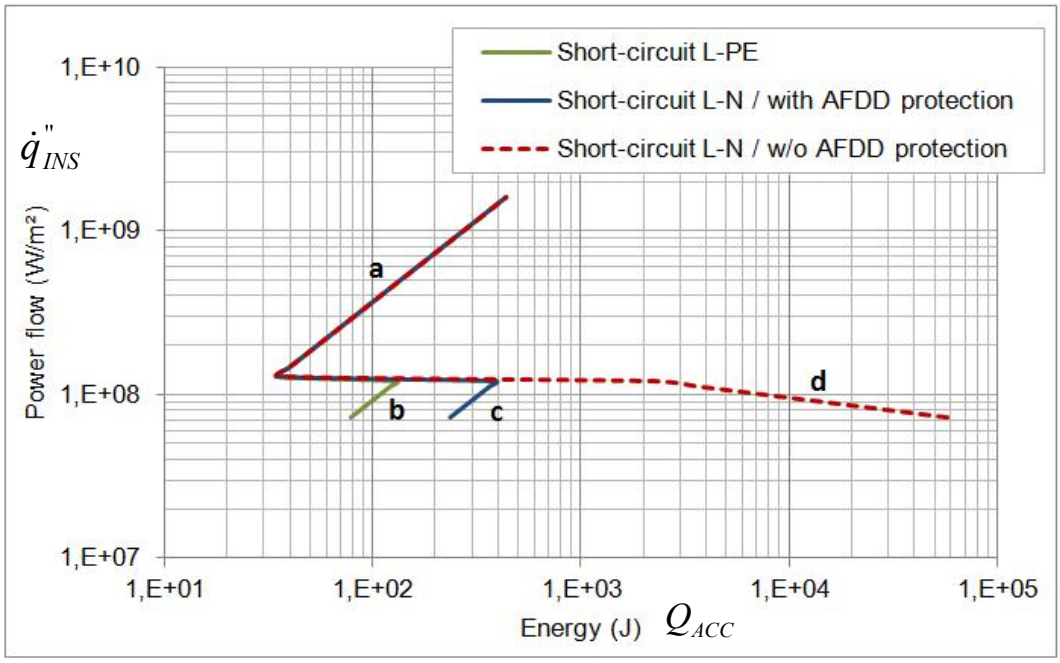

Figure 74: Heat flow through the insulation as a function of the accumulated energy for the parallel arc for currents above 45 A

6.4 Earth leakage

An earth leakage is an unintended current flow between a live conductor and the protection earth or any other part at the earth potential. If the impedance of the fault is low, the fault quickly turns into a bolted short-circuit or a parallel arc. This case was already considered in 3.4. If the impedance is higher, a small leakage current can flow and heat the fault location without being detected by the overcurrent protections. The available protection is the RCD that must trip according to the characteristic displayed in Table 9. $I_{\Delta n}$ is the rated residual operating current of the RCD that can be 30 mA to provide protection for people and 300 mA to ensure fire protection. Most residential circuits are protected with 30 mA RCDs. Only those circuits that are not directly accessible can be protected with a 300 mA RCD.

Current	$I_{\Delta n}$	$2\times I_{\Delta n}$	$5\times I_{\Delta n}$
Maximum break time t_B	0.3 s	0.15 s	0.04 s

Table 9: Limiting values of break time for RCD according IEC 61008-1 [DIN10b]

The high impedance isolation fault is most probably a carbonized track. The creepage distance between the phase conductor and the earthed part must have a significant influence on the value of the impedance. The shortest distance is the distance separating the phase and protection earth conductor in a cable, so twice the insulation thickness of a single conductor. The conductors of a NYM-J cable with 1.5 mm² cross-section have an insulation thickness of 0.35 mm, so the shortest distance will be 0.7 mm. The biggest possible distance is related to the necessary conditions to initiate a first carbonized track. Dry and wet tracking cannot take place if the separation distance is too big. One possibility is to consider the required creepage distances that are defined for electrical equipment in IEC 60664-1 [IEC07]. For 250 V AC, the maximum required creepage distance is 4 mm and corresponds to the material group III (CTI values from 100 to 400) and pollution degree 3 (Conductive pollution occurs or dry non-conductive pollution occurs and can become conductive at condensation).

Figure 75 displays a model of the earth leakage fault between two conductors that are separated by distance x of the insulation material. An initial carbonized track that bridges the insulation is already established. Since the most probable cause of the carbonized track is

surface tracking, we expect that the initial width y of the track is much bigger than its thickness z. We chose an initial ratio y/z of 10. The generated heat is dissipated in the metallic parts and the insulation by conduction and in the air space above the fault by radiation and convection. The track is directly exposed to the air and it is quickly oxidized if the temperature is too high. Complete oxidation would mean a dramatic drop in electrical conductivity and an interruption of the leakage current. We expect that this scenario will not happen in a worst-case situation so the temperature will be limited to a value where the oxidation of the polymer cannot be completed. According to the thermogravimetric analysis in 7.4, this maximum temperature would be 700 °C for the PVC-based polymer. A rough estimate of the radiation and convection losses at this temperature shows that the contributions of these dissipations are negligible. For the remaining conduction losses, the proportion α of the heat that pyrolizes the insulation can be roughly estimated with the thermal resistances κ of the materials and the corresponding exchange surfaces:

$$\alpha(t) \approx \frac{\kappa_{INS}\ (x\ \ y(t) + 2\ (x + y(t))\ z(t))}{\kappa_{INS}\ (x\ \ y(t) + 2\ (x + y(t))\ z(t)) + \kappa_{Cu}\ \ 2\ \ y(t)\ z(t)} \tag{101}$$

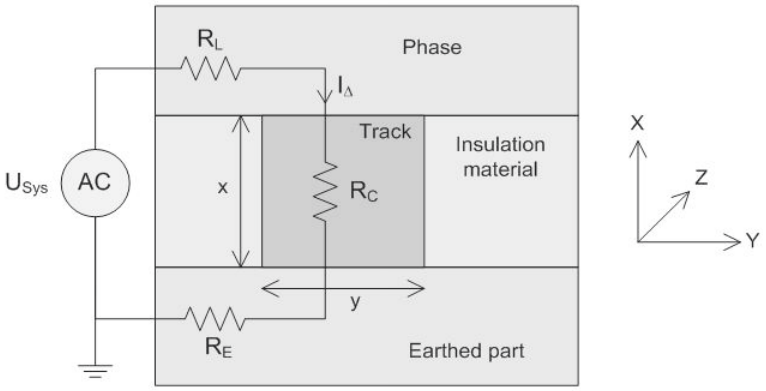

Figure 75: Model of earth leakage fault with equivalent electrical circuit

The primary power source is the electrical system at voltage *Usys*. The impedances of conductors R_L and R_E are negligible if compared with the impedance of carbonized track *Rc*. The power generated $\dot{q}_{heat}$ at the fault is:

$$\dot{q}_{heat}(t) = U_{sys}\ \ I_{\Delta}(t) \tag{102}$$

The initial value of leakage current I_Δ was chosen to be equal to 150 mA, the non-tripping residual current of the 300 mA RCD. Therefore, the initial value of *Rc* is 1533 Ω. The initial dimensions and mass m_c of the carbonized track can be estimated with these equations:

$$R_c(t) = \frac{x}{\sigma \; y(t) \; z(t)} = \frac{\rho \; x^2}{\sigma \; m_c(t)} \tag{103}$$

Rough estimates of density ρ and electrical conductivity σ of the carbonized track are obtained in 7.3.3. Thickness z and mass m_c of the carbonized material are not constant because they increase if the decomposition temperature of the PVC insulation is exceeded and the heat produces new carbonized material (with the enthalpy of carbonization L_c):

$$m_c(t) = m_c(0) + \int_0^t \frac{\alpha \; \dot{q}_{heat}(t)}{L_c} \; dt = m_c(0) + \int_0^t \frac{\alpha \; U_{sys} \; I_\Delta(t)}{L_c} \; dt \tag{104}$$

If the impedance decreases as the degradation of the insulation progresses, leakage current I_Δ must increase:

$$I_\Delta(t) = \frac{U_{sys}}{R_c(t)} = U_{sys} \; \frac{\sigma}{\rho \; x^2} \left(m_c(0) + \int_0^t \frac{\alpha \; U_{sys} \; I_\Delta(t)}{L_c} \; dt \right) \tag{105}$$

It becomes a differential equation that can be easily solved:

$$\frac{dI_\Delta(t)}{dt} = U_{sys}^{\;2} \; \frac{\alpha \; \sigma}{\rho \; x^2 \; L_c} \; I_\Delta(t) \tag{106}$$

$$I_\Delta(t) = I_\Delta(0) \; \exp\left(\frac{\sigma \; U_{sys}^{\;2} \; \alpha}{\rho \; x^2 \; L_c} \; t \right) \text{ with } I_\Delta(0) = \frac{\sigma \; U_{sys} \; m_c(0)}{\rho \; x^2} \tag{107}$$

The time while the maximum tripping current of 0.3 A is reached is:

$$t_B = \frac{\ln\left(\frac{0.3 \; A}{I_\Delta(0)} \right) \; \rho \; x^2 \; L_c}{\sigma \; U_{sys}^{\;2} \; \alpha} \tag{108}$$

The maximum heat flow in the direction of the insulation can be calculated with the equation (109):

$$\dot{q}''_{INS} = \frac{\alpha \; U_{sys} \; 0.3 \; A}{x \; y(t_B) + 2 \; (x + y(t_B)) \; z(t_B)} \tag{109}$$

The accumulated energy at the carbonized track is:

$$Q_{ACC} = \int_0^{t_B} U_{sys} \; I_\Delta(t) \; dt = I_\Delta(0) \; \frac{\rho \; x^2 \; L_c}{\sigma \; U_{sys} \; \alpha} \left(\exp\left(\frac{\sigma \; U_{sys}^{\;2} \; \alpha}{\rho \; x^2 \; L_c} \; t_B \right) - 1 \right) \qquad (110)$$

Two variables in these equations are roughly estimated:

- the enthalpy of carbonization L_c is extrapolated from the carbonization test in 7.3.2. The median value is 3.5 kJ/g and we perform the analysis in the range of 2 to 5 kJ/g.
- The electrical conductivity of the carbonized material is estimated in the range of 1.6 to 21.4 S/m.

As expected, it takes more time for a carbonized track with lower electrical conductivity and higher enthalpy of carbonization to increase the current and power dissipation, and lead to the RCD trip (see Figure 76). Electrical conductivity has a greater influence: the fault durations are in the range of 0.2 to 8 s for 21.4 S/m and 10 to 350 s for 1.6 S/m. According to our observations [Dur05] and the all-round opinion of electricians that earth leakage faults last for a very long time and gradually become hazardous, we believe that the scenarios that result in longer fault durations are more probable. This would mean that the electrical conductivity and/or the proportion of power dissipated in the insulation are lower than the values used in the model. This hypothesis is plausible because the presence of oxygen may result in an important oxidation of the carbonized material that becomes less conductive. In addition, it was reported that the pyrolized polymer may have a higher thermal resistance [FAA05] and act as a barrier between the heat source and the intact polymer; the power dissipation in the copper conductors will be higher and the decomposition of the polymer will be reduced. Figure 77 displays the thermal stress parameters of the fault at a system voltage of 230 V AC for the four combinations of extreme values of electrical conductivity and enthalpy of carbonization. As explained above, the values corresponding to the lower electrical conductivities (dashed lines) will be more probable. We obtain values for heat flow to the insulation in the same range as for the glowing fault, but they are a factor 100 lower than at series arcing.

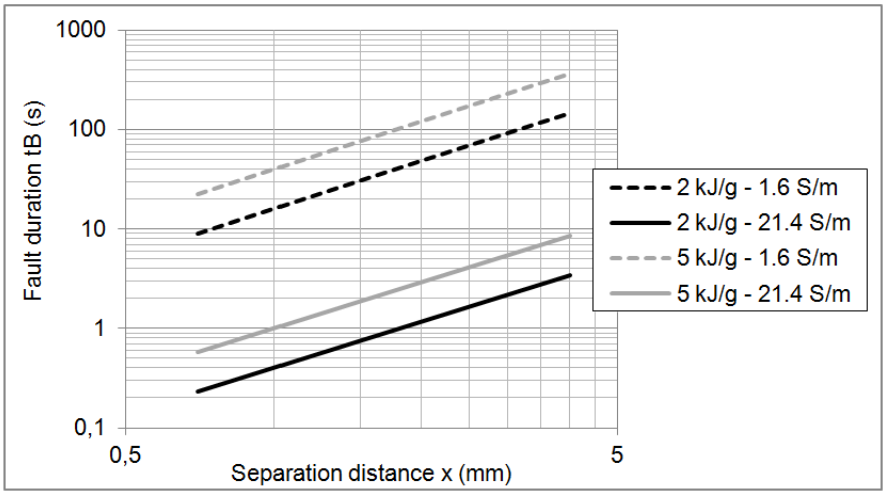

Figure 76: Duration of the earth fault if the circuit is protected by a 0.3 A RCD
Scenario: leakage current starting at 0.15 A / 230 V AC across a gap of 0.7 to 4 mm

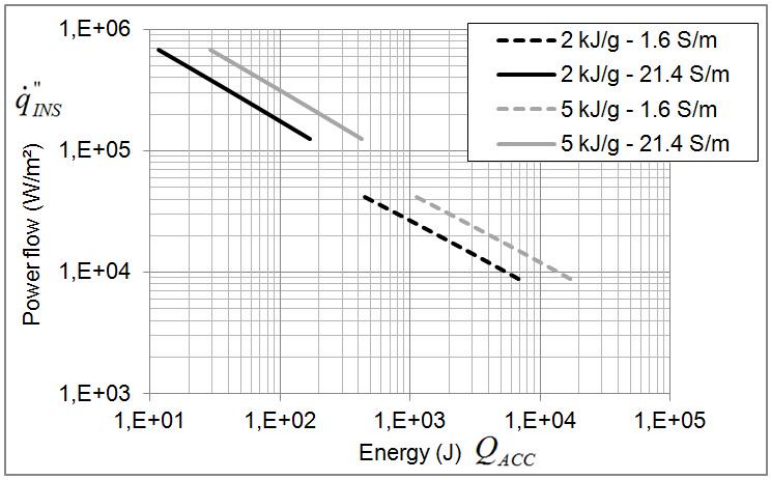

Figure 77: Heat flow to the insulation as a function of the accumulated energy at the carbonized track. Scenario: leakage current starting at 0.15 A / 230 V AC
across a gap of 0.7 to 4 mm

6.5 Summary of thermal stresses

Figure 78 displays the estimated values of the six criteria of thermal stress for the different faults that could occur in a circuit rated at 16 A, wired with a PVC NYM-J 3x1.5 mm² cable, and protected by MCB and RCD. These parameters are related to the probability of ignition of the cable and of fire spreading.

The protection function of the MCB results in a very low thermal stress at a bolted short-circuit fault. The overload fault can dissipate a lot of energy, but it is spread through all the wiring and over a long time, hence the temperature and heat flow are very low. A fire cannot be ignited since the ignition temperature of the insulation is not exceeded. A fire due to these faults can only start if many installation rules are ignored or if the protection device is faulty or non-existent. The earth leakage presents higher values for heat flow and temperature because the carbonized track has very small dimensions compared with the complete wiring. Fortunately, the RCD with a 0.3 A rated residual operating current can limit the energy and reduce the risk of ignition. Since a majority of circuits are protected by 0.03 A RCDs, the risk is even lower. The lower risk represented by these "conventional faults" is the result of the installation rules defined in the standards and the performance of the MCB and RCD breakers which have been state-of-the-art for decades. The glowing fault presents similar values for temperature and heat flow as the earth leakage fault. Unfortunately, there is no protection device available for this fault. The fault can last for hours, days, or weeks and the released energy can be extremely high. Nevertheless, this energy is spread over a very long time and theoretical estimates show that this fault can only sustain a sufficient heat flow for ignition during a very limited time (less than one minute); the flame point cannot be reached. Investigations with ignition tests on insulation polymers (see 7.5) confirmed this assumption. Nevertheless, the hazard resulting from the glowing fault cannot be ignored: other materials with a much higher flammability than PVC (dry dust, chipped wood…) could come into direct contact with the glowing bridge and ignite. Research on the detection and mitigation of such electrical faults will be continued and the electrical safety rules for electrical installations, especially for the quality of the connections, must always be observed.

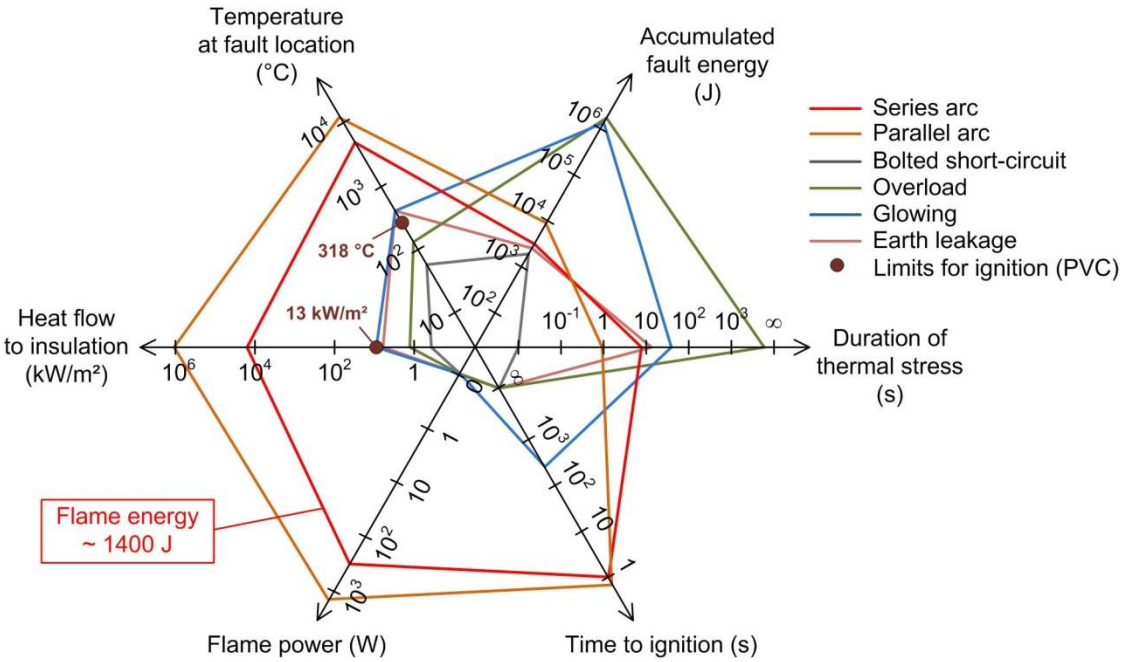

Figure 78: Thermal stress parameters of different electrical faults that can occur in a circuit wired with PVC NYM-J 3×1.5 mm² cable and protected by MCB B16, RCD 0.3 A

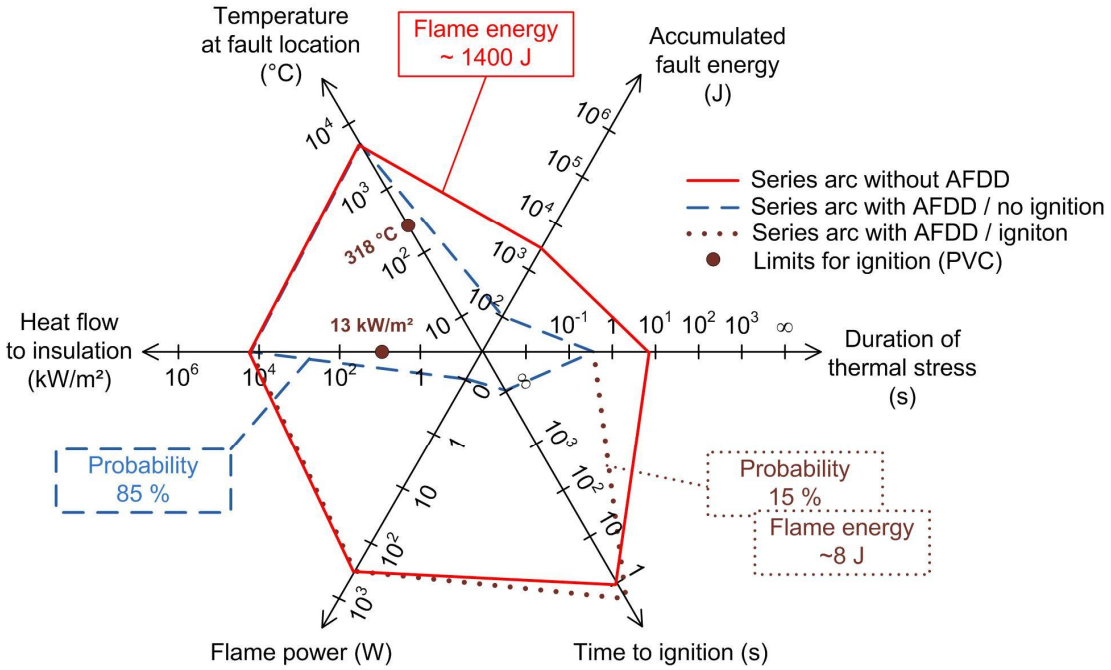

Figure 79: Thermal stress parameters for series arc faults that can occur in a circuit wired with PVC NYM-J 3×1.5 mm² cable and protected by MCB B16, RCD 0.3 A, and with/without AFDD

6.6 Statistical analysis and evaluation of the safety increase with AFDD

The probability p_{FIRE} of an electrical fire starting at a series arc fault is:

$$p_{FIRE} = p_{SAF} \; p_{IGN} \; p_{SPREAD} \tag{111}$$

where p_{SAF} is the probability of a stable series arc fault being initiated, p_{IGN} the probability of the cable igniting, and p_{SPREAD} the probability of the fire spreading to another flammable material. We assume that p_{SPREAD} is proportional to the flame energy. The probability p_{IGN} and the flame energy are very much dependent on the arc current. Therefore, a distinction must be made between the probabilities in different current ranges. This results in the following equation:

$$p_{FIRE} = p_{SAF} \; \sum_i p_{c,i} \; p_{IGN,i} \; \alpha \; Q_{F,i} \tag{112}$$

where α is the proportionality factor between p_{SPREAD} and the flame energy $Q_{F,i}$ (see equation (75)) and $p_{c,i}$ the probability that the value of the load current is in the current range *i*:

$$p_{c,i} = \frac{I_{\max,i} - I_{\min,i}}{16\,A} \tag{113}$$

If an AFDD protects the circuit, the limitation of the flame energy and the probability p_{AFDD} that the device detects the series arc fault within the maximum break time (or energy limitation) must be taken into account:

$$p_{FIRE}\big|_{AFDD} = p_{SAF} \; \sum_i p_{c,i} \; p_{IGN,i} \; \left(1 - p_{AFDD,i}\right) \; \alpha \; Q_{F,i}\big|_{AFDD} \tag{114}$$

p_{AFDD} is determined by calculating the proportion of tests where the ignition energy Q_{IGN} (see equation (2)) is lower than the threshold energy of 100 J. If the arc current is lower than detection current I_d, the AFDD cannot trip and p_{AFDD} is zero. In the case of ignition, the power of the flame is calculated using equation (73) and the energy of the flame is calculated with the equation (76). The parameters arc power and gap distance must be determined. A mean arc power is estimated with the mean values of the arc voltage, the arc current, and the arc stability $\bar{\delta}_{arc,i}$ at the flame ignition:

$$\bar{\dot{q}}_{arc,i} = \bar{I}_{arc,i} \;\; \overline{U}_{arc,i} \;\; \bar{\delta}_{arc,i} \tag{115}$$

The gap distance is estimated by making a comparison between the measured electrical characteristic of the arc displayed in Figure 80 and the theoretical characteristic displayed in Figure 57: a distance of approximately 0.3 mm can be deduced. This small gap distance is plausible since the tests reproduced stable series arcing that resulted mostly from contact arcing.

The series arc tests in PVC cables using the method explained in part 3.2 were repeated at 230 V AC in order to determine the different probabilities and arc characteristics. 50 samples were tested for each test current and the results are displayed in Table 10:

$I_{\max,i} - I_{\min,i}$	$\overline{U}_{arc,i}$	$\bar{I}_{arc,i}$	$\bar{\delta}_{arc,i}$	$\bar{\dot{q}}_{arc,i}$	$\bar{\dot{q}}_{F,i}$	$p_{c,i}$	$p_{IGN,i}$	$p_{AFDD,i}$	$\overline{Q}_{F,i}\big\vert_{AFDD}$
(A)	(V)	(A)	(%)	(W)	(W)				(J)
< 0.5	-	-	0 %	-	-	0.03	0	0	-
0.5 - 1.5	56.2	0.8	77 %	32.0	6.9	0.06	0.11	0.60	3.6
1.5 - 2.5	45.2	1.6	80 %	57.8	10.6	0.06	0.58	1	-
2.5 - 4	36.5	2.5	78 %	71.6	12.3	0.09	0.68	1	-
4 - 6.5	29.3	4.4	75 %	95.8	15.2	0.16	0.90	1	-
6.5 - 8.5	27.4	6.6	65 %	118.1	18.3	0.13	0.46	0.96	3.2
8.5 - 13	25.3	8.9	56 %	125.6	29.3	0.28	0.16	0.89	11.9
13 - 16	20.2	14.6	46 %	134.9	20.2	0.19	0.14	0.57	8.5

Table 10: Mean physical parameters and statistical analysis of the test results of series arcing in PVC cable using the method described in part at 230 V AC

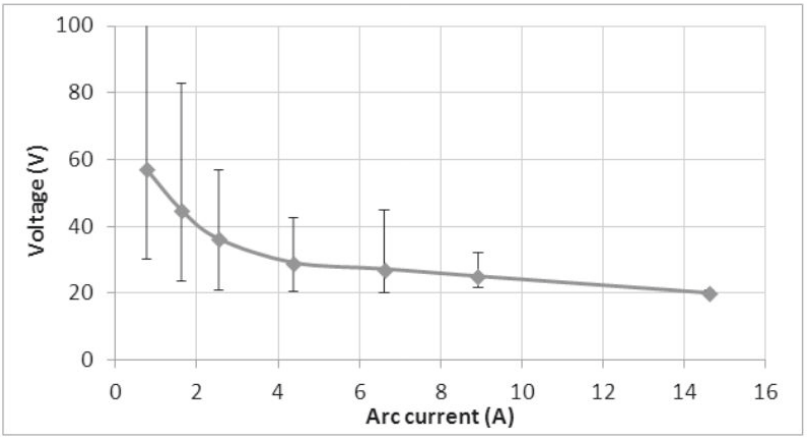

Figure 80: Mean arc voltage as a function of the mean arc current
Test according to the method described in part 3.2 at 230 V AC
(50 samples per current value)

The mean probability that the cable will ignite before the AFDD interrupts the current and the mean energy of the resulting flame are determined with equations (116) and (117). The mean flame energy is 8.4 J and the maximum calculated value is 15 J.

$$\overline{\left(1-p_{AFDD}\right)}=\frac{\sum_i p_{c,i}\ \left(1-p_{AFDD,i}\right)}{\sum_i p_{c,i}}=15\ \% \tag{116}$$

$$\overline{Q_F\big|_{AFDD}}=\frac{\sum_i p_{c,i}\ \ Q_{F,i}\big|_{AFDD}}{\sum_i p_{c,i}}=8.4\ J \tag{117}$$

Probability p_{SAF} and factor α remain unknown, but they do not need to be determined if we consider the ratio between the fire probability without and with AFDD protection. This ratio represents the safety factor increase based on fires caused by series arc faults that results from using the AFDD:

$$\frac{p_{FIRE}\big|_{NO\ AFDD}}{p_{FIRE}\big|_{AFDD}}=\frac{Q_F\big|_{NO\ AFDD}\ \sum_i p_{c,i}\ \ p_{IGN,i}}{\sum_i p_{c,i}\ \ p_{IGN,i}\ \left(1-p_{AFDD,i}\right)\ Q_{F,i}\big|_{AFDD}} \tag{118}$$

Table 11 displays the estimated values of the safety factor. If the AFDD fulfills the minimum series arc detection requirements of the standards IEC/EN 62606 (minimum detection current Id = 2.5 A and arc energy $Q_{ARC} \leq 100$ J), safety is increased by a factor of 9. The

protection devices usually present a performance margin above the minimum requirements; we can expect that most AFDDs can detect series arc faults at lower currents than the standard threshold of 2.5 A. With a detection threshold of 1.5 A, safety is increased by a factor of 53 and with a threshold of 0.5 A, this factor increases to 3695. The same estimate was performed for an arc energy limitation of 50 J: the improvement is very marginal because it only has an effect on the rare cases where ignition occurs before the AFDD is tripped. In contrast, lowering the detection current threshold results in a much greater improvement since it provides protection against series arc faults in a current domain that was previously not covered. The detection of series arc faults at arc currents below 0.45 A is not necessary since a stable arc cannot be sustained in these conditions between copper electrodes [Bab03 (p546)]. A minimum arc trip current of 1 A seems to be a reasonable compromise between safety and technical feasibility: with a safety factor of 264, the remaining risk of fire ignition is below 0.4 %. These results are very rough estimates and must be taken with caution since they are based on many statistical assumptions and data from testing in specific conditions. Nevertheless, they show that the safety factor is strongly dependent on AFDD sensitivity.

Detection current	*Id*	0.5 A	1 A	1.5 A	2 A	2.5 A
Safety factor	$\frac{p_{FIRE}\big\vert_{NO\ AFDD}}{p_{FIRE}\big\vert_{AFDD}}$	3695	264	53	19	9

Table 11: Safety factor against fire due to series arc fault in 230 V / 16 A branch circuits provided by the AFDD protection that limit the arc energy to 100 J

7 Investigations on insulation polymers

The thermal properties of an insulation material have a significant influence on the initiation of stable series arcs. One reason that was often mentioned is the charring of the polymer that results in a conductive track and supports the restrike of the arc after each current zero-crossing. The purpose of this chapter is to evaluate the behavior of the different insulation polymers at arcing conditions and to understand the relationship with the charring. The findings could be used to identify "arc-resistant" polymers and improve the passive protection. Therefore, specific tests that generate different thermal stresses were performed on the polymers and the performance levels were analyzed. Table 12 shows a list of the tested polymers that includes the technical information provided by the manufacturer. The base polymers and the presence of additives were verified using infrared spectroscopy. There are three halogen-free polymers (two on a PE basis and one on a PP basis) and three PVC-based polymers with different temperature ratings.

Polymer designation from manufacturer	Other material designation	Infrared spectroscopy analysis	Flame resistance acc. to	Specificity	Our designation
Halogen free 90 °C	TI6 acc. to DIN EN 50363-7	PE	IEC 60332-1-2	Halogen free	PE 90 °C
Cross linked Polyolefin 125 °C	No info available	PE low density	IEC 60332-1-2	Halogen free Heavy duty acc. to EN 50525-3-41	XLPE 125 °C
PP halogen free 90 °C	No info available	PP	No info available	Halogen free	PP 90 °C
PVC 70 °C	TI2 acc. to DIN EN 50363-3	PVC + CaCO3	IEC 60332-1-2		PVC 70 °C
PVC 90 °C Kälteflexibel	TI4 acc. to DIN EN 50363-3	PVC + CaCO3	IEC 60332-1-2	flexible at cold	PVC 90 °C
PVC UL 105 °C	No info available	PVC + CaCO3	No info available		PVC 105 °C

Table 12: List of tested polymers used as conductor insulation

7.1 Series arcing at 230 V AC

The purpose of this method is to determine the ability of the material to promote arcing and to ignite in the realistic conditions of a low-voltage circuit (230 V AC / 50 Hz).

7.1.1 Test setup

The reproduction of a series arc in an installation cable was already presented in 0. The same test setup is used for single conductors with a 1.5 mm² cross-section. The cable manufacturer provided flexible copper conductors in different fashions (tin or silver coating). In order to obtain comparable results, the strands were removed and new massive copper conductors were introduced in the insulation. The test setup is displayed in Figure 81. The fault zone is completely covered with the insulation (the opening visible in the 3D sketch is only there to display the arc location and conductors). Load R is resistive and adjusted to obtain a load current of 5 A without an arc. The positioning of the electrodes with a linear actuator is similar to the apparatus described in 3.2. The test duration is limited to 200 s after the first arc initiation. The current and voltage at the fault are recorded and a possible ignition of the probe is noted by the operator.

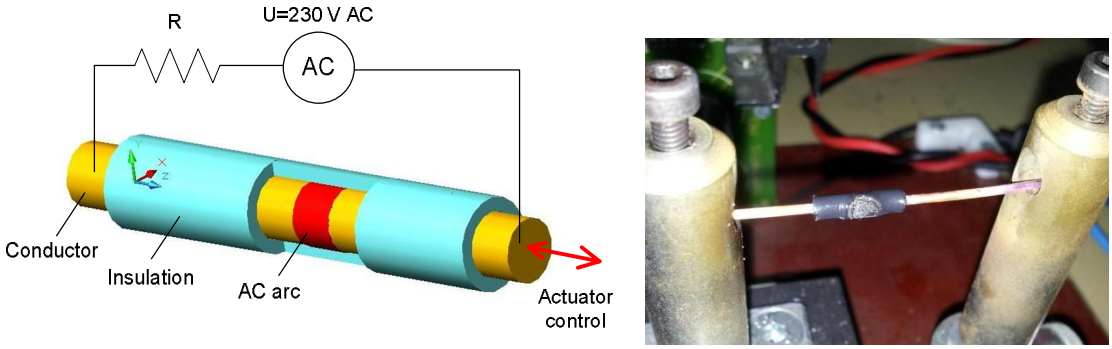

Figure 81: Sketch and picture of the test setup with series arcing at 230 V AC

7.1.2 Experimental results

The electrical values are analyzed to extract the energy that is necessary to initiate a stable series arc. At each half-cycle of the system voltage (10 ms), the current and voltage at the fault are analyzed to determine if there is an arc or not. An arc is detected if the voltage is at least 13 V and the current at least 0.1 A at the same time. The resulting logical signal is filtered with a moving average on a period of 100 ms in order to achieve arc stability (see

definition in 3.2). The amount of energy that is necessary to initiate a stable arc (with at least 70 % stability) is extracted from the data as displayed in Figure 82.

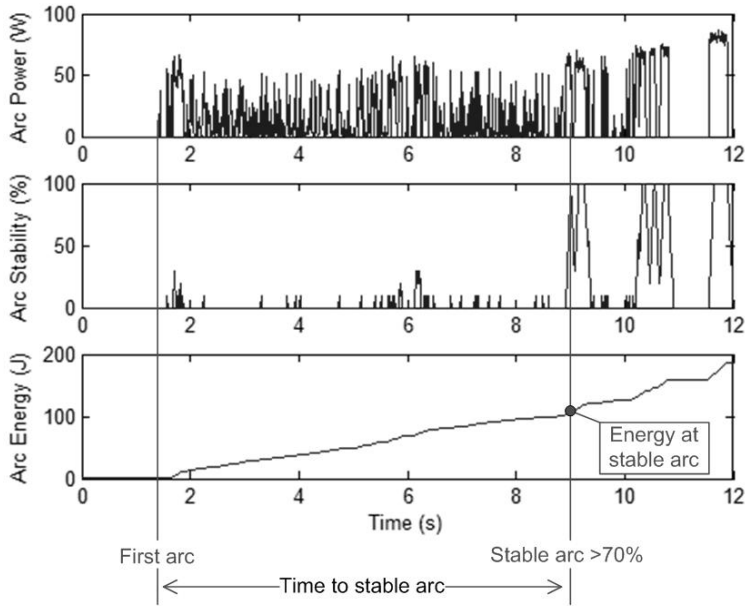

Figure 82: Electrical parameters of a series arc in PVC 70 °C insulated conductor at 230 V AC / 5 A load. Determination of energy and time to initiate a stable arc

The ignition probability is the proportion of ignited probes within the 200 s test time (at least 10 probes are tested for each polymer). In the case of ignition, the operator disconnects the probe from the power source and notes if the material self-extinguishes promptly. The results are displayed in Table 13. An "arc-resistant" material must have a low ignition probability. In the case of ignition, it will self-extinguish within seconds and the energy amount and time to initiate a stable arc will be as high as possible.

As expected, the PVC-based polymers have a high probability of ignition that is directly related to the initiation of a stable arc. The amount of energy needed to obtain a stable arc is in the range of 10 J to 1000 J. The median values are between 63 J and 110 J for the PVC-based polymers and this result is in line with the previous investigation on cables (see part). The corresponding duration is in the range of 0.5 s to 100 s. They all extinguish readily within 1 s or 2 s. The PE-based polymers do not ignite because it is not possible in these conditions to initiate a stable arc. For a few additional tests, the duration was extended to 5 minutes instead of 200 s. No stable arc and no ignition could be observed. The PP-based

polymer has a moderate performance. The ignition probability is lower than for PVC-based polymers because this material quickly melts and often fills the gap between the conductors. This positive behavior is counterbalanced by the fact that in the case of ignition, this material does not self-extinguish quickly. The material burns as long as there is flammable material to burn. The polymer often drops down and the fallen materials continue to burn.

Polymer	Ignition probability	Energy to stable arc (median)	Time to stable arc (median)	Self-extinguish
	%	J	s	Yes/No
PE 90 °C	**0 %**	not applicable / no stable arc		
XLPE 125 °C	**0 %**	not applicable / no stable arc		
PP 90 °C	64 %	45.5	10.4	**No**
PVC 70 °C	**90 %**	100.5	7.5	Yes
PVC 90 °C	**90 %**	64.3	14.2	Yes
PVC 105 °C	**100 %**	63.3	13.6	Yes

Table 13: Test results at series arcing at 230 V AC / 5 A load

7.2 Series arcing at 230 V DC

Arcs at DC current are very stable, reproducible, and easy to initiate. They offer a good opportunity to compare the behavior of insulation materials when they are exposed to this thermal stress. In addition, applications with higher DC voltages are becoming increasingly widespread (photovoltaic generators, data centers, servers, electrical cars, full electrical control in aircrafts…); the need for protection against arc faults has increased [UL11] and it is interesting to observe the behavior of ordinary insulation materials in the case of faults.

7.2.1 Test setup

The same electrode holder is used as in the test setup for AC low-voltage series arcing. A DC supply replaces the AC supply. The actuator is replaced by a mechanism that can quickly (within 20 ms) separate the conductors at a distance of 1 mm. A circuit detects the arc with the value of the arc voltage as an indicator and sends a command to open the solid-state relay S in order to limit the arc duration to exactly 1 s. The load current is adjusted to 4 A without

an arc. The current and voltage at the fault are recorded and a possible ignition of the probe is noted by the operator. In addition, the mass of the probes is measured with a precision balance before and after the test in order to determine the mass of polymer that was vaporized. The residues are scraped away from the intact base material and the mass difference is deduced. At least ten probes of each material are tested for each polymer.

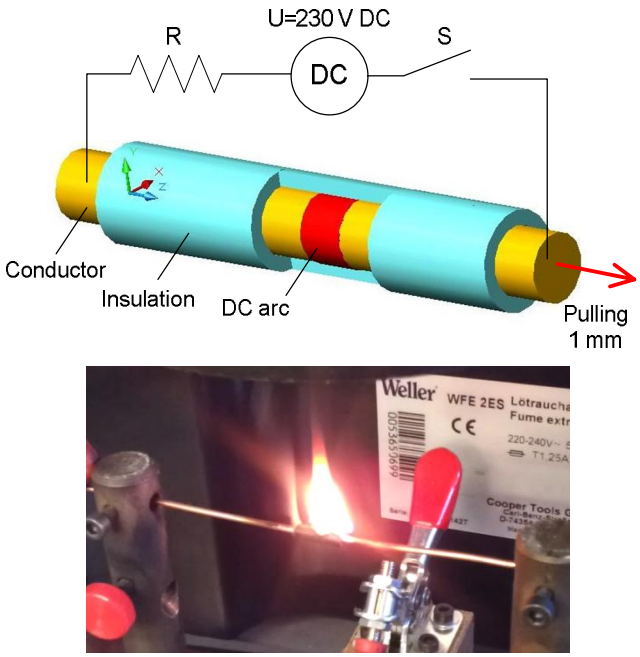

Figure 83: Sketch of the test setup with series arcing at 230 V DC and picture of an ignited probe (PP 90 °C) that still burns after the arc has been interrupted

7.2.2 **Experimental results**

In order to limit the disturbances while the arc is initiated and when the probe is burning, the electrical parameters are analyzed in a limited time that lasts 0.2 s and starts 0.2 s after initiation of the arc. Figure 84 displays the arc voltage and current during a test. The power of this arc is on average 135 W. The arc power is also determined without insulation and its average value is 89 W. In the short duration for measurement, the probe is still intact and the arc is confined between conductors and insulation; power dissipation by radiation and convection is neglected and we assume that the complete power is dissipated by conduction in the conductors and in the insulation. The additional cooling power that is due to the cooling effect of the insulation can be estimated using the equation (119):

$$\Delta\dot{q}_{cool} = \frac{\int_{0.2s}^{0.4s} U_{arc}(t)\ I_{arc}(t)\ dt}{0.2s} - 89\,W \tag{119}$$

This additional cooling power includes two components: cooling due to gassing and conduction to insulation. Since many parameters are not known, especially the specific heat capacity of the gas (which probably varies for each type of polymer) and the proportion of this gas flow that really reaches the arc column, it is not possible to estimate each component.

The mean values of the additional cooling power are displayed in Table 14. Since the standard deviations are in the range of 5 W to 8 W, we can assume that PE 90 °C and PVC 105 °C cool the arc more than the other materials. This would mean that the heat capacity of the gasified mass of the polymer is more important (higher mass and/or higher specific heat capacity) and/or the atoms present in these gases have higher ionization energies.

The mass losses show that the PVC-based polymers were more vaporized than the PE-based polymers. The mass loss per unit of energy could be estimated using equation (120) with a test duration t_{test} equal to 1 s. For each Joule of energy dissipated in the polymer, the PVC-based polymers lost twice as much mass as the PE-based polymers. The reason is most probably the loss of the chlorine HCl that is quickly released at thermal stress and represents approximately 50 % of the mass. Another explanation could be a higher concentration of inert fillers in the PE-based polymers.

$$\frac{\Delta\overline{m}}{\Delta Q_{cool}} = \frac{\Delta\overline{m}}{\Delta\overline{\dot{q}}_{cool}\ \ t_{test}} \tag{120}$$

The proportion of ashes varied from 8 % to 27 %. Producing a lot of ash during combustion is an appropriate means of protection from burning. The ashes that remain are materials that do not vaporize and this limits the concentration of flammable gases. The high performance polymer XLPE 125 °C had the maximum proportion of ashes of 27 %.

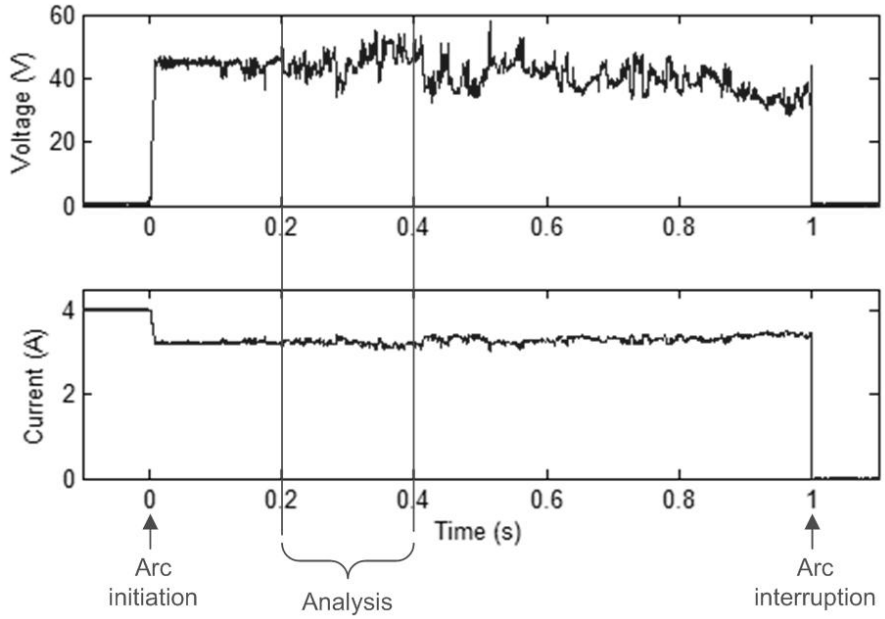

Figure 84: Electrical parameters of a series arc in PE 90 °C insulated conductor at 230 V DC / 4 A load

All the probes of PVC and PP-based polymers ignite and burn readily. As expected, the PP-based polymer does not extinguish just after arc interruption (see Figure 83). The ignition probability for PE-based polymers is in the range of 50 %. It can be observed that these polymers have a better mechanical stability at higher temperatures and can sometimes withstand the heat of the arc for a limited duration. Many tests were repeated for longer arc durations and it was observed that all probes ignited if the arc lasted for two seconds. This shows that all the tested polymers can burn at arcing. In DC applications, a series arc may last much longer and the short additional time (~ 1 s) that can be gained by using one of these PE-based polymers will only be useful in combination with an adequate arc fault detector that can quickly interrupt the current. This shows that active protection devices and highly reliable connectors are necessary for DC applications at important voltages. Systems with voltages below 30 V are not considered here since the measured arc voltages at series arcing in cables are in the range of 30 V to 100 V (see Figure 54 and Figure 56 in part 6.1.1.2). Protection of photovoltaic generators is already mandatory in the United States and a UL product standard is available [UL11]. Specific requirements for installations covered by the IEC standards are in discussion.

Polymer	Ignition probability	Self extinguish	Additional Cooling power $\Delta\bar{\dot{q}}_{cool}$	Mean mass loss per probe $\Delta\overline{m}$	Mass loss per unit of energy $\Delta\overline{m} / \Delta Q_{cool}$	Proportion of ashes μ
	%	Yes/No	W	mg	μg/J	%
PE 90 °C	50 %	Yes	68	5.3	78	10 %
XLPE 125 °C	60 %	Yes	64	4.5	71	27 %
PP 90 °C	**100 %**	**No**	51	not measurable / material melts		
PVC 70 °C	**100 %**	Yes	56	9.4	167	13 %
PVC 90 °C	**100 %**	Yes	60	9.1	152	8 %
PVC 105 °C	**100 %**	Yes	69	10.2	149	8 %

Table 14: Test results at series arcing at 230 V DC, 4 A load, and 1 s duration

7.3 Carbonization at high-voltage

Carbonization at high voltage is a method that is already used in the test standards for AFCI and AFDD [UL13, IEC13] to condition cable samples and initiate very stable arcs. It is particularly appropriate to produce rapidly a carbonized track between the conductors. This method allows an evaluation of the relationship between thermal stress and carbonization for different polymers with a better reproducibility than with the test at 230 V AC (see 7.1).

7.3.1 Test setup

The massive conductors are inserted in the insulation and the gap distance between them is adjusted to 1 mm using a precision linear translator. A ceramic holder is tightened around the sample in order to improve the mechanical stability of the system (see Figure 85). The sample is placed in the high-voltage conditioner and tested in two steps. At the first step, a transformer supplying a voltage of 7.5 kV AC with a short-circuit current of 18 mA is switched during 10 seconds in parallel with the probe. The goal of this first step is to initiate an electrical discharge and provoke a first degradation of the polymer. At the second step, the same procedure is repeated with a transformer supplying 2.5 kV AC with a maximum current of 200 mA. At every step, the voltage and current at the sample are recorded. After the test, the conductance between the two conductors is measured at low voltage and the mass loss of each single probe is determined.

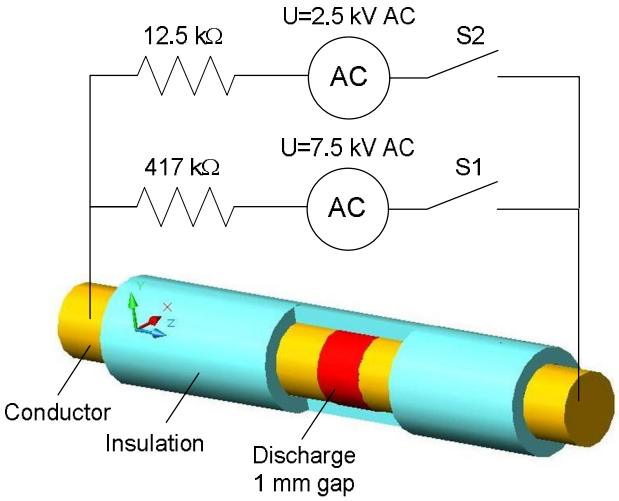

Figure 85: Sketch of test setup with discharge at AC high-voltage

7.3.2 **Experimental results**

It appears from the analysis of the electrical data that there is either an electrical discharge or a resistive path between the conductors. The resistive path is a carbonized track that was formed during the test. A distinction can be made in Figure 87 for the PVC 70 °C: a transition from discharge to carbonized track is visible. The discharge voltage has a typical shape with steep edges and higher voltage values. The carbonized track results in a sinus waveform of the electrical signals with a much lower voltage and an increased current value. The thermal stress from the discharge carbonizes the PVC and forms a carbonized track between the conductors (see Figure 86). While the resistance of this carbonized track decreases, the current is shared between this parallel path (current I_C) and the discharge (current I_D). Since the current from the transformer is limited, the discharge current I_D decreases. Below a critical value, the discharge cannot be sustained any more.

The discharge can be distinguished from the carbonized track by calculating the conductance that is determined by dividing the average current at each half-cycle by the average voltage. The analysis of the tests shows that the conductance of the discharge is in the range of 10^{-5} S and the conductance of a carbonized track in the range of 10^{-3} S. A conductance threshold is set at 3.10^{-4} S in the analysis script. This method allows splitting of the energy dissipation into two components: the energy dissipated by the discharge and the ohmic heat dissipated by the carbonized track. The energy values are calculated by integrating the electrical power. Figure

88 displays the conductance and the energies during the first test step for a PVC 70 °C sample. It shows that the initial discharge lasts 2 s, has a power of 5 W, and dissipates 9.5 J to produce a stable carbonized track. After the transition, the carbonized track dissipates 3.1 J at a much lower power of 0.4 W.

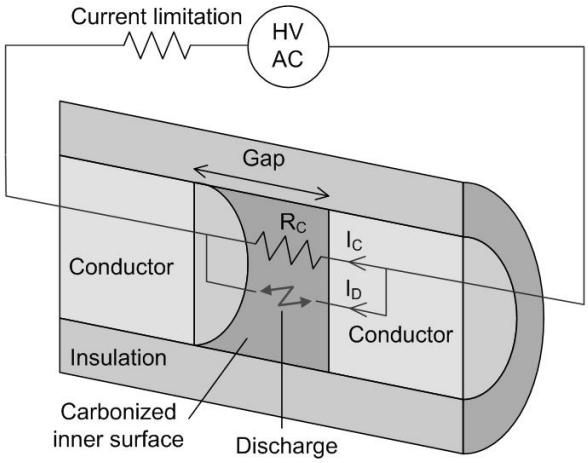

Figure 86: Sketch and equivalent circuit of the system during high-voltage carbonization test

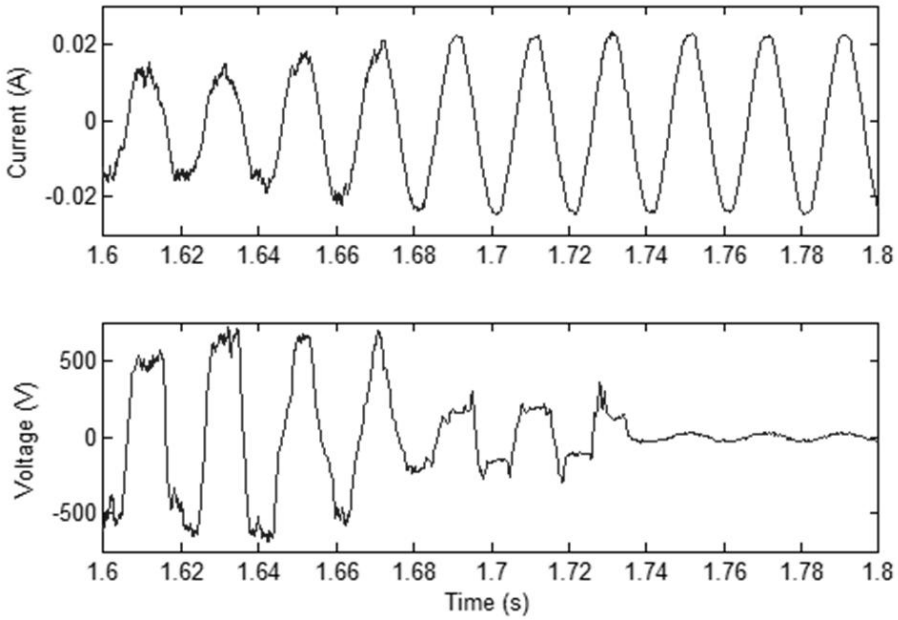

Figure 87: Voltage and current of the 1st step with PVC 70 °C (zoom at the transition from discharge to carbonized track)

The same data analysis is also performed for the second step. The energy values reveal two different trends for the polymers. As displayed in Figure 89, the PVC-based polymers

present the highest values of ohmic heat and the PE-based polymers do not carbonize (the discharge lasted during the complete test). Despite the presence of the ceramic holder, the mechanical stability of the samples of PP-based polymers is very low and only a few test results are available.

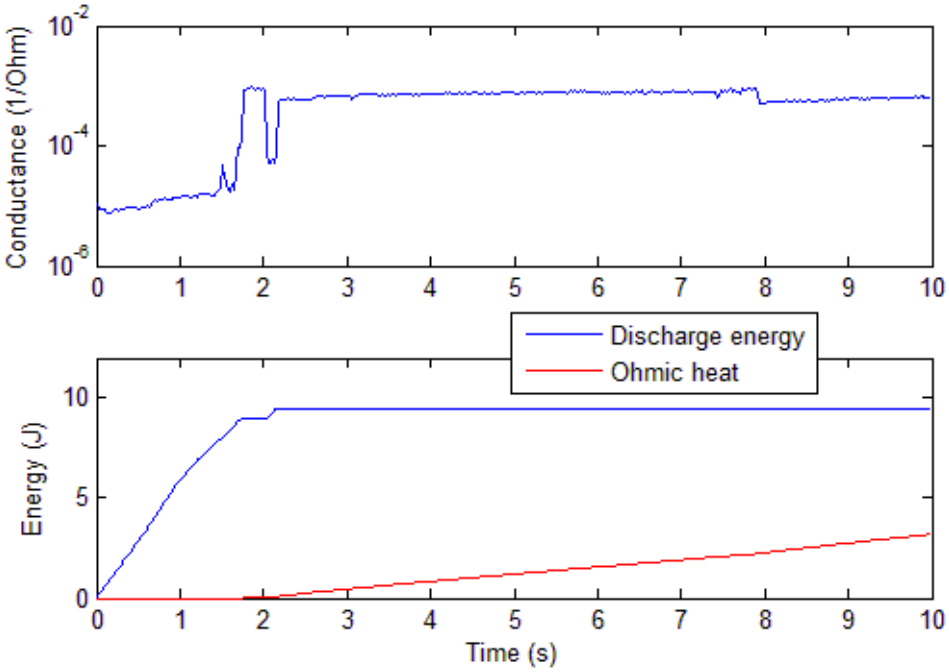

Figure 88: Extrapolated electrical parameters at the 1st step with PVC 70 °C

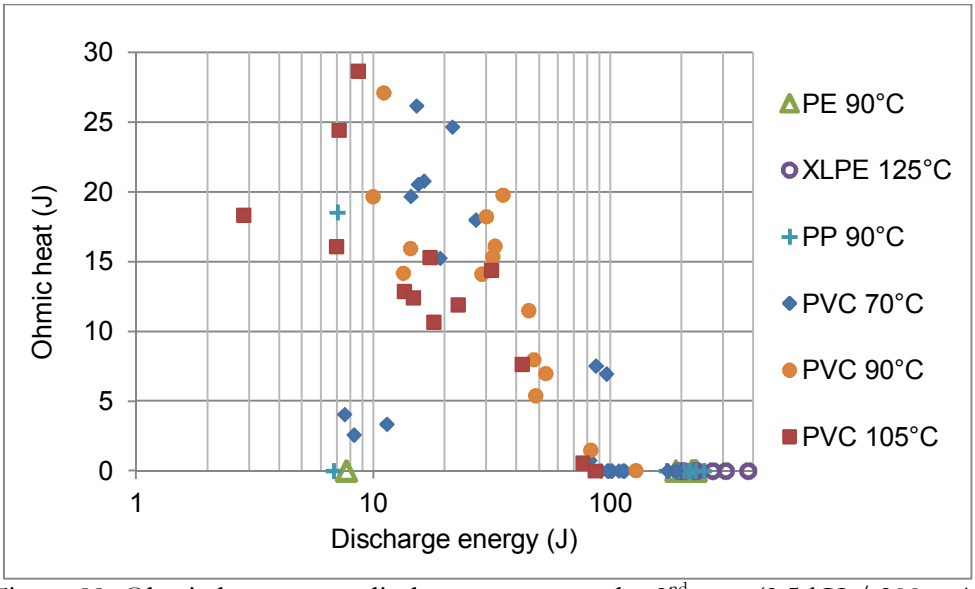

Figure 89: Ohmic heat versus discharge energy at the 2nd step (2.5 kV / 200 mA)

The mass losses displayed in Figure 90 show a tendency to increase in a linear fashion with the energy for all the polymers. The PVC-based polymers lose on average 33 μg/J and the PE-based polymers 13 μg/J. The ratio of mass losses per unit of energy between PVC and PE is 2.5 and this result is in accordance with the factor 2.1 that can be extrapolated from the test at 230 V DC (see Table 14).

The proportion of ashes is in the range of 40 % to 60 % for all the materials (see Table 15). This result differs from the test at 230 V DC. Since the available amount of oxygen at the location of the load is very limited, the samples do not burn and there is no heat feed-back from a flame; the oxidation and dissociation of the polymer are reduced. This hypothesis is confirmed with the result of the thermogravimetric test explained in part 7.4.

If the ashes can conduct electrical current, the conductance of the sample will increase with the mass of ashes. The ratio of the conductance to the mass of ashes is displayed in Figure 91 and shows again the two distinct behaviors of the PVC and PE-based materials. The conductivity of the ashes from PVC is in general 100 times higher. This means that the thermal stress on the PVC results in the production of carbon-based residues (char) that are able to conduct electrical current.

The required energy to vaporize and carbonize 1 g of the PVC insulation is on average 15 kJ. The gasification enthalpy provided by [FAA05] is between 1.2 and 2.1 kJ/g. The important difference between both values means that a significant proportion of the energy that was dissipated during both carbonization steps is not used to carbonize and evaporate the insulation. Most of it is dissipated in the conductors. On the one hand, the ohmic heat is produced directly by the carbonized track itself and we would expect most of this heat to contribute to the degradation of the polymer. On the other hand, the discharge is not too close to the insulation and most of the heat will be absorbed by the conductors. We assumed that 90 % of the ohmic heat and only 5 % of the discharge energy contribute to degrading the insulation and we obtained a plausible result of 1.9 kJ/g. Since 55% of the mass of the PVC-based polymer remains as carbonized residue, we can conclude that approximately 3.5 kJ of energy is necessary to produce 1 g of this conductive material.

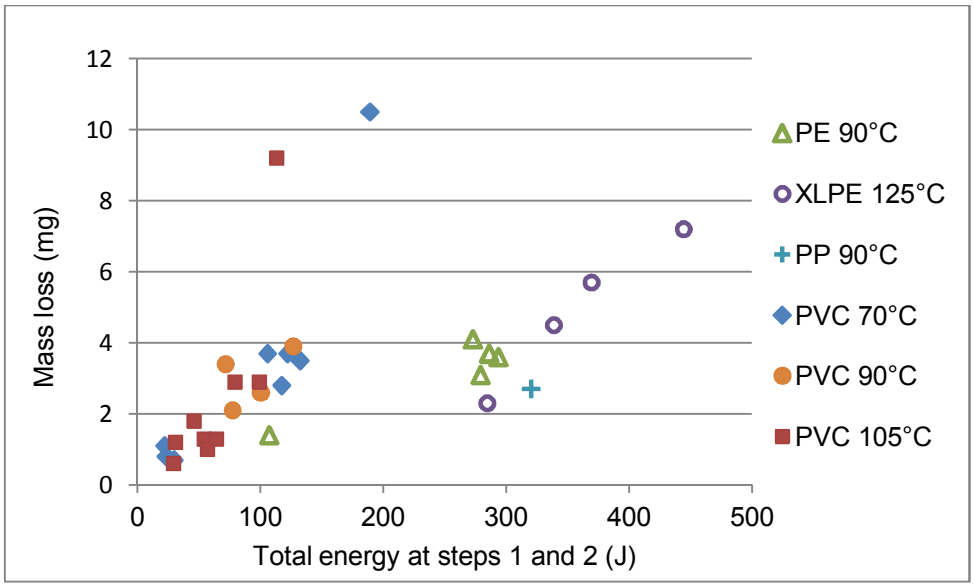

Figure 90: Mass loss versus cumulated discharge energy at steps 1 and 2

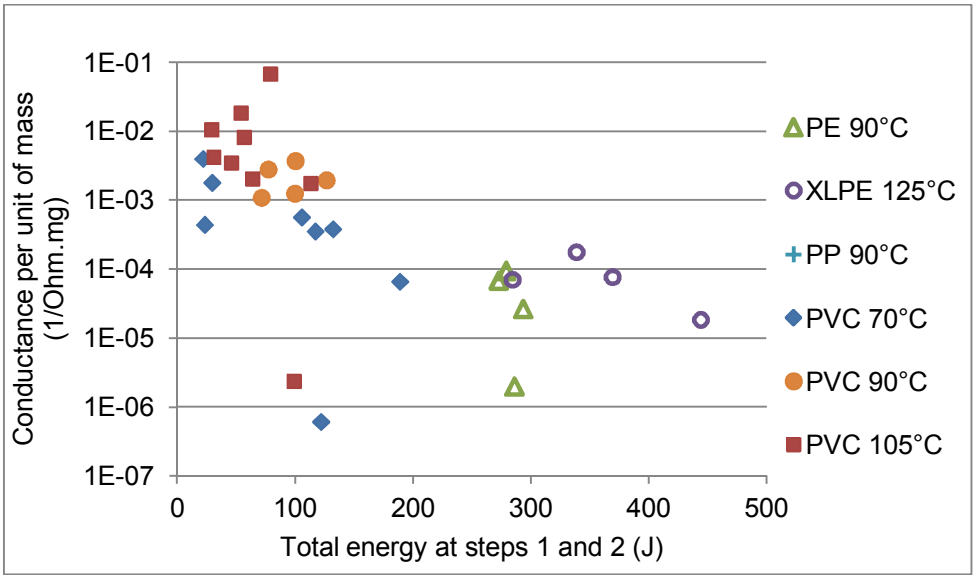

Figure 91: Conductance per unit of ashes' mass versus cumulated discharge energy at steps 1 and 2

Polymer	HV conditioning leads to conducting path	Mass loss per unit of energy	Proportion of ashes
	%	µg/J	%
PE 90 °C	0 %	13	42 %
XLPE 125 °C	0 %	13	47 %
PP 90 °C	20 %	no data	
PVC 70 °C	100 %	35	57 %
PVC 90 °C	100 %	31	56 %
PVC 105 °C	100 %	34	49 %

Table 15: Results of the tests at high-voltage AC

7.3.3 **Further considerations on the carbonized track**

If we assume that the carbonized materials are homogeneously spread on the internal surface of the insulation between the conductors (see Figure 92), we can make a rough estimate of the electrical conductivity of this material with the following equation:

$$\sigma = \frac{\overline{G}\ \ gap^2\ \ \rho}{\Delta\overline{m}} \tag{121}$$

where $\overline{G}$ is the mean value of conductance, $\Delta\overline{m}$ the mean mass of ashes, *gap* the gap distance of 1 mm, and ρ the density of the carbonized material (1650 kg/m^3 for the ashes of the PVC 70 °C). The obtained values vary between 1.6 and 21.4 S/m; the value of 10 S/m was chosen for this theoretical analysis. The temperature dependency shows a semiconducting behavior with a positive temperature coefficient of 5.3 10^{-3} /K (see Figure 93).

The voltage drop and electrical power at a carbonized track that forms a resistance R_c in series with an electrical load R_{Load} in a circuit at the voltage U_{sys} are:

$$U_c(t) = U_{sys}(t)\ \frac{R_c(t)}{R_c(t) + R_{Load}} \tag{122}$$

$$R_c(t) = \frac{gap^2\ \ \rho}{\Delta m\ \ \sigma\ \ \left(1 + 5.3\ 10^{-3}\ \ T(t)\right)} \tag{123}$$

$$\dot{q}_{heat}(t) = \frac{U_c(t)^2}{R_c(t)} \tag{124}$$

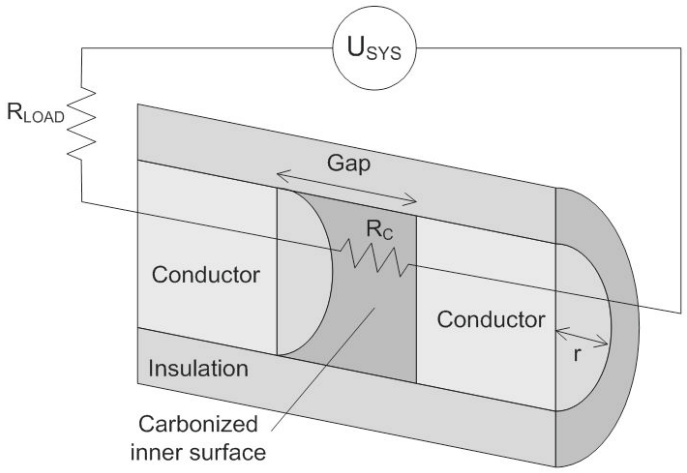

Figure 92: Sketch and equivalent circuit of the model

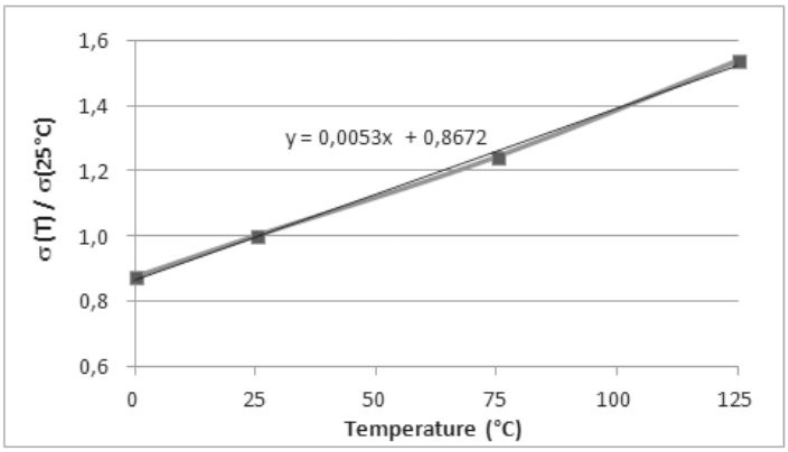

Figure 93: Temperature drift of electrical conductivity of the carbonized residue (for PVC 70°C)

If we consider only the conduction losses, the cooling power is divided into two terms: the dissipation in the PVC insulation with thermal resistance $R_{th,r}$ and the dissipation in the conductors with $R_{th,z}$.

$$\dot{q}_{cool}(t) = \frac{T(t) - T_{amb}}{R_{th,r}} + 2\ \frac{T(t) - T_{amb}}{R_{th,z}} = \frac{T(t) - T_{amb}}{R_{th}} \tag{125}$$

with

$$R_{th,r} = \frac{Film\ thickness}{\kappa_c \ 2\pi \ r \ gap} = \frac{\Delta m}{\kappa_c \ 4\pi^2 \ r^2 \ gap^2 \ \rho} \tag{126}$$

$$R_{th,z} = \frac{gap}{\kappa_c \ 2\pi \ r \ Film\ thickness} = \frac{gap^2 \ \rho}{\kappa_c \ \Delta m} \tag{127}$$

$$Film\ thickness = \frac{\Delta m}{2\pi \ r \ gap \ \rho} \tag{128}$$

$$\frac{1}{R_{th}} = \frac{1}{R_{th,r}} + \frac{2}{R_{th,z}} \tag{129}$$

Thermal conductivity κ_c and specific heat capacity c_c of the film of carbonized material are not known. The values for amorphous carbon are used: 0.2 W/m K and 907 J/kg K respectively [Yaw11].

The temperature of the carbonized track can be expressed with the equation (130) that leads to the differential equation (131):

$$T(t) = T(0) + \frac{\int_0^t (\dot{q}_{heat}(t) - \dot{q}_{cool}(t)) \ dt}{m \ c_c} \quad \text{with } T(0) = T_{amb} \tag{130}$$

$$\frac{dT(t)}{dt} = \frac{1}{m \ c_c} \left(\frac{R_c \ \hat{U}_{sys}^{\ 2} \ \sin^2(\omega \ t)}{(R_c(t) + R_{Load})^2} - \frac{T(t) - T(0)}{R_{th}} \right) \tag{131}$$

The differential equation is simplified by neglecting the time dependency in *Rc* and using new parameters α and β:

$$\frac{dT(t)}{dt} = -\alpha \ T(t) + \alpha \ T(0) + \beta \ \sin^2(\omega \ t) \tag{132}$$

with

$$\alpha = \frac{1}{m \ c_c \ R_{th}} \tag{133}$$

$$\beta = \frac{R_c \ \hat{U}_{sys}^{\ 2}}{m \ c_c \ (R_c + R_{Load})^2} \tag{134}$$

Since there is a term $-\alpha$ multiplied with $T(t)$, the solution of the differential equation must have the following form:

$$T(t) = \exp(-\alpha\ t)\left(\beta\ \int_0^t \exp(\alpha\ t)\ \sin^2(\omega\ t)\ dt + T(0)\ (\exp(\alpha\ t)+1) + C\right) \quad (135)$$

The integral of $\exp(\alpha\ t)\ \sin^2(\omega\ t)$ is calculated by applying the product rule method:

$$u\ v = \int (u'\ v + u\ v') \quad (136)$$

$$\int u'\ v = u\ v - \int u\ v' \quad (137)$$

If we define $u = \exp(\alpha\ t)$ and $v = \sin^2(\omega\ t)$, we obtain:

$$\int \exp(\alpha\ t)\ \sin^2(\omega\ t)\ dt = \frac{1}{\alpha}\ \left(\exp(\alpha\ t)\ \sin^2(\omega\ t) - \omega\ \int \exp(\alpha\ t)\ \sin(2\omega\ t)\ dt\right) \quad (138)$$

The term with sin² is now outside of the integral and the remaining integral of $\exp(\alpha\ t)\ \sin(2\omega\ t)$ is calculated using the same method. We obtain:

$$\int \exp(\alpha\ t)\ \sin(2\omega\ t)\ dt = \frac{1}{\alpha^2 + 4\omega^2}\ \exp(\alpha\ t)\ (\alpha\ \sin(2\omega\ t) - 2w\ \cos(2\omega\ t)) \quad (139)$$

and finally:

$$\int_0^t \exp(\alpha\ t)\ \sin^2(\omega\ t)\ dt = \exp(\alpha\ t)\left(\frac{\sin^2(\omega\ t)}{\alpha} - \frac{w\ \sin(2\omega\ t) - \frac{2\omega^2}{\alpha}\ \cos(2\omega\ t)}{\alpha^2 + 4\omega^2}\right) \quad (140)$$

Constant C is determined with the initial conditions at the time t=0. We obtain:

$$C = -\frac{2\beta\ \omega^2}{\alpha^3 + 4\alpha\ \omega^2} \quad (141)$$

The final solution is:

$$T(t) = \exp(-\alpha\ t)\left(\beta\ \int_0^t \exp(\alpha\ t)\ \sin^2(\omega\ t)\ dt + T(0)\ (\exp(\alpha\ t)+1) - \frac{2\beta\ \omega^2}{\alpha^3 + 4\alpha\ \omega^2}\right) \quad (142)$$

Figure 94 displays the maximum temperature, the electrical power, and the voltage drop at the carbonized track that can be reached during a half-cycle of 10 ms for different impedance values R_c at the system voltage 230 V AC and with a 2.5 A load in series: the mass of carbonized residue is increased step by step, starting at 20 µg and the calculation is stopped when the film thickness exceeds the radius r of the conductor. The calculated values are purely theoretical and are used for comparison purposes. They are only valid for the hypothesis that the carbonized track remains stable and does not lead to an arc strike. If the impedance of the track is too low or too high, the heating power and the temperature are

lower. The temperature is at a maximum for the intermediate values of impedance (50 Ω to 300 Ω) and reaches 1600 K. This shows that the arc strike due to creepage on char is less probable if the impedance of the track is too low or too high. If it is too low, the voltage drop is too low and the arc striking voltage cannot be reached. If it is too high, the current is too low and cannot sufficiently heat the fault area to initiate the arc. This behavior was observed during preparation of cord specimens and the test of AFDDs according to IEC 62606 [IEC13]. If the cord specimens were insufficiently or excessively carbonized, initiation of a series arc with a small load in series was difficult to obtain. The same analysis is displayed in Figure 95 for a 16 A load in series. The lower load impedance results in a higher voltage drop and available electrical power at the fault. For the same initial impedance of the carbonized track, the probability of an arc strike is greater with a higher load in series.

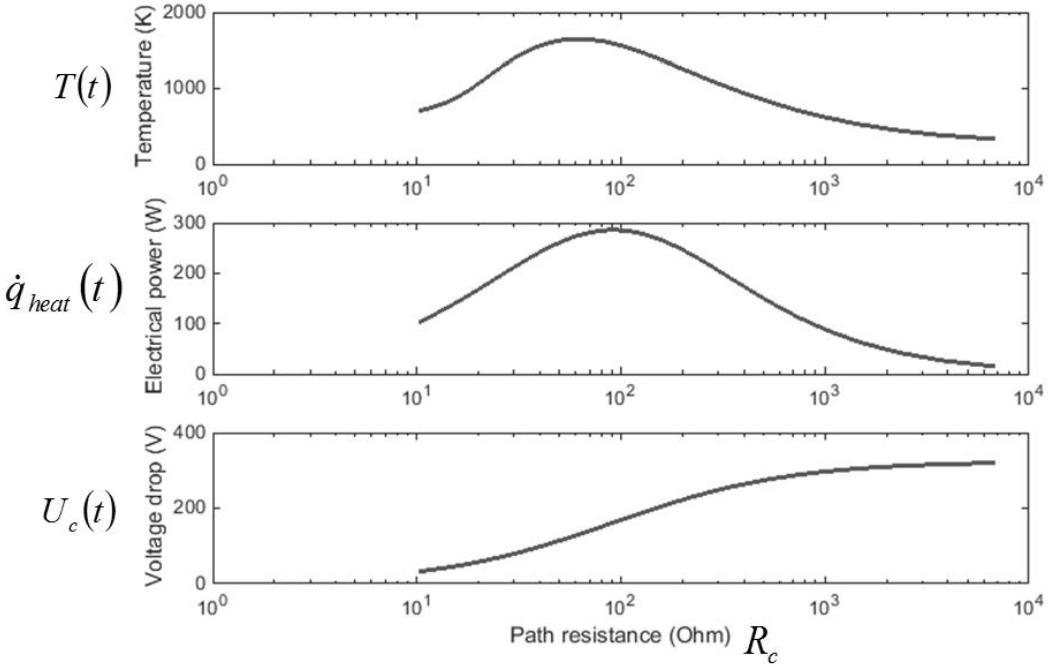

Figure 94: Electrical and thermal characteristics of the carbonized track for 230 V AC, 2.5 A load, and 1 mm gap distance

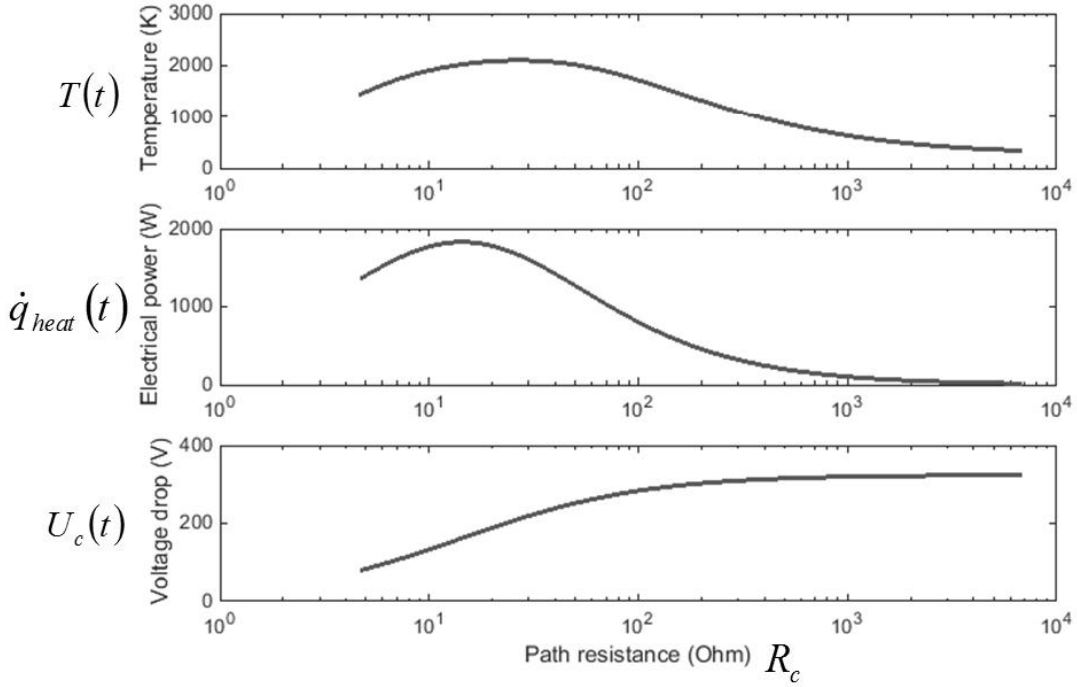

Figure 95: Electrical and thermal characteristics of the carbonized track for 230 V AC, 16 A load, and 1 mm gap distance

7.4 Thermogravimetric analysis

The thermogravimetric analysis is an analytical method for measuring the physical and chemical changes in a material as the temperature increases [Ben99, DIN05]. A small quantity of the polymer is placed in a ceramic holder. The mass of the sample is monitored as the temperature increases at a constant rate of 10 K/min in an atmosphere of pure nitrogen. The same procedure is performed with pure oxygen and a comparison with the results with pure nitrogen reveals the chemical changes related to oxidation reactions. Figure 96 displays the evolution of the mass up to 800 °C of the PVC 70 °C and PE 90 °C.

As displayed in Figure 95, the PVC 70 °C starts to decompose at 230 °C with the splitting of the chlorine HCl and loses 42 % of its mass. This process is completed at 350 °C. The further decomposition of the PVC takes place in two steps while flammable gases are vaporized. Between 400 °C and 500 °C, 9 % of the mass is lost with pure nitrogen and 16 % with pure oxygen. Between 625 °C and 740 °C, 9 % of the mass is lost independently of the test gas. The remaining proportion of ashes is 36 % when testing with nitrogen and 29 %

with oxygen. This means that 7 % of the mass of the remaining ashes after the test with nitrogen is composed of carbonized residues. In contrast, the PE 90 °C has a better thermal stability because it starts to decompose at 290 °C. 56 % of the mass is lost in two steps that take place at a much lower temperature under oxidizing conditions. The proportion of ashes is nearly the same for the tests with nitrogen and oxygen (45 %). The ashes of the PE-based polymer contain a very low concentration of carbon after complete thermal degradation. An EDX spectroscopy was performed and the identified elements were aluminum, magnesium, and oxygen (probably the elements of the fillers). Only traces of carbon and silicon were detected. This analysis shows that the ashes from the PE-based polymers are carbon-depleted compared with the ashes from the PVC-based polymers. This observation may explain the huge differences regarding the formation of a conductive track and the initiation of stable arcs with both polymers. Other polymers collected from electrical equipment were tested in the same conditions and the results are displayed in Table 17. PC, PPO, and PUR-based polymers do not seem to be arc-resistant. PP, PBT, and ABS-based polymers are supposed to be arc-resistant.

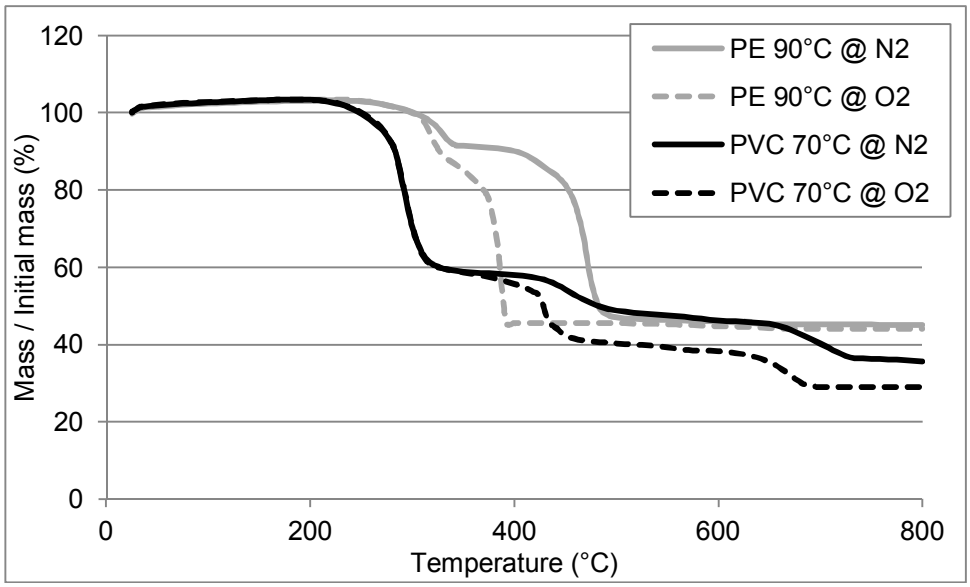

Figure 96: Thermogravimetric curve for PE 90 °C and PVC 70 °C polymers with pure nitrogen and pure oxygen

Ash from the PVC 70 °C was collected after the carbonization at high voltage and was analyzed with the thermogravimeter at pure nitrogen (see Figure 97, continuous line). An

important mass loss of 30 % was observed at temperatures below the decomposition temperature of 230 °C. The only possible explanation is the presence of water in the ashes that was captured during the storage period (few days). This finding could explain the observation of small water drops that were discovered on carbonized cables (see Figure 98). This property to absorb water could be an aggravating factor: the water droplets could increase the conductance of the complete fault zone in addition to the carbonized track, thus forming a combination of dry and wet tracking fault.

After the complete evaporation of the water at 130 °C, the same mass losses corresponding to the splitting of the chlorine and the decomposition of the rest of the polymer were observed. The same ashes were used for a second test, this time with pure oxygen: an additional mass loss of 20 % was observed. The EDX spectroscopy showed that the ashes are mainly composed of calcium and chlorine. These last observations show that the polymer is not completely decomposed during the thermal stress of an electrical fault. We can assume that if a carbonized track exists between two conductors at different polarities, the ohmic heat dissipated by the current flow in this track can still generate gases. These hot gases may quickly heat the space between the conductors and facilitate the striking of the arc.

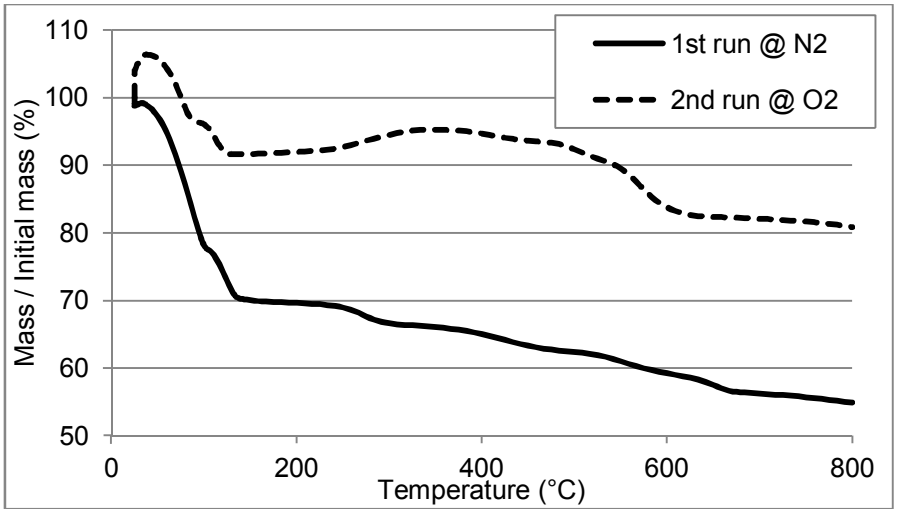

Figure 97: Thermogravimetric curve for the ashes of PVC 70 °C after carbonization at high-voltage

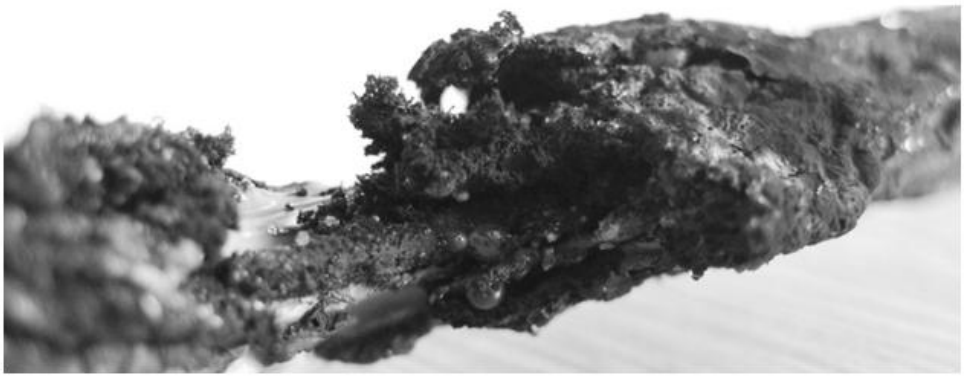

Figure 98: Presence of water droplets on a carbonized NYM-J cable (PVC based) after a series arc test

7.5 Glowing at 230 V AC

The possible thermal stress at glowing faults and the relationship with series arcing has already been discussed in part 3.3. The behavior of the electrical polymers under glowing conditions is observed using a simple method. The same test setup for a series arc at 230 V AC is used with 1.5 mm² massive copper conductors without insulation (Figure 99). The load current is set to 2 A because glowing is very stable at this value. After the initial oxidation at contact arcing (see 3.3.1), a glowing connection is initiated and the movable conductor is slowly retracted in order to extend the glowing bridge and increase its power dissipation. The voltage and current values are monitored and as soon as the power is in the range of 8 to 14 W, a piece of polymer is applied manually on the glowing bridge. The application force and position are varied and 5 to 10 trials per polymer are performed. The alteration of the polymers and possible ignition are observed. The test of a PVC sample is shown in Figure 33 of part 3.3.2. Table 16 displays the results for the polymers that were tested with other methods and also additional polymers for wire and cable jacket insulation provided by the same cable manufacturer. It appears that the PE-based and halogen-free polymers are very stable and cannot be ignited. The PVC, PP, and PUR-based polymers are quickly damaged. They are deformed, melted, and generate smoke. They can ignite, but the ignitions are always associated with the initiation of a stable series arc.

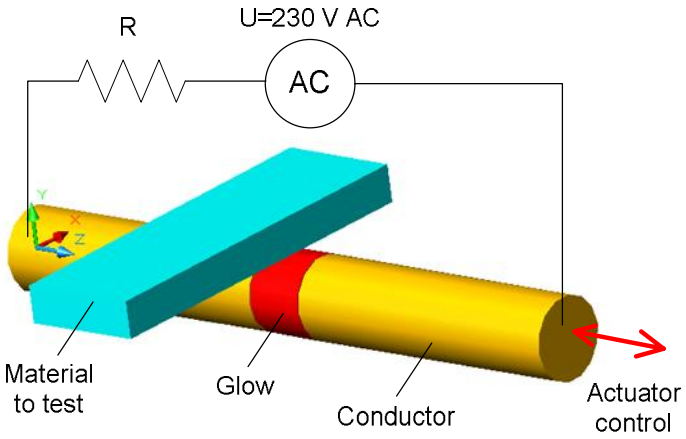

Figure 99: Sketch of test setup with glowing at 230 V AC / 2 A

Designation	Insulation for	Alteration	Ignition
PUR	Jacket	Melting + smoke	Seldom, only at arcing
PUR flame resistant	Jacket	Melting + smoke	Seldom, only at arcing
PUR not flame resistant	Jacket	Melting + smoke	Small flames, only at arcing
Polyolefin Halogenfrei	Jacket	Melting + smoke	Small flames, only at arcing
PVC 90 °C	Jacket	Melting + smoke	Small flames, only at arcing
PVC 70 °C	Jacket	Melting + smoke	Small flames, only at arcing
PVC 70 °C transparent	Jacket	Melting + smoke	Small flames, only at arcing
Polyolefin halogen free	Jacket	Almost no damage	No
PE 90 °C	Wire	Almost no damage	No
XLPE 125 °C	Wire	No damage	No
PP 90 °C	Wire	Melting + smoke	Small flames, only at arcing
PVC 70 °C	Wire	Melting + smoke	Small flames, only at arcing
PVC 90 °C	Wire	Melting + smoke	Small flames, only at arcing
PVC 105 °C	Wire	Melting + smoke	Small flames, only at arcing
Polyolefin halogen free 90 °C	Wire	No damage	No
PVC UL 90 °C	Wire	Melting + smoke	Small flames, only at arcing

Table 16: Results of the glowing test for different polymers

7.6 Conclusions on the relationship between series arcing and insulation polymers

The evidence from the investigations shows a clear relationship between the decomposition of the polymers into char and the initiation of stable series arcs that can lead to the ignition of the insulating material. All the tested polymers could burn, but only the PVC and the PP-based polymers were able to produce a carbonized track under the thermal stress provoked by electrical faults and anomalies such as glowing connections and contact arcing. This carbonized track can initiate a very stable arc (of the type arc due to creepage on char) that has a higher power density than other faults and can quickly ignite the flammable materials. The PUR-based polymers may have the same behavior since the important difference between the proportion of residues after TGA at pure nitrogen and TGA at pure oxygen reveals the tendency of this material to carbonize (see Table 17). In contrast, the PE-based polymers and in general the halogen-free polymers do not easily carbonize and seem to be very "arcing-resistant".

Other polymer types that may be used to manufacture the housing or other parts may also carbonize and promote arcing. Considering the proportion of residues after the TGA analysis, this will be the case with the PC and PPO-based polymers. The ABS, PBT, and PP-based polymers do not carbonize. This thesis shows that stable arc faults can also be produced in wires insulated with PP-based polymer. This means that the thermal stress that leads to arcing due to creepage on char (from contact arcing or glowing) does not result in a complete and homogenous degradation of the polymer. A polymer that is supposed to be arc-resistant after judgment using the TGA method can also carbonize in real electrical fault conditions and result in stable arcing. The TGA analysis is not sufficient to determine if a polymer is arc-resistant or not.

Polymer	Application	Decom-position temperature [FAA05]	Char yield (μ) [FAA05]	Measured decom-position temperature at TGA	Residual mass after TGA at N_2	Residual mass after TGA at O_2
ABS	Housing	390 °C	0 %	370 °C	3.1 %	2.2 %
PA	Housing	350-411 °C	4 %	390 °C	2.6 %	3.1 %
PBT	Housing	382 °C	7 %	360 °C	35 %	35 %
PC	Housing	476 °C	25 %	460 °C	25.7 %	2 %
PPO	Housing	441 °C	25 %	400 °C	14.1 %	4.5 %
PE	Wire insulation (PE 90 °C)	399-411 °C	0 %	310 °C	45.2 %	44.1 %
PP	Wire insulation (PP 90 °C)	354 °C	0 %	410 °C	2.2 %	1.7 %
PUR	Cable jacket	324 °C	13 %	320 °C	11.9 %	2.5 %
PVC	Wire insulation (PVC 70 °C)	249-273 °C	8 %	260 °C	35.8 %	29 %

Table 17: Measured decomposition temperature and proportion of residues at TGA analysis with pure nitrogen or pure oxygen

7.7 High-voltage arc-tracking rate

An additional indicator is necessary to verify that a polymer is arc-resistant. The method of carbonization at high-voltage described in 7.3 could be used. It could be implemented as described in the test standards for AFCI and AFDD: if no arc can be initiated after this high-voltage conditioning, the polymer can be declared to be arc-resistant. Such an approach would give a qualitative result: the polymer is arc-resistant or not. Alternative methods could also produce quantitative results and help the material specialists to optimize the polymer recipes. This is the thermogravimetric analysis that can provide the amount of carbonized mass and the high-voltage arc-tracking rate test from the UL 746A [UL12b] that indicates at different performance levels how quick a polymer can produce a carbonized track at high-voltage discharges. This method has been used to estimate the performance level of three insulation polymers (PE 90 °C, PVC 70 °C, and PVC 90 °C). Two stainless steel electrodes are placed at the surface of the probe at a distance of 4 mm apart. The power source (5.2 kV AC with 2.36 mA short-circuit current) is connected to the electrodes and a discharge is initiated. The distance between both electrodes is quickly increased while the discharge is taking place. If the discharge is interrupted, the distance is decreased. It is increased again at restrike. An average speed of the distance increase is determined. A high value means that the material easily produces a conductive carbonized track. We assume in this case that the polymer is not arc-resistant or less arc-resistant. The results are displayed in Table 18. As expected, the PE-based polymer obtained the best possible performance level (PLC 0) and the tracking rate was zero. This means that a small increase in distance between the electrodes is sufficient to interrupt the discharge. In contrast, the PVC-based polymers could sustain the discharge at speeds above 15 mm/min. These results are in accordance with the observations made with other methods. It must be mentioned that the PVC-based polymers reached the second best performance level category (PLC 1) defined in the standard UL 746A. The limit between PLC 0 and 1 is 10 mm/min. The worst PLC is 4 for tracking rates above 150 mm/min. This means that PLC 0 would be mandatory for arc-resistant material, but it would be better to determine the tracking rate limit between an arc-resistant and a non-arc-resistant polymer (supposed to be between 0 and 15 mm/min) and redefine the PLC with a higher resolution in this range.

Polymer	High-voltage arc tracking rate	Performance level category
	mm/min	
PE 90 °C	0	0
PVC 70 °C	15.8	1
PVC 90 °C	21.5	1

Table 18: Performance level at high-voltage arc-tracking rate test according to UL 746A §25 [UL12b]

7.8 Conclusions on the relationship between insulation polymers and thermal stress at electrical faults

Using arc-resistant polymers as insulation for wiring and other electrical parts would lead to a great improvement in electrical safety. Nevertheless, the gains in safety must be weighed against possible disadvantages that this measure could bring. The polymer PVC is widely used in electrical equipment not only due to the lower costs, but also because of its excellent chemical and mechanical properties. In addition, the extension cords, the internal wiring of electrical appliances and housing materials that are used behind the socket by the electricity user may also be subject to electrical faults and this cannot be planned or checked by an electrician. The generalization of the arc-resistant polymers will only be reached by updating the product and installation standards. This task can take years or decades and it can only start on the basis of many reports that can reproduce and confirm our findings. As long as arc faults cannot be completely inhibited by passive safety measures, the use of active protection against arc faults, the AFDD or AFCI, is recommended.

8 Improvements in the test standard for AFDD and electrical safety

Our comprehensive characterization of arc faults in this thesis allows us to analyze the current test standard of the IEC for AFDD, verify if the tests and criteria are appropriate, determine if the methods to generate arcs are compatible with real arc fault characteristics, and make improvement proposals if necessary.

8.1 Improving and amending test standard IEC 62606

8.1.1 **Series arc tests**

The three test scenarios described in part 1.5.1 are appropriate: the simulated fault characteristics are plausible and they cover the most hazardous fault scenarios. However, the fact that the series arc fault can start at the neutral conductor was not taken into account and one additional verification test in this configuration should be performed.

8.1.2 **Parallel arc tests**

At test §9.9.3.1, the generated parallel arc is of the type "arcing due to creepage on char" (as described in 3.1.1.2). The arc voltage is in the range of 20 V to 70 V and the obtained arc current at the lowest prospective test current of 75 A is approximately 60 A. Most of the residential circuits in Germany are protected by B16 MCBs that have an instantaneous trip threshold between 48 and 80 A. In the case of a parallel arc, it is likely that the MCB trips before the AFDD. We stated in a previous study [MAHBE11] that short-circuits involving parallel arcs are reliably interrupted by MCBs; the only situation in which the parallel arc may not be interrupted is if the fault occurs at the end of an excessively long extension cord with a high wiring impedance. Therefore, it would be sensible to perform this test with a target arc current that is equal to or slightly lower than the lowest test current for an instantaneous trip test of the MCB (Test §9.10.3 of the IEC 60898 [IEC15]). A simple method would be to adjust the prospective short-circuit current to the lowest test current for an instantaneous trip test of the MCB: this means for example 48 A for a MCB B16 or 80 A for a MCB C16.

At test §9.9.3.2, the high arc currents from 75 A to 500 A are quickly interrupted by the MCB or fuse before the AFDD can detect the arc. An additional test at a lower current than the lowest test current for instantaneous trip test of the MCB would also be sensible. The tests at currents up to 500 A do not really seem to be useful.

8.1.3 **Masking and unwanted tripping tests**

For the unwanted tripping tests, only the disturbing appliance is powered and the AFDD is not allowed to trip (see 1.5.3). For the masking tests, the AFDD should be able to detect the arc while a disturbing load is powered upstream or downstream of the arc location. The placement of the arc location, the disturbing load, and the test load are varied in multiple combinations. This procedure is correct, but it must be mentioned that the most adverse testing condition in this standard is if a single disturbing appliance and a resistive load are powered at the same time. In reality, more appliances may be used at the same time in an electrical circuit; it is not unusual in a living room to have a television, a notebook, a ventilator, and a lamp powered at the same time on the same circuit. Tests at combinations with a larger number of appliances should be also performed. Figure 100 displays an example of wiring and a combination of appliances that could be appropriate for such a test. The series arc is initiated at every section of wiring where a sufficient load current flows (greater than the minimum detection current of AFDD). For each test, the break time of the AFDD and the arc current are measured and compared with the thresholds of Table 1 (see 1.5.1). The series arcs are generated using the carbonized cable specimen (see 8.2.4.1) or using an arc generator (see 8.2.2.1).

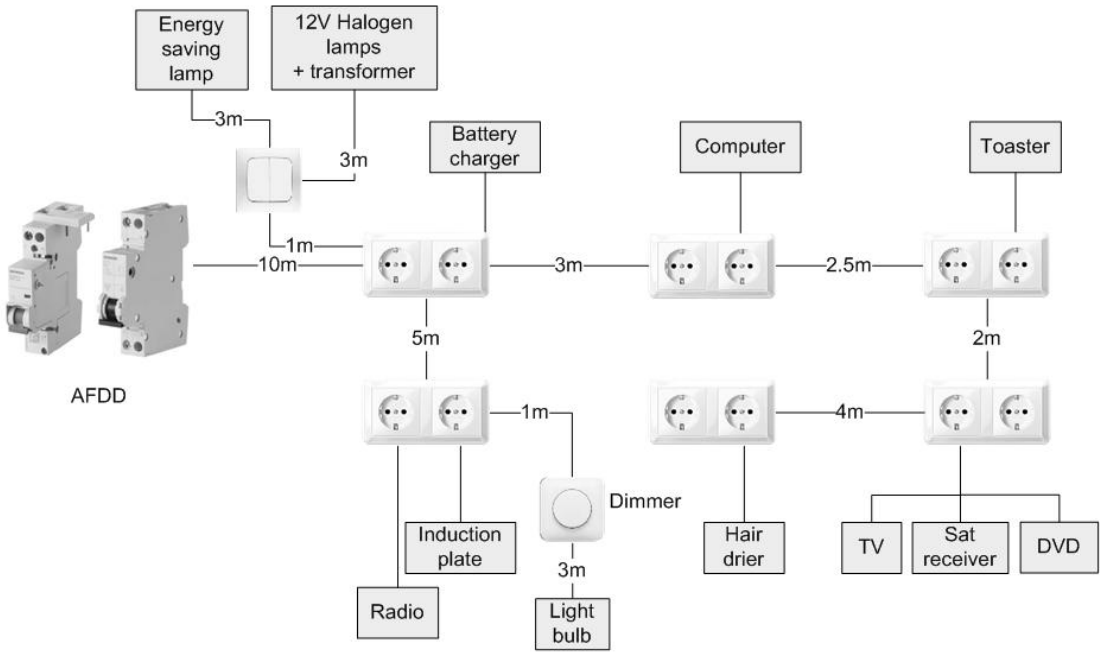

Figure 100: Example of enhanced masking/nuisance test for AFDD

8.1.4 **New tests for AFDD with 3 or 4 poles**

The requirements for 3 and 4 pole AFDD should be included soon in the standard IEC 62606. The main complements regarding arc detection are:

- Series arc detection test for every phase, including verification with only two conductors connected (phase-to-phase or phase-to-neutral).
- Series arc detection at the neutral conductor if the 3-phase load has a star point connected to neutral and the load is unbalanced.
- Parallel arc test phase-to-phase.
- Masking test and verification of the immunity against nuisance tripping with 3-phase loads such as motors with and without frequency inverter.

The definition of a new tripping characteristic for 400 V is necessary. This topic is discussed in 0.

8.2 Generation of series arcs for testing

8.2.1 **Requirements**

It is necessary that the methods of arc generation produce arcs that are in accordance with the characteristics of the most probable and most hazardous types of series arc faults that can occur in low-voltage electrical installations. The following observations and conclusions regarding series arc faults that have been put forward in this thesis can be used to define the requirements on arc generation methods:

- Series arcing in the form of non-contact arcing due to creepage on char is hazardous because the carbonized track enables a stable arc that dissipates a sufficient power to ignite the insulation polymer and spread the fire (see 3.2 and 6.1.1.3).
- Non-contact arcing due to creepage on char is likely to occur because other electrical faults such as contact arcing or glowing can carbonize the insulation and initiate this type of arc (see 3.3.2 and 3.2).
- Series contact arcing dissipates much less power than series arcing due to creepage on char because it is less stable and the arc voltage is lower (see 3.2).
- Non-contact arcing due to voltage breakdown is unlikely and if it occurs, the duration will not exceed a few half-cycles (see 3.1.1.1); this type of arcing does not represent an immediate hazard.
- All types of arc faults have physical characteristics that present important variations at the initiation and during the life of the arc: the mean values of arc voltage and current can be predicted for defined conditions, but with every test, important variations around the mean value are expected (see Figure 56). The variance is due to the number of key parameters (e.g. gap distance, material properties, preparation of the sample…), the interdependencies involved in the physical mechanisms, and the interactions between the arc and the environment.

Based on these conclusions, we can assume that the series arc that is generated for AFDD testing must fulfill two conditions:

- the type should be non-contact arcing due to creepage on char with a high stability. By high stability we mean a stability of at least 70 % (see Figure 24 for the determination of the value).
- the electrical characteristics of the arcs should present a realistic variance. The variance in arc voltage and arc striking voltage after current zero-crossing should result in a variance of at least 30 % in the arc energy. The series arc generated in cables fulfills this requirement as described in Figure 109.

On the one hand, the required variance of the arc is not compatible with the expectations on standard tests that should be reproducible. On the other hand, the generation of reproducible and constant arc characteristics would not prove the adequacy of the AFDD to protect the installation; there is a potential risk that the AFDD is designed to detect only the defined and reproducible arcs of the test procedure. For this reason, the variance of the arc must be understood, accepted, and implemented in the test method.

The next parts describe the different test methods that are used in the standard IEC 62606 [IEC13] and alternative methods discovered in publications and other standards. They are classified by the type of arc they can generate. Their adequacy to be used in a test method for AFDD is judged based on the findings of this thesis.

8.2.2 Non-contact arcing due to breakdown

8.2.2.1 Arc generator according to IEC 62606 / §9.9.2.7 [IEC13]

This generator consists of a fixed electrode and a moving electrode that can be positioned with a precision translator (see Figure 101). The movement of this electrode is usually controlled manually, but a fully automated version is also possible [Zue08]. One of the electrodes is made of copper and the other electrode is made of graphite. This configuration of electrodes can produce very stable arcs at very small separation distances. The resulting short arcs have a low arc voltage in the range of 13 V to 20 V. Hence, the arc power is lower than for the arcs that are initiated in cables and for a given test current, the AFDD is

permitted to interrupt the arc fault within a time that is 2.5 times longer than the break time specified in Table 1. It is verified in part 8.4 that this criterion is correct.

The stability requirement is fulfilled, but the other requirement on variance is not met. This high stability is obtained because of the small gap distance and the carbon of the graphite electrode that cannot melt. The electrical characteristics (arc voltage and effect on arc current) present a very small variance. In addition, there is always an air separation between the electrodes and this is not an arc due to creepage on char. The series arcs that are generated with this method present characteristics that are not compatible with real arc faults. Furthermore, the use of a graphite electrode is questionable. Carbon is not used as a conductor or connection material in electrical installations. The presence of this material in a pure form may result in a different electrical signature of the arc (see 1.3) and the AFDD may be designed to detect these specific arcs that do not exist as arc faults in reality. The requirement of detecting such types of arcs does not prove the protection function of the AFDD and it results in a risk of nuisance tripping since arcing with carbon electrodes are generated in brush motors.

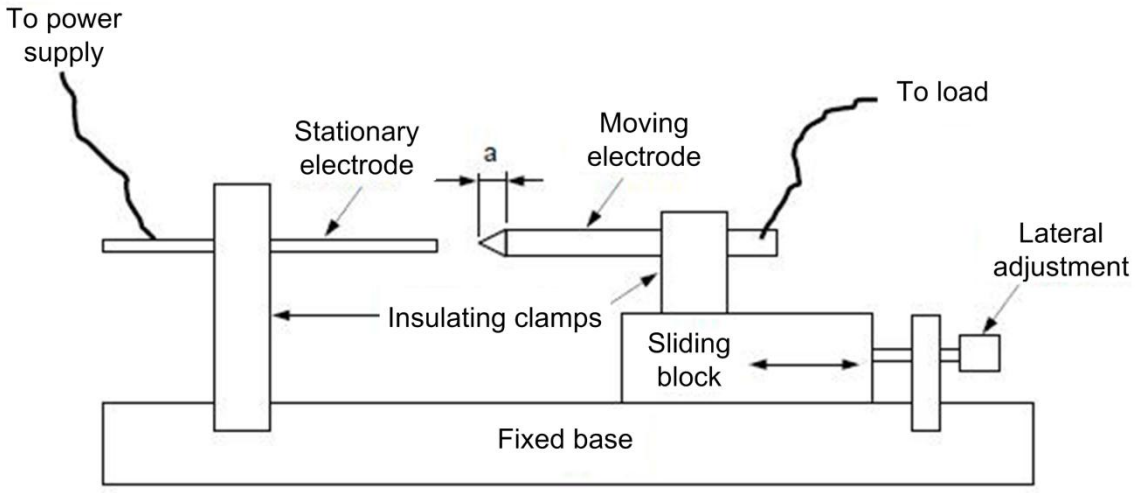

Figure 101: Arc generator according to IEC 62606 / §9.9.2.7 [IEC13]

8.2.2.2 Series arcs initiated with high-voltage impulses

The arc generator of J. Andrea [AST10b] consists of a circuit that combines a low-voltage power source and a high-voltage impulse generator (see Figure 102). A discharge is initiated between the copper electrodes with a voltage impulse of many kilovolts. Then, the discharge turns into an arc with a higher current supplied by the low-voltage power source. This arc generator is capable of initiating arcs at DC and AC supply, whereas, at AC supply, the high-voltage impulse initiation must be repeated after each current zero-crossing.

The initiation point of the arcs is very reproducible and this would correspond to a constant striking voltage. The arc voltage is also nearly constant during a test since the electrodes are free of insulation (no disturbance effects due to gassing of a polymer). Therefore, the variance of the generated arcs is extremely low and inappropriate for AFDD testing. The variance could be increased by means of a programmable generator to trigger the high-voltage impulse generator at a random striking time and by testing with an insulated wire instead of electrodes separated by air. However, the presence of the coupling transformer placed in series in the circuit disqualifies this method for AFDD testing: the impedance of this generator may strongly attenuate the electrical signature of the arc, especially at high frequencies, and handicap the arc detection.

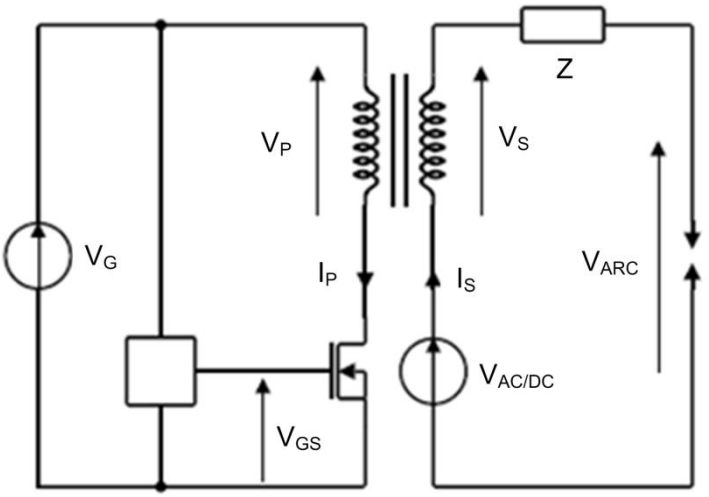

Figure 102: Arc generator with high-voltage impulse generator for arc initiation

8.2.3 **Contact arcing**

As explained in 3.1.2 and 8.2.1, contact arcing as a series arc fault does not represent an immediate danger, but in the long term (accumulation of arcing events in a time frame that can be days, months, or years), it could lead to a stable arc fault. The detection of this type of fault is not considered in the AFDD standard, but it would be sensible to do so.

8.2.3.1 Modified arc generator

The graphite electrode of the arc generator described in 8.2.2.1 can be replaced by a copper electrode or another metal used for electrical connection. The resulting arc is not stable (interruptions or shorting with metal bridges) and the position of the electrodes must be steadily adjusted to reinitiate the arc. The resulting power dissipation is much lower than at non-arcing due to creepage on char. This method enables a correct reproduction of the real series contact arc faults.

8.2.3.2 Loose terminal connection – Vibration test according to SAE AS5692 [SAE09] / §4.7.7.6.3

The standard SAE AS5692 describes the requirements of Arc Fault Circuit Breakers (AFCB) for the protection of aircraft electrical circuits (115 V AC / 400 Hz). At test §4.7.7.6.3, many connectors are placed in series at a terminal strip to increase the probability of contact faults. The conductors are intentionally loosened and vibrations are applied to the terminal strip (see Figure 103). The AFCB must trip within five minutes. This test is appropriate to reproduce electrical faults in environments where vibrations are always present or very likely to occur. In fixed low-voltage circuits, similar conditions can be present in appliances with moving parts such as washing machines, dryers, and pumps.

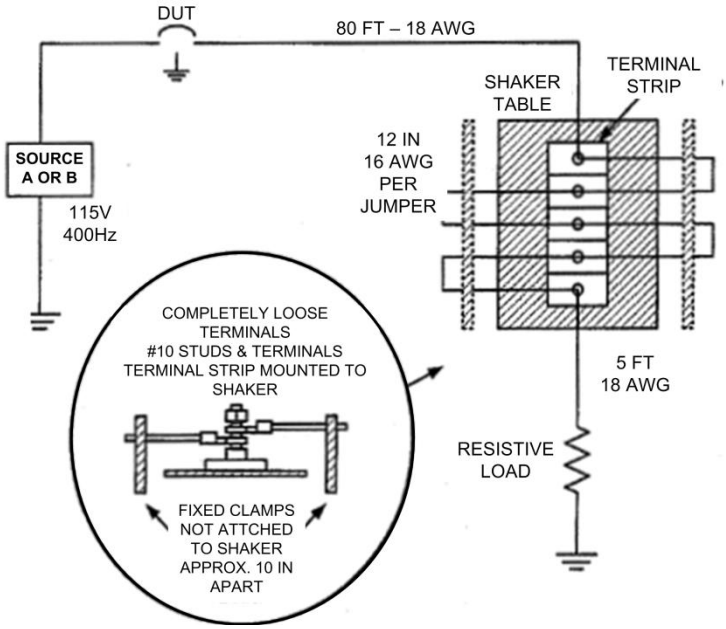

Figure 103: Loose terminal test according to SAE AS5692 / §4.7.7.6.3 [SAE09]

8.2.4 **Arcing due to creepage on char**

8.2.4.1 Series arcing with cables prepared according to IEC 62606 / §9.9.2.6 [IEC13]

This method has as its origin the carbonized path arc clearing time test according to UL 1699 / §40.4 [UL13]. The description of the conditioning specifies that only cables or cords with PVC insulation may be used. This detail matches the result of our investigations in chapter 7: initiating a stable series arc is much easier with the capability of PVC to char and build a carbonized path. A perpendicular slit is made across the conductor insulation as displayed in Figure 104. Then, the fault area is covered with PVC and glass-fiber tape. A conditioning that consists of different steps of carbonization at high-voltage (similar to the test procedure presented in 7.3.1) is performed. The exposed insulation between the conductors is carbonized by low-current discharges. The carbonization is optimized by the presence of the tape that prevents direct contact with the air and oxidation of the track. Afterwards, the cable specimen is placed in series with the load, the circuit is energized, and a very stable arc is initiated. The choice of the type of cable, the manual preparation of the specimens, and the interaction between the arc and the insulation material result in important variations of the arc characteristics. All the requirements that are defined in 8.2.1 are fulfilled and this method is appropriate for testing AFDD.

Figure 104: Damage done on a cable specimen (SPT2) for testing

The arc in the cable specimen is actually not initiated at an interrupted conductor, but between two isolated conductors of the cable (like for a parallel arc). The specific connection according to Figure 10 ensures that the arc is really in series with the load.

8.2.4.2 Carbonized path arc ignition test according to UL 1699 / §40.2

A cord specimen is conditioned by separating one of the conductors of an NMB cable. One of the cut conductors is pulled a bit in order to make a small separation gap. The slit is covered with PVC tape and fiber glass tape. A fire indicator (cotton) is placed on the fault area. Then, the cable specimen is periodically loaded (cycle of 20 seconds) with high -voltage (15 kV AC / 30 mA) to carbonize the fault area and with a load current at 120 V AC. The AFCI should trip before the cotton ignites. In this case, the break time of the AFDD is not measured and only the result of the ignition test is considered. This method also results in stable series arcs due to creepage on char, but the use of a fire indicator as criterion is an issue: the test conditions may strongly affect the result, especially the relative air humidity and the quality of the cotton. Therefore, the measurement of the break time of the AFDD is the preferred criterion.

8.2.5 Alternative methods

Alternative methods exist but they are complex to implement and are only used for the study of the arc faults in laboratory:

- Rotational flexing according to the UL report from 09/2005 [UL95]
  A cord is slowly twisted until one of the conductors becomes damaged. Then, the cable is loaded with a current of 16.5 A until an ignition occurs. In most cases, the insulation becomes hot and darkened and a series arc is initiated. The process takes hours and is not reproducible.

- Transition from contact to non-contact arcing in PVC cables [MAF10, She06b]
  This method produces contact arcing at a separated conductor of a cable in order to generate glowing and series arcing (see 3.2 and 3.3). The process generally takes a few minutes. The variance is important but the results are statistically reproducible.
- Series arc initiated with oxidized bus bars [MTMA10]
  Busbars are oxidized for hours at many hundreds of degrees. Then, they are loosely tightened with a bolt and loaded with load currents above 40 A. The results are not very reproducible and the required current levels to produce arcing are only compatible with specific industry applications.

8.2.6 **Conclusion on the methods for generating series arcs**

The generation of stable series arcs due to creepage on char according to IEC 62606 / §9.9.2.6 is the most appropriate method for AFDD testing because it reproduces the most hazardous type of arc and the important variance in the electrical characteristics which is inherent to real arc faults (see Table 19).

Test method	Part	Non-contact arcing due to creepage on char	High arc stability *	Realistic variance of the arc characteristics *	Remarks
Arc generator	8.2.2.1	No	Yes	No	Variance is too low, not recommended
Series arcs initiated with HV impulse	8.2.2.2	No	Yes	No	Not realistic and too predictable
Modified arc generator	8.2.3.1	No	No	Yes	Only for detection of contact arcing
Loose terminal connection vibration test	8.2.3.2	No	No	Yes	
Series arcing in cables	8.2.4.1	Yes	Yes	Yes	Preferred method
Carbonized path arc ignition test	8.2.4.2	Yes	Yes	Yes	Use of fire indicator, not recommended

Table 19: Overview of test methods and evaluation regarding the adequacy for series arc test (* see for definition in part 8.2.1)

The test with contact arcing is not present in the IEC standard except for parallel arc faults. The series contact arc faults present a real danger in the long term and it would be wise to take it into account. A simple consideration can clarify if the detection of contact arcing is sensible or not: harmless contact arcing is initiated under control in relays or switches. Most of these devices are employed in appliances such as light switches, irons, and washing machines. The frequency of switching is usually very low. If we consider one switching operation per second that results in one half-cycle of arcing every time, the stability of the arc is only 1 %. If we define a stability threshold of 10 % for contact arcing, the AFDD will trip if such arcing events happen 10 times per second on average. Setting the tripping threshold to 10 % stability will not result in unwanted tripping unless someone deliberately provokes arcing at a light switch or a plug.

We can suggest the following test procedure:

- Use the arc generator as described in part 8.2.3.1
- Generate the series contact arcing with a low stability (for example 10 %). This can be done manually or with an automatic adjustment of the gap distances as described in [Zue08] that has been programmed for this specific test (in this case the make and break actions shall be randomly distributed over the time)
- Record the arc current and arc voltage with an oscilloscope
- Calculate the mean power of the fault with the equation (143) at regular time intervals (for example 10 seconds)

$$\bar{\dot{q}}_{ARC} = \frac{\int_0^{10s} U_{ARC}(t)\ I_{ARC}(t)\ dt}{10s} \tag{143}$$

At contact series arcing, an arc voltage of 13 V is expected. If the target stability is 10 %, the expected mean power of the contact arc fault shall be close to this value:

$$\bar{\dot{q}}_{ARC} \approx 0.1\ 13V\ \ I_{LOAD} \tag{144}$$

Then, the following criteria can be used:

- If the AFDD tripped and the measured mean power before tripping was in the range of 50 % to 200 % of the expected mean power, the test is passed

- If the AFDD did not trip and the measured mean power before tripping was in the range of 50 % to 200 % of the expected mean power, the test is failed
- Independently from the action of the AFDD, if the mean power is not in the range of 50 % to 200 % of the expected mean power, the test must be repeated

8.3 Tripping characteristics for series arcing

8.3.1 Tripping characteristics for AFCI according to UL 1699 [UL13]

The UL tripping characteristic that is displayed in Figure 11 has its origin in a report [UL96] from the Underwriters Laboratories. The scenario of the broken wire with carbonized track was identified as a repeatable method and the most representative series arc fault able to start an electrical fire. The surgical cotton was chosen as a fire indicator and the tests were performed with the cord SPT2 16 AWG prepared as described in 8.2.4.1. Carbonization was performed in two steps at 15 kV / 30 mA and 1.8 kV / 300 mA. The prepared cord specimen was placed in series in a circuit with an adjustable load. The circuit was energized at 120 V AC during a limited time by means of a relay. It was checked if the cotton ignited for each combination of time and load current. Figure 105 displays the results; the red markers and the red line represent the time – current curve chosen for the AFCI.

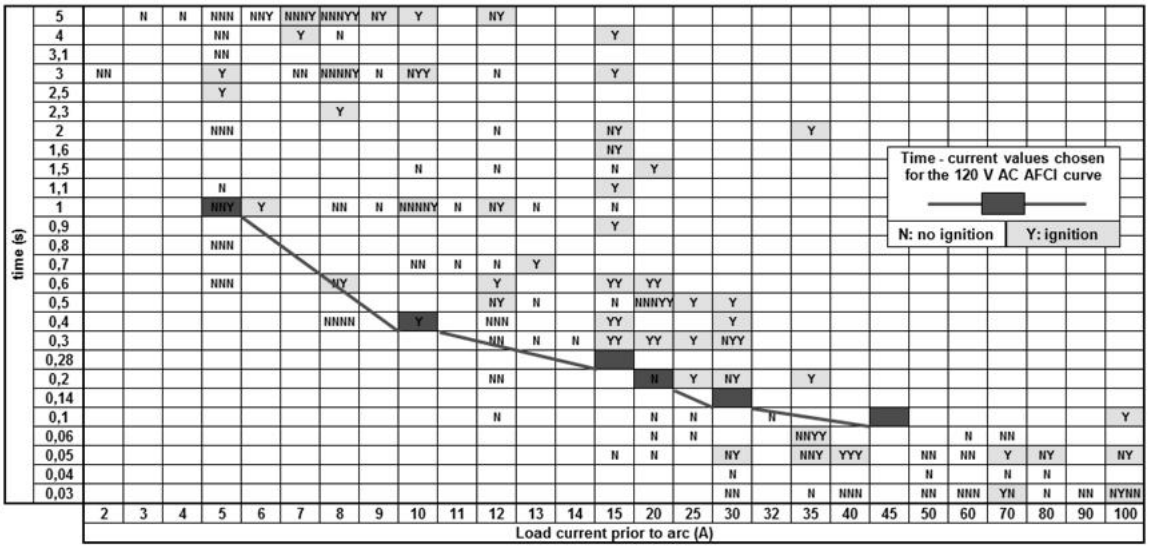

Figure 105: Ignition results on SPT2 with cotton as fire indicator and ignition threshold curve [UL96]

Below the tripping characteristic, also named "fire curve", the fire indicator did not ignite, except at currents equal to or above 30 A. At these currents, ignitions were observed at arc durations as short as 0.03 s. It would have been barely possible to design an AFCI that can interrupt the fault so fast. Therefore, a compromise between safety and technical feasibility was reached with break times greater than 0.1 s. The same tripping characteristic has been defined for the AFDD with 120 V rated voltage, but with one difference: the maximum break time is a function of the arc current and not of the load current that flows before the arc initiation. The reason for this difference is not known.

8.3.2 **Tripping characteristics for AFCI and AFDD 230/240 V AC**

Experts of Leviton used the same method to determine a fire curve at 240 V AC [KCS07]; they found out that the probability of ignition was much higher at 240 V than at 120 V and the break times were lower for the same current in order to reach the same safety level. Shea [She08] showed that the reason for the higher probability of ignition at 240 V AC was the higher arc power:

- The probability of restrike after every current zero-crossing is greater at a higher system voltage, thus increasing the stability of the arc and the mean value of the arc power.
- The current-limiting effect of the series arc is a function of the arc voltage and the system voltage. At a higher system voltage, this effect is reduced and the arc current and power are higher.

The definition of the tripping characteristic for AFDD at 230 V rated voltage was based on a different approach. As already explained in part 3.2, stable series arcs were produced in PVC cables by degrading the insulation with contact arcing and glowing. The required energy to ignite the polymer was in the range of 100 J to 800 J [MAF10]. The energy value of 100 J was chosen as reference for the tripping characteristic for series arcing according to IEC 62606; with an arc voltage assumed to be in the range of 40 V, the maximum break time t_B of the AFDD was defined by the following relations:

$$t_B = \frac{100\,J}{40\,V\;\;I_{arc}} = \frac{2.5\;A\,s}{I_{arc}} \text{ for } I_{arc} \le 20\,A \text{ and } t_B = 0.12\,s \text{ for } I_{arc} > 20\,A \qquad (145)$$

It must be mentioned that the variance on the ignition energy values was very important and in rare cases, cable specimens ignited at energy levels below the threshold of 100 J. This was the case if glowing preceded the stable series arc fault. This means that the 100 J threshold cannot prevent all ignitions of the insulation material. Nevertheless, the AFDD can promptly interrupt the current and limit the duration of combustion of the self-extinguishing polymer, thus significantly reducing the risk of the fire spreading.

The energy threshold could be defined at a lower value in order to increase the safety level. This measure would result in lower maximum break times and would increase the risk of nuisance tripping. The detection of series arc faults requires complex algorithms that are based on the relationship between low-frequency and high-frequency electrical signals [MAHBE11, Res08, RST11]. The AFDD must distinguish between the real series arcs that may occur in combination with disturbing loads and ignore situations where the switching arcs and disturbing signals are produced. The analysis requires a sufficient amount of data and time to take the decision if an arc fault is detected or not (see 1.3). If the quantity of data is limited, the risk of taking a wrong decision is higher. In addition, there are harmless switching arcs (not distinguishable from series arc faults) that may last too long and force the AFDD to trip. In the scope of a field test during the development phase of the Siemens AFDD 5SM6 [Bra17], many trips due to series arcing were reported. Approximately 90 devices were installed during many months in family homes, apartments, offices, and workshops. The reason for two of the reported trips was an electrical fault: the switch of a light dimmer and the heating rod of a drier were faulty. For two other trips, the bimetal-controlled switch of irons had low contact forces and a slow opening speed; they produced arcs that lasted up to two seconds. These irons did not present any damage or danger since the heat from the arc was dissipated in the part of the device that is designed to withstand elevated temperatures. 30 additional irons were analyzed and four of them produced arcs that lasted up to 80 ms. The solution for reducing the probability of unwanted tripping due to switching arcs was to program the tripping characteristic of the AFDD as close as possible to the tripping characteristic of the standard IEC 62606.

These observations show that reducing the energy threshold and break time will significantly increase the likelihood of unwanted tripping, annoy consumers, and burden the AFDD

manufacturers with complaints. This means that even if a technology is capable of detecting series arc faults much quicker than the IEC standard requires, the reaction time may be intentionally delayed because there is a minority of appliances that generate long switching arcs.

The minimum arc tripping current is equal to 2.5 A. Below this value, there is no guarantee that the AFDD can trip at a series arc fault. Tests at series arcing in PVC cables under the conditions described in part 3.2 were performed at very low currents. The probability of ignition at a 1 A load was 11 % and the arc current was in the range of 0.8 A. At a 2 A load (1.6 A arc current), the probability of ignition was above 50 %. It is strongly recommended that the tripping characteristic at 230 V starts at 1 A arc current.

8.3.3 **Electrical simulation and analysis**

The tripping characteristics for AFDD at 120 V AC and 230 V AC system voltages are different (see Figure 11). The main reason is the different methodology employed to determine them (fire curve for 120 V and energy limitation for 230 V). Another reason is the use of different references to determine the break time: the load current preceding the arc for 120 V and the value of the arc current for 230 V. In addition, the minimum arc detection current is 2.5 A for 230 V and 5 A for 120 V. We assume that the electrical power of the arc does not directly depend on the system voltage. At the same arc current and under the same environmental conditions, the arcs at 120 V and 230 V will dissipate the same amount of power. For this reason, the same tripping characteristic should be used for both system voltages. The same consideration can be made for the 400 V system voltage that is currently being discussed for the next update of the IEC 62606 standard. The following parts give more clarification on these problems. Theoretical considerations and experiments were performed to explain and address these issues. The results are described in the next parts.

8.3.3.1 **Electrical model of series arc**

The purpose of the electrical model [MAF14] is to understand the interaction of the series arc fault in electrical circuits and the influence of the main parameters on the arc characteristic and the power dissipation. The scenario of a separated conductor in a cable is

used and the equivalent circuit is displayed in Figure 107. Prior to arcing, switch S is closed and the current in the circuit can be calculated by solving this differential equation:

$$\frac{dI(t)}{dt} = -\frac{R}{L}\ I(t) + \frac{\hat{U}_{SYS}\ \sin(\omega\ t)}{L} \tag{146}$$

We assume that the electrical arc is a conductance of arc column G_{col} in series with voltage source U_{AC} equal to the sum of the anodic and cathodic voltages. R_C represents the resistance of the carbonized path in parallel to the arc. The modified version of the model of Mayr [May43 (p588-608)] is used to calculate the variation of conductance for arc column G_{col}:

$$\frac{dG_{col}(t)}{dt} = \frac{G_{col}(t)}{\theta}\ \left(\frac{(U_{arc}(t) - U_{AC})\ I_{arc}(t)}{\dot{q}_{out}(I_{arc}(t))} - 1 \right) \tag{147}$$

Cooling power $\dot{q}_{out}$ is a function of the arc current; we use a static electrical characteristic that fits with the computed and measured values in part 6.1.1.3:

$$\dot{q}_{out} = \dot{q}_{ARC} = U_{ARC}\ \ I_{ARC} = \left(a + b\ \ (z_1 - 2\ \ z_{INT}) + \frac{c + d\ \ (z_1 - 2\ \ z_{INT})}{I_{ARC}} \right)\ I_{ARC} \tag{148}$$

with $a = U_{AC} = 13$ V, $b = 35$ V/mm, $c = 10$ V A, $d = 12$ V A/mm.

Time constant θ is the ratio between the energy content and the cooling power of the arc column [Rie67] and can be expressed with the equation (149):

$$\theta = \frac{\int_{T_R}^{T_1} \rho\ \ c_p\ \ dT}{\sigma\ \ E^2} \tag{149}$$

where T_1 is the temperature of the arc column, T_R the temperature of the cooling walls, ρ the density, c_p the specific heat capacity, σ the electrical conductivity of the plasma, and E the electric field. Values in the range of 10 µs are obtained with the simulation data from our model presented in part 6.1.1.1. After determining conductance G_{col}, the complete arc conductance is calculated with the equation (150) and the arc voltage is deduced with the equation (151):

$$G_{arc}(t) = \frac{I_{arc}(t)}{U_{arc}(t)} = \frac{I_{arc}(t)}{U_{AC} + \frac{I_{arc}(t)}{G_{col}}} = \frac{G_{col}(t)\ I_{arc}(t)}{U_{AC}\ \ G_{col}(t) + I_{arc}(t)} \tag{150}$$

$$U_{arc}(t) = \frac{I_{arc}(t)}{G_{col}(t)} + U_{AC} \tag{151}$$

Before the equation (147) can be used, the arc must first be initiated. We assume that a discharge with a limited current is initiated if the voltage drop at the carbonized path exceeds a defined striking voltage *Us*. This current flow in parallel with resistance R_C must result in an increase in the complete fault conductance and a decrease in the voltage. It became apparent after many trials that a voltage decrease of 15 V gives an appreciable agreement between the model and the measurements. After the arc initiation, the arc current is calculated by solving this differential equation:

$$\frac{dI_{arc}(t)}{dt} = -\frac{R}{L} I_{arc}(t) + \frac{\hat{U}_{SYS} \sin(\omega t) - U_{arc}}{L} \tag{152}$$

An example of a computed signal is displayed in Figure 106. The results of the measurement and the model are in agreement.

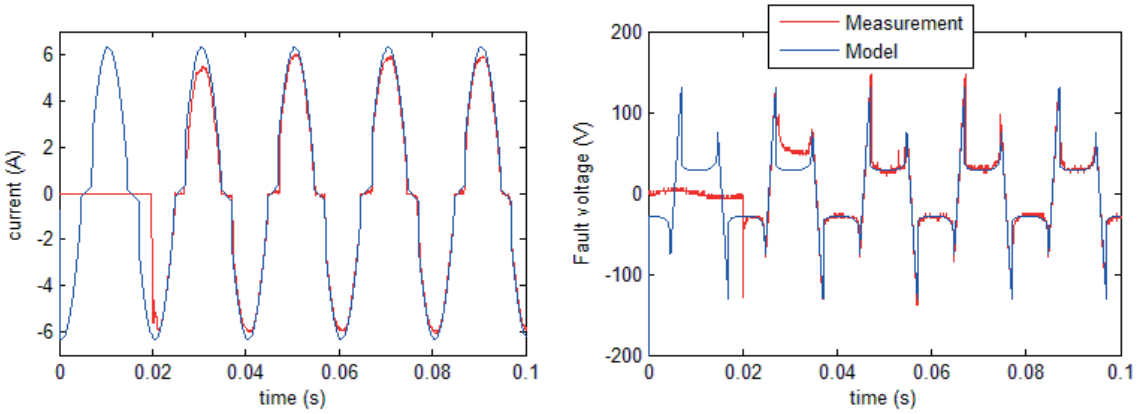

Figure 106: Computed and measured arc voltage and current at 230 V AC system voltage, 5 A resistive load, and 1 mm gap distance

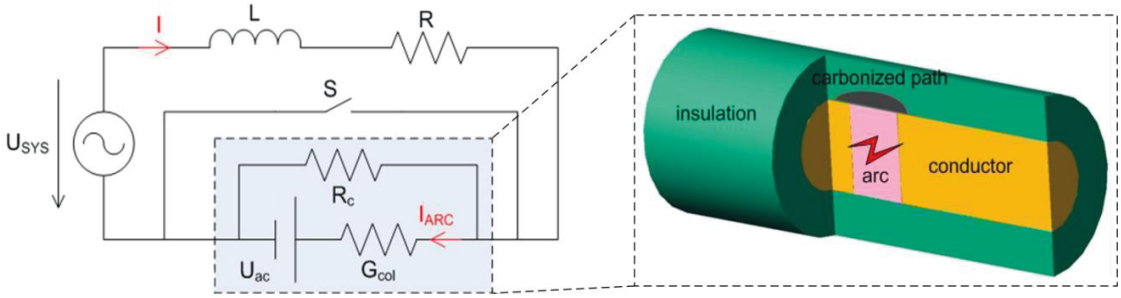

Figure 107: Equivalent circuit of the series arc with sketch of the faulty conductor

8.3.3.2 Investigations on the tripping characteristics for different system voltages

The model is used to compute duration t_B that requires the series arc to dissipate an amount of energy equal to 100 J. This duration corresponds to the maximum break time of the AFDD to limit the arc energy to the threshold of 100 J. The computation is based on equation (153). All electrical and mechanical conditions are defined to be constant except for the system voltage that is set successively at 120 V, 230 V, and 400 V. The results are displayed in Figure 108. Tests were performed under the same conditions as with PVC-insulated cables.

$$100\ J = \int_0^{t_B} U_{ARC}(t)\ I_{ARC}(t)\ dt \tag{153}$$

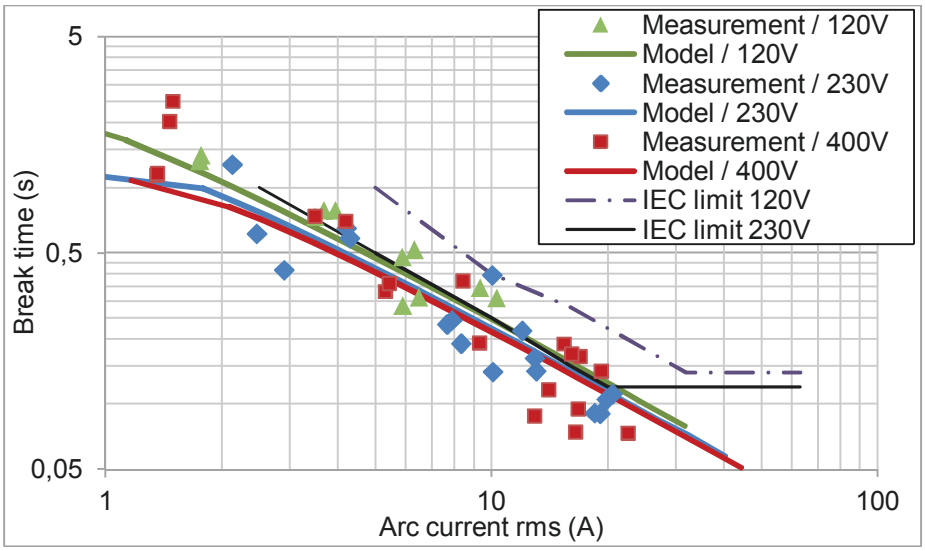

Figure 108: Required break times to limit arc energy to 100 J at different system voltages. Measured and computed data (Us = 103 V, Rc = 400 Ω, L = 10 µH, gap distance = 1 mm)

A fair agreement between computed and measured data is observed. As expected, the calculated break times are nearly the same for the different system voltages. There is a slight trend toward obtaining higher break times at a lower system voltage and arc current. The reason is that the electrical power of the arc is slightly lower at lower electrical voltages because the same striking voltage is reached later after the zero-crossing of the current. Nevertheless, the difference is small and does not explain the factor 2 between the tripping characteristics for 120 V and 230 V. The same tripping characteristic could be defined for the system voltage 400 V AC. This statement is confirmed with the extrapolated break times

from measurements that have the same trend as the calculated data and do not present significant differences regarding the system voltage.

8.4 Other considerations on the test criteria

The purpose of the tripping characteristic is to limit the energy to 100 J. This is done by extrapolating a break time with the equation (154). A constant arc voltage of 40 V is assumed:

$$t_B = \frac{100\,J}{I_{arc}\ \ 40\,V} \tag{154}$$

Since the real arc presents important variations of voltage and power, this simple extrapolation may lead to under- or over-estimates of the required break time. For example, a series arc that has an arc voltage of 50 V at 2.5 A dissipates approximately 125 W. In order to limit the energy to 100 J, the AFDD should trip within 0.8 s, but according to the official tripping characteristic for 230 V, it must trip within 1 s. If this is the case, the arc energy will reach 125 J. The real energy limitation was determined by conducting many tests using PVC cables and an arc generator. Figure 109 displays the real arc energies that have been measured from the arc initiation to the maximum break time calculated with equation (154). As expected, the variance is important. For the tests with cables, the mean arc energy is 100 J, but deviations from -40 % to 70 % are observed. The arc energy has the tendency to be greater at lower currents because of the voltage-current characteristic of the arc (see Figure 44). The variance when testing with an arc generator is much lower because the short arcs are more stable and reproducible. The break times were multiplied by a factor 2.5 for the test with an arc generator and the assumption made in 8.2.2.1 that the arc generator dissipated approximately 2.5 times less energy is verified.

Based on an extrapolated time-current tripping characteristic, the AFDD cannot limit the arc energy to a specific value. It may interrupt the current earlier or later depending on the arcing conditions. If this fact is not accepted, an alternative method would be to measure the arc voltage and the arc current, calculate the arc energy for every test with equation (155), and compare the results with the maximum energy threshold:

$$Q_{ARC} = \int_0^{t_B} U_{arc}(t)\ I_{arc}(t)\ dt \qquad (155)$$

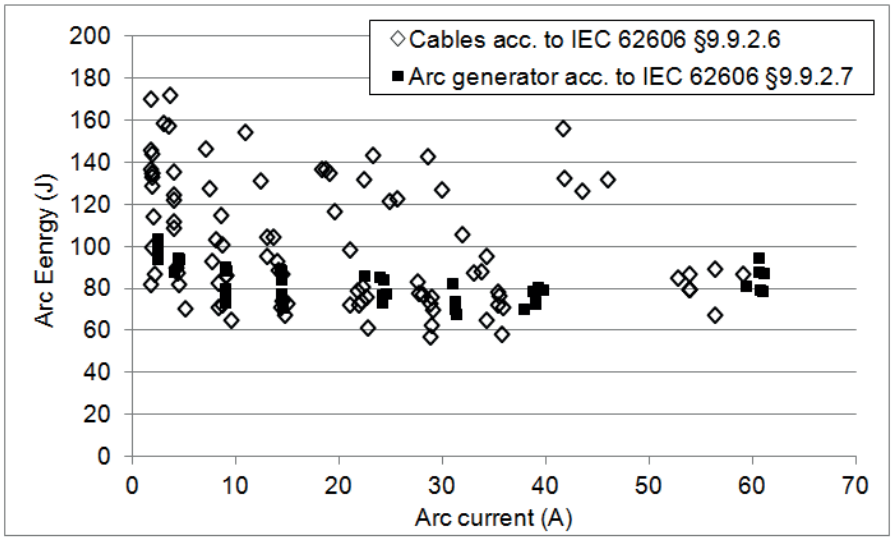

Figure 109: Arc energy dissipated during the maximum break time of the tripping characteristic for 230 V AC. The break time is multiplied by 2.5 for the test with an arc generator

At high series arc currents, the corresponding break times to limit the energy to 100 J may be below 50 ms and this could represent a risk of unwanted tripping with appliances that generate longer switching arcs. For this reason, a compromise can be reached by checking that the AFDD trips within 100 ms even if the arc energy exceeds the threshold of 100 J. The logical criterion is:

$$Q_{arc} \leq 100\,J \text{ or } (Q_{arc} > 100\,J \ \& \ t_B \leq 0.1\,s)$$

An equivalent circuit of the test setup is represented in Figure 110. Measurement of the arc voltage represents a risk of influencing the test results since the voltage probe could filter the high-frequency signals generated by the series arc (see part 1.3); the AFDD would be masked and would not be able to detect the fault. In this case, a specific filter for the measurement would have to be used in agreement with the AFDD manufacturer.

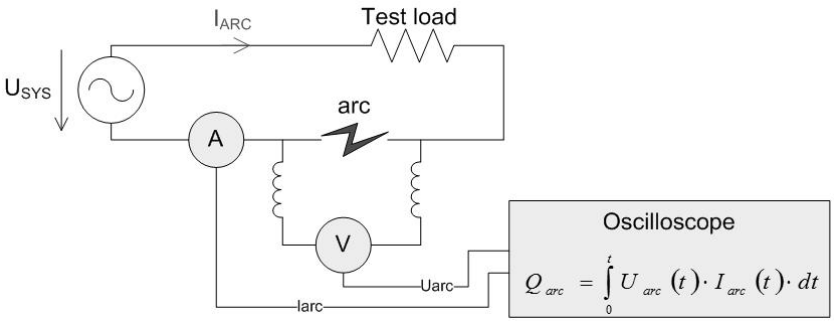

Figure 110: Proposed test setup for verifying the AFDD at series arcing

8.5 Summary of recommendations for IEC/EN 62606

Based on our analysis of the current version of the standards IEC/EN 62606 and the findings on the characteristics of the different types of arc faults, we can suggest the following modifications and complements:

- Start the verification of the series arc detection at 1 A (see 8.3.2)
- Add the verification of the contact arcing detection (see 8.2.6)
- Use carbonized cables to generate series arcs and avoid using an arc generator with graphite and copper electrodes (see 8.2.4.1)
- Use the energy limitation as a test criterion for series arc detection instead of a time-current characteristic (see 8.4)
- Use the same test criteria for series arc detection as for AFDD with 120 V, 230 V, and 400 V rated voltage (see 8.3.3.2)
- Add the requirements for the 3 and 4 poles AFDD (8.1.4)
- Perform masking and nuisance trip tests with combinations of more than two appliances (see 8.1.3)
- Create a product standard for AFDD for DC circuits and photovoltaic generators (see 7.2)

9 Conclusion

The series arc fault in low-voltage installations is a hazardous electrical fault that can generate sufficient heat to start an electrical fire. This fault is in series in the electrical circuit, the effect on the current value is limited, and the current flows in the path that it is intended to use. For this reason, the regular protection devices (fuse, RCD, MCB) are not able to detect the fault and interrupt the current. In order to estimate how hazardous this type of fault can be, the statistical fire data in different countries was reviewed. Electrical faults are particularly hazardous since people may be surprised by a fire at night. Therefore, electrical fires are potentially much more lethal and result in higher losses than other types of fires. Unfortunately, the statistical data do not provide reliable evidence on the part played by series arc faults in the occurrence of electrical fires. Forensic experts can find the location where a fire started and also the nature of the primary heat source, but in the case of an electrical fire, they are normally not able to identify the responsible electrical fault.

Nevertheless, stable series arcs and fire ignitions of insulation materials could be easily initiated in realistic conditions in the laboratory and similar observations were published by other authors. Investigations show that a stable series arc can be initiated by other electrical faults such as glowing connections or contact arcing and the fault can start at small currents in the range of only 1 A. Since the arc is a thermal phenomenon that consists of a conducting air plasma column, it requires a minimum electric field and current flow to exist. The resulting power dissipation is in the range of 50 W to 800 W if the fault occurs in a 16 A rated circuit. The temperature of the arc column exceeds 5000 °C and power dissipation to the insulation material can reach many millions of watts per square meter. This intense thermal stress can lead to quick degradation of the insulation polymer and to vaporization of flammable gases. An estimate of the fault characteristic in a PVC-insulated cable for a 16 A circuit that was not protected by an AFDD, shows that the fault may last from one second to one minute and dissipate heat in the range of many thousand Joules. The high temperature and longevity of the series arc fault results in a high probability of ignition. The fire may spread to other materials that do not have the self-extinguishing properties of electrical polymers.

Figure 111 displays the main thermal stress parameters at series arc faults in PVC-insulated cables for low-voltage electrical circuits. The required temperature and heat flow to ignite the PVC are widely exceeded. The arc fault duration also exceeds the estimated time to ignition and the ignition of the cable in these conditions is very probable without an appropriate protection device. The AFDD cannot reduce the heat flow and the temperature since these parameters depend only on the physical characteristics of the arc, but it can limit the fault duration and the amount of released energy. At this energy level (up to 100 J), the probability of ignition of the insulation is significantly reduced. In the worst-case situations (probability of approximately 15 %), the PVC may ignite before the AFDD interrupts the current; in this case, the flame is likely to extinguish quickly because the AFDD trip and mandatory self-extinguishing properties of the insulation polymers result in an efficient limitation of the flame duration and energy (< 12 J instead of 1400 J).

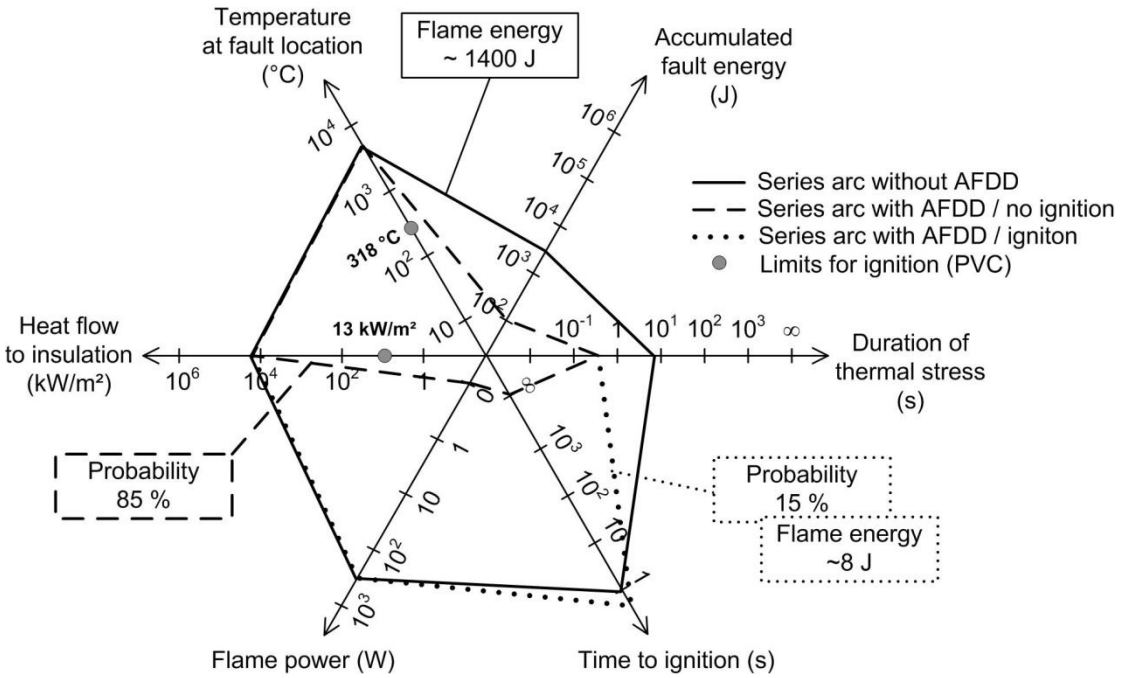

Figure 111: Thermal stress and safety enhancement with AFDD at series arc faults in PVC cables for 230 V / 16 A branch circuits

The same analysis of the thermal stress was performed for other faults that may be the causes of electrical fires (see Figure 78, page 118). Overcurrent, bolted short-circuits, and earth leakage result in much lower thermal stresses because their energy levels are more

evenly spread in the wiring and/or they can be promptly detected and interrupted by regular protection devices. The glowing faults that result from contact arcing and weakened connections are very stable and can last much longer than series arcs, but the expected power dissipation into the insulation is many hundred times lower. The thermal stress on the insulation is in theory sufficient to ignite the PVC, but it cannot be sustained long enough to reach the flame point. Only parallel arc faults can generate a higher thermal stress than at series arcing, but their nuisance is very limited since they can be reliably interrupted by conventional protection devices. The contribution of series arc faults to the initiation of electrical faults cannot be estimated exactly, but these last arguments show that it is significant. Therefore, the use of AFDD to increase electrical safety is advisable. The risk of starting an electrical fire with series arc faults is reduced by a factor of 9 to 3700 depending on the real performance of the AFDD. This device is not mandatory in IEC installations yet. It is currently recommended in the German national installation standard [DIN16] and a mandatory installation where the fire risk is critical (museums, historic buildings, nurseries, retirement homes etc) has been proposed in an amendment of the standard [DIN15]. A requirement of the AFDD protection in low-voltage installations, for example by protecting the residential branch circuits as a priority, would be appropriate.

The requirements for the AFDD are described in the standards IEC/EN 62606. The specific requirements for detecting series arc faults were analyzed and it appeared that the test scenarios involving cables with carbonized insulation are suitable for reproducing the most hazardous form of series arcing. The series arcs due to creepage on char combine stability, longevity, and flammable material at the fault location. The variations introduced during the conditioning of the cable specimen are in agreement with the important variance of the electrical parameters of real arc faults. In contrast, the contact arcs are very astable and do not present an immediate risk. However, the detection of such arcs is also recommended because they can lead to glowing faults or stable series arc faults in the long term. Further recommendations were made for the next review of the IEC and EN standards. Ignitions at only 1 A arc current were observed: reducing the minimum detection current to this value instead of the standard 2.5 A threshold would appear to make sense. The arc energy could be directly measured instead of measuring a break time and comparing the result with a tripping characteristic. This method would enable reliable verification of the arc energy limitation.

The investigations also revealed that the system voltage has a very small influence on power dissipation of the series arc and it is recommended that the same tripping characteristic at series arcing be used for different AC low-voltage systems.

In addition to the active protection provided by the AFDD, further research efforts should be aimed at increasing passive protection from series arc faults. The investigations on the insulation polymers provide evidence of a clear relationship between the tendency of many polymers, especially PVC, to produce conducting ashes at thermal degradation and to promote the initiation of stable series arcs at AC voltage. In contrast, PE and other halogen-free polymers are very resistant against series arcing. The practical use of these arc-resistant polymers in the different electrical applications should be studied in terms of the costs and other technical requirements. These findings should be taken into account in installation and product standards.

Table 20 displays our recommendations for the combined active and passive protection systems for series arc faults. Initiation of hazardous stable series arcs is only possible if the system can produce a minimum arc voltage of 13 V. This is the case if the following relation is verified:

$$U_{SYS} - R\ I \quad 13V \tag{156}$$

The worst-case situation corresponds to the minimum resistance of circuit R_{MIN} which is a function of system voltage U_{SYS}, rated current I_N, and a safety factor for overload (a value of 1.5 is recommended):

$$R_{MIN} = \frac{U_{Sys}}{1.5 \times I_N} \tag{157}$$

The maximum arc current can be estimated with the equation (158). If this current exceeds the minimum current that an arc can sustain (0.45 A for copper), the electrical circuit should be protected by an AFDD.

$$I_{ARC\_MAX} = \frac{U_{SYS} - 13V}{R_{MIN}} = 1.5 \times I_N \times \frac{U_{SYS} - 13V}{U_{SYS}} \tag{158}$$

For AC low-voltage circuits where series arc faults are possible, it is recommended that arc-resistant materials be used. A verification of this feature could be based on our recommendations in part 7.8. For DC circuits, the initiation of stable series arcs is not directly related to the insulation materials and the requirements can be focused on flame resistance. The glowing fault is also a problem that requires an answer, but there is no technical solution yet. If a detection device becomes available, AC and DC circuits with current rating above 0.45 A should be protected.

Low-voltage system	$I_{ARC\_MAX} \geq 0.45$ A see Eq. (158)	Active protection against series arc faults	Passive protection / Insulation	
			Arc resistant	Flame retardant/proof
AC	Yes	Yes *	Yes	Yes
	No	-	-	Yes
DC	Yes	Yes **	-	Yes
	No	-	-	Yes

Table 20: Recommendations for passive and active protection against series electrical faults
* with AFDD acc. to IEC/EN 62606 if applicable
** with specific AFDD for DC applications and/or photovoltaic generators

The introduction of the AFDD is an important step in improving electrical safety and new generations of AFDD are expected in the near future. The findings and conclusions of this study show that there is still a need as well as a potential for improving electrical safety in low-voltage electrical installations. The efforts required in industry and in standardization work to exploit this potential are considerable, but the gain in electrical safety and the benefits to saving human lives that it implies have no price.

List of abbreviations

ABS: Poly(acrylonitrile-co-butadiene-co-styrene)

AC: Alternating Current

AFCI: Arc Fault Circuit Interrupter

AFDD: Arc Fault Detection Device

C/H: Ratio of carbon atoms to hydrogen atoms in the polymer composition

CPSC: Consumer Product Safety Commission

DC: Direct Current

DSB: Norwegian directorate for civil protection

EDX: Energy-dispersive X-ray spectroscopy

GFCI: Ground Fault Circuit Interrupter

HOC: Effective heat of combustion

HRP: Heat release parameter

HRR: Heat release rate

ICF: International Cable makers Federation

IEC: International Electrotechnical Commission

IFS: Institut für Schadenverhütung und Schadenforschung der öffentlicher Versicherer e.V.

LFL: Lower Flammability Limit

MCB: Miniature Circuit Breaker

NEC: Net Emission Coefficient

NEC: National Electrical Code

NEMA: National Electrical Manufacturers Association

PA: Polyamide

PBT: Poly(butylene terephtalate)

PC: Polycarbonate

PE: Polyethylene

PLC: Performance Level Category

PMMA: Poly(methyl methacrylate)

PP: Polypropylene

PPO: Poly(phenylene oxide)

PS: Polystyrene

PVC: Poly(vinyl chloride)

RCD: Residual Current Detector

RMS: Root Mean Square

RSSI: Received Signal Strength Indication

TGA: Thermogravimetric Analysis

TRP: Thermal Response Parameter

UL: Underwriters Laboratories

Polymer properties

Polymer	T_d	T_{ign}	h_g	μ	h_c	χ
	°C	°C	kJ/g	g/g	kJ/g	kJ/kJ
ABS	390	394	2.3	0	36.6	0.79
PA 6.6	411	456	2	0.04	27.4	0.92
PBT	382	382	1.3	0.07	23.8	0.91
PC	476	500	1.8	0.25	23.3	0.91
PE (LD)	399	377	1.9	0	41.4	0.97
PVC flexible	249	318	1.2	0.08	19.3	0.59

Polymer	k	ρ	c_p	*HRP*	*TRP*	*HRR*
	W/m K	Kg/m^3	kJ/kg K	kJ/kJ	kW $s^{0.5}/m^2$	kW/m^2
ABS	0.26	1050	1.5	13	210	359
PA 6.6	0.23	1140	1.57	18	246	240
PBT	0.22	1350	1.61	15	220	341
PC	0.2	1200	1.22	9	229	89
PE (LD)	0.38	925	1.55	21	231	145
PVC flexible	0.17	1255	1.38	4	142	91

Symbols

A_F	Surface of the flame	[m²]
A_{INS}	Surface of insulation exposed to thermal stress	[m²]
$\overline{A}_L$	Mean transition probability	[/s]
A_m^n	Transition probability from level m to n	[/s]
$\overline{A}_R$	Recombination probability	[/s K]
b_x	Mobility of particle x	[m²/V s]
c	Specific heat capacity	[J/kg K]
C	Heat capacity	[J/K]
D	Diffusion speed of particles	[m²/s]
D_F	Diameter of the flame base	[m]
e	Charge of the electron = 1.6021765 10^{-19} C	[A s]
E	Electric filed	[V/m]
f_{en}	Frequency of electron-neutral collisions	[/s]
f_P	Frequency of a photon	[Hz]
f_x	Degree of liberty of a particle x	[no unit]
f_S	Safety factor	[no unit]
F_p	Flow of particles	[1/m² s]
g_x	Statistical weight of a particle x	[no unit]
G	Electrical conductance	[1/Ω]
h_c^0	Heat of combustion	[J/kg]
h_g	Enthalpy of gasification per mass of polymer	[J/kg]
h_P	Planck constant = 6.62606957 10^{-34} J.s	[J s]
HOC	Effective heat of combustion	[J/Kg]
HRP	Heat release parameter	[no unit]
HRR	Heat release rate	[W/m²]
HRR_b^*	Critical heat release rate for sustained burning	[W/m²]

I	Electrical current	[A]
I_{ARC}	Arc current	[A]
I_{Δ}	Residual current	[A]
$I_{\Delta n}$	Rated residual operating current	[A]
I_f	Radiation intensity per unit of volume in the space 4π	[W/m³]
I_{LOAD}	Load current	[A]
I_N	Rated current	[A]
I_P	Prospective short-circuit current	[A]
I_{SC}	Current at short-circuit	[A]
j	Current density	[A/m²]
K	Effective emissivity coefficient of the flame	[/m]
k_B	Boltzmann constant = 1.3806488 10^{-23} J/K	[J/K]
k_M	Material coefficient	[A $s^{0.5}$/m²]
$\overline{L}_B$	Mean beam length	[m]
L_C	Enthalpy of polymer carbonization	[J/kg]
L_F	Length of the flame	[m]
L_g	Enthalpy of gasification per mass of vaporizable polymer	[J/kg]
m	Mass	[kg]
$\dot{m}''$	Mass flow	[kg/m² s]
$\dot{m}''\big\|_{ign}$	Critical mass flow for ignition	[kg/m² s]
n_x	Density of particles x	[1/m³]
N_m	Excitation probability of an atom at the level m	[no unit]
p	Pressure, Probability	[Pa], [no unit]
$\dot{q}$	Power	[W]
$\dot{q}''$	Heat flow	[W/m²]
$\dot{q}''_{INS}$	Heat flow from the electrical fault to the insulation	[W/m²]

$\dot{q}'''$	Power density	[W/m³]
Q	Energy	[J]
Q_{ACC}	Accumulated energy of the electrical fault	[J]
Q'''	Density of energy	[J/m³]
Q_x^C	Effective cross-sectional area of particle x	[m²]
r	Radius	[m]
R	Electrical resistance	[Ω]
R_{th}	Thermal resistance	[K/W]
S	Cross-section	[m²]
t	Time	[s]
T	Temperature	[K]
U	Voltage	[V]
U_{AC}	Anodic and cathodic fall voltage	[V]
U_{ARC}	Arc voltage	[V]
U_{BR}	Breakdown voltage	[V]
U_S	Arc striking voltage	[V]
U_{SYS}	System voltage	[V]
V	Volume	[m³]
V_F	Volume of the flame	[m³]
v	Velocity	[m/s]
W	Kinetic energy of a particle	[eV]
$\overline{W}$	Mean excitation energy	[eV]
W_i	Ionization energy	[eV]
W_{sp}	Energy transported by a single particle	[eV]
W_t	Energy transported by a flow of particle	[W/m²]
Z	Degree of ionization	[no unit]
ε	Emissivity factor	[no unit]

κ	Thermal conductivity	[W/m K]
λ	Mean free path	[m]
θ	Time constant	[s]
μ	Proportion of residue	[no unit]
ρ	Density	[kg/m³]
σ	Electrical conductivity	[1/Ω m]
σ_{SB}	Stefan-Boltzmann constant = 5.6704 10-8 J/m^2sK^4	[J/m^2 s K^4]
χ	Combustion efficiency	[no unit]
ω	Angular frequency	[rad/s]

Symbols for derivates

P	Any physical quantity
$\dot{P}$	Derivate in the time domain $= \frac{dP}{dt}$
P'	Derivate in one space dimension $= \frac{dP}{dx}$
P''	Derivate in two space dimensions $= \frac{d^2P}{dx\ dy}$
P'''	Derivate in three space dimensions $= \frac{d^3P}{dx\ dy\ dz}$
$\dot{P}'''$	Derivate in three space dimensions and time $= \frac{d^4P}{dx\ dy\ dz\ dt}$

Definitions of specific terms

Arc stability: ratio of arcing half-cycles to the total number of half-cycles during a defined time lap (see 0)

Bolted short-circuit: short-circuit between two conductors at different polarities with stable metal-to-metal contact

Char: carbonized residue or ash of a polymer at thermal degradation

Electrical fire: fire exclusively initiated by the heat of an electrical fault

Ignition energy at arcing: energy dissipated by the series arc fault from the instant where it becomes stable (arc stability > 70 %) to the instant where the insulation is ignited (flame that lasts at least 50 ms)

Masking test: verification of the arc detection function of the AFDD in combination with a load that may generate disturbing electrical signals and mask the specific arc signals

Nuisance trip: tripping operation of a protection device without the presence of a real electrical fault (also called unwanted tripping)

References

AnLü09 M. Anheuser, C. Lüders, "Numerical arc simulations for low-voltage circuit breakers",Siemens AG, 18th Symposium on Physics of Switching Arc (FSO), September 2009

AST10a ASTM D3874-12, "Standard Test Method for Ignition of Materials by Hot Wire Sources", March 2010

AST10b J. Andrea, P. Schweitzer, E. Tisserand, P. Roth, S. Weber, "Calibrated AC and DC Arcing Fault Generator", Université Henri Pointcaré Nancy, IEEE/ICEC Holm Conference on Electric Contacts, 2010

Ayr03 H. Ayrton, "The electric arc", Chapter 6, ISBN-10 0548410194, 1903

Bab01 V. Babrauskas, "How do electrical wiring faults lead to structure ignitions?", Fire science and technology Inc., Fire and materials 2001 Conference, London, 2001

Bab03 V. Babrauskas, "Ignition Handbook", ISBN 0-9728111-3-3, Fire Science Publishers, 2003

Bab05 V. Babraukas, "Mechanisms and modes for ignition of low-voltage PVC wires, cables, and cords", p. 291-309 in Fire & Materials 2005, Interscience Communications Ltd., London, 2005

BCTG12 T. Billoux, Y. Cressault, Ph. Teulet, A. Gleizes, "Calculation of the net emission coefficient of an air thermal plasma at very high pressure", 12th High-Tech Plasma Processes Conference, 2012

Bea05 P. A. Beaulieu, "Flammability Characteristics at heat flux levels up to 200 kW/m² and the effect of oxygen on flame heat flux", Table C.1, Worcester Polytechnic Institute, October 2005

Ben99 B. Benzler, "Thermische Analyse von PVC", Mettler Toledo GmbH, January 1999

Ber09 F. Berger, "Der Störlichtbogen – Ein Überblick", TU Ilmenau, VDE Albert-Keil-Kontaktseminar, 2009

BHSL06 W. Benenson, J. Harris, H. Stocker, H. Lutz, "Handbook of Physics", part 17.1.1.2, ISBN 0-387-95269-1, Springer, 2006

Bla98 U.S. Patent 5,729,145, R. Blades, "Method and apparatus for detecting arcing in AC power systems by monitoring high frequency noise", March 17th 1998

Bra17 www.brandschutzschalter.de

ChCo90 S. Chapmann, T. Cowling, "The mathematical theory of non-uniform gases", 3rd edition, Cambridge Univ. Press, ISBN 052140844X, 1990

ChPo72 W.K. Chu, D. Powerd, "Calculation of mean excitation energy for all elements", Baylor University, Waco, 1972

Com27 K. Compton, "The electric arc", Trans. AIEE 46, 868-883, 1927

Cro06 T. Crompton, "Polymer Reference Book", ISBN: 098-1-84735-025-1, Smithers Rapra Technology, 2006

Dah99 Y. Dahmouni, Hannover University, "Brandentstehung in Niederspannungsanlagen", 1999

DIN00 DIN VDE 0250-0204, "Isolierte Starkstromleitungen / PVC-Installationsleitung NYM", December 2000

DIN01 DIN VDE 0281-3, "PVC-isolierte Leitungen mit Nennspannung bis 45/750V – Aderleitungen für feste Verlegung", January 2001

DIN03a DIN VDE 0100-482, "Errichten von Niederspannungsanlagen, Brandschutz bei besonderen Risiken oder Gefahren", June 2003

DIN03b DIN VDE 0298-4, "Verwendung von Kabeln und isolierten Leitungen für Starkstromanlagen / Empfohlene Werte für die Strombelastbarkeit von Kabeln und Leitungen für feste Verlegung in und an Gebäuden und von flexiblen Leitungen", August 2003

DIN05 DIN 51006, "Thermische Analyse (TA) – Thermogravimetrie (TG) – Grundlagen", July 2005

DIN10a DIN VDE 0100-430, "Errichten von Niederspannungsanlagen – Teil 4-43: Schutzmassnahmen – Schutz bei Überstrom", October 2010

DIN10b DIN EN 61008-1, "Residual current operated circuit-breakers without integrated overcurrent protection for household and similar uses (RCCB's) – Part 1: General rules", January 2010

DIN11 DIN VDE 0860, §20.1.2, "Audio, video and similar electronic apparatus, Safety requirements", October 2011

DIN14 DIN EN 62606, "Allgemeine Anforderungen an Fehlerlichtbogen-Schutzeinrichtungen", August 2014

DIN15 DIN VDE 0100-420/A1, "Low-voltage installations – Part 4-42: Protection for safety – Protection against thermal effects", April 2015

DIN16 DIN VDE 0100-420 „Errichten von Niederspannungsanlagen – Teil 4-42: Schutzmaßnahmen – Schutz gegen thermische Auswirkungen", Kapitel 421.7, February 2016

DIN99 DIN VDE 0636-2011, "Niederspannungssicherungen", Teil 2.1, May 1999

Dry11 D. Drysdale, "An Introduction to Fire Dynamics", University of Edinburgh, 3rd edition, 2011

DSB17 Norvegian directorate for civil protection, DSB, Database available on web site www.dsb.bo, Status 2017

Dur05 M. Durchholz, Siemens internal report EL2-10-151 on material ignition by wet tracking in combination with RCD protection, May 2005

FAA05 "Polymer flammability", DOT/FAA/AR-05/14, U.S. Federal Aviation Administration, May 2005

Fen95 J. Fenghui, "Prediction of Flame Radiation and Temperature in Polymer Combustion", State Key Laboratory of Science, USTC, International Association for Fire Safety Science, AOFST, 1995

FIC13 Federation of Indian chambers of Commerce and Industry, "India risk survey 2013", page 24, http://www.ficci.com/surveys.asp, 2013

FrKe11 A. Fridman, L. A. Kennedy, "Plasma Physics and Engineering", 2nd edition, ISBN 978-1-4398-1228-0, CRC Press, 2011

GBP11 D. Gonzales, F. Berger, H. Pursch, "Experimental investigation of the interaction of interrupting arcs and gassing polymer walls", IEEE Holm Conference on Electric Contacts, 2011

GCT10 A. Gleizes, Y. Cressault, Ph. Teulet, "Mixing rules for thermal plasma properties in mixtures of argon, air and metallic vapors", Plasma Sources Science and Technology 19, IOP Publishing, 2010

GrSe05 W. Grellmann, S. Seidler, "Kunstoffprüfung", ISBN 3-446-22086-0, Carl Hanser Verlag, 2005

HABB13 JM. Martel, M. Anheuser, F. Berger, B. Barbu, "Die thermischen Auswirkungen von Störlichtbögen auf Isolationsmaterialien", VDE Albert-Keil-Kontaktseminar, 2009, October 2013

HBG83 J. R. Hall, R. Bukowski, A. Gomberg, "Analysis of electrical fire investigations in ten cities", NBSIR 83-2803, US Dpt of commerce, December 1983

HeZu01 E. Hetzmannseder, J. Zuercher, "Lichtbogenfehler", Eaton Corp., VDE Albert-Keil-Kontaktseminar, 2001

Hoc03 A. Hochbaum, "Störungsarme Elektroinstallationen", GDV, VdS-Schadenverhütung Verlag, Heft 4, 2003

HoPr01 A. Horrocks, D. Price, "Fire retardant materials", ISBN 1-85573-419-2, Woodhead Publishing Limited, 2001

ICF04 "Residential wiring and electrical safety in Europe", ICF congress Prague Issue 50, December 2004

IEC04 IEC 60695-11-10, "Test flames – 50 W horizontal and vertical flame test methods", May 2004

IEC07 IEC 60664-1, "Insulation coordination for equipment within low-voltage-systems", Ed. 2, Table F.4, April 2007

IEC10a IEC 60695-2-12, "Glowing/hot-wire based test methods – Glow-wire flammability index (GWFI) test method for materials", Edition 2.0, October 2010

IEC10b IEC 60695-2-13, "Glowing/hot-wire based test methods – Glow-wire ignition temperature (GWIT) test method for materials", Edition 2.0, October 2010

IEC13 IEC 62606 Ed. 1.0, "General requirements for Arc Fault Detection Devices", March 2013

IEC15 IEC 60898-1 Ed. 2.0, "Electrical accessories – Circuit breakers for overcurrent protection for household and similar installations – Part 1: Circuit breakers for a.c. operation", March 2015

IFS14 Instituts für Schadenverhütung und Schadenforschung der öffentlichen Versicherer e.V., "IFS-Brandursachenstatistik 2013", http://ifs-ev.org/archiv/statistik/ifs_brandursachenstatistik_2013.pdf, Status April 2014

Kal12 M. Kalsen-Frise, "Leistungsberechnung", www.dieleitungsberechnung.de, Version 3.2, 2012

KCS07 D. Kolker, S. Campolo, N. Di Salvo, , "A study of Time/Current Characteristics of the Ignition Processes in Cellulosic Material Caused by Electrical Arcing for Application in 240V Arc-Fault Circuit Interrupters", Leviton Manufacturing, IEEE Holm Conference on Electric Contacts, 2007

Kin02 W. King, NFPA Technical committee proposal for National Electrical Code, Paragraph 210.12, October 2002

Kos11 S. Kosse, "Einfluss gasender Materialien auf die Lichtbogenbewegung", Siemens AG, VDE Albert-Keil-Kontaktseminar, 2011

Lan83 A. Landrock, "Handbook of plastics flammability and combustion toxicology", Chapter 5, ISBN 0-8155-0940-5, Noyes Publications, 1983

Lat80 D. Latham, "A channel model for long arcs in air", Physics of fluids Vol. 23, p. 1710-1715, 1980

Low74 J. J. Lowke, "Predictions of arc temperature profiles using approximate emission coefficients for radiation losses", J.Q.S.R.T. Vol. 14, p.111-112, 1974

Mae51 H. Maecker, "Der elektrische Lichtbogen", Ergebnisse der exakten Naturwissenschaften, Band XXV, pages 293-358, 1951

MAF10 JM. Martel, M. Anheuser, F. Berger, "A study of series arcing fault in the low-voltage electrical installation", IEEE Holm Conference on Electric Contacts, 2010

MAF14 JM. Martel, M. Anheuser, F. Berger, "Time-current tripping characteristics at series arcing for Arc Fault Detection Devices", VDE-ICEC Conference, June 2014

MAHBE11 JM. Martel, M. Anheuser, A. Hueber, F. Berger, F. Erhard, "Schutz gegen parallele Störlichtbögen in der Hauselektroinstallation", VDE Albert-Keil-Kontaktseminar, 2011

May43 O. Mayr, "Beiträge zur Theorie des statistischen und des dynamischen Lichtbogens", Archiv für Elektrotechnik, vol. Band 37, No. Heft 12, 1943

MeBe77 W. Meese, R. Beausoleil, "Exploratory study of glowing electrical connections", US Dpt of commerce, October 1977

Mil13 D. Miller, Consumer Product Safety Commission USA, "2009-2011 Residential Fire loss estimates", July 2013

MoGi06 A. P. Mouritz, A. G. Gibson, "Fire Properties of Polymer Composite Materials", ISBN-10 1-4020-5355-X, Springer, 2006

MTMA10 P. Müller, S. Tenbohlen, R. Maier, M. Anheuser, "Characteristics of series and parallel low current arc faults in the time and frequency domain", Univ. of Stuttgart, Siemens AG, IEEE Holm Conference on Electric Contacts, 2010

MuGo56 E. L. Murphy, R. H. Good, "Thermionic, Field Emission, and the Transition Region", Physical Review, Vol. 102, Number 6, Page 1464, 1956

Noa03 F. Noak, "Einführung in die elektrische Energietechnik", ISBN 3-446-21527-1, Fachbuchverlag Leipzig, 2003

Pat05 V. Patel, "Electrical Wiring Systems and Fire Risk in Residential Dwellings", ISBN 0-478-28436-5, Energy Safety Service New Zealand, 2005

PMGB01 G. Parise, L. Martirano, U. Grasselli, L. Benetti, "The Arc-Fault Circuit Protection", Univ. of Rome, IEEE Industry Applications Conference, Chicago, 2001

PSZ09 B. Pahl, T. Schoepf, X. Zhou, "Arc faults in residential electrical systems", Eaton Corp., VDE Albert-Keil-Kontaktseminar, 2009

Rac11 W. Racky, "Studie von Störlichtbogenfällen in der Niederspannungselektroinstallation", Hochschule Deggendorf, Siemens, Germany, August 2011

ReBa15 Plasma data for air provided by F. Reichert and computed by B. Barbu from TU Ilmenau, 2015

Res08 C. Restrepo, "Arc fault detection and discrimination methods", Siemens, IEEE Holm conference on Electric Contacts, 2008

Rie67 W. Rieder, "Plasma und Lichtbogen", Friedr. Vieweg & Sohn GmbH, Verlag, Braunschweig, 1967

RST11 M. Rabla, P. Schweitzer, E. Tisserand, "Method to design arc fault detection algorithm using FPGA", IEEE Holm Conference on Electric Contacts, 2011

RSZ11 C. Rümpler, H. Stammberger, A. Zacharias, "Low-Voltage arc simulation with out-gassing polymers", IEEE Holm Conference on Electric Contacts, 2011

SAE09 SAE International, SAE AS5692, part 4.7.7.6.3, release 2009/30/7

ShCa11 J. Shea, J. Carrodus, "RF Current Produced from Electrical Arcing", IEEE Holm Conference on Electric Contacts, 2011

She06a J. Shea, "Identifying causes for certain types of electrically initiated fires in residential circuits", Conference for proceeding on aged electrical systems, NFPA, Chicago, 2006

She06b J. Shea, "Glowing Contact Physics", Eaton Corp., IEEE Holm Conference on Electric Contacts, 2006

She07a J. Shea, "Conditions for series arcing phenomena in PVC wiring", Eaton Corp., IEEE Transactions on Components and Packaging Technologies, 2007

She07b J. Shea, "Conditions that can cause upper thermal limits on residential wiring to be exceeded", Fire and Materials, 2007

She08 J. Shea, "Comparing 240 Vrms to 120 Vrms Series Arcing Faults in Residential Wire", Eaton Corp., IEEE Holm Conference on Electric Contacts, 2008

ShZh07 J. Shea, X. Zhou, "Material Effect on Glowing Contac Properties", Eaton Corp, IEEE Holm Conference on Electric Contacts, 2007

SiCa11 E. Sili, J. Cambronne, "Pressure and temperature effects on the Paschen curve", Université de Toulouse, 2011 annual report conference on electrical insulation and dielectric phenomena, 2011

SKSNR91 J. Sletbak, R. Kristensen, H. Sundklakk, G. Navik, M. Runde, "Glowing contact areas in loose copper wire connections", p. 244-248 in Proc. 37th IEEE Holm Conference on Electric Contacts, 1991

SmCo87 L. Smith, D. McCoskrie, "Residential Electrical distribution system fires", CPSC, December 1987

SmWi01 B. Smirnov, M. Wiley, "Physics of Ionized Gases", ISBN 0-471-17594-3, 2001

Str98 A. von Streitberg, "Elektrische Brandursachen – Erfolgversprechende Ansätze zur Schadenverhütung", Allianz report 6-98, 1998

Tro90 J. Troitzsch, "International plastics flammability handbook", Chapters 3 and 4, 2nd edition, ISBN 3-446-15156-7, Carl Hanser Verlag, 1990

UL01 UL 817, "Cord Sets and Power-Supply Cords", Edition 11, March 2001

UL10 UL 62, "Flexible Cords and Cables", Edition 18, May 2010

UL11 UL 1699B, "Outline of investigation for photovoltaic arc-fault circuit protection", April 2011

UL12a UL 94, "Tests for Flammability of Plastics Materials for Parts in Devices and Appliances", Tests 7 & 8, Edition 5, January 2012

UL12b UL 746A, "Polymeric Materials – Short Term Property Evaluations", Tests 33 & 34, Edition 6, October 2012

UL13 UL 1699, "Standard for Safety for Arc-Fault Circuit-Interrupters", January 2013

UL95 Underwritters Lab. Inc., "Technology for detecting and monitoring conditions that could cause electrical wiring system fires", CPSC-C-94-1112, September 1995

UL96 Underwritters Lab. Inc., "Arc-Fault detection circuit breakers for National Electrical Manufacturers Association", Project 95NK6832, File NC3054, March 1996

Urb08 J. Urbas, "Glowing connections experiments with alternating currents below 1 Arms", IEEE Holm Conference on Electric Contacts, 2008

USD08 U.S. Department of Homeland Security, "Residential Building Electrical Fires", Volume 8, Issue 2, March 2008

Tur12 S. Turns, "An introduction to combustion", p. 293-295, 3rd Ed., McGraw-Hill, ISBN 978-007-108687-5, 2012

Wag01 R. Wagner, "Special services investigation on branch/feeder arc fault circuit interrupter incorporating equipment ground fault protection", Cutler-Hammer, File E45310, May 2001

Wyp12 G. Wypych, "Handbook of polymers", ISBN 978-1-895198-47-8, ChemTec Publishing Toronto, 2012

XiHn14 J. Xin, C. Fu Huang, "Fire risk assessment of residential buildings based on fire statistics from China", Fire Technology, 50, 1147-1161, 2014

Yaw11 C. Yaws, "Yaws handbook of properties of the chemical elements", Lamar university Beaumont Texas, 2011

YNN84 N. Yoshimura, M. Nishia, F. Noto, "Light Emission from Tracking Discharges on Organic Insulation", IEEE Transactions on Electrical Insulation EI-19, 149-155, 1984

ZhSh07 X. Zhou, J. Shea, "Characterization of glowing contacts using optical emission spectroscopy", IEEE Holm Conference on Electric Contacts, 2007

Zim87 M. Zimmer, "Damit sich das Feuer nicht ausbreitet", Elektro-Handel 32. Jahrgang 1987 Nr. 12

Zue08 J. Zuercher, Patent application WO 2008/053329 A2, Eaton Corp., May 8th 2008